UNIVERSITAT POLITÈCNICA DE VALÈNCIA

INSTITUTO INTERUNIVERSITARIO DE INVESTIGACIÓN DE RECONOCIMIENTO MOLECULAR Y DESARROLLO TECNOLÓGICO

DEVELOPMENT OF SMART DEVICES FOR THE DETECTION OF METABOLITES OF TOXIC SUBSTANCES AND DISEASE-RELATED ENZYME OVEREXPRESSION

PhD THESIS

Submitted by

Marcia Domínguez Rodríguez

PhD Supervisors:

Prof. Ramón Martínez Máñez
Dr. Juan F. Blandez

Valencia, Diciembre 2023

RAMÓN MARTINÉZ MÁÑEZ PhD in Chemistry and Professor at the Universitat Politècnica de València and JUAN F. BLANDEZ PhD in Suitinable Chemistry.

CERTIFY:

That the work "***Development of smart devices for the detection of metabolites of toxic substances and disease-related enzyme overexpression***." has been developed by Marcia Domínguez Rodríguez under their supervision in the Instituto Interuniversitario de Investigación de Reconocimiento Molecular y Desarrollo Tecnológico (IDM) of the Universitat Politècnica de València, as a Thesis Project in order to obtain the degree of PhD in Chemistry at the Universitat Politècnica de València.

Valencia, Diciembre 2023.

Prof. Ramón Martínez Máñez

Dr. Juan F. Blandez

A mi familia

"In the book of life, the answers aren't in the back." - **Charlie Brown**

"The most beautiful thing we can experience is the mysterious. It is the source of all true art and science." - **Albert Einstein**

Acknowledgements

Agradecimientos

Hoy, al llegar al final de este emocionante viaje, me gustaría tomar un momento para expresar mi más sincero agradecimiento a todas las personas que han contribuido de alguna manera a la realización de esta tesis.

En primer lugar, quiero agradecer a mis directores de tesis, Ramón Martínez Mañez y Juan Francisco Blandez, por su orientación, apoyo y sabios consejos a lo largo de todo el proceso de investigación. Me siento afortunada de haber tenido la oportunidad de trabajar bajo sus tutelas y de aprender de sus experiencias. Gracias Ramón por permitirme formar parte del grupo y haber depositado tu confianza en mí. Gracias JuanFran por tu infinita paciencia y tus innumerables consejos. Has hecho que cada obstáculo sea mucho más llevadero.

Muchas gracias, Félix, por tu apoyo y dedicación constantes. Siempre has estado ahí, dispuesto a ayudar en los momentos más difíciles.

A Alba García, quien me ha llevado de la mano por el mundo de la biología. Gracias por tu paciencia y disposición.

A Bea Lozano, gracias por haberme adentrado en el fascinante mundo de los sensores. Eres un ejemplo de trabajo constante.

A Vicente Martí, por sus sabios consejos y disposición para ayudarme en cada momento.

Por otra parte, quisiera agradecer a todos mis compañeros del grupo del IDM, con los que he compartido todo este tiempo, en especial a mis compañeros del 2.6: Jessie, Eva Garrido, Guillermo, Giovanni, Andy, Toni, Laura…. Con ustedes he vivido un sinfín de aventuras y retos. Muchas gracias por el inmenso apoyo y ayuda que me han brindado durante todos estos años.

Gracias a mis compañeros del equipo de comunicación, Paula, Andrea E., Javi, por estar siempre allí, por hacerme reír y por todos los momentos compartidos.

Me gustaría también agradecer a mis compañeros del CIPF, en especial a David y Araceli, por su paciencia y ayuda a la hora de comprender ese maravilloso mundo de la biología y por complementar en gran medida esta tesis.

Gracias también a Andrea Bernardos y Elena Aznar, así como a la parte más administrativa del grupo, que también ha desempeñado un papel fundamental en la realización de esta tesis. Eva Brun y Tania, gracias por estar siempre dispuestas a ayudar.

Además, quiero agradecer a todos mis compañeros de la CPI y de la Fe: Angy, Serena, Miguelito, Yoel, Isa, Marina …, con quienes he compartido momentos inolvidables.

Me es imposible mencionarlos a todos. Han sido muchos los que me han acompañado durante este emocionante camino. ¡Gracias, Gracias a todos! Siempre me han hecho sentir en casa a pesar de estar lejos de ella.

A mi tati, quien ha sido mi soporte y motor impulsor en los últimos 7 años. Siempre has estado ahí para escucharme y recordarme que juntos podemos lograr cualquier cosa que nos propongamos.

A Olgui y Toni por aceptarme como otra hija más.

A mis abuelos, por ser mi primera escuela. Aunque hoy no puedan ver ni ser conscientes de este logro, sé que se sentirían muy felices y orgullosos.

A mis queridos gordis, infinitas gracias por siempre estar presentes a pesar de la distancia y por apoyarme en cada una de mis decisiones. La persona que hoy soy es gracias a ustedes.

A mis hermanos, uno de los mejores regalos que me ha dado la vida por siempre estar ahí para su gordita.

¡Gracias infinitas!

Resumen

La presente tesis doctoral, titulada "Desarrollo de dispositivos inteligentes para la detección de metabolitos de sustancias tóxicas y sobreexpresión enzimática relacionada con enfermedades", se enfoca en el diseño, síntesis, caracterización y evaluación de nanopartículas para la detección de metabolitos del benceno en orina y el uso de sondas moleculares fluorogénicas para la detección de enzimas sobreexpresadas mediante medidas en la orina o a través de la misma.

En el primer capítulo se discuten las limitaciones de las técnicas de diagnóstico convencionales y se destaca el valor de la orina como muestra biológica para la detección y seguimiento de biomarcadores relacionados con patologías específicas. También se introducen los conceptos básicos de los materiales mesoporosos de sílice, el reconocimiento molecular y el desarrollo de sondas moleculares, así como el estado del arte en el desarrollo de sondas moleculares fluorogénicas y su aplicación actual en la detección de enzimas, cuya sobreexpresión está ligada a la evolución de diversas patologías. Finalmente, se discute la necesidad creciente de desarrollar nuevas sondas moleculares fácilmente eliminables renalmente como herramientas de diagnóstico no invasivas para el paciente y para el seguimiento de la eficacia del tratamiento de enfermedades.

En el segundo capítulo se exponen los objetivos generales de la presente tesis doctoral, así como los objetivos concretos que son abordados en los diferentes capítulos experimentales.

En el tercer capítulo se describe un nuevo nanodispositivo inteligente (**S4**) para la detección del ácido *trans,trans*-mucónico (*t,t*-MA), que es un metabolito del benceno, en orina. En concreto, se plantea la síntesis y caracterización de un material constituido por nanopartículas de sílice mesoporosas cargadas con sulfrodamina B y funcionalizadas en su superficie externa con un derivado del ácido tereftálico, capaz

de coordinarse con el complejo Cu_2bistren (previamente sintetizado y caracterizado), cerrando así los poros y permitiendo la encapsulación del colorante. En presencia del dicarboxilato *t,t*-MA se observó una marcada liberación de sulforodamina B debido a la coordinación preferencial del *t,t*-MA con el complejo Cu_2bistren. La apertura de poros y la liberación de carga se induce rápidamente (10 minutos) y de manera selectiva en muestras de orina real adulterada con *t,t*-MA, utilizando un simple fluorímetro y sin tratamiento previo de la muestra.

El cuarto capítulo presenta el diseño de una nueva sonda fluorogénica (**NB-ALA**) cuya emisión se localiza en el infrarrojo cercano (NIR-I). **NB-ALA** está constituida por el fluoróforo Azul de Nilo unido mediante un enlace amida hidrolizable al aminoácido L-alanina. La formación de este enlace produce la desactivación de la emisión de fluorescencia del Azul de Nilo. Esta fluorescencia es recuperada en presencia de la enzima aminopeptidasa-N (APN), la cual hidroliza el enlace entre el Azul de Nilo y el resto peptídico. Las propiedades fotoquímicas del Azul de Nilo, con alto rendimiento cuántico de fluorescencia, permite detectar de forma sensible y selectiva la presencia de la enzima APN en muestras de orina. **NB-ALA** se validó de forma eficaz para la detección de APN en muestras de orina humana dopadas, así como en un modelo murino de fibrosis renal inducido por perfusión con ácido fólico, donde el daño renal promueve la presencia en orina de elevados niveles de APN. En este modelo, marcadores de daño renal tradicionales como los niveles séricos de urea y creatinina se recuperan con el tiempo (o más bien se compensan mientras persiste cierto daño renal) siendo la única lectura patológica que puede relacionarse con el daño renal la densidad de la orina. Dichos valores de densidad tomados en función del tiempo se evaluaron frente a los resultados obtenidos con **NB-ALA** para detectar el daño en riñón, mostrándose señal únicamente en la orina procedente de riñones fibróticos.

Basándonos en la necesidad de desarrollar métodos de diagnóstico y seguimiento de enfermedades más eficaces y menos tóxicos, en el capítulo cinco se describe una

nueva sonda (**NB-SO_3-Leu**) para la detección de elevados niveles de leucina aminopeptidasa (LAP) como biomarcador de cáncer. Para ello, se modificó la estructura del fluoróforo comercial Azul de Nilo con la introducción de un grupo sulfónico, generando una estructura zwitteriónica que favorece la solubilidad en agua de la sonda y promueve su eliminación renal, disminuyendo los posibles efectos tóxicos por acumulación de la sonda, o el fluoróforo libre, en diferentes órganos del sistema reticuloendotelial. Los resultados mostraron una alta selectividad y sensibilidad del **NB-SO_3-Leu** en la detección de LAP, incluso en la presencia de potenciales interferentes. Un ejemplo especialmente importante del uso de LAP como biomarcador es su aplicación para la detección del melanoma, en el que la detección precoz es esencial para la resección. Por ello, la sonda se validó *in vitro* en la detección de LAP en células de cáncer de melanoma SK-Mel-103, caracterizado por la sobreexpresión de esta enzima. Los estudios finales con inhibidores enzimáticos demostraron la selectividad de la sonda en el mecanismo propuesto.

Partiendo de la idea anterior, en el sexto capítulo se describe una sonda molecular similar (**NB-SO_3-Ala**) para la detección de niveles elevados de alanina aminopeptidasa (APN) como biomarcador de cáncer. Para ello inicialmente se modificó el esqueleto del fluoróforo comercial Azul de Nilo con restos de ácido sulfónico para aumentar su solubilidad. Una vez obtenido el fluoróforo modificado, este se conjugó a un residuo de alanina, que actúa como unidad reactiva de APN produciendo, además, la desactivación de la fluorescencia del fluoróforo modificado. En presencia de APN está fluorescencia se recupera permitiendo la monitorización de los niveles de la enzima. Por otra parte, la nueva sonda es capaz de detectar la sobreexpresión de la enzima APN en diferentes líneas celulares de cáncer, observándose mayor expresión en células de cáncer de pulmón humano A549.

Finalmente, el capítulo siete se centra en un nuevo concepto de sondas moleculares no invasivas que proporcionan una señal fácilmente legible a través de

simples medidas de fluorescencia de la orina. Con tal fin, se partió de un fluoróforo de hemicianina-7 (Cy7), cuya estructura se modificó con ácidos sulfónicos, generando una estructura zwitteriónica que favorece su eliminación a través de la orina. Este fluoróforo se empleó en el diseño de una sonda para la detección, a través de la orina, de la enzima monoamina oxidasa (MAO), cuyos elevados niveles se asocian a enfermedades relacionadas con el envejecimiento. La sonda (**Cy7-MAO**), constituida por el fluoróforo Cy7 modificado con grupos sulfónicos unido a un grupo propilamino, es hidrolizada en presencia de dicha enzima, recuperando la fluorescencia inicial del fluoróforo. Esta sonda, tiene la gran ventaja de que tras su administración se hidroliza en presencia de la enzima MAO, dando lugar a la liberación de un fluoróforo Cy7 altamente emisivo que puede cuantificarse en la orina de forma directa. **Cy7-MAO** se validó con éxito *in vitro* utilizando células humanas HepG2 de hígado, con altos niveles endógenos de MAO. Por otra parte, la sonda **Cy7-MAO** se empleó para la detección de la enzima MAO *in vivo* en ratones jóvenes y viejos. Estos estudios indicaron que la expresión de MAO en ratones ancianos sanos aumenta significativamente en comparación con los animales jóvenes, lo que sugiere que la sobreexpresión de MAO puede utilizarse como biomarcador del envejecimiento.

Por último, en el capítulo ocho, se presentan las conclusiones principales de los diferentes capítulos experimentales, así como las conclusiones generales extraídas de esta tesis doctoral. El desarrollo de nanomateriales y sondas moleculares para detectar selectivamente sustancias tóxicas y enzimas que han sido empleadas como biomarcadores de enfermedades constituye un campo novedoso y con gran potencial para el desarrollo de nuevas técnicas de diagnóstico. Se espera que los resultados obtenidos en esta tesis puedan servir como base para el desarrollo de nuevas sondas moleculares para el diagnóstico y tratamiento temprano de diferentes enfermedades, así como para el seguimiento de tratamientos en pacientes.

Resum

Aquesta tesi doctoral, titulada "Desenvolupament de dispositius intel·ligents per a la detecció de metabòlits de substàncies tòxiques i sobreexpressió enzimàtica relacionada amb malalties", s'enfoca en el disseny, preparació, caracterització i aplicació de nanopartícules per a la detecció de metabòlits del benzè reen orina i l'ús de sondes moleculars fluorogèniques per a la detecció d'enzims sobreexpressats mitjançant mesures a l'orina a través d'aquesta.

Al primer capítol es discuteixen les limitacions de les tècniques de diagnòstic convencionals i es destaca el valor de l'orina com a mostra biològica per a la detecció i seguiment de biomarcadors relacionats amb patologies específiques. També s'introdueixen els conceptes bàsics dels materials mesoporosos de sílice, el reconeixement molecular i el desenvolupament de sondes moleculars, així com l'estat de l'art en el desenvolupament de sondes moleculars fluorogèniques i la seva aplicació actual a la detecció d'enzims, la sobreexpressió dels quals està lligada a l'evolució de diverses patologies. Finalment, es discuteix la necessitat creixent de desenvolupar noves sondes moleculars fàcilment eliminables renalment com a eines de diagnòstic no invasives per al pacient i per al seguiment de l'eficàcia del tractament de malalties.

Al segon capítol s'exposen els objectius generals de la present tesi doctoral, així com els objectius concrets que són abordats en els diferents capítols experimentals. En el tercer capítol es descriu un nou nanodispositiu intel·ligent (**S4**) per a la detecció de l'àcid *trans, trans*-mucònic (*t,t*-MA), que és un metabòlit del benzè, en orina. En concret, es planteja la síntesi i caracterització d'un material constituït per nanopartícules de sílice mesoporoses carregades amb sulfrodamina B i funcionalitzades a la superfície externa amb un derivar de l'àcid tereftàlic, capaç de coordinarse amb el complex Cu_2bistren (prèviament sintetitzat i caracteritzat),

tancant així els porus i permetent l'encapsulació del colorant. En presència del dicarboxilat *t,t*-MA es va observar un marcat alliberament de sulforodamina B a causa de la coordinació preferencial del *t,t*-MA amb el complex Cu_2bistren. L'obertura dels porus i l'alliberament de la càrrega s'indueix ràpidament (10 minuts) i de manera selectiva a mostres d'orina reals adulterades amb *t,t*-MA, utilitzant un simple fluorímetre i sense tractament previ de la mostra.

El quart capítol presenta el disseny d'una nova sonda fluorogènica (**NB-ALA**) l'emissió de la qual es localitza a l'infraroig proper (NIR-I). **NB-ALA** està constituïda pel fluoròfor Blau de Nil unit mitjançant un enllaç amida hidrolitzable a l'aminoàcid L-alanina. La formació d'aquest enllaç produeix la desactivació de l'emissió de fluorescència del Blau de Nil. Aquesta fluorescència és recuperada en presència de l'enzim aminopeptidasa-N (APN), la qual hidrolitza l'enllaç entre el Blau de Nil i el fragment peptídic. Les propietats fotoquímiques del Blau de Nil, amb un alt rendiment quànticde fluorescència, permeten detectar de manera sensible i selectiva la presència de l'enzim APN en mostres d'orina. **NB-ALA** es va validar de manera eficaç per a la detecció d'APN en mostres d'orina humana dopades, així com, en un model murí de fibrosi renal induït per perfusió amb àcid fòlic, on el dany renal promou la presència en orina d'elevats nivells d'APN. En aquest model, marcadors de dany renal tradicionals com els nivells sèrics d'urea i creatinina es recuperen amb el temps (o més aviat es compensen mentre persisteix cert dany renal) sent l'única lectura patològica que es pot relacionar amb el dany renal la densitat de la orina. Aquests valors de densitat presos en funció del temps es van avaluar davant dels resultats obtinguts amb **NB-ALA** per detectar el dany en ronyó, mostrant-se senyal únicament a l'orina procedent de ronyons fibròtics.

Basantnos en la necessitat de desenvolupar mètodes de diagnòstic i seguiment de malalties més eficaços i menys tòxics, al capítol cinc es descriu una nova sonda (**NB-SO_3-Leu**) per a la detecció d'elevats nivells de leucina aminopeptidasa (LAP) com a biomarcador de càncer. Per això, es va modificar l'estructura del fluoròfor comercial Blau de Nil amb la introducció d'un grup sulfònic, generant una estructura zwitteriònica que afavoreix la solubilitat de la sonda en aigua i en promou l'eliminació renal, disminuint els possibles efectes tòxics per acumulació de la sonda i del fluoròfor lliure en diferents òrgans del sistema reticuloendotelial. Els resultats van mostrar una alta selectivitat i sensibilitat de **NB-SO_3-Leu** a la detecció de LAP, fins i tot en la presència de potencials interferents. Un exemple especialment important de l'ús de LAP com a biomarcador és la seva aplicació per a la detecció del melanoma, en què la detecció precoç és essencial per a la resecció. Per això, la sonda es va validar in vitro a la detecció de LAP en cèl·lules de càncer de melanoma SK-Mel-103, caracteritzat per la sobreexpressió d'aquest enzim. Els estudis finals amb inhibidors enzimàtics van demostrar la selectivitat de la sonda al mecanisme proposat.

Partint de la idea anterior, al sisè capítol es descriu una sonda molecular similar (**NB-SO_3-Ala**) per a la detecció de nivells elevats d'alanina aminopeptidasa (APN) com a biomarcador de càncer. Per això inicialment es va modificar l'esquelet del fluoròfor comercial Blau de Nil incorporant grups d'àcid sulfònic per augmentar-ne la solubilitat. Una vegada s'ha obtingut el fluoròfor modificat, aquest es va conjugar amb l'aminoàcid alanina, que actua com a unitat reactiva d'APN produint, a més, la desactivació de la fluorescència del fluoròfor modificat. En presència d'APN aquesta fluorescència es recupera i permet la monitorització dels nivells de l'enzim. D'altra banda, la nova sonda és capaç de detectar la sobreexpressió de l'enzim APN en diferents línies cel·lulars de càncer, observant-se més expressió en cèl·lules de càncer de pulmó humà A549.

Finalment, el capítol setè es centra en un nou concepte de sondes moleculars no invasives que proporcionen un senyal fàcilment llegible mitjançant simples mesures de fluorescència de l'orina. Amb aquesta finalitat, es va partir d'un fluoròfor d'hemicinanina-7 (Cy7), l'estructura del qual es va modificar amb àcids sulfònics, generant una estructura zwitteriònica que n'afavoreix l'eliminació a través de l'orina. Aquest fluoròfor es va fer servir en el disseny d'una sonda per a la detecció, a través de l'orina, de l'enzim monoamina oxidasa (MAO), els nivells elevats dels quals s'associen a malalties relacionades amb l'envelliment. La sonda (**Cy7-MAO**), constituïda pel fluoròfor Cy7 modificat amb grups sulfònics unit a un grup propilamina, és hidrolitzada en presència d'aquest enzim, recuperant la fluorescència inicial del fluoròfor. Aquesta sonda té el gran avantatge que després de la seva administració s'hidrolitza en presència de l'enzim MAO, donant lloc a l'alliberament del fluoròfor Cy7 altament emissiu que es pot quantificar a l'orina de manera directa. El compost **Cy7-MAO** es va validar amb èxit *in vitro* utilitzant cèl·lules humanes HepG2 de fetge, amb alts nivells endògens de MAO. D'altra banda, la sonda **Cy7-MAO** es va fer servir per a la detecció de l'enzim MAO *in vivo* en ratolins joves i vells. Aquests estudis van indicar que l'expressió de MAO en ratolins vells augmenta significativament en comparació dels animals joves, cosa que suggereix que la sobreexpressió de MAO es pot utilitzar com a biomarcador de l'envelliment.

Finalment, al capítol vuitè, es presenten les conclusions principals dels diferents capítols experimentals, així com les conclusions generals extretes d'aquesta tesi doctoral. El desenvolupament de nanomaterials i sondes moleculars per detectar selectivament substàncies tòxiques i enzims que han estat emprats com a biomarcadors de malalties constitueix un camp nou i amb gran potencial per al desenvolupament de noves tècniques de diagnòstic. S'espera que els resultats obtinguts en aquesta tesi puguin servir com a base per al desenvolupament de noves

sondes moleculars per al diagnòstic i el tractament primerenc de diferents malalties, així com per al seguiment de tractaments en pacients.

Abstract

This PhD thesis, entitled "Development of smart devices for the detection of metabolites of toxic substances and disease-related enzyme overexpression", focuses on the design, preparation, characterization, and evaluation of nanoparticles for the detection of benzene metabolites in urine and the use of fluorogenic molecular probes for the detection of overexpressed enzymes by measurements in or through urine.

The first chapter discusses the limitations of conventional diagnostic techniques and highlights the value of urine as a biological sample for the detection and monitoring of biomarkers related to specific pathologies. The basic concepts of mesoporous silica materials, molecular recognition and the development of molecular probes are also introduced, as well as the state of the art in the development of fluorogenic molecular probes and their current application in the detection of enzymes, whose overexpression is linked to the evolution of various pathologies. Finally, the growing need to develop new renal clearable molecular probes as non-invasive diagnostic tools for the patients and for monitoring the efficacy of disease treatments are discussed.

In the second chapter, the general objectives of this PhD thesis are presented, as well as the specific objectives that are addressed in the different experimental chapters.

The third chapter describes a new smart nanodevice (**S4**) for the detection of *trans,trans*-muconic acid (*t,t*-MA), which is a metabolite of benzene, in urine. Specifically, the synthesis and characterization of a material consisting of mesoporous silica nanoparticles loaded with sulfrodamine B and functionalized on its external surface with a terephthalic acid derivative, capable of coordinating with Cu_2bistren complex (previously synthesized and characterized), thus closing the

pores and allowing the encapsulation of the dye. In the presence of *t,t*-MA dicarboxylate, a marked release of sulforhodamine B was observed due to the preferential coordination of *t,t*-MA with the Cu_2bistren complex. Pore opening and charge release is induced rapidly (10 min) and selectively in real urine samples adulterated with *t,t*-MA, using a simple fluorimeter and without sample pre-treatment.

The fourth chapter presents the design of a new fluorogenic probe (**NB-ALA**) whose emission is localized in the near infrared (NIR-I) region. **NB-ALA** consists of the fluorophore Nile Blue linked, through a hydrolyzable amide bond, with the amino acid L-alanine. The formation of this amide bond results in the deactivation of the Nile Blue fluorescence emission. This fluorescence is recovered in the presence of the enzyme aminopeptidase-N (APN), which hydrolyzes the bond between Nile Blue and the peptide residue. The photochemical properties of Nile Blue, with high fluorescence quantum yield, allow sensitive and selective detection of the presence of the APN enzyme in urine samples. **NB-ALA** was effectively validated for the detection of APN in doped human urine samples as well as in a murine model of folic acid perfusion-induced renal fibrosis, where renal damage promotes the presence of elevated levels of APN in urine. In this model, traditional renal damage markers, such as serum urea and creatinine levels, recover over time (or rather compensate while some renal damage persists) with the only pathological reading that can be related to renal damage being urine density. These density values taken as a function of time were evaluated against the results obtained with **NB-ALA** to detect kidney damage, showing signal only in urine from fibrotic kidneys.

Centered on the need to develop more efficient and less toxic methods for disease diagnosis and monitoring, chapter five describes a new probe (**NB-SO_3-Leu**) for the detection of elevated levels of leucine aminopeptidase (LAP) as a cancer biomarker. For this purpose, the structure of the commercial fluorophore Nile Blue was modified

with the introduction of a sulfonic group, generating a zwitterionic structure that favors the water solubility of the probe and promotes its renal clearance, decreasing the possible toxic effects due to accumulation of the probe, or the free fluorophore, in different organs of the reticuloendothelial system. The results showed a high selectivity and sensitivity of **NB-SO_3-Leu** in the detection of LAP, even in the presence of potential interferents. A particularly important example of the use of LAP as a biomarker is its application for the detection of melanoma, where early detection is essential for resection. Therefore, the probe was validated *in vitro* in the detection of LAP in SK-Mel-103 melanoma cancer cells, characterized by overexpression of this enzyme. Final studies with enzyme inhibitors demonstrated the selectivity of the probe in the proposed mechanism.

Based on the above idea, the sixth chapter describes a similar molecular probe (**NB-SO_3-Ala**) for the detection of elevated levels of alanine aminopeptidase (APN) as a cancer biomarker. For this purpose, the backbone of the commercial fluorophore Nile Blue was initially modified with sulfonic acid moieties to increase its solubility. Once the modified fluorophore was obtained, it was conjugated to an alanine residue, which acts as a reactive unit of APN producing, in addition, the deactivation of the fluorescence of the modified fluorophore. In the presence of APN this fluorescence is recovered allowing the monitoring of enzyme levels. On the other hand, the new probe can detect APN enzyme overexpression in different cancer cell lines, with higher expression observed in A549 human lung cancer cells.

Chapter seven focuses on a new concept of non-invasive molecular probes that provide an easily readable signal through simple urine fluorescence measurements. To this end, we started from a hemicyanin-7 (Cy7) fluorophore, whose structure was modified with sulfonic acids, generating a zwitterionic structure that favors its elimination through urine. This fluorophore was used in the design of a probe for the detection, through urine, of the enzyme monoamine oxidase (MAO), whose elevated

levels are associated with aging-related diseases. The probe (**Cy7-MAO**), consisting of the fluorophore Cy7 modified with sulfonic groups attached to a propylamino group. This propylamino moiety is hydrolyzed in the presence of MAO recovering the initial fluorescence of the fluorophore. This probe has the great advantage that after administration it is hydrolyzed in the presence of the MAO enzyme, resulting in the release of a highly emissive Cy7 fluorophore that can be directly quantified in urine. **Cy7-MAO** was successfully validated *in vitro* using human HepG2 liver cells with high endogenous MAO levels. Moreover, the **Cy7-MAO** probe was employed for the detection of MAO enzyme *in vivo* in young and old mice. These studies indicated that MAO expression in healthy old mice is significantly increased compared to young animals, suggesting that MAO overexpression can be used as a biomarker of aging.

Finally, in chapter eight, the main conclusions of the different experimental chapters are presented, as well as the overall conclusions drawn from this PhD thesis. The development of nanomaterials and molecular probes to selectively detect toxic substances and enzymes that have been used as biomarkers of diseases constitutes a novel field with great potential for the development of new diagnostic techniques. It is expected that the results obtained in this PhD thesis can serve as a basis for the development of new molecular probes for the early diagnosis and treatment of different diseases, as well as for the follow-up of treatments in patients.

Publications

Results of this PhD Thesis and other contributions have resulted in the following scientific publications.

- **Domínguez, M.**, Azorín-Soriano, D., Martí-Centelles, V., García-Fernández, A., Blandez, J. F., Sancenón, F. & Martínez-Máñez, R. Leucine Aminopeptidase (LAP) activatable Nile Blue-based NIR fluorescent probe for cancer detection. Submitted, **2023.**
- **Domínguez, M.**, Azorín-Soriano, D., Martí-Centelles, V., García-Fernández, A., Blandez, J. F., Sancenón, F. & Martínez-Máñez, R. NIR fluorescent probe for detection of alanine aminopeptidase (APN) overrepresentation as a cancer biomarker. Submitted, **2023.**
- **Domínguez, M.**, Lérida-Viso, A., Azorín-Soriano, D., Martí-Centelles, V., Blandez, J. F., García-Fernández, A., Sancenón, F. & Martínez-Máñez, R. A renal clearable probe for *in vivo* Monoamine Oxidase (MAO) detection. Submitted, **2023.**
- **Domínguez, M.**, Blandez, J. F., Sancenón, F., Martí-Centelles, V., Martínez-Máñez, R. Optical renal clearable probes for the detection and monitoring of diseases. Submitted, **2023.**
- **Domínguez, M.**, Meyer, K., Sancenón, F., Blandez, J. F., Serrano, M., & Martínez-Máñez, R. A NIR fluorescent probe for the detection of renal damage based on overrepresentation of alanine aminopeptidase enzyme. *ChemComm.*, **2023**, *59*, 2481-2484.
- Lozano-Torres, B., García-Fernández, A., **Domínguez, M.**, Sancenón, F., Blandez, J. F., & Martínez-Máñez, R. β-Galactosidase-Activatable Nile Blue-Based NIR Senoprobe for the Real-Time Detection of Cellular Senescence. *Anal. Chem.,* **2023**, *95*, 1643–1651.
- **Domínguez, M.**, Blandez, J. F., Lozano-Torres, B., de la Torre, C., Licchelli, M., Mangano, C., Amendola, V., Sancenón, F. & Martínez-Máñez, R. A Nanoprobe Based on Gated Mesoporous Silica Nanoparticles for The Selective and Sensitive Detection of Benzene Metabolite *t,t*-Muconic Acid in Urine. *Chem. Eur. J.*, **2021**, *27*, 1306-1310.

Abbreviations and Acronyms

^{13}C-NMR	Carbon-13 nuclear magnetic resonance
^{1}H-NMR	Hydrogen-1 nuclear magnetic resonance
8-OHdG	8-hydroxy-deoxyguanosine
ACGIH	American Conference of Governmental Industrial Hygienists
Ala-AMC	Ala-7-amido-4-methylcoumarin
APN	Alanine aminopeptidase
ATCC	American Type Culture Collection
Boc	tert-butyloxycarbonyl protecting group
Boc-Ala-OH	Boc-L-alanine
Boc-Leu-OH	Boc-L-leucine
BPA	Bisphenol A
CE	Capillary electrophoresis
CL	Clorgyline
CT	Computed tomography
CTAB	Hexadecyltrimethylammonium bromide
d	Doublet
dd	Double doublet
dt	Double triplet
DLS	Dynamic light scattering
DMEM	Dulbecco's Modified Eagle Medium
DMF	N,N-dimethylformamide
DMSO	Dimethyl Sulfoxide
DMSO-d_6	Dimetil sulfóxido-d_6
EA	Elemental Analysis

EEDQ	1-ethoxycarbonyl-1,2-dihydroquinoline
ELISA	Enzyme-linked immunosorbent assay
ESI-MS	Electrospray ionization mass spectrometry
ESPT	Excited-state proton transfer
ETS	Electron transfer space
FA	Folic acid
FBS	Fetal bovine serum
FDA	Food and Drug Administration
Fmoc	Fluorenylmethyloxycarbonyl protecting group
Fmoc-Ala-OH	Fluorenylmethyloxycarbonyl -L-alanine
FRET	Förster resonance energy transfer
FTIR	Fourier-transform infrared spectroscopy
GC-MS	Gas chromatography coupled to mass spectrometry
GFM	Glomerular filtration membrane
HEPES	4-(2-hydroxyethyl)-1-piperazineethanesulfonic acid
HPLC-MS	High-performance liquid chromatography–mass spectrometry
HPLC-UV	High-perfromance liquid chromatography-ultraviolet spectroscopy
HPβCD	2-Hydroxylpropyl-β-cyclodextrin
HRMS	High-resolution mass spectrometry
HR-TEM	High-resolution transmission electron microscopy
ICP-MS	Inductively coupled plasma mass spectrometry
ICT	Intramolecular charge transfer
IUPAC	International Union of Pure and Applied Chemistry
J	Coupling constant

LAP	Leucine aminopeptidase
LOD	Limit of detection
LOQ	Limit of quantification
m	Multiplet
M41S	Molecular 41 sieves
MAO	Monoamine oxidase
MeCN	Acetonitrile
MeOD	Metanol-d_4
MRI	Magnetic resonance imaging
MSNs	Mesoporous Silica Nanoparticles
$NaBH_4$	Sodium borohydrate
NB	Nile Blue
NIR	Near-infrared
NIRF	Neari-infrared fluroescence
NMR	Nuclear magnetic resonance
PA	Pargyline
PAHs	Polycyclic aromatic hydrocarbons
PAI	Photoacoustic imaging
PEG	Polyethylene glycol
PET	Positron emission tomography
PIET	Photon-induced electron transfer
PVP	Polyvinylpyrrolidone
PXRD	Powder X-ray diffraction
q	Quartet
qd	Quarte doublet
RES	Reticuloendothelial system

ROS	Reactive oxygen species
STEM	Scaning transmission electron microscopy
s	Singlet
S_N2	Bimolecular nucleophilic substitution
SRh B	Sulforhodamine B
t	Triplet
***t,t*-MA**	*t,t*-muconic acid
TBSCl	Tertbutyldimethylsilyl chloride
TEC	Triggers tubular epithelial cell
TEOS	Tetraethyl orthosilicate
TFA	Trifluoroacetic acid
TGA	Thermogravimetric analyses
TLC	Thin layer chromatograpy
TSC	Thiosemicarbazide
US	Ultrasound
UTIs	Urinary tract infections
VEGF	Vascular endothelial growth factor
VOCs	Volatile organic compounds
WHO	World Health Organization
λ_{em}	Emission wavelength
λ_{exc}	Excitation wavelength

Table of Contents

Chapter 1 I General Introduction..... 6

1.1 Diagnostic Tools 6

1.2 Advantages of urine as a biological sample 10

1.3 Biological information in urine samples 12

1.3.1 Urine metabolites originated by exposure to toxic substances. 14

1.3.2 Disease-related enzymes in urine..... 16

1.4 Methods for detecting diseases and toxic substances in urine samples..... 19

1.5 Nanotechnology and nanomedicine 23

1.6 Mesoporous silica materials in advanced applications 24

1.6.1 Synthesis of mesoporous silica nanoparticles..... 26

1.6.2 Functionalization of mesoporous silica materials 27

1.7 Molecular probes 29

1.8Activable fluorescent probes..... 34

1.8.1 Molecular probes for detection of overexpressed enzymes 35

1.8.1.1 Molecular probes for *in vivo* detection of enzymes..... 36

1.8.1.2 Molecular probes for enzyme detection through urine 38

1.9. Near-infrared zwitterionic fluorescent agents with potential applications for urine-based disease detection 42

Chapter 2 I Objectives..... 47

Chapter 3| A nanoprobe based on gated mesoporous silica nanoparticles for the selective and sensitive detection of benzene metabolite *t,t*-muconic acid in urine. 50

3.1 ABSTRACT 53

3.2 INTRODUCCION..... 54

3.3 RESULTS AND DISCUSSION..... 55

3.4 MATERIALS AND METHODS..... 62

3.5 CONCLUSION 74

3.6 REFERENCES..... 75

Chapter 4| NIR fluorescent probe for the detection of renal damage based on overrepresentation of alanine aminopeptidase enzyme..... 80

4.1 ABSTRACT 83

4.2 INTRODUCTION..... 84

4.3RESULTS AND DISCUSSION..... 86

4.4 MATERIALS AND METHODS..... 93

4.5 CONCLUSIONS..... 104

4.6 REFERENCES..... 105

Chapter 5| Leucine aminopeptidase (LAP) activatable nile blue-based NIR fluorescent probe for cancer detection. 108

5.1 ABSTRACT 111

5.2 INTRODUCTION..... 112

5.3 RESULTS AND DISCUSSION..... 115

5.4 EXPERIMENTAL SECTION..... 122

5.5 CONCLUSIONS..... 137

5.6 REFERENCES..... 138

Chapter 6| NIR fluorescent probe for detection of alanine aminopeptidase (APN) overrepresentation as a cancer biomarker..... 143

6.1 ABSTRACT 147

6.2 INTRODUCTION..... 148

6.3 RESULTS AND DISCUSSION..... 151

6.4 EXPERIMENTAL SECTION..... 159

6.5 CONCLUSIONS..... 167

6.6 REFERENCES..... 168

Chapter 7| A renal clearable probe for *in vivo* monoamine oxidase (MAO) detection..... 176

7.1 ABSTRACT 179

7.2 INTRODUCTION 180
7.3 RESULTS AND DISCUSSION 182
7.4 MATERIALS AND METHODS 193
7.5 CONCLUSIONS 209
7.6 REFERENCES 210
Chapter 8| Conclusions and Perspectives 218

Chapter 1 I General Introduction

Chapter 1 I General Introduction

1.1 Diagnostic Tools

Diagnosis is an essential tool for an effective healthcare. The importance of diagnostics has been revelated with COVID-19 pandemic, which has demonstrated not only the crucial need for fast, easy, and accurate diagnostics as well as the existence of problems in virtually each of their aspect, including personnel safety, equipment and the lack of adequate techniques or failure in the supply chain. The scope of the diagnosis methodology is broad. For the patient, diagnostics allows a better comprehension of its pain and know its source and possible amelioration. On the other hand, diagnostics allow to a specialist guide treatment, prognosticate, monitor progression, and measure response to treatment. Broadly, diagnostics are crucial for universal health coverage, public health, epidemiology, and global health security. Worldwide access to high-quality diagnostics is scarce, and even when they are available, they are often of low quality. Access is also inequitable, as diagnostics are often more accessible in populated urban areas and for people of elevated socioeconomic status. Because of this, low-income and developing countries are particularly affected (Figure 1).[1]

[1] Fleming, K. A., Horton, S., Wilson, M. L., Atun, R., DeStigter, K., Flanigan, J., et al. The Lancet Commission on diagnostics: transforming access to diagnostics. *The Lancet*, **2021**, *398*, 1997-2050.

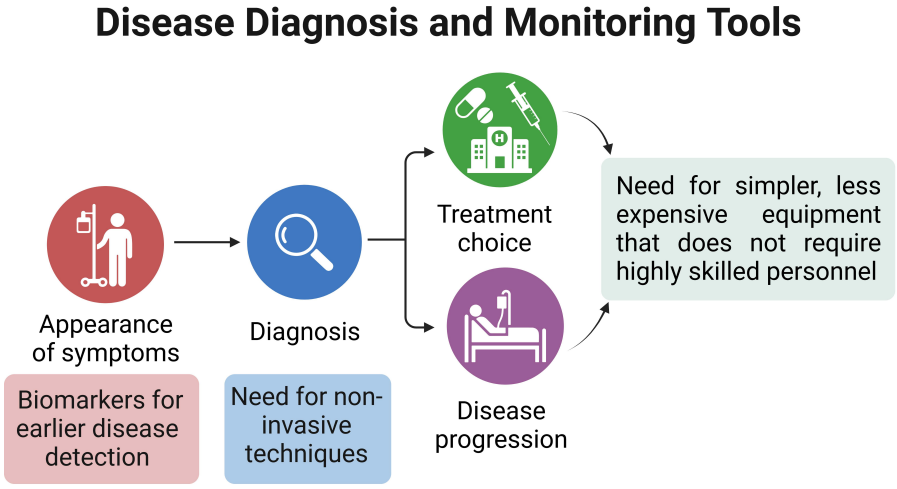

Figure 1. Main challenges in the development of new tools for the diagnosis and monitoring of diseases.

Medical imaging is a highly effective tool for early diagnosis of diseases, intraoperative image-guided surgery, and precision therapy.[2] Optical imaging such as fluorescence, chemiluminescence or bioluminescence, compared to magnetic resonance imaging (MRI) and computerized tomography (CT), has numerous advantages. These benefits include the use of non-ionizing radiations, high spatiotemporal resolution, sensitivity, multiplexing capabilities, and the availability of various imaging agents.[3] Photoacoustic imaging (PAI) also enables deep tissue imaging by combining optical and ultrasound (US) techniques.[4] The development of

[2] a) Naumova, A. V., Modo, M., Moore, A., Murry, C. E., & Frank, J. A. Clinical imaging in regenerative medicine. *Nat. Biotechnol.*, **2014**, *32*, 804-818; b) Cheng, P., & Pu, K. Molecular imaging and disease theranostics with renal-clearable optical agents. *Nat. Rev. Mater.*, **2021**, *6*, 1095-1113.

[3] James, M. L., & Gambhir, S. S. A molecular imaging primer: modalities, imaging agents, and applications. *Physiol. Rev.*, **2012**, *92*, 897-965.

[4] Wang, L. V., & Hu, S. Photoacoustic tomography: *in vivo* imaging from organelles to organs. *Science*, **2012**, *335*, 1458-1462.

optical instruments, such as endoscopes, microscopes, and photoacoustic tomography devices, has greatly facilitated the application of optical imaging in preclinical and clinical settings. Optical imaging techniques have enabled the detection of molecular and cellular pathways in living cells and animals, preclinical drug screening, the discovery of new disease biomarkers, and *in vivo* tissue imaging. Despite all these advances, it is still necessary the development of new techniques and probes.[5] In this regard, renal clearable probes are excellent candidates for medical imaging as they are rapidly blood-distributed and removed by the glomerular filtration membrane (GFM), transported through the renal tubules and finally excreted into the bladder via the ureter. Along this process, probes are minimally metabolized and their rapidly cleared decrease toxicity issues and side effects, two of the most important criteria for their clinical translation.

Encouraged by the preclinical results and the potential of optical imaging, several agents have been developed, mainly based on inorganic nanoparticles and organic fluorophores, each with its own advantages and disadvantages. Inorganic nanoparticles have size- and composition-tunable signal wavelength, high photostability and large Stokes shift, due to their quantum confinement properties.[6] In comparison, organic materials, such as macromolecular or small-molecule fluorophores, show great structural versatility with clear structure-properties relationships.[7] These optical agents are composed by several reactive units that allow

[5] Beard, P. Biomedical photoacoustic imaging. *Interface focus*, **2011**, *1*, 602-631.

[6] a) Zhou, C., Long, M., Qin, Y., Sun, X., & Zheng, J. Luminescent gold nanoparticles with efficient renal clearance. *Angew. Chem. Int. Ed.*, **2011**, *50*, 3168-3172; b) Burns, A., Ow, H., & Wiesner, U. Fluorescent core–shell silica nanoparticles: towards "Lab on a Particle" architectures for nanobiotechnology. *Chem. Soc. Rev.*, **2006**, *35*, 1028-1042.

[7] Li, J., & Pu, K. Development of organic semiconducting materials for deep-tissue optical imaging, phototherapy and photoactivation. *Chem. Soc. Rev.*, **2019**, *48*, 38-71.

the combination of different functional groups to obtain desired biochemical properties for the detection, targeting and even treatment of diseases.

The design and development of new cost-effective and easy-implementation diagnostic tools is one of the main goals in health research. In this context, diagnostic systems capable of detecting target biomarkers in readily accessible biofluids constitute a potential solution for non-invasive longitudinal studies. Building on these concepts, the present thesis has been developed and divided in two main approaches (Figure 2). The first one is the development of systems capable of detecting specific analytes (such as metabolites, enzymes, proteins, or toxic compounds) which are overexpressed in urine by direct fluorescence measurements. The second approach is focused on the design of probes that are specifically transformed by the action of targeted biomarkers located in cells and tissues and exhibit a rapid renal clearance, being excreted by the urine system and thus allowing a simple detection way through fluorescence measurements in this biofluid.

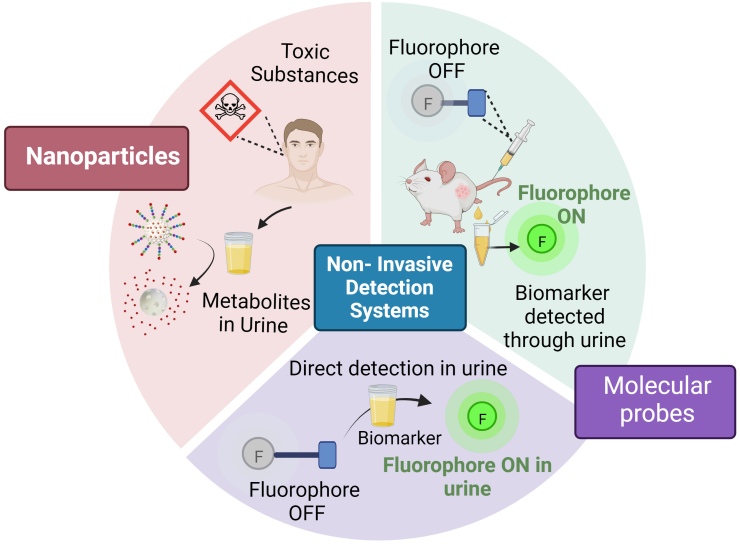

Figure 2. Probes for non-invasive disease detection and monitoring.

1.2 Advantages of urine as a biological sample

For a long time, blood plasma has been considered the primary biofluid in biomarker research, either in the search for new biomarkers or monitoring those that have already been well established. Plasma (which constitutes 5% of body weight) and tissue fluid (which constitutes 15% of body weight) are responsible for providing materials to cells, receiving cellular effluent, and maintaining suitable conditions for cellular activity. Homeostasis mechanisms, such as nervous or body fluids regulations, are crucial to keep constant physicochemical properties of tissue and cells and their surrounding (such as temperature, pH, osmotic pressure, or chemical composition) which are essential for normal metabolism. From a biomarker discovery standpoint, the homeostasis mechanism is in charge to remove and excrete cell wastes, modifying its composition with numerous potential biomarkers, particularly in the early-stages of various diseases.[8] These biomarkers are excreted through plasma, by the inherent homeostasis mechanism to minimize or avoid possible harms in neighbouring healthy tissues or cells. However, some of these biomarkers are not stable in an extracellular environment and, as a result, only are present in plasma for a relatively short time *in vivo*. This low stability of plasma samples reveals the importance of preserving it correctly and the need to carry out measurements rapidly after sample collection. As commented above, this sample manipulation cannot be easy in rural areas or even in developing countries, together with the need of specific materials for their collection. All these drawbacks increased in the case of longitudinal treatment monitoring. This constitutes a significant, maybe

[8] a) Gao, Y. (Ed.). Urine: Promising Biomarker Source for Early Disease Detection. *Springer Nature*, **2019**; b) Decramer, S., de Peredo, A. G., Breuil, B., Mischak, H., Monsarrat, B., Bascands, J. L., & Schanstra, J. P. Urine in clinical proteomics. *Mol. Cell Proteomics*, **2008**, *7*, 1850-1862.

the main, challenge in the study of plasma-derived biomarkers. A great alternative to these drawbacks is the use of urine as a biological sample for biomarker detection.[9]

In this context, urine is non-invasively obtained and contains essential information about the patient's health, dietary intake, and exposure to environmental contaminants.[10] In addition, urine can be collected in large quantities without harming the patient. Although, as with other biofluids, sample preservation is a crucial step in achieving an accurate and sensitive disease-biomarkers detection, in this case, urine, once produced, is stored in the bladder for hours at 37°C before being excreted. Bladder urine storage supposes a very stable phase that minimizes or stops protein degradation, as well as the alteration of other biomarkers.[11]

Although, the use of urine as biofluid in disease diagnosis is an ancient practice, its current importance became evident after its application in protein mass spectrometry, a technique that allowed the discovery of new protein biomarkers in urine and the development of proteomic profiles. Large-scale proteomic profiles in healthy human urine samples have revealed the presence of at least 1,000 different genetic protein products, as well as a great number of metabolic compounds.[12] These studies have supposed a significant advance in the discovery of urinary protein

[9] Zhang, Z., Liu, J., Cheng, Y., Chen, J., Zhao, H., & Ren, X. Urine analysis has a very broad prospect in the future. *Front. Anal. Sci.*, **2022**, *1*, 1-13.

[10] Smolders, R., Schramm, K. W., Nickmilder, M., & Schoeters, G. Applicability of non-invasively collected matrices for human biomonitoring. *Environ. Health.,* **2009**, *8*, 1-10.

[11] Harpole, M., Davis, J., & Espina, V. Current state of the art for enhancing urine biomarker discovery. *Expert Rev. Proteomics.*, **2016**, *13*, 609-626.

[12] a) Spahr, C. S., Davis, M. T., McGinley, M. D., Robinson, J. H., Bures, E. J., Beierle, J., Morat, J., Courchesne, P. L., Chen, K., Wahl, R. C., Yu, W., Luethy, R. & Patterson, S. D. Towards defining the urinary proteome using liquid chromatography-tandem mass spectrometry I. Profiling an unfractionated tryptic digest. *Proteomics*, **2001**, *1*, 93-107. b) Pang, J. X., Ginanni, N., Dongre, A. R., Hefta, S. A., & Opiteck, G. J. Biomarker discovery in urine by proteomics. *J. Proteome Res.*, **2002**, *1*, 161-169.

excretion profiles and their clinical uses for tasks such as early disease detection and classification, prognostic evaluation, or monitoring of a specific treatment.[13]

1.3 Biological information in urine samples

Urine is a biofluid produced by the blood after its filtration by renal glomerular cells and its renal tubules collection. This intermediated fluid undergoes different reabsorption processes in which its composition is altered to obtain the final urine, which is stored in the bladder until its excretion. Changes in urine composition, which can undergo through the different steps commented, can reflect the metabolism and state of organs. Each day, millions of urine chemical analyses are performed to identify metabolic diseases in newborns, diagnose diabetes, monitor kidney function, confirm bladder infections, detect illegal drug use, etc. Currently, it is known that the urine composition of healthy individuals is mainly composed by water, inorganic salts, urea, uric acid, etc. This composition can be altered by some diseases, showing elevated levels of proteins, sugar, amino acids, or ketone bodies, among others. The latest studies have added the urinary monitoring of biomarkers for the detection of lung, bladder or prostate cancer, failures in the blood coagulation system or for the monitoring of Alzheimer's and autoimmune diseases.[14]

Among these new biomarkers, mesothelin and β2-microglobulin are two of the most widespread in urinalysis (Figure 3). Mesothelin is a glycoprotein that can be detected in both blood and urine and is employed as specific biomarker of pancreatic

[13] Pisitkun, T., Johnstone, R., & Knepper, M. A. Discovery of urinary biomarkers. *Mol. Cell Proteomics*, **2006**, *5*, 1760-1771.
[14] Jing, J., & Gao, Y. Urine biomarkers in the early stages of diseases: current status and perspective. *Discov. Med.*, **2018**, *25*, 57-65.

cancer,[15] while β2-microglobulin, produced by nucleated cells, is employed to assess proximal tubule damage in kidney related diseases. [16] Another well-stablished example of a urine biomarker is diacetylspermine, a low-molecular-weight aliphatic amine, employed in the early cancer diagnosis, treatment, prognosis, and recurrence monitoring.[17] In this context, probably the most widespread urinary biomarker is 8-hydroxy-deoxyguanosine (8-OHdG), an indicator of oxidative DNA damage.[18] It is caused by ionizing radiation and chemical carcinogens and reflects the burden of oxidative damage in the body. Some studies have suggested a possible correlation between changes in 8-OHdG levels in urine and Parkinson's disease.[19]

[15] Qian, L., Li, Q., Baryeh, K., Qiu, W., Li, K., Zhang, J., Yu, Q., Xu, D., Liu, W., Brand, R. E., Zhang, X., Chen, W. & Liu, G. Biosensors for early diagnosis of pancreatic cancer: a review. *Transl Res.,* **2019**, *213*, 67-89.

[16] Zhang, A., Wang, B., Yang, M., Shi, H., & Gan, W. β2-microglobulin induces epithelial-mesenchymal transition in human renal proximal tubule epithelial cells *in vitro*. *BMC Nephrol.*, **2015**, *16*, 1-8.

[17] Stejskal, D., Humenanska, V., Hanulova, Z., Fiala, R., Vrtal, R., Solichova, P., & Karpisek, M. Evaluation of urine N1, N12-Diacetylspermine as potential tumor marker for urinary bladder cancer. *Biomed Pap Med Fac Univ Palacky Olomouc Czech Repub*, **2006**, *150*, 235-237.

[18] Valavanidis, A., Vlachogianni, T., & Fiotakis, C. 8-hydroxy-2'-deoxyguanosine (8-OHdG): a critical biomarker of oxidative stress and carcinogenesis. *J. Environ. Sci. Health. Part C.*, **2009** *27*, 120-139.

[19] Seet, R. C., Lee, C. Y. J., Lim, E. C., Tan, J. J., Quek, A. M., Chong, W. L., Looi, W. F., Huang, Sh. H., Wang, H., Chan, Y. H. & Halliwell, B. Oxidative damage in Parkinson disease: Measurement using accurate biomarkers. *Free Radic. Biol. Med.*, **2010**, *48*, 560-566.

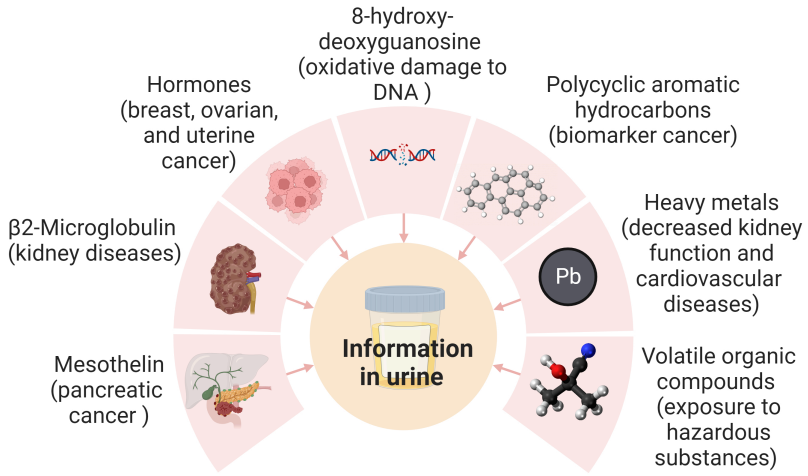

Figure 3. Urinary biomarkers and metabolites originating from exposure to toxic substances.

1.3.1 Urine metabolites originated by exposure to toxic substances

Urine is the main way employed by the body to eliminate toxic substances and its monitoring allows determine patient's exposure, environmental or occupational, to health-hazardous compounds. Some examples of metabolites that can be detected in urine include polycyclic aromatic hydrocarbons (PAHs) obtained after exposure to cigarette smoke, atmospheric pollution, coal, or other petroleum-derived products.[20] Among PAHs metabolites, bisphenol A (BPA) is the most studied and its presence in urine has been related to an increased risk of cancer.[21]

[20] Wang, Z., Zheng, Y., Zhao, B., Zhang, Y., Liu, Z., Xu, J., Chen, Y., Yang, Z., Wang, F., Wang, H., He, J., Zhang, R., & Abliz, Z. Human metabolic responses to chronic environmental polycyclic aromatic hydrocarbon exposure by a metabolomic approach. *J. Proteome Res.*, **2015**, *14*, 2583-2593.

[21] Prins, G. S., Hu, W. Y., Shi, G. B., Hu, D. P., Majumdar, S., Li, G., Huang, K., Nelles, J. L., Ho, S. M., Walker, C. L., Balla, A. K. & van Breemen, R. B. Bisphenol A promotes human prostate stem-progenitor cell self-renewal and increases *in vivo* carcinogenesis in human prostate epithelium. *Endocrinology*, **2014**, *155*, 805-817.

Other toxic substances that can be detected in urine are heavy metals such as lead[22] or mercury,[23] whose presence can be mainly found in water, soil, fish, and some consumer products. Prolonged exposure to lead can promote health problems mainly related to the nervous system as well as anaemica or renal failure.[24] In the same way, high levels of mercury in urine have been related to an increased risk of cardiovascular diseases.[25]

Pesticides and volatile organic compounds (VOCs) can also be detected in urine.[26] In addition to pesticides, VOCs can come from common chemical compounds (such as paints, solvents or cleaning products).[27] Among VOCs, muconic acid, a dicarboxylic acid witch three isomeric forms, is one of the most important urine biomarkers from hazardous chemical exposition, and their presence in urine certifies the exposure of the patient to benzene or its derivatives.[28] The detection of metabolites in urine can

[22] Sommar, J. N., Hedmer, M., Lundh, T., Nilsson, L., Skerfving, S., & Bergdahl, I. A. Investigation of lead concentrations in whole blood, plasma and urine as biomarkers for biological monitoring of lead exposure. *J. Expo. Sci. Environ. Epidemiol*., **2014**, *24*, 51-57.

[23] Park, J. D., & Zheng, W. Human exposure and health effects of inorganic and elemental mercury. Journal of preventive medicine and public health, **2012**, *45*, 344.

[24] World Health Organization. Preventing disease through healthy environments: exposure to lead: a major public health concern (No. WHO/CED/PHE/EPE/19.4.7). World Health Organization, **2019**.

[25] Mozaffarian, D., Shi, P., Morris, J. S., Spiegelman, D., Grandjean, P., Siscovick, D. S.,Willett, W. C. & Rimm, E. B. Mercury exposure and risk of cardiovascular disease in two US cohorts. *N. Engl. J. Med.*, **2011**, *364*, 1116-1125.

[26] Singh, B., Singh, K., & Singh, R. K. Biomonitoring of pesticide residues in human biological matrices. *Indian J. Clin. Biochem.*, **2017**, *32*, 365-373.

[27] Fan, R., Li, H., Liang, X., Li, L., & Xing, Y. Recent advances in the detection of volatile organic compounds in exhaled breath and urine for clinical diagnosis. *J. Pharm. Anal.*, **2019**, *9*, 293-303.

[28] a) Ducos, P., Gaudin, R., Bel, J., Maire, C., Francin, J. M., Robert, A., & Wild, P. *Trans, trans*-Muconic acid, a reliable biological indicator for the detection of individual benzene exposure down to the ppm level. *Int. Arch. Occup. Environ. Health.*, **1992**, *64*, 309-313. b) Gagné, S. Determination of *trans, trans*-muconic acid in workers' urine through ultra-performance liquid chromatography coupled to tandem mass spectrometry. *Biomed. Chromatogr*., **2013**, *27*, 664-668.

help determine the extent of exposure to toxic substances and guide the prevention and treatment of potential adverse health effects.

1.3.2 Disease-related enzymes in urine

Among the above-mentioned compounds and metabolites that can be found in urine, enzymes play a particular role because their levels (or presence and absence) are a direct indicative of various diseases (Table 1).[29] These diseases are usually related to the digestive or urinary systems, but also the presence of some enzymes indicate fails in other organs. For instance, in digestive system-related diseases, high levels of lipase (which promotes fat digestion) or amylase (which helps digest carbohydrates) in urine are indicative of pancreatic diseases, such as pancreatitis or inflammation processes.[30]

Another important group of enzymes are proteases, whose high urine levels may indicate kidney diseases such as nephritis or glomerulonephritis.[31] Among these proteases chymotrypsin, a proteolytic enzyme mainly produced in the pancreas, has been further studied as an unequivocal sign of pancreatic dysfunction.[32] In the same way, the presence of metalloproteases in urine is an indicator of inflammation or

---

[29] Jung, K. Enzyme activities in urine. How should we express their excretion? *Eur. J. Clin. Chem. Clin. Biochem.*, **1991**, *29*, 725-729.

[30] a) Rompianesi, G., Hann, A., Komolafe, O., Pereira, S. P., Davidson, B. R., & Gurusamy, K. S. Serum amylase and lipase and urinary trypsinogen and amylase for diagnosis of acute pancreatitis. *Cochrane Database Syst. Rev.*, **2017**, *4*, 1-113. b) Simmons, C. W. The Malabsorption Syndrome. *J. Natl. Med. Assoc.*, **1962**, *54*, 597-605. c) Cañamares-Orbis, P., Bernal-Monterde, V., Sierra-Gabarda, O., Casas-Deza, D., Garcia-Rayado, G., Cortes, L., & Lué, A. Impact of liver and pancreas diseases on nutritional status. *Nutrients*, **2021**, *13*, 1650. d) Berk, J. E. Diagnostic features of pancreatic disease. *JAMA*, **1955**, *159*, 1079-1085.

[31] Tan, R. J., & Liu, Y. Matrix metalloproteinases in kidney homeostasis and diseases. *Am. J. Physiol. Renal Physiol.*, **2012**, *302*, F1351-F1361.

[32] Aggarwal, A., Gupta, R., Negi, V. S., Rajasekhar, L., Misra, R., Singh, P., Chaturvedi, V. & Sinha, S. Urinary haptoglobin, alpha-1 anti-chymotrypsin and retinol binding protein identified by proteomics as potential biomarkers for lupus nephritis. *Clin. Exp. Immunol.*, **2017**, *188*, 254-262.

tissue injury and even, in some cases, cancer. [33] On the other hand, one of the most widely studied biomarkers of renal damage is *N*-acetyl-β-D-glucosaminidase, which is involved in the breakdown of complex carbohydrates in the lysosomes of renal tubular cells, and its increased presence in urine is an indicator of tubular cell injury or damage.[34] In addition, it has been widely reported that the presence of peptidases in the urine is directly related to kidney failure and inflammation.[35] In this context, the most common aminopeptidase is aminopeptidase N, which is found on the surface of renal cells and whose release though the urine is associated to inflammatory and diseases in kidney and to prostate cancer.[36]

[33] Moses, M. A., Wiederschain, D., Loughlin, K. R., Zurakowski, D., Lamb, C. C., & Freeman, M. R. Increased incidence of matrix metalloproteinases in urine of cancer patients. *Cancer Res.*, **1998**, *58*, 1395-1399.

[34] Sheira, G., Noreldin, N., Tamer, A., & Saad, M. Urinary biomarker *N*-acetyl-β-D-glucosaminidase can predict severity of renal damage in diabetic nephropathy. *J. Diabetes Metab. Disord.*, **2015**, *14*, 1-5.

[35] Sun, A. L., Deng, J. T., Guan, G. J., Chen, S. H., Liu, Y. T., Cheng, J., Li, Z. W., Zhuang, X. H., Sun, F. D. & Deng, H. P. Dipeptidyl peptidase-IV is a potential molecular biomarker in diabetic kidney disease. *Diab. Vasc. Dis. Res.*, **2012**, *9*, 301-308.

[36] He, X., Xu, Y., Shi, W., & Ma, H. Ultrasensitive detection of aminopeptidase N activity in urine and cells with a ratiometric fluorescence probe. *Anal. Chem.*, **2017**, *89*, 3217-3221.

Table 1. Some enzymes used as biomarkers in urine, their functions, associations, and advantages.

Enzyme	Function	Associations	Advantages	Ref.
Aminopeptidase N	Present on cell surface, released in urine	Inflammation and cancer	Found on cell surface and detectable in urine, making it a non-invasive diagnostic tool	37
γ-Glutamyl transpeptidase	Enzyme present in liver and other tissues	Liver damage and liver disease	GGT activity in urine can aid in the diagnosis of liver disease and liver damage	38
Matrix metalloproteinase	Degrades extracellular matrix	Inflammation and cancer progression	Enzymatic activity can be directly detected in urine, allowing for early cancer detection	39
Bone morphogenetic protein 7	Bone growth factor	Chronic kidney disease	Detection of BMP-7 may indicate early-stage chronic kidney disease	40
***N*-Acetyl-β-glucosaminidase**	Lysosomal enzyme	Tubular renal injury	NAG activity in urine has been linked to tubular renal injury, aiding in the diagnosis of kidney diseases	41
Lactate dehydrogenase	Intracellular enzyme	Cell damage and cancer	LDH activity in urine can aid in the diagnosis of cell damage and cancer	42
Alkaline phosphatase	Present in bone, liver, and other tissues	Bone and liver disease	ALP activity in urine can aid in the diagnosis of bone and liver diseases	43
Amylase	Produced in pancreas and salivary glands	Pancreatic and salivary gland diseases	Amylase activity in urine can aid in the diagnosis of pancreatic and salivary gland diseases	44
Lipase	Produced in pancreas and other tissues	Pancreatic diseases	Elevated levels of lipase in urine may indicate pancreatitis and other pancreatic diseases	45

[37] Barnieh, F. M., Loadman, P. M., & Falconer, R. A. Is tumour-expressed aminopeptidase N (APN/CD13) structurally and functionally unique? *Biochimica et Biophysica Acta (BBA)-Reviews on Cancer*, **2021**, *1876*, 1-9.

[38] McIntyre, N., & Rosalki, S. Biochemical investigations in the management of liver disease. *Hepatobiliary diseases*, **1992**, 39-71.

[39] Szarvas, T., Vom Dorp, F., Ergün, S., & Rübben, H. Matrix metalloproteinases and their clinical relevance in urinary bladder cancer. *Nat. Rev. Urol.*, **2011**, *8*, 241-254.

[40] Gao, L., Zhong, X., Jin, J., Li, J., & Meng, X. M. Potential targeted therapy and diagnosis based on novel insight into growth factors, receptors, and downstream effectors in acute kidney injury and acute kidney injury-chronic kidney disease progression. *Signal Transduct. Target. Ther.*, **2020**, *5*, 1-9.

[41] Rosner, M. H. Urinary biomarkers for the detection of renal injury. *Adv. Clin. Chem.*, **2009**, *49*, 73-97.

[42] Raab, W. P. Diagnostic value of urinary enzyme determinations. *Clin. Chem.*, **1972**, *18*, 5-25.

[43] Thapa, B. R., & Walia, A. Liver function tests and their interpretation. *Indian J. Pediatr.*, **2007**, *74*, 663-671.

[44] Pieper-Bigelow, C., Strocchi, A., & Levitt, M. D. Where does serum amylase come from and where does it go? *Gastroenterol. Clin. North Am.*, **1990**, *19*, 793-810.

[45] Yadav, D., Agarwal, N., & Pitchumoni, C. S. A critical evaluation of laboratory tests in acute pancreatitis. *Am. J. Gastroenterol.*, **2002**, *97*, 1309-1318.

In conclusion, urine is a biological fluid produced by the kidneys that plays a fundamental role in the elimination of waste and toxic substances from the body. In addition, it contains valuable information about the health of individuals and its composition analysis can reveal the presence of diseases and patient exposition to toxic substances. Taking advantage of these characteristics, the development of systems capable of detecting diseases and toxic substances in urine, as well as the monitoring of treatments, will be a novel and crucial field of research in the coming years. These systems will enable early disease detection and monitoring patient's health in a non-invasive way, which can significantly improve the use of accurate treatments and expand patient lifespan.

1.4 Methods for detecting diseases and toxic substances in urine samples

Currently, different methods are employed to urine analysis at the clinical level (Figure 4). Among these techniques, the easiest to handle is urine analysis with reagent strip, constituted by strips containing chemical reagents whose colour changes when they react with specific compounds.[46] This method is commonly employed to identify the presence of glucose, proteins, ketones, and other metabolites. However, it can only be applied for qualitative detection. The methods employed for quantitative detection are based on chromatographic techniques coupled with mass spectrometry, mainly used to detect drugs or illegal compounds together with capillary electrophoresis (CE), [47] commonly used to separate proteins and other metabolites in urine. These techniques are also useful to detect anomalies

[46] Fujita, K., & Nonomura, N. Urinary biomarkers of prostate cancer. *Int. J. Urol.*, **2018**, *25*, 770-779.

[47] Zhang, T., & Watson, D. G. A short review of applications of liquid chromatography mass spectrometry based metabolomics techniques to the analysis of human urine. *Analyst*, **2015**, *140*, 2907-2915.

in the composition of the urine, such as some proteins or blood cells.[48] Furthermore, another technique used to monitor changes in analytes and metabolites levels in urine is nuclear magnetic resonance spectroscopy (NMR). This technique is especially valuable in the early detection of metabolic diseases. Finally, immunoassays are employed to identify the presence of specific antigens or antibodies in the urine, with make it possible to determine the presence of certain diseases, such as prostate cancer.[49]

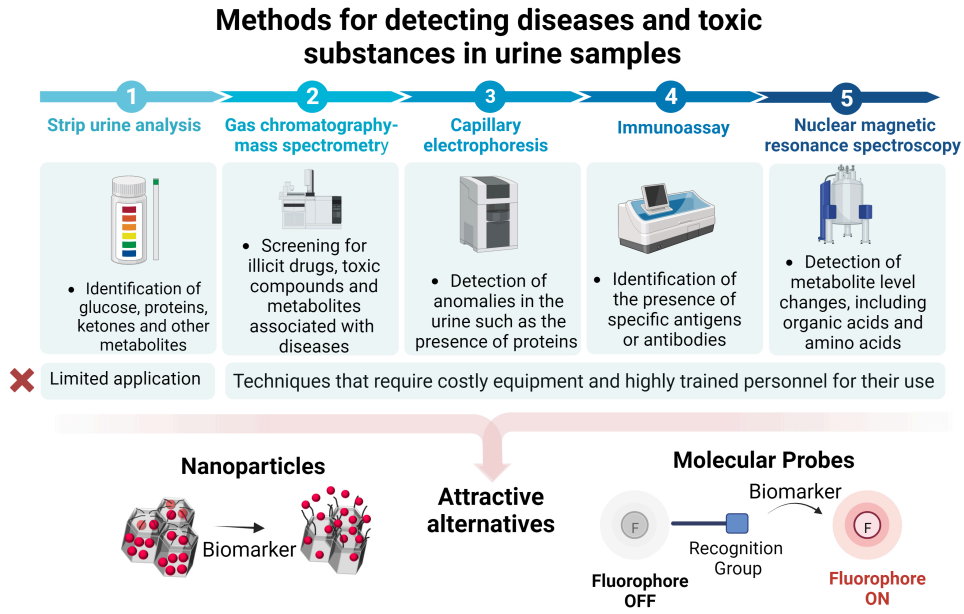

Figure 4. Main methods for detection of biomarkers in urine developed to date.

[48] Ma, Y., Liu, G., Du, M., & Stayton, I. Recent developments in the determination of urinary cancer biomarkers by capillary electrophoresis. *Electrophoresis*, **2004**, *25*, 1473-1484.

[49] Bales, J. R., Higham, D. P., Howe, I., Nicholson, J. K., & Sadler, P. J. Use of high-resolution proton nuclear magnetic resonance spectroscopy for rapid multi-component analysis of urine. *Clin. Chem.*, **1984**, *30*, 426-432.

However, despite the advantages achieved with these techniques, they have some significant drawbacks, related with their high cost and the impossibility to use them in resource-constrained areas. In addition, they require a high level of skills and technical expertises to perform the analysis and analyse the results, which can increase training time and costs.

Considering the above-mentioned facts, systems based on cromo-fluorogenic measurements are revealed as an interesting alternative for the urine detection of analytes and metabolites. Among the different processes that allow the detection and quantification based on chromogenic changes or fluorescence emission signals, the use of nanoparticles as diagnostic technique had been tested with excellent results for the detection of some bacteria and viruses.[50] These systems are based on nanoparticles, whose surface or pores (in the case of porous nanoparticles), incorporate a chromophore or fluorophore.[51] These nanoparticles are designed in such a way that, in the presence of an analyte, changes in their external surface, induce variation in the fluorophores attached on the surface or the release of the entrapped dye. These processes result in changes in the colour or in the emission that can be monitored by UV-visible or by fluorescence, which are simple, cheap, and easy-to-use techniques.

Another way to detect urine analytes through chromo-fluorogenic measurements is the use of molecular probes. These probes are made up of molecules specifically designed to selectively bind to a target biomarker. Commonly, these probes are

[50] a) Kadadou, D., Tizani, L., Wadi, V. S., Banat, F., Alsafar, H., Yousef, A. F., Barceló, D. & Hasan, S. W. Recent advances in the biosensors application for the detection of bacteria and viruses in wastewater. *J. Environ. Chem. Eng.*, **2022**, *10*, 1-13. b) Tuna, B. G., Durdabak, D. B., Ercan, M. K., Dogan, S., Kavruk, M., Dursun, A. D., Tekol, S. D., Celik, C. & Ozalp, V. C. Detection of viruses by probe-gated silica nanoparticles directly from swab samples. *Talanta*, **2022**, *246*, 1-5.

[51] Okuyama, K., & Lenggoro, I. W. Preparation of nanoparticles via spray route. *Chem. Eng. Sci.*, **2003**, *58*, 537-547.

designed to detect nucleic acids or proteins. For the detection of nucleic acids, probes are designed to selectively bind to specific DNA or RNA sequences and are primary used for urine detection of infectious diseases, such as human papillomavirus or chlamydia.[52] These probes can detect the presence of viral or bacterial DNA or RNA in urine samples, allowing for early detection of infection and the design of more effective treatments. On the other hand, protein detection probes are designed to bind selectively to specific proteins or protein fragments.[53] In this context, protein probes have been designed for the detection of proteins associated with kidney diseases, such as albumin or creatinine, which can be used as an indirect indicator of changes in kidney function.[54] However, the most common use of these probes is for enzyme detection. Additionally, molecular probes can be used to monitor diseases progression and treatments efficacy over time, allowing for personalized treatment plans and better patient outcomes, exhibiting a linear relationship between analyte concentration and signal with a very low limit of detection (LOD) and quantification (LOQ).

Overall, molecular probes and sensors based on nanoparticles are promising tools for the sensitive and accurate detection of biomarkers such as metabolites, enzymes, or proteins in urine. As nanotechnology continues to improve, these tools will likely become even more accurate and reliable, enabling earlier and more effective diagnosis and treatment of a wide range of conditions.

[52] Pfaller, M. A. Molecular approaches to diagnosing and managing infectious diseases: practicality and costs. *Emerg. Infect. Dis.*, **2001**, *7*, 312-318.
[53] Gubala, V., Harris, L. F., Ricco, A. J., Tan, M. X., & Williams, D. E. Point of care diagnostics: status and future. *Anal. Chem.*, **2012**, *84*, 487-515.
[54] Yao, B., Giel, M. C., & Hong, Y. Detection of kidney disease biomarkers based on fluorescence technology. *Mater. Chem. Front.*, **2021**, *5*, 2124-2142.

1.5 Nanotechnology and nanomedicine

Nanotechnology involves the handling of matter at the atomic and molecular level to create small-size structures, ranging from one to a few hundred nanometers (Figure 5). This multidisciplinary field has made considerable advances since its introduction by Richard Feynman in 1959[55] and the establishment of the new field of nanotechnology by Norio Taniguchi in 1974.[56] Nanomaterials have unique features, due to their small size, which have been employed for the development of nanosystems and nanodevices applied in several fields of chemistry, biotechnology, or medicine.[57]

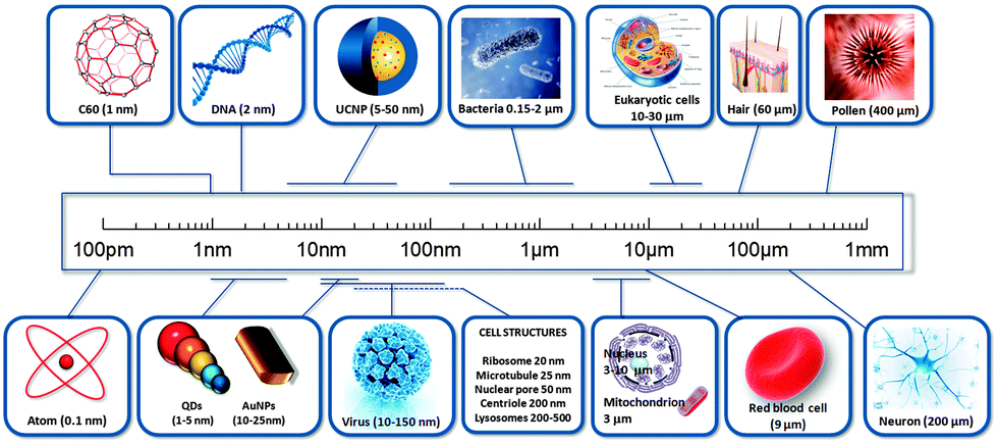

Figure 5. Illustration of the size range from macromaterials to nanomaterials. Adapted from Gnach, A., Lipinski, T., Bednarkiewicz, A., Rybka, J., & Capobianco, J. A. Upconverting nanoparticles: assessing the toxicity. *Chem. Soc. Rev.*, **2015**, *44*, 1561-1584.

[55] Feynman, R. P. An invitation to enter a new field of physics. *Int. J. Eng. Sci*, **1960**, *23*, 22-36.
[56] Taniguchi, N. Proc. Intl. Conf. Prod. Eng. Part II, Japan Society of Precision Engineering, Tokyo, **1974**.
[57] Alagarasi, A. Chapter 1—Introduction to nanomaterials. Nanomaterials; Viswanathan, B., Ed.; Narosa Publishing House: Mumbay, India, **2009**, 2-25.

Nanomedicine, a subfield of nanotechnology, combines nanotechnology with biomolecular interactions to develop diagnostic tools, regenerative medicine, and drug delivery systems. Among these areas, drug delivery nanosystems are the most developed. These drug delivery nanosystems can target drugs release at specific sites to improve their efficacy and reduce side effects. Both organic (such as liposomes and polymers) and inorganic supports (including quantum dots, gold, metal oxides, and silica-based materials) have been used for the development of drug delivery systems.[58]

Although over 100 nanomedicines have been approved by the Food and Drug Administration (FDA), there are still clinical challenges that require further research efforts.[59] However, significant advancements have been made in nanomedicine in recent decades, and new breakthroughs are anticipated in the future.[60]

1.6 Mesoporous silica materials in advanced applications

Throughout the last decades, there has been a significant increase in interest in porous materials due to their potential applications in various scientific and

[58] a) Bawarski, W. E., Chidlowsky, E., Bharali, D. J., & Mousa, S. A. Emerging nanopharmaceuticals. *Nanomedicine: NBM*, **2008**, *4*, 273-282.b) Choi, Y. H., & Han, H. K. Nanomedicines: current status and future perspectives in aspect of drug delivery and pharmacokinetics. *J. Pharm. Investig.*, **2018**, *48*, 43-60.

[59] Thapa, R. K., & Kim, J. O. Nanomedicine-based commercial formulations: Current developments and future prospects. *J. Pharm. Investig.*, **2023**, *53*, 19-33.

[60] Genchi, G. G., Marino, A., Tapeinos, C., & Ciofani, G. Smart materials meet multifunctional biomedical devices: current and prospective implications for nanomedicine. *Front. Bioeng. Biotechnol.*, **2017**, *5*, 1-8.

technological fields such as catalysis,[61] adsorption,[62] sensing,[63] or drug delivery.[64] This interest is mainly due to the large specific surface area and tunable pore size that present these types of materials. These solids are classified by the International Union of Pure and Applied Chemistry (IUPAC) based on pore size as microporous (< 2 nm), mesoporous (2-50 nm), and macroporous (>50 nm) materials.[65] Of these, mesoporous silica materials, such as the M41S phases, have attracted considerable attention since their synthesis, which was first reported in 1992.[66] The M41S family consists of materials such as MCM-41, MCM-48, and MCM-50 with hexagonal, cubic, and lamellar structures, respectively.[67] Among these materials, MCM-41 is the most studied and has remarkable applications due to its easy synthesis process based on inexpensive and non-hazardous chemicals.

In addition, M41S in general, and MCM-41 in particular, exhibit high chemical and thermal stability, biocompatibility, and easy surface functionalization using alkoxysilane derivatives. These features have led to advanced functionalities and

[61] Perego, C., & Millini, R. Porous materials in catalysis: challenges for mesoporous materials. *Chem. Soc. Rev.*, **2013**, *42*, 3956-3976.
[62] Thomas, K. M. Hydrogen adsorption and storage on porous materials. *Catal. Today*, **2007**, *120*, 389-398.
[63] Wales, D. J., Grand, J., Ting, V. P., Burke, R. D., Edler, K. J., Bowen, C. R., Mintova, S. & Burrows, A. D. Gas sensing using porous materials for automotive applications. *Chem. Soc. Rev.*, **2015**, *44*, 4290-4321.
[64] Slowing, I. I., Trewyn, B. G., Giri, S., & Lin, V. Y. Mesoporous silica nanoparticles for drug delivery and biosensing applications. *Adv. Funct. Mater.*, **2007**, *17*, 1225-1236.
[65] IUPAC, *J. Colloid interface chem. Pure Appl. Chem.,* **1972**, *31*, 577-638.
[66] Kresge, A. C., Leonowicz, M. E., Roth, W. J., Vartuli, J. C., & Beck, J. S. Ordered mesoporous molecular sieves synthesized by a liquid-crystal template mechanism. *Nature*, **1992**, *359*, 710-712.
[67] Kresge, C. T., & Roth, W. J. The discovery of mesoporous molecular sieves from the twenty-year perspective. *Chem. Soc. Rev.*, **2013**, *42*, 3663-3670.

improved properties than make MCM-41 a very attractive material for several applications.[68]

1.6.1 Synthesis of mesoporous silica nanoparticles

M41S materials are obtained following the Stöber method, which involves template molecules acting as structure directing agents and silica precursors that polymerizes around the template to form the final mesoporous structure.[69] Template molecules, namely surfactants, are dissolved into polar solvents to form liquid crystals, which aggregate into micelles and self-assemble into supermicellar structures. The structure of these supermicelles, which can be hexagonal, cubic, or laminar, determines the resulting mesoporous framework. Silica precursor molecules are added in the final step and hydrolysed to form silanol groups that condensate over the supermicelles, resulting in a network of siloxane bonds that form the characteristic porous structure (Figure 6). The nature of the silica precursor, pH, ionic forces, temperature, and time, control the porous structure and morphology of the final material.[70] The most widely studied material within the M41S family, MCM-41, is synthesized by polymerizing the silica precursor tetraethyl orthosilicate (TEOS) over the supermicelles formed by the surfactant hexadecyltrimethylammonium bromide (CTAB). The resulting silica scaffold has a spherical shape of around 80-100 nm diameter with cylindrical unidirectional empty channels of approximately 2.5 nm diameter arranged in a hexagonal distribution. The nanoparticles size as well as pore

[68] Croissant, J. G., Fatieiev, Y., Almalik, A., & Khashab, N. M. Mesoporous silica and organosilica nanoparticles: physical chemistry, biosafety, delivery strategies, and biomedical applications. *Adv. Healthc. Mater.*, **2018**, *7*, 1-75.

[69] Stöber, W., Fink, A., & Bohn, E. Controlled growth of monodisperse silica spheres in the micron size range. *J. Colloid Interface Sci.*, **1968**, *26*, 62-69.

[70] Raman, N. K., Anderson, M. T., & Brinker, C. J. Template-based approaches to the preparation of amorphous, nanoporous silicas. *Chem. Mater.*, **1996**, *8*, 1682-1701.

volume and pore size are easily tuneable as function of synthesis parameters while nanoparticles surface can also be modified introducing small changes in the synthesis route or through post-synthesis treatment using alkoxysilane chemistry.

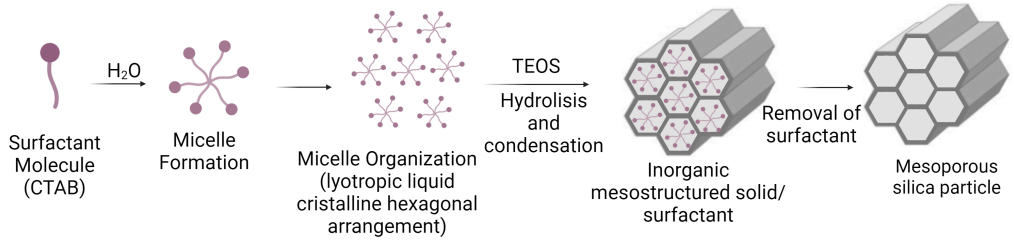

Figure 6. Schematic representation of the synthetic route of mesoporous silica MCM-41 type.

1.6.2 Functionalization of mesoporous silica materials

In recent years, the functionalization of inorganic materials with molecular or supramolecular assemblies has enabled the preparation of advanced hybrid materials in the nanoscale range, with a wide range of applications in various scientific fields. These organic (bio)molecules or supramolecules are selected based on the nature, size, and shape of the inorganic solid, leading to the development of smart nanodevices with advanced functionalities.

One of the most attractive concepts in the field of smart nanodevices is the design of gated materials,[71] which are constructed to precisely control the release of (bio)chemicals from porous supports into a solution in response to an external stimulus. These nanodevices typically consist of two subunits: (i) a porous inorganic support, in which a molecule is entrapped, and (ii) selected molecular and/or

[71] Escriche-Navarro, B., Escudero, A., Lucena-Sánchez, E., Sancenón, F., García-Fernández, A., & Martínez-Máñez, R. Mesoporous silica materials as an emerging tool for cancer immunotherapy. *Adv. Sci.*, **2022**, *9*, 1-24.

supramolecular entities grafted onto the external surface, which control mass transport from the pores. Mesoporous solids, mainly silica-based micro- or nanoparticles, are commonly used as the inorganic support, while gating mechanisms take advantage of different external stimuli like pH, change in redox potential, chemical affinity, or temperature, among others (Figure 7).

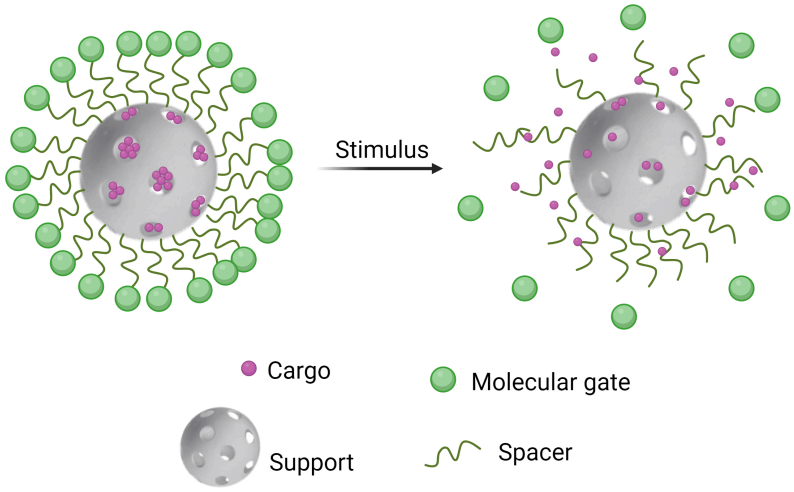

Figure 7. Schematic representation of a molecular gate for on-command release.

Mesoporous silica in the shape of nanoparticles (MSNs) have been extensively studied as drug delivery systems due to their biodistribution and accumulation effects in major target organs such as the liver, lungs, kidneys, spleen, brain, and gastrointestinal tract.[72] MSNs have also been shown to be safe and biocompatible,

[72] a) Chen, Y., Chen, H., & Shi, J. *In vivo* bio-safety evaluations and diagnostic/therapeutic applications of chemically designed mesoporous silica nanoparticles. *Adv. Mater.*, **2013**, *25*, 3144-3176. b) Wu, T., & Tang, M. Review of the effects of manufactured nanoparticles on mammalian target organs. *J. Appl. Toxicol.*, **2018**, *38*, 25-40.

although some toxic effects have been observed in some cases.[73] The biodegradability of silica-based materials is another critical factor in nanoparticles safety. The MSNs scaffold is composed of -Si-O-Si bonds, which are susceptible to hydrolytic breakdown, resulting in the generation of orthosilicic acid ($Si(OH)_4$), a well-tolerated substance that is excreted through urine.[74] This evidence confirms that renal clearance is the primary excretion pathway for MSNs. Furthermore, some studies have demonstrated that MSNs can also be excreted via the hepatobiliary pathway, albeit to a lesser extent.[75]

1.7 Molecular probes

Molecular probes are molecules designed to bind to a specific substrate (such as cations, anions, proteins, nucleic acids, lipids, or enzymes) and emit an output signal after this interaction. Inside the vast realm of output signals empolyed in the design of molecular probes, fluorescence is perhaps the most used. In this respect, fluorescent molecular probes are mainly composed of a fluorescent molecule (reporter unit) attached to a specific reactive unit designed to selectively bind to the target substrate to be detected. Upon binding, the target induces an electronic change in the fluorescent probe that results in a modulation of its fluorescence properties, thus in a measurable analytical signal. The change in emission and/or

[73] a) Lindén, M. Biodistribution and excretion of intravenously injected mesoporous silica nanoparticles: implications for drug delivery efficiency and safety. *The enzymes*, **2018**, *43*, 155-180.

[74] a) Bunker, B. C. Molecular mechanisms for corrosion of silica and silicate glasses. *J. Non. Cryst. Solids.*, **1994**, *179*, 300-308.; b) Hao, N., Liu, H., Li, L., Chen, D., Li, L., & Tang, F. *In vitro* degradation behavior of silica nanoparticles under physiological conditions. *J. Nanosci. Nanotechnol.*, **2012**, *12*, 6346-6354.

[75] Vallet-Regí, M., Colilla, M., Izquierdo-Barba, I., & Manzano, M. Mesoporous silica nanoparticles for drug delivery: Current insights. *Molecules*, **2017**, *23*, 1-19.

colour provides information about the amount and location of the target in the sample.[76]

In this regard, it is important to consider the term "molecular recognition". Molecular recognition is a fundamental process in chemistry, biochemistry, and molecular biology. It refers to the ability of molecules to specifically recognize and bind to other molecules through non-covalent interactions, such as hydrogen bonds, Van der Waals forces, electrostatic interactions, or coordination bonds.[77] Molecular recognition involves guest and host molecules that display complementarity in terms of geometric and electronic characteristics. This phenomenon plays a critical role in biological systems and is evident in various interactions such as antigen-antibody, receptor-ligand, sugar-lectin, DNA-protein, and RNA-ribosome interactions.[78]

Dr. Emil Fischer proposed, in 1894, the lock and key model of molecular recognition, which is a fundamental concept in host-guest interactions, especially in the case of enzymes and substrates. In this model, enzymes act as the "lock" and their substrates act as the "key," which must have complementary size and shape (Figure 8).[79] The "lock-key" principle, which simplifying the mechanism of action of most biological systems, can account for their remarkable selectivity and specificity. Selectivity refers to the ability of the host to differentiate between different guests, whereas specificity relates to the accuracy of molecular recognition.[80]

---

[76] Hulanicki, A., Glab, S., & Ingman, F. O. L. K. E. Chemical sensors: definitions and classification. *Pure Appl. Chem.*, **1991**, *63*, 1247-1250.

[77] Lehn, J. M. Supramolecular chemistry—scope and perspectives molecules, supermolecules, and molecular devices (Nobel Lecture). *Angew. Chem. Int. Ed.*, **1988**, *27*, 89-112.

[78] Breiten, B., Lockett, M. R., Sherman, W., Fujita, S., Al-Sayah, M., Lange, H., Bowers, C., M., Heroux, A., Krilov, G. & Whitesides, G. M. Water networks contribute to enthalpy/entropy compensation in protein–ligand binding. *J. Am. Chem. Soc.*, **2013**, *135*, 15579-15584.

[79] Fischer H. E. "Chemistry". Nobel Lecture, **1996**.

[80] Bergmann, G., Von Oepen, B., & Zinn, P. Improvement in the definitions of sensitivity and selectivity. *Anal. Chem.*, **1987**, *59*, 2522-2526.

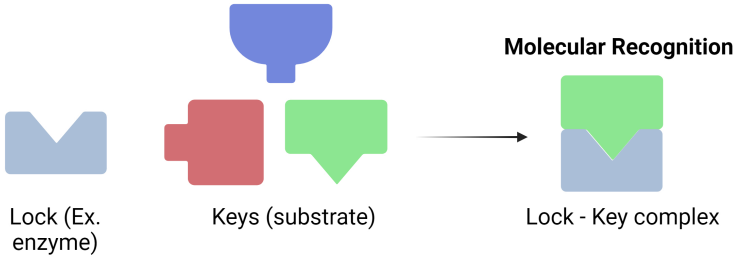

Figure 8. Representative scheme of the "lock-key" principle, a fundamental concept in molecular recognition.

Molecular probes have been extensively investigated and used for their ability to improve analytical sensitivity and, in particular, to provide greater temporal and spatial sampling capability in *in vivo* imaging studies. Typically, these probes consist of three different parts: (1) a reporter unit, namely a fluorophore or dye, whose optical features changed upon interaction with the target analyte of interest; (2) a recognition unit, responsible for selective interaction with the target analyte; and (3) a spacer or linker molecule that connects the reporter with the recognition units (in certain cases the two components are integrated without any linker but forming a supramolecular ensemble) (Figure 9).[81]

[81] a) Martínez-Mañez, R., & Sancenon, F. Fluorogenic and chromogenic chemosensors and reagents for anions. *Chem. Rev.*, **2003**, *103*, 4419-4476; b) Santos-Figueroa, L. E., Moragues, M. E., Climent, E., Agostini, A., Martínez-Máñez, R., Sancenón, F. Chromogenic and fluorogenic chemosensors and reagents for anions. A comprehensive review of the years 2010–2011. *Chem. Soc. Rev.*, **2013**, *42*, 3489-3613; c) Garrido, E., Pla, L., Lozano-Torres, B., El Sayed, S., Martínez-Máñez, R., & Sancenón, F. Chromogenic and fluorogenic probes for the detection of illicit drugs. *ChemistryOpen*, **2018**, *7*, 401-428.

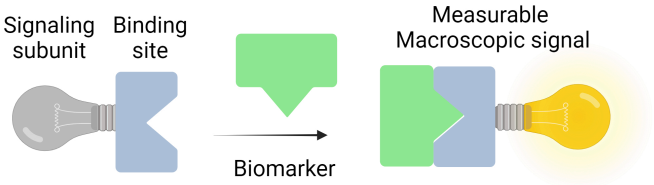

Figure 9. Schematic representation of a molecular probe.

The fluorescence of molecular probes can be modulated through different mechanisms such as the J-aggregate effect, the H-aggregates, the solvation effect, and electron transfer processes. The J-aggregate effect occurs when molecules stack in an organized structure, causing electronic transitions to change and increased light emission. Moreover, H-aggregates constitute a particular supramolecular arrangement that emerges when molecules are densely and systematically organized in a stacked or aggregated conformation. This geometric configuration gives rise to distinct optical characteristics and is frequently linked to substantial intermolecular interactions that exerts an influence on their light absorption and emission properties.[82] The solvation effect appears when the molecule is in a polar environment, affecting electronic transitions. Energy transfer is another important mechanism in molecular probe fluorescence. In this case, the molecule that emits light (donor) transfers energy to another nearby molecule (acceptor), causing the latter to emit light at a different wavelength. This requires not only the proximity of the molecules but also a spectral overlap between the donor's emission and the acceptor's absorption. This process is known as Förster resonance energy transfer (FRET) and is frequently used in detecting interactions between molecules. In general, the mechanisms that allow molecular probes to fluoresce are complex and

[82] Hestand, N. J., & Spano, F. C. Expanded theory of H-and J-molecular aggregates: the effects of vibronic coupling and intermolecular charge transfer. *Chem. Rev.*, **2018**, *118*, 7069-7163.

depend on many factors, such as the molecule structure, the environment in which they are found, the experimental conditions, and the interactions with other molecules. Additionally, it is important to note that in the design of molecular probes, specific photoinduced processes must be considered, such as intramolecular charge transfer (ICT), electron transfer through space (ETS), and excited-state proton transfer (ESPT). ICT involves the movement of electrons within a molecule when it is excited by light, whereas in photon-induced electron transfer (PIET), electrons move between two spatially separated molecular groups when the probe is excited. On the other hand, ESPT is a process in which a proton is transferred from one region of the molecule to another upon it is excited.[83]

Therefore, proper design and selection of molecular probes are crucial for their use in specific applications, such as biomolecule detection or cell imaging. In biological research, fluorescent molecular probes are used to visualize and quantify cellular and molecular processes. For example, fluorescent probes can bind to specific proteins in cells and allow the real time visualization of their distribution. They are also used to study protein interactions with other molecules, such as nucleic acids.[84]

One application of fluorescent molecular probes is their use in the detection of contaminants in water, air, and soil. The probes can be designed to selectively bind to specific contaminants (such as heavy metals or organic compounds) allowing their

[83] a) Tachibana, R., Kamiya, M., Suzuki, S., Morokuma, K., Nanjo, A. & Urano, Y. Molecular design strategy of fluorogenic probes based on quantum chemical prediction of intramolecular spirocyclization. *Commun Chem.*, **2020**, *3*, 1-8. b) Yang, X., Zhang, Q., Zhang, S., Lai, M., Ji, X., Ye, Y., Li, & Zhao, M. Molecule fluorescent probes for sensing and imaging analytes in plants: Developments and challenges. Coord. Chem. Rev., **2023**, *487*, 1-34.

[84] a) Zhang, J., Campbell, R. E., Ting, A. Y., & Tsien, R. Y. Creating new fluorescent probes for cell biology. *Nat. Rev. Mol. Cell Biol.*, **2002**, *3*, 906-918; b) Singh, H., Tiwari, K., Tiwari, R., Pramanik, S. K., & Das, A. Small molecule as fluorescent probes for monitoring intracellular enzymatic transformations. *Chem. Rev.*, **2019**, *119*, 11718-11760.

detection and quantification.[85] They can also be designed to bind/interact with specific proteins or biomarkers associated with diseases such as cancer or cardiovascular disorders.[86] By binding to these target molecules, fluorescent probes can detect the presence of the disease and monitor its progression.

1.8 Activable fluorescent probes

Activatable fluorescent probes represent an innovative tool in the field of biomedical research and have garnered increasing interest in recent years. These probes offer a unique ability to detect and quantify biological and chemical processes in a specific and controlled manner. Activatable fluorescent probes exist in two primary states: inactive and active. In their inactive state, the probe does not emit fluorescence, while in their active state, the probe emits detectable fluorescence.[87] This change of state occurs in response to a specific stimulus. These stimuli can vary, including changes in the chemical environment, interactions with specific biomolecules, variations in pH, temperature, the presence of metal ions, or changes in the pathological tissue microenvironment.[88] The probe responds to this stimulus and becomes active, emitting fluorescence. Furthermore, if the probe remains continuously active until interacting with the target tissues or cells at the desired site, it is also classified as an activatable probe. Activatable fluorescent probes have the

[85] a) Li, X., Wang, L., Du, D., Ni, L., Pan, J., & Niu, X. Emerging applications of nanozymes in environmental analysis: Opportunities and trends. *Trends Analyt. Chem.*, **2019**, *120*, 1-13.
[86] a) Huang, J., & Pu, K. Near-infrared fluorescent molecular probes for imaging and diagnosis of nephro-urological diseases. *Chem. Sci*., **2021**, *12*, 3379-3392. b) Huang, J., & Pu, K. Activatable molecular probes for second near-infrared fluorescence, chemiluminescence, and photoacoustic imaging. *Angew. Chem. Int. Ed.*, **2020**, *59*, 11717-11731.
[87] Lacivita, E., Leopoldo, M., Berardi, F., A Colabufo, N., & Perrone, R. Activatable fluorescent probes: a new concept in optical molecular imaging. *Curr. Med. Chem.*, **2012**, *19*, 4731-4741.
[88] Liu, Y., Teng, L., Xu, C., Ren, T. B., Xu, S., Lou, X., Yuan, L. & Zhang, X. B. An integration strategy to develop dual-state luminophores with tunable spectra, large stokes shift, and activatable fluorescence for high-contrast imaging. *CCS Chem.*, **2022**, *4*, 2153-2164.

potential to enhance target signals while reducing background, resulting in the generation of high signal-to-noise ratios.[89]

The mechanisms underlying the activation process may vary depending on the type of activatable probe. Some mechanism are based on changes in the chemical or physical properties of the probe as response to the stimulus. For instance, a change in pH can induce a structural modification in the probe, rendering it fluorescent. Other probes may function through interactions with specific biomolecules. For example, a probe designed to detect a specific biomarker, such as an enzyme, becomes active when it binds to that particular biomarker, initiating its emission of fluorescence.[90] The choice of the activation mechanism depends on the application and specific research or diagnostic objectives. Understanding these mechanisms is essential for the design and interpretation of experiments utilizing activatable fluorescent probes.

1.8.1 Molecular probes for detection of overexpressed enzymes

Classical imaging technologies such as MRI, CT, and positron emission tomography (PET) are unable to monitor many biological phenomena in real-time. This is because traditional imaging methods use non-specific binding materials, whose *in vivo* locations are guided by their different permeabilities or perfusions in tissues or cells. In contrast, optical imaging has gained significant interest due to its inherent ability to obtain high-quality spatial resolution images of live animals in a minimally invasive manner.[91] Although optical probes offer several advantages over

[89] Duan, Q. J., Zhao, Z. Y., Zhang, Y. J., Fu, L., Yuan, Y. Y., Du, J. Z., & Wang, J. Activatable fluorescent probes for real-time imaging-guided tumor therapy. *Adv. Drug Deliv. Rev.*, **2023**, *196*, 1-19.

[90] Wu, X., Wang, R., Kwon, N., Ma, H., & Yoon, J. Activatable fluorescent probes for in situ imaging of enzymes. *Chem. Soc. Rev.*, **2022**, *51*, 450-463.

[91] a) Liu, H., Ren, G., Miao, Z., Zhang, X., Tang, X., Han, P., Gambhir, S. S. & Cheng, Z. Molecular optical imaging with radioactive probes. *PloS one*, **2010**, *5*, 1-9; b) Massoud, T. F.,

their radiological counterparts, they are generally less sensitive and have less tissue penetration. However, in terms of development costs, safety, and handling processes, they are superior to MRI, CT, and radioactive probes.

Furthermore, fluorescence-based optical probes that target enzymes can be used to real time monitoring of biological processes *in vivo*.[92]

1.8.1.1 Molecular probes for *in vivo* detection of enzymes

Enzymes play a crucial role as biological catalysts in various physiological and biological processes. They enable chemical reactions to occur under mild conditions in a biological environment and are essential for keeping normal bodily functions. Consequently, enzyme expression levels are closely related to healthy function of biological systems. In clear opposition, this means that abnormal enzyme activities are closely associated with diseases and pathological process.[93] Thus, not only enzymatic levels can be used to determine the presence or absence of diseases, even their intra or intercellular location can facilitate this discrimination. Therefore, it is crucial to monitor the activity and biodistribution of enzymes in real-time to identify their function and provide optimal conditions for early diagnosis and treatment of possible disfunctions.

Taking into account the above, *in vivo* detection of enzymatic activity has become a key technique for biological process research and disease diagnosis. In this sense, molecular probes are valuable tools for specific detection of enzymes in real-time and in *in vivo* studies. These systems are specifically designed to interact with the

& Gambhir, S. S. Molecular imaging in living subjects: seeing fundamental biological processes in a new light. *Genes Dev.*, **2003**, *17*, 545-580.

[92] a) Weiss, S. Fluorescence spectroscopy of single biomolecules. *Science*, **1999**, *283*, 1676-1683; b) Hanash, S. Disease proteomics. *Nature*, **2003**, *422*, 226-232.

[93] Zhang, J., Chai, X., He, X. P., Kim, H. J., Yoon, J., & Tian, H. Fluorogenic probes for disease-relevant enzymes. *Chem. Soc. Rev.*, **2019**, *48*, 683-722.

enzyme of interest, resulting in a detectable signal that can be measured and quantified. This allows for real-time monitoring of enzymatic activity in cells and tissues, which can be useful for early disease detection, treatment efficacy monitoring, and understanding of biological processes.[94]

One of the most commonly used signals for *in vivo* enzymatic detection employing molecular probes is fluorescence due to its high sensitivity, low cost, ease of operation, and non-invasiveness.[95] However, it is important to note that to allow for *in vivo* fluorescence imaging, near-infrared (NIR) fluorescent probes need to be designed to reduce absorption and scattering of UV and visible light by biological tissues, thus improving penetration depth and detection sensitivity. To date, numerous NIR fluorescent probes have been developed for *in vivo* enzymatic activity detection, providing sensitive NIR fluorescence useful for early disease diagnosis and image-guided tumour surgery.[96]

However, the use of molecular probes for detection of abnormal levels of enzymes also presents several drawbacks. One of the main limitations is the lack of penetration in tissues, which may limit their capacity to detect enzymes in certain areas of the body. Additionally, the sensitivity of some probes may be insufficient for early disease detection or long-term biological process monitoring. There is also a risk of adverse reactions and side effects, although these are generally minimal.[97]

---

[94] Massoud, T. F., & Gambhir, S. S. Molecular imaging in living subjects: seeing fundamental biological processes in a new light. *Genes Dev.*, **2003**, *17*, 545-580.

[95] Schäferling, M. The art of fluorescence imaging with chemical sensors. *Angew. Chem. Int. Ed.*, **2012**, *51*, 3532-3554.

[96] a) Hong, G., Antaris, A. L., & Dai, H. Near-infrared fluorophores for biomedical imaging. Nat. Biomed. Eng., **2017**, *1*, 1-22. b) Wang, Y., Weng, J., Wen, X., Hu, Y., & Ye, D. Recent advances in stimuli-responsive in situ self-assembly of small molecule probes for *in vivo* imaging of enzymatic activity. *Biomater. Sci.*, **2021**, *9*, 406-421.

[97] Herschman, H. R. Molecular imaging: looking at problems, seeing solutions. *Science*, **2003**, *302*, 605-608.

1.8.1.2 Molecular probes for enzyme detection through urine

A novel area of interest for the development of minimally invasive methods for disease detection and monitoring is the design of renal clearable molecular probes. The pharmacokinetic properties of optical probes are crucial for their clinical implementation. Upon intravenous administration, probes are distributed towards organs and tissues by the bloodstream, followed by *in vivo* metabolism and, subsequent hepatobiliary or renal elimination.[98] The elimination pathways are determined by the inherent properties of the probes, such as size, shape, or surface charges, among other factors. In this context, several molecular probes and optical agents are cleared by the reticuloendothelial system (RES). In these cases, the metabolites of the probes are secreted into the duodenum through the bile duct and accumulate in the liver or spleen, so non-biodegradable probes can lead to acute or chronic toxicity.[99] Therefore, there is a need to investigate and design renal clearable molecular probes for diseases detection and monitoring. In this regard, the design of probes that can be specifically transformed (as a turn-on of the fluorescence emission) by the action of certain biomarkers at the disease area and then renally cleared, thus allowing direct detection in urine, is a major challenge in this research area. This is a novel research field with clear potential for probe implementation in human research for non-invasive biomarker monitoring (Figure 10).

[98] Cheng, P., & Pu, K. Molecular imaging and disease theranostics with renal-clearable optical agents. *Nat. Rev. Mater.*, **2021**, *6*, 1095-1113.
[99] Poon, W., Zhang, Y. N., Ouyang, B., Kingston, B. R., Wu, J. L., Wilhelm, S., & Chan, W. C. Elimination pathways of nanoparticles. *ACS nano*, **2019**, *13*, 5785-5798.

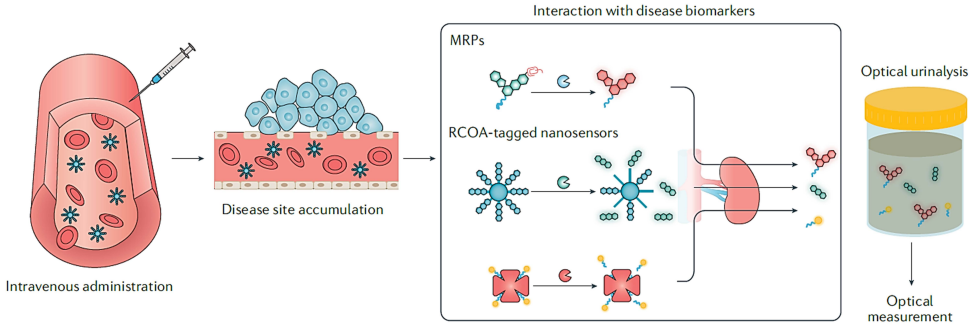

Figure 10. Mechanism of biomarker detection using renal clearable molecular probes. Adapted Cheng, P., & Pu, K. Molecular imaging and disease theragnostic with renal-clearable optical agents. *Nat. Rev. Mater.*, **2021**, *6*, 1095-1113.

Recently, a series of molecular probes have been developed to detect enzymes through urine. Typically, these diuretic probes consist of organic fluorophores composed of an organic optical unit (organic fluorophore with fluorescent, chemiluminescent, or photoacoustic signals) and a water-soluble unit that provides renal clearable features (such as cyclodextrin, inulin, polyethylene glycol (PEG), sinistrin, dextran, polyvinylpyrrolidone (PVP), or zwitterionic groups) (Figure 11).[100]

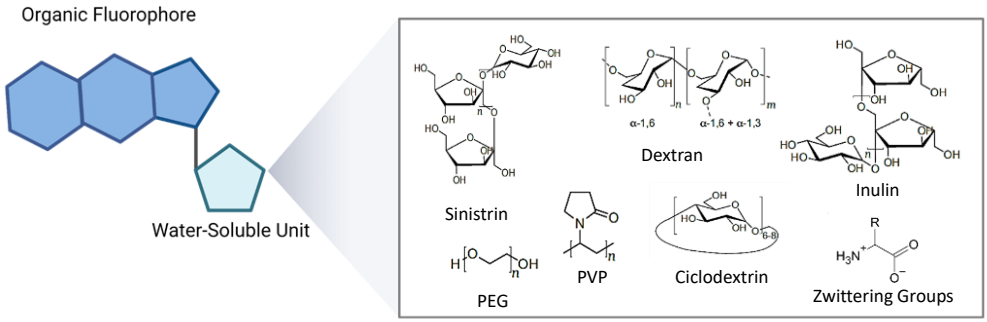

Figure 11. General structure of renal clearable molecular probes.

[100] Cheng, P., & Pu, K. Molecular imaging and disease theranostics with renal-clearable optical agents. *Nat. Rev. Mater.*, **2021**, *6*, 1095-1113.

Renal clearance leads to rapid elimination of this type of molecular probes, reducing the clearance time from days to just hours with little metabolic degradation. In the kidneys, renal molecular probes are filtered in the glomerulus through the glomerular filtration membrane (GFM), and then transported to the renal tubules where they can be secreted or reabsorbed.[101] Finally, these molecular probes are secreted in the urine through the bladder. This rapid elimination process results in lower long-term organ toxicity and side effects compared to agents eliminated by the mononuclear phagocyte system.[102]

As previously mentioned, renal clearance can be facilitated by modifying fluorophores with organic molecules such as dextran, PVP or PEG. The use of these organic molecules allows renal clearance to depend solely on glomerular filtration, unlike globular protein clearance where tubular reabsorption plays an important role.[103] Another compound used to improve the renal properties of molecular probes are cyclic oligosaccharides called cyclodextrins. Cyclodextrins can be used as drug transporters, showing excellent renal clearance (90% at 6 hours and 99% at 12 hours). An interesting example of the application of cyclodextrins is the development of a renal-clearable molecular probe for near-infrared fluorescence (NIRF) imaging and urinalysis of SARS-CoV-2 (Figure 12). The probe consists of a NIR dye and a peptide that binds to a substrate of main protease (M^{prop}) involved in SARS-CoV-2 polypeptide processing. The authors demonstrated that the probe could detect the

---

[101] Guyton, A. C., & Hall, J. E. Textbook of medical physiology. *Elsevier Saunders*. **2006**, *889*,955-956.

[102] a) J. Huang, et al., Molecular optical imaging probes for early diagnosis of drug-induced acute kidney injury, *Nat. Mater*. **2019**, *18*, 1133-1143; b) B. Du, et al., Tailoring kidney transport of organic dyes with low-molecular-weight PEGylation, *Bioconjug. Chem*. **2020**, *31*, 241-247.

[103] Venturoli, D., & Rippe, B. Ficoll and dextran vs. globular proteins as probes for testing glomerular permselectivity: effects of molecular size, shape, charge, and deformability. *Am. J. Physiol. Renal Physiol.*, **2005**, *288*, F605-F613.

virus in urine samples from infected mice, as well as in clinical samples from COVID-19 patients. [104]

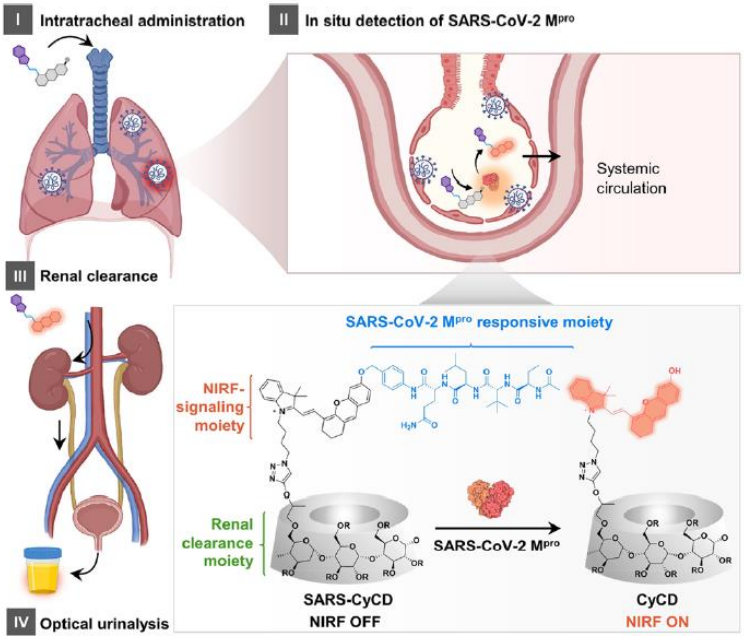

Figure 12. Scheme depicting *in vivo* detection of SARSCoV-2 via i.t. Injection of Mpro activatable NIRF probe (SARS-CyCD), followed by NIRF imaging and optical urinalysis; lower right: chemical structure of SARSCyCD (R = H or 2-Hydroxylpropyl) and its activated form, CyCD, in response to Mpro. Adapted from Liew, S. S., Zeng, Z., Cheng, P., He, S., Zhang, C., & Pu, K. Renal-clearable molecular probe for near-infrared fluorescence imaging and urinalysis of SARS-CoV-2. *J. Am. Chem. Soc.*, **2021**, *143*, 18827-18831.

[104] Liew, S. S., Zeng, Z., Cheng, P., He, S., Zhang, C., & Pu, K. Renal-clearable molecular probe for near-infrared fluorescence imaging and urinalysis of SARS-CoV-2. *J. Am. Chem. Soc.*, **2021**, *143*, 18827-18831.

Following this line, an attractive alternative is the introduction of zwitterionic charges into the structure of the fluorophore. These zwitterionic groups reduce binding to proteins and favor their excretion from the body.[105]

1.9. Near-infrared zwitterionic fluorescent agents with potential applications for urine-based disease detection

NIR zwitterionic fluorescent molecules have been employed in the last decade as signaling units in optical imaging for biomedical applications. Zwitterionic compounds have both positive and negative charges in their structure, increasing their solubility in water and stability under physiological conditions and avoiding non-specific binding to proteins.[106] Along with these improvements, provided by the presence of zwitterionic charges, the features of these probes have been enhanced over traditional NIR imaging agents, with high quantum yields, low toxicity, and high photostability, making them a useful tool for long-term imaging studies. Their initial applications were based on their use as tracer for the detection of abnormalities or diseases in the urinary system.[107]

[105] Dey, G., Singh, V., Dewangan, J., Daniel, P. V., Kamthan, M., Ghosh, D., Mondal, P. & Ghosh, S., Renal Clearable New NIR Probe: Precise quaqntification of albumin in biofluids and fatty liver disease state identification through tissue specific high contrast imaging *in vivo*. *Anal. Chem.*, **2017**, *89*, 10343-10352.

[106] Hyun, H., Henary, M., Gao, T., Narayana, L., Owens, E. A., Lee, J. H., Park, G., Wada, H., Ashitate, Y., Frangioni, J. V. & Choi, H. S. 700-nm zwitterionic near-infrared fluorophores for dual-channel image-guided surgery. *Mol. Imaging Biol.*, **2016**, *18*, 52-61.

[107] a) Choi, H. S., Gibbs, S. L., Lee, J. H., Kim, S. H., Ashitate, Y., Liu, F., Hyun, H., Park, G., Xie, Y., Bae, S., Henary, M. & Frangioni, J. V. Targeted zwitterionic near-infrared fluorophores for improved optical imaging. *Nat. Biotechnol.*, **2013**, *31*, 148-153; b) Haque, A., Faizi, M. S. H., Rather, J. A., & Khan, M. S. Next generation NIR fluorophores for tumor imaging and fluorescence-guided surgery: A review. *Bioorg. Med. Chem.*, **2017**, *25*, 2017-2034.

The continuous development of this type of probes has led to its activation with specific targets and its read-out through urine.[108] Their higher water solubilities, coupled with their renal clearance performances have improved their biocompatibility when they are compared to traditional optical agents. Taking advantage of these characteristics, recent studies have used fluorophores with long wavelengths (NIR-I: 650–1000 nm or NIR-II: 1000–1700 nm)[109], which can penetrate deep into tissues, making them useful for non-invasive imaging of internal organs and tissues. Additionally, their use in biomedical imaging has become more common due to the improved sensitivity and selectivity of NIR imaging techniques (Figure 13).[110]

Overall, NIR zwitterionic fluorescent agents show promise features and could be used as a non-invasive and efficient methods for detecting urinary tract abnormalities and diseases, including urinary tract infections (UTIs), bladder cancer and acute kidney injury.[111]

---

[108] Huang, J., Weinfurter, S., Daniele, C., Perciaccante, R., Federica, R., Della Ciana, L., Pill. J. & Gretz, N. Zwitterionic near infrared fluorescent agents for noninvasive real-time transcutaneous assessment of kidney function. *Chem. Sci.*, **2017**, *8*, 2652-2660.

[109] Chen, C., Tian, R., Zeng, Y., Chu, C., & Liu, G. Activatable fluorescence probes for "turn-on" and ratiometric biosensing and bioimaging: from NIR-I to NIR-II. *Bioconjug. Chem.*, **2020**, *31*, 276-292.

[110] a) Choi, H. S., Nasr, K., Alyabyev, S., Feith, D., Lee, J. H., Kim, S. H., Ashitate, Y., Hyun, H., Patonay, G., Strekowski, L., Henary, M. & Frangioni, J. V. Synthesis and *in vivo* fate of zwitterionic near-infrared fluorophores. *Angew. Chem. Int. Ed.*, **2011**, *50*, 6258-6263; b) Yao, C., Chen, Y., Zhao, M., Wang, S., Wu, B., Yang, Y., & Zhang, F. A bright, renal-clearable NIR-II brush macromolecular probe with long blood circulation time for Kidney disease bioimaging. *Angew. Chem. Int. Ed.*, **2022**, *61*, e202114273.

[111] a) Huang, J., Li, J., Lyu, Y., Miao, Q., & Pu, K. Molecular optical imaging probes for early diagnosis of drug-induced acute kidney injury. *Nat. Mater.*, **2019**, *18*, 1133-1143. b) Xue, D., Wu, D., Lu, Z., Neuhaus, J., Zebibula, A., Feng, Z., Cheng, S., Zhouh, J., Qian, J. & Li, G. Structural and functional NIR-II fluorescence bioimaging in urinary system via clinically approved dye methylene blue. *Engineering*, **2023**, *22*, 149-158.

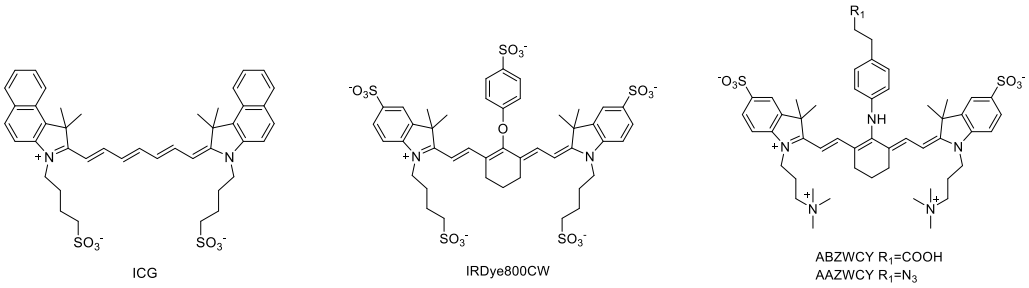

Figure 13. Structures of zwitterionic cyanine dyes.

In this context, this PhD thesis has explored the development of different detection systems mainly focused on two fields of application: (1) detection of metabolites originated by exposure to toxic environments directly in urine and (2) detection of diseases related to the overexpression of enzymes either directly in urine or through urine.

Chapter 2 I Objectives

Chapter 2 I Objectives

Given the need and relevance of the development of non-invasive and easily accessible diagnostic techniques, the present PhD thesis aims to contribute to the development of detection systems focused mainly on two fields of application: (1) detection of metabolites originated by exposure to toxic environments directly in urine and (2) non-invasive detection of overexpressed enzymes (related with certain diseases) through fluorescence measurements (in urine, in other biofluids or in cells) using renal clearable molecular probes.

The specific objectives of each chapter are:

• To design and validate an intelligent nanodevice based on mesoporous silica nanoparticles loaded with sulforhodamine B and capped with a copper complex for the detection of *t,t*-muconic acid in urine.

• To develop an OFF-ON probe based on Nile blue fluorophore for the detection of elevated levels of alanine aminopeptidase in the urine of mice with renal damage induced by folic acid.

• To synthesize and characterize a new fluorescence probe based on a Nile blue fluorophore modified with sulfonic groups to increase its solubility and to detect elevated levels of leucine aminopeptidase as a cancer biomarker.

• To design and synthesize of a NIR fluorescent probe based on a Nile blue fluorophore modified with sulfonic groups conjugated to alanine, to detect overexpression of aminopeptidase enzyme as a cancer biomarker.

- To develop a non-invasive NIR fluorescent molecular probe based on a zwitterionic hemicianine fluorophore Cy7, with renally-clearable features, to detect high levels of monoamine oxidase (MAO) related to ageing diseases, in natural ageing mice model through a readable fluorescent signal in urine.

Chapter 3| A nanoprobe based on gated mesoporous silica nanoparticles for the selective and sensitive detection of benzene metabolite *t,t*-muconic acid in urine.

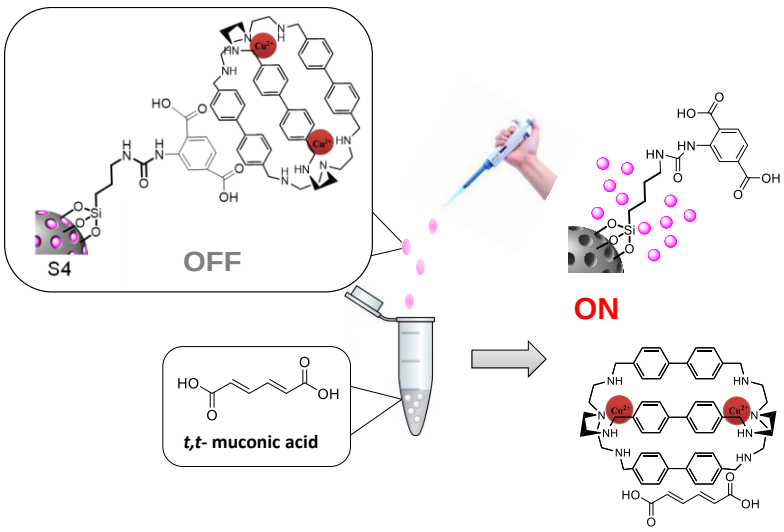

A nanoprobe based on gated mesoporous silica nanoparticles for the selective and sensitive detection of benzene metabolite *t,t*-muconic acid in urine.

Marcia Domínguez,[a] Juan F. Blandez,[a,b,c] Beatriz Lozano-Torres,[a,b,c,d] Cristina de la Torre,[a,d,e] Maurizio Licchelli,[e*] Carlo Mangano,[e] Valeria Amendola,[e] Félix Sancenón,[a,b,c,d] and Ramón Martínez-Máñeza,[b,c,d*]

[a] M. Domínguez, Dr. J. F. Blandez, B. Lozano-Torres, Dr. C. de la Torre, Dr. F. Sancenón, Prof. R. Martínez-Máñez
Instituto Interuniversitario de Investigación de Reconocimiento Molecular y Desarrollo Tecnológico (IDM)
Universitat Politècnica de València
Camino de Vera s/n, 46022, Valencia (Spain)
E-mail: rmaez@qim.upv

[b] Dr. J. F. Blandez, B. Lozano-Torres, Dr. F. Sancenón, Prof. R. Martínez-Máñez
Unidad Mixta UPV-CIPF de Investigación en Mecanismos de Enfermedades y Nanomedicina
Universitat Politècnica de València, Centro de Investigación Príncipe Felipe
Carrer d'Eduardo Primo Yúfera, 3, 46012, Valencia (Spain)

[c] Dr. J. F. Blandez, B. Lozano-Torres, Dr. F. Sancenón, Prof. R. Martínez-Máñez
Unidad Mixta de Investigación en Nanomedicina y Sensores
Universitat Politècnica de València, Instituto de Investigación Sanitaria La Fe
Avenida Fernando Abril Martorell, Torre 106 A 7planta, 46026, Valencia (Spain)

[d] B. Lozano-Torres, Dr. C. de la Torre, Dr. F. Sancenón, Prof. R. Martínez-Máñez
CIBER de Bioingeniería, Biomateriales y Nanomedicina (CIBER-BBN)
Madrid, 28019, Spain.

[e] Dr. C. de la Torre, Prof. M. Licchelli, Dr. C. Mangano, Dr. V. Amendola
Dipartimento di Chimica, Università di Pavia
Via Taramelli 12, I-27100, Pavia (Italy)
E-mail: maurizio.licchelli@unipv.it

Published online: 18 January 2021
(Reprinted with permission from *Chem. Eur. J*. **2021**, *27*, 1306-1310)

3.1 ABSTRACT

Benzene is a highly toxic aromatic hydrocarbon. Inhaling benzene can cause dizziness, vertigo, headaches, aplasia, mutations and, in the most extreme cases, cancer. *Trans, trans*-muconic acid (*t,t*-MA) is one of the metabolization products of benzene. Although different analytical methods have been reported for the determination of *t,t*-MA, these are often expensive, require trained personnel, are not suitable for on-site measurements, and use hazardous organic solvents. For these reasons, the development of reliable, selective and sensitive methods for rapid and *in situ* detection of *t,t*-MA are gain importance. Addressing this challenge, a nanodevice for the selective and sensitive quantification of *t,t*-MA in urine is reported. The nanodevice used is achieved using mesoporous silica nanoparticles loaded with a dye reporter and capped with a dicopper(II) azacryptand. Pore opening and payload release is induced rapidly (10 min) and selectively with *t,t*-MA in urine, using a simple fluorimeter without sample pretreatment.

3.2 INTRODUCCION

Benzene is one of the most commonly used aromatic hydrocarbons in chemical, petrochemical, and pharmaceutical industries due to its ability to dissolve and disperse a large number of compounds of different polarities.[1] Benzene, and its derivatives, are mainly generated by tobacco smoke, combustion engines, or chemical processes, among other sources.[2-4] Therefore, humans are both environmentally and occupationally exposed to benzene mainly via inhalation.[5] Besides, benzene can also enter into the human body across the skin or through the gastrointestinal tract.[6] In recent years, attempts have been made to reduce the use of benzene as a result of its toxic effects on human health.[7] It has been described that continued exposure at high concentrations of benzene can trigger a series of symptoms such as dizziness, headaches, loss of consciousness, aplasia, mutations or cancer.[8] For these reasons, biomonitoring of benzene is extremely important to assess global exposure of workers to this lethal chemical. Recent studies have shown that benzene is a potent carcinogen (classified as group I by the International Agency for Research on Cancer and by the US Environmental Protection Agency) related with acute non-lymphocytic leukemia, lymphocytic leukemia, multiple myeloma and non-Hodgking`s lymphoma. Furthermore, benzene can act over the bone marrow, resulting in hematological adverse effects such as pancytopenia and aplastic anemia.[9-11]

Taking into account these facts, many countries have implemented health and monitoring programs to control human exposure to benzene. These programs are based in the detection of benzene metabolites, such as *t,t*-MA, phenylmercapturic acid or phenol in urine.[12,13] As a result, *t,t*-MA has been proposed by the American Conference of Governmental Industrial Hygienists (ACGIH) as an indicator of benzene continuous exposure with an established limit of 0.5 mg/g creatinine.[14,15]

Different analytical methods have been reported for the determination of *t,t*-MA based in liquid chromatography–mass spectrometry (HPLC-MS), liquid chromatography-ultraviolet spectroscopy (HPLC-UV) and gas chromatography coupled to mass spectrometry (GC-MS). However, these analytical methods are usually expensive, need trained personnel, are not suitable for *in situ* measurements and use hazardous organic solvents.[16-26] For these reasons, the development of reliable, selective and sensitive methods for the rapid and *in situ* detection of *t,t*-MA is of importance. In this respect, very recently, the use of nanostructured materials for the detection of benzene and other aromatic compounds has been reported.[27.28]

From another point of view, azacryptands are supramolecular metal complexes that are constituted by an organic core (azacryptand) with two coordinated metal ions.[29] Within these metal complexes, those formed by bistren cryptands (obtained by the reaction of two tris(2-aminoethyl)amine and three dialdehyde linkers and Cu(II)) have been extensively used for the selective coordination of several dicarboxylates.[30-32] In particular, very recently, Amendola and coworkers have demonstrated that *t,t*-MA can coordinate effectively to a dicopper(II) bistren azacryptand and developed an indicator displacement assay for the fluorescence sensing of this benzene metabolite.[33]

3.3 RESULTS AND DISCUSSION

Based on the above, and following our interest in the development of hybrid organic-inorganic materials for the design of chromo-fluorogenic sensing protocols as an alternative to molecular based probes,[34-41] we report herein the synthesis and characterization of a gated nanodevice for the selective and sensitive quantification of *t,t*-MA in urine. The nanodevice used MSNs as inorganic scaffold with the pores loaded with sulforhodamine B (SRh B) and capped with an inclusion complex formed

between a terephthalic acid derivative (grafted onto the external surface of the solid) and a dicopper(II) bistren azacryptand (Scheme 1).[42,43]

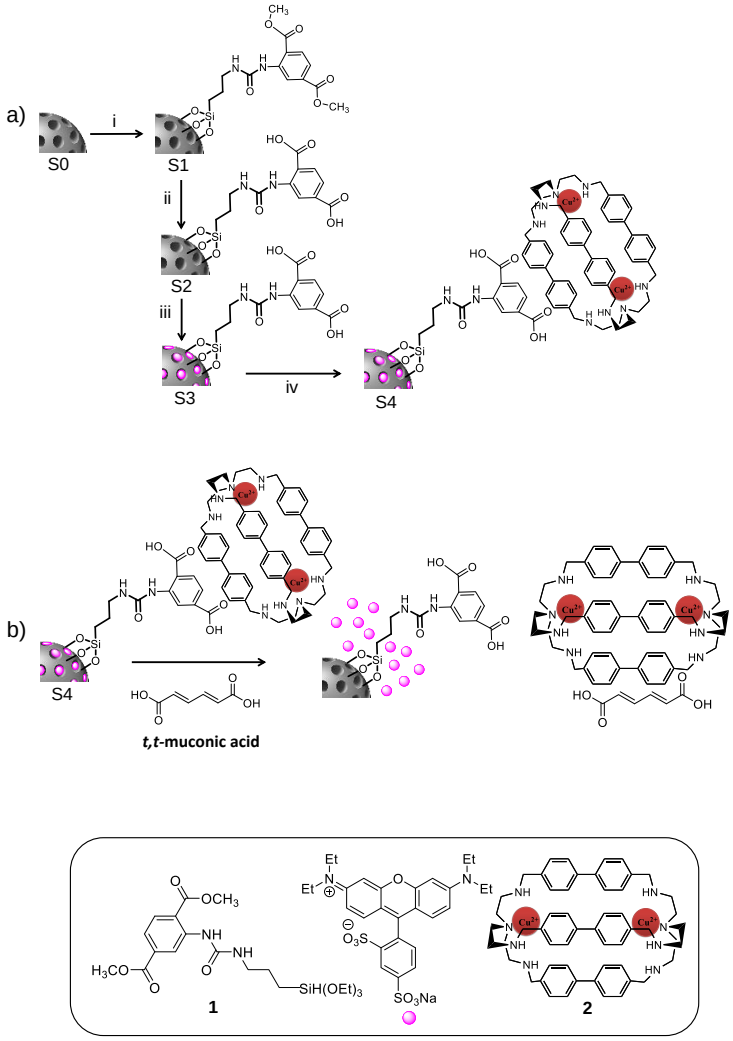

Scheme 1. (a) MSNs loaded with SRh B and capped with a derivative of terephthalic acid coordinated with a dicopper(II) bistren complex (**S4**). Reagents and conditions: (i) **1**, CH_3CN; (ii) CH_2Cl_2, H^+; (iii) SRh B; (iv) **2**, CH_3CN (b) In the presence of *t,t*-MA, the dicopper(II) bistren azacryptand is dethreaded with subsequent pore opening and SRh B release.

In the absence of *t,t*-MA, pores are tightly capped due to the presence of the bulky inclusion complex onto the external surface of the nanoparticles. However, in the presence of *t,t*-MA (which is also a dicarboxylate) a marked SRh B release was expected to occur due to preferential coordination of *t,t*-MA with the dicopper(II) bistren azacryptand, azacryptand displacement, with the consequent pore opening and cargo delivery (Scheme 1).

MSNs were prepared using TEOS as silica source and CTAB as a micellar template.[44,45] The as-made nanoparticles were then calcined at 550 ^{o}C to obtain the starting material (**S0**). On the other hand, the alkoxysilane-containing terephthalate derivative **1** was prepared by reaction between (3-isocyanatopropyl) triethoxysilane and dimethyl 2-aminoterephthalate. **1** was grafted onto the external surface of the calcined nanoparticles yielding **S1**. Then the acidic hydrolysis in **S1** of the dimethyl esters of the grafted terephthalate derivative yielded **S2** nanoparticles. Afterward, the pores of the mesoporous material were loaded with SRh B (**S3**) and then capped upon addition of dicopper(II) bistren cryptand via the coordination of the appended terephthalic with the azacryptand (**S4**) (Scheme 1). The bistren cryptand was prepared by reaction of 4,4'-biphenyldicarboxaldehyde with tris(2-aminoethyl)amine and further reduction of the imine bonds with sodium borohydride. The final dicopper(II) complex **2** was obtained by refluxing the azacryptand with copper(II) nitrate.[33]

All prepared solids were characterized using standard techniques (Supporting Information). Figure 1a shows the powder X-ray diffraction (PXRD) patterns of the as made, **S0** and **S**4 nanoparticles. As could be seen, all three patterns showed the characteristic (100) diffraction peak confirming the preservation of the mesoporous structure during the preparation procedure. The presence of the mesoporous structure was also corroborated by high-resolution transmission electron microscopy (HR-TEM) (Figures 1b and S2). The presence of Cu in the final **S4** nanoparticles was

confirmed by scaning transmission electron microscopy (STEM) images (Figure 1c). Besides, from N_2 adsorption-desorption isotherms, **S0** presented a specific surface area of 1090. $m^2 \cdot g^{-1}$ and a pore volume 0.95 $cm^3 \cdot g^{-1}$ while for **S4** the specific surface area decreased to 43 $m^2 \cdot g^{-1}$ and pore volume was 0.04 $cm^3 g^{-1}$ (Figure S3 and Table S1).

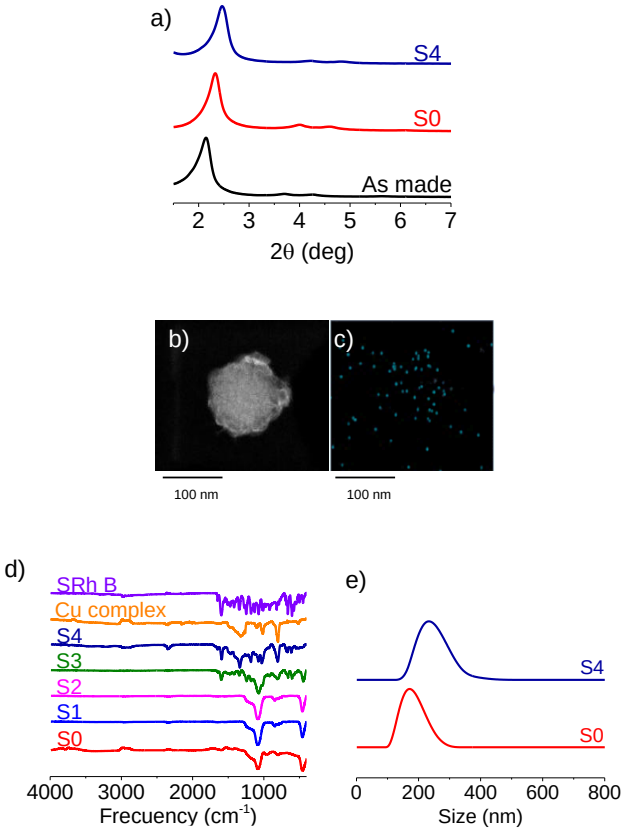

Figure 1. (a) Power X-ray diffraction patterns of as-made MSNs, **S0** and **S4** nanoparticles. (b) HR-TEM image of **S4** nanoparticles. (c) STEM images of **S4** nanoparticles. (d) FTIR spectra of **S0**, **S1**, **S2**, **S3**, **S4**, dicopper(II) bistren complex and SRh B. (e) Hydrodynamic diameter of **S0** and **S4** nanoparticles determined by dynamic light scattering (DLS).

The different functionalization steps (i.e. from **S0** to **S4**) were followed by Fourier-transform infrared spectroscopy (FTIR), DLS, thermogravimetric analysis (TGA) and elemental analysis (EA). The FTIR spectrum of **S0** nanoparticles showed the typical band of Si-O-Si stretching vibrations at 1079 cm^{-1} (Figure 1d), which was also present in the **S1-S4** solids. **S3** and **S4** presented a band at ca. 1590 cm^{-1} ascribed to the C=N stretching vibration of the SRh B loaded inside the pores. Bands at 1310 and 803 cm^{-1} ascribed to stretching vibrations of Cu-N bonds, indicated the presence of the dicopper(II) bistren azacryptand on **S4**. Besides, Z-potential (Table S2) changed from -23.6 mV for **S0** to -31.5 mV for **S3** (loaded with SRh B and functionalized with the terephthalate derivative, both negatively charged) and then to 50.2 mV for **S4** (capped with the positively charged dicopper(II) bistren cryptand). DLS measurements showed an increase in the hydrodynamic nanoparticle diameter, from 120 nm for **S0** to 225 nm for **S4** (Figure 1e). **S1** amounted 0.82 $mmol \cdot g^{-1}$ of solid of therephthalic methyl ester derivative, whereas in **S4** the amount of dye and dicopper(II) bistren cryptand were 0.303 $mmol \cdot g^{-1}$ of solid and 0.465 $mmol \cdot g^{-1}$ of solid, respectively (Table S3).

Dye release from **S4** was tested in the absence and in the presence of *t,t*-MA. For this purpose, **S4** was suspended in HEPES 0.05 M at pH 7.0 and the resultant suspension was separated in two aliquots. *t,t*-MA was added to one of the aliquots (final analyte concentration of 0.11 mM) while HEPES was added to the other. Both suspensions were stirred at 25°C.

Samples were taken at scheduled times and centrifuged for 3 min to remove the solid. Finally, the fluorescence of the released SRh B was measured at 580 nm (λ_{ex} = 510 nm). Cargo delivery profiles obtained are shown in Figure 2a. In the absence of *t,t*-MA (Figure 2a, black curve) a nearly zero release was observed (less than 5% of the maximum amount delivered after 15 min) indicating an effective pore closure. In contrast, when *t,t*-MA was present, a remarkable enhancement of the fluorescence

recorded at 580 nm was found (Figure 2a, red curve). This is consistent with a preferential coordination of *t,t*-MA with dicopper(II) cage complex **2** that induces dicopper(II) bistren cryptand displacement from **S4**, pore opening and dye delivery.

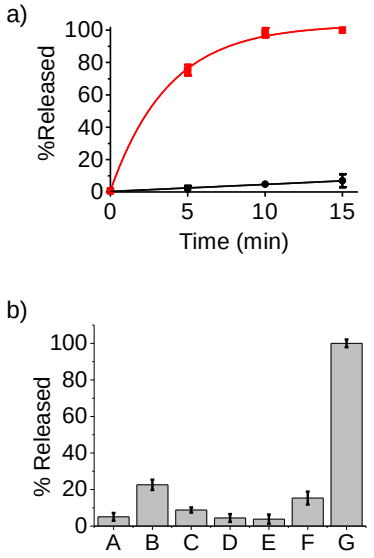

Figure 2. (a) Release profiles of SRh B from HEPES suspensions of solid **S4** at pH 7.0 in the absence (black curve) and in the presence of *t,t*-MA (0.11 mM) (red curve); 100% release was attributed to the maximum dye released after 15 min. Error bars are expressed as 3σ for three independent experiments. (b) Emission intensity of SRh B at 580 nm (λex = 510 nm) released from **S4** nanoparticles (HEPES 0.05M, pH 7.0) in the presence of dicarboxylic acids (0.19 mM): A (adipic acid), B (maleic acid), C (fumaric acid), D (succinic acid), E (suberic acid), F (sebacic acid) and G (*t,t*-MA) after 10 min upon addition. Error bars are expressed as 3σ for three independent experiments.

In order to confirm this sensing paradigm we carried out additional studies on complex formation between *t,t*-MA and the dicopper(II) bistren cryptand by UV-visible titrations. From these studies a logarithm of the stability constant of 8.45 was determined (Supporting Information), which is higher than that reported for the interaction of terephthalate dianion and dicopper(II) bistren cryptand (logK = 8.0).[30]

This is in agreement with the displacement of the dicopper(II) bistren cryptand from **S4** in the presence of *t,t*-MA which induced dye delivery. Besides, addition of increasing amounts of *t,t*-MA to an HEPES suspension of **S4** induced a progressive dye release (Figure S6), which also supports the displacement protocols shown in Scheme 1. From the titration profile a limit of detection as low as 0.027 mM for *t,t*-MA was calculated.

The selective response of **S4** nanoparticles toward *t,t*-MA was also studied. For this purpose, to HEPES suspensions of **S4** selected dicarboxylates were added at 0.19 mM concentration and the emission of the SRh B in the solution at 580 nm was measured after 10 min. As could be seen in Figure 2b from all dicarboxylates tested only *t,t*-MA was able to induce a remarkable emission enhancement due to selective pore opening and SRh B release.

Taking into account the high selectivity found and the low LOD of **S4** toward *t,t*-MA (see Table S5 for a comparison of the sensing features of **S4** with the traditional methods reported in the literature[18-26]), we take a step forward and evaluated possible use of the sensing nanoparticles to determine *t,t*-MA in urine. For this purpose, urine was spiked with known amounts of *t,t*-MA and the concentration was determined using **S4** nanoparticles by means of a calibration curve in the same media (LOD of *t,t*-MA in urine of 0.017 mM). Results are shown in Table 1. As it can be seen, **S4** was satisfactorily applied to the detection of *t,t*-MA with high recovery ratios in the 97-99% range. These results demonstrate the potential application of **S4** for the detection and quantification of *t,t*-MA, related with benzene exposure, in realistic urine samples.

Table 1. Determination of *t,t*-MA spiked in urine using S4 nanoparticles.

Sample	*t,t*-MA spiked (μM)	*t,t*-MA determined (μM)	Recovery (%)
1	45.0	44.5	98.9
2	54.0	53.0	98.2
3	62.9	61.0	97.1

3.4 MATERIALS AND METHODS

TEOS, CTAB, sodium hydroxide, methanol, dichloromethane, SRh B, acetonitrile (MeCN), (3-isocyanatopropyl)triethoxysilane, *N*,*N*'-bis(2-aminoethyl)ethane-1,2-diamine , sodium borohydride ($NaBH_4$), 4-(2-hydroxyethyl)-1-piperazineethanesulfonic acid (HEPES), *t,t*-MA, adipic acid, maleic acid, fumaric acid, succinic acid, suberic acid and sebacic acid were purchased from Sigma-Aldrich. Dimethyl-2-aminoterephthalate was obtained from 2-aminoterephthalatic acid according to a published procedure,[46] whereas 4,4'-biphenyl-dialdehyde was synthesized by a Suzuki cross-coupling reaction using a modification of the synthetic procedure reported by Huff et al.[47]

HR-TEM images were carried out in a 200 KV in a JEOL JEM 2100F microscope equipped with a X ray detector and PXRD measurements were recorded on a Philips D8 Advance Diffractometer with CuKα radiation. Porosity was studied by N_2 adsorption-desorption isotherms recorded in a Micromeritics ASAP2010 automated sorption analyzer. TGA were recorded a TGA/SDTA 851e Mettler Toledo balance, employing a heating program that have a heating ramp of 10°C per min from 25°C to 100°C, the temperature was kept at 100°C for 60 min and finally was applied a new heating ramp of 10°C per min from 100°C to 1000°C, and an isothermal heating step at the final temperature for 30 min. All process was carried out in an oxidant

atmosphere (air, 80 mL·min^{-1}). FTI) spectra were obtained in a Nicolet 6700 instrument (Thermo scientific, USA) in the range 4000–400 cm^{-1}. DLS and Z potential measurements were recovered whit a Malvern Zetasizer Nano ZS. Fluorescence spectroscopy was carried out in a JASCO spectrofluorometer FP-8500. Mass spectra were acquired on a Thermo-Finnigan ion-trap LCQ Advantage Max instrument equipped with an electron spray ionizing source. Real urine samples employed for this work were from voluntary individuals and informed consent was obtained for any experimentation.

Synthesis of materials

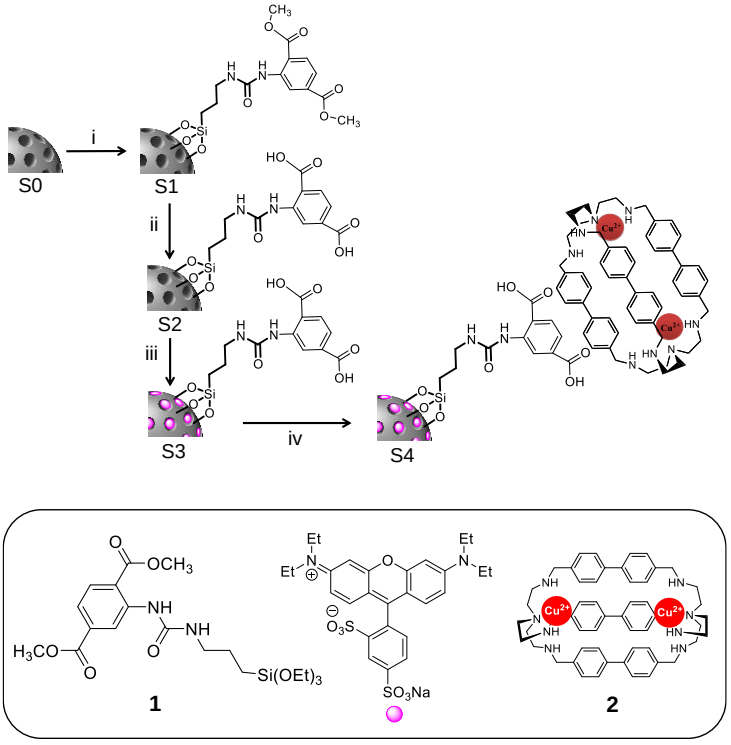

Scheme S1. Synthetic procedure for the preparation of solid **S4**. Reagents and conditions: (i) **1**, CH_3CN; (ii) CH_2Cl_2, H^+; (iii) SRh B; (iv) **2**, CH_3CN.

Synthesis of terephthalic acid derivative 1:

(3-isocyanatopropyl)triethoxysilane (1.1 mL, 4.4 mmol) was added to a suspension of dimethyl-2-aminoterephthalate[1] (0.578 g., 2.8 mmol) in dry ethyl acetate (20 mL). The resulting mixture was stirred and heated to 80°C (reflux) under an inert atmosphere (Ar) and left to react for 24 h. The reaction was monitored by thin layer chromatography (TLC), eluent: hexane/ethyl acetate 7:3, and electrospray ionization mass spectrometry (ESI-MS). Both techniques showed the presence of the expected product and some unreacted dimethyl-2-aminoterephtalate reagent. An additional amount of (3-isocyanatopropyl)triethoxysilane (0.28 mL, 1.1 mmol) was then added and the reaction continued under the same condition until no further increase in the concentration of the product was detected by MS-ESI (two days). The mixture was left to cool to room temperature, concentrated to dryness and taken up with hexane/ ethyl acetate 7:3 (10 mL), which results in the separation of a white solid. It was filtered out and washed with several portions of hexane to yield the pure product (0.45 g., yield: 35.2%). ^{1}H-NMR: (400 MHz, $CDCl_3$): δ = 10.21 (broad s, 1H); 9.11 (d, 1H, J = 1.6 Hz); 7.96 (d, 1H, J = 8.3 Hz); 7.53 (dd, 1H, J_1= 8.3 Hz,J_2 = 1.7 Hz); 4.96 (broad s, 1H); 3.86-3.85 (s,6H); 3,77 (q, 6H, J = 7.0 Hz), 3,25 (m, 2H), 1,64 (m, 2H), 1,17 (m, 9H, J = 7.0 Hz), 0,62 (t, 2H, J = 8.1 Hz). ESI-MS: for $C_{20}H_{33}N_2O_8Si$ ($M+H^+$), calculated: 457.6 m/z; measured: 457.7 m/z.

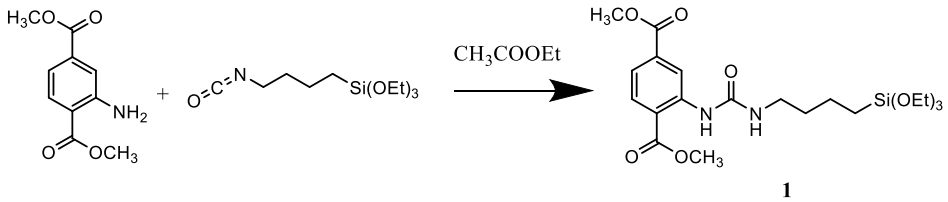

1

Scheme S2. Synthetic procedure used for the preparation of 1.

Synthesis of dicopper(II) bistren cryptand (2):

Imino bistren cryptand (3): A solution of *N*,*N*'-bis(2-aminoethyl)ethane-1,2-diamine (468 mg, 3.2 mmol) in CH_3CN (100 mL) was added dropwise (over 1 h) to a magnetically stirred solution of 4,4'-biphenyl-dialdehyde (1 g, 4.8 mmol) in CH_3CN (100 mL) under inert atmosphere at room temperature. The mixture was then left to react for 20 h. The white precipitate formed was obtained by filtration, washed with CH_3CN, and dried in vacuo, to yield 1.14 g (1.4 mmol, 88%). The product was characterized by ESI-MS: $C_{54}H_{54}N_8$ ($M+H^+$), theoretical: 814.4 m/z; measured: 815.0 m/z).

Bistren cryptand (4): A magnetically stirred solution of **3** (1 g, 1.2 mmol) in methanol (150 ml) was reduced by addition of solid $NaBH_4$ (2.72 g, 72 mmol), in small portions over a period of 1 h. After complet addition, the mixture was heated to reflux for 3 h and then left to react at room temperature overnight. The solvent was removed under vacuum, yielding a white precipitate that was taken up with 20 ml of dichloromethane and 25 ml of water. The mixture was transferred to an extraction funnel, thoroughly mixed and the organic layer recovered. The water layer was furtherly extracted with 2 x 20 ml of dichloromethane. The combined organic portions were added of Na_2SO_4 and left to dry overnight, then filtered, evaporated to dryness, yielding 0.794 g (0.96 mmol, 80%) of product. ^{1}H-NMR: (400 MHz, CD_3OD): δ = 7.14 (d, 12H, J = 8.2 Hz); 7.02 (d, 12H, J = 8.2 Hz), 3.82 (s, 12H), 2.95 (m, 12H); 2.28 ppm (m, 12H). ESI-MS: for $C_{54}H_{66}N_8$ ($M+H^+$), theoretical: 826.5 m/z; experimental: 827.8m/z . EA: theoretical $C_{54}H_{66}N_8$: C 78.41; H 8.04; N 13.55%, experimental $C_{54}H_{66}N_8$: C 78.38; H 8.11; N 13.51%;

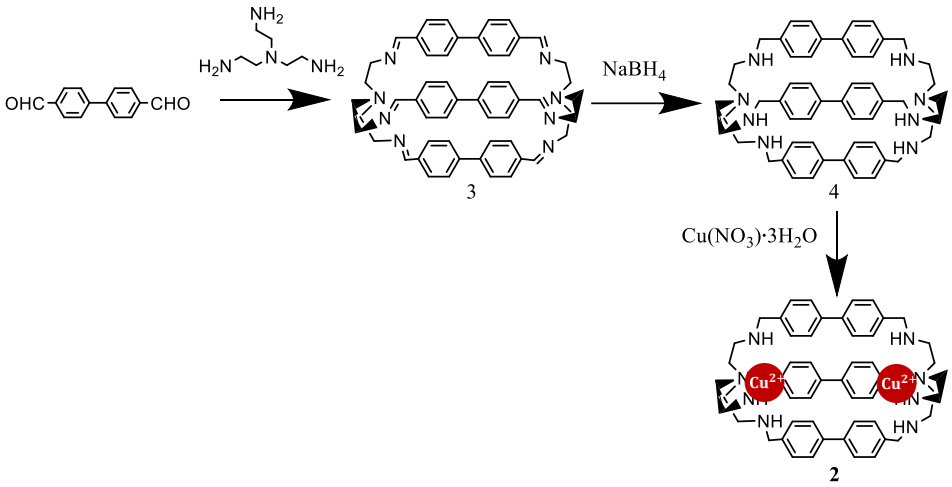

Scheme S3. Synthetic procedure used for the preparation of dicopper(II) bistren cryptand **2**.

Dicopper(II) complex (2): $Cu(NO_3)_2 \cdot 3H_2O$ (19.3 mg. 0.08 mmol) was added to a solution of **4** (35mg, 0.04 mmol) in 5ml of methanol. The suspension was stirred at room temperature overnight. The solvent was removed under reduced pressure and the complex salt [Cu^{II}_2(**4**)](NO3)4.3H2O precipitated as a bright blue powder, which was collected by vacuum filtration (40 mg, 0.04 mmol, yield 80%). ESI-MS: for $C_{54}H_{66}N_8Cu_2$ ($M+H^+$), theoretical: 952.4 m/z; experimental 953.4 m/z. EA: theoretical for $C_{54}H_{72}Cu_2N_{12}O_{15}$: C, 51.63; H, 5.78; N, 13.38%; experimental for C, 51.57; H, 5.82; N, 13.42%.

Synthesis of mesoporous silica nanoparticles (S0): CTABr (1.00 g, 2.74 mmol) was first dissolved in 480 mL of deionised water before adding 3.5 mL of a solution of NaOH 2M until a basic pH 8 was reached. Then, the solution was heated to 80°C and TEOS (5.00 mL, $2.57 \cdot 10^{-2}$mol) was added dropwise to the surfactant solution at maximum stirring. The mixture was stirred for 2 h at 80°C. A white precipitate was obtained and isolated by centrifugation. Once isolated, the solid was washed with deionized water and ethanol until a neutral pH in the solution was obtained. Then

the solid was dried at 60°C (MCM-41 as-synthesized). To prepare the final porous material (**S0**), the as-synthesized solid was calcined at 550°C using an oxidant atmosphere for 5 h in order to remove the template phase.

Synthesis of S1: S0 nanoparticles (100 mg) and terephthalic acid derivative **1** (25 mg, 0.06 mmol) were suspended in acetonitrile (15 mL). The suspension was stirred at room temperature overnight. Then, solution was centrifuged and the solid (**S1**) washed twice with acetonitrile and dried under vacuum.

Synthesis of S2: S1 nanoparticles (42 mg) were suspended in 5 ml of dichloromethane, and 50 µL of HCl were added dropwise to the solution. The mixture was heated at 50°C for 24 hours. Then, the solution was allowed to room temperature and subsequently neutralized with sodium hydroxide (NaOH). Finally, the solution was centrifuged, and the solid (**S2**) was washed twice with dichloromethane and dried under vacuum.

Synthesis of S3: S2 (200 mg) and SRh B (92.9 mg, 0.16 mmol) were suspended in CH_3CN (7 mL). The suspension was stirred at room temperature for 24 h. Solid **S3** was recovered by centrifugation as a pink powder.

Synthesis of S4: S3 (34 mg) and dicopper (II) bistren cryptand **2** (100 mg, 0.083 mmol) were suspended in CH_3CN (4 mL) and the suspension was stirred for 24 h. Final **S4** was obtained by centrifugation and washed with water to eliminate the residual dye. **S4** was dried in an oven at 37°C overnight to obtain a pink powder.

Characterization of solids

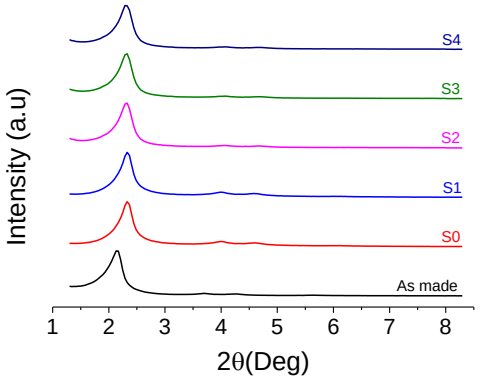

Figure S1. Powder X-ray diffraction (PXRD) patterns of the prepared solids.

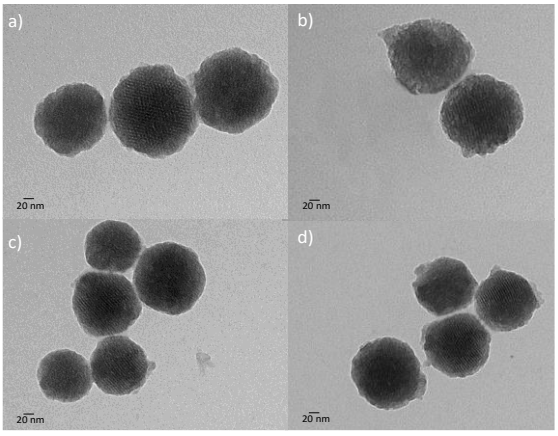

Figure S2. HR-TEM images of (a) solid **S0**, (b) solid **S2**, (c) solid **S3** and (d) solid **S4**. The images show the spherical shape of the nanoparticles with diameters of ca. 100 nm. The mesopores of the nanoparticles are also observed as alternate black and white strips.

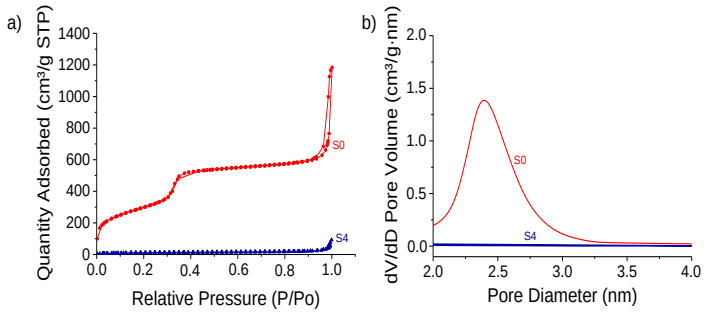

Figure S3. (a) N_2 adsorption-desorption isotherms of **S0** and **S4**, (b) pore sizes for **S0** and **S4** nanoparticles.

Table S1. BET specific surface values, pore volumes and pore sizes calculated from N_2 adsorption-desorption isotherms for selected materials. [a] An accurate pore volume, could not be obtained.

Sample	SBET [m^2g^{-1}]	Pore Volume [cm^3g^{-1}]	Pore size [nm]
S0	1090.7	0.95	3.35
S3	42.7	0.04	--[a]

Table S2. Z-potential and DLS values for the prepared nanoparticles.

	S0	**S1**	**S2**	**S3**	**S4**
Z-potential (mV	-23.6	-22.5	35.2	-31.5	50.2
DLS (nm)	120	-	137	-	225

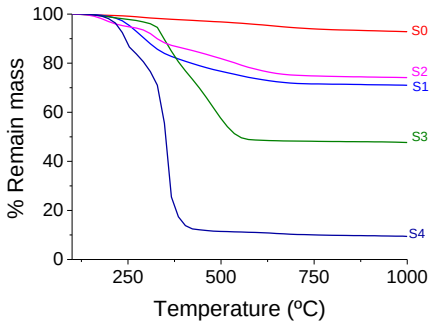

Figure S4. Thermogravimetric analysis for **S0**, **S1**, **S2**, **S3** and **S4** nanoparticles.

Table S3. Elemental composition of **S1** and **S4** nanoparticles determined by elemental analysis and ICP-MS measurements. [a] Elemental analysis. [b] ICP-MS.

	% N[a]	% C[a]	% H[a]	% S[a]	% Cu[b]
S1	2.30	15.53	2.92	-	-
S4	9.73	53.25	5.14	1.82	5.91

Cargo release experiment in HEPES

1 mg of **S4** was suspended in 1300 µL of HEPES (0.05 M, pH=7). The suspension was divided in two aliquots of 500 µL and HEPES was added until a volume of 1200 µL was reached. Then, 20 µL of *t,t*-MA (6.8 mM) were added to one aliquot and, in parallel, 20 µL of HEPES (0.05 M, pH=7) were added to the second aliquot. Both suspensions were stirred at 25°C for 10 min. Aliquots of 150 µL were taken at scheduled times and centrifuged for 3 min at 12000 rpm (to remove the solid). Fluorescence of the released SRh B was measured at 580 nm (λ_{ex} = 510 nm). The release profile of **S4** in presence or absence of *t.t-MA* is shown in Figure 2a.

Stability constant determination

The interaction of dicopper (II) bistren cryptand with *t,t*-MA was studied by UV-vis measurements. A solution of dicopper (II) bistren cryptand (1×10^{-5} M in HEPES 0.05M, pH=7) was prepared and UV-vis band at 260 nm was monitored upon addition of increasing amounts of *t,t*-MA. The absorption band at 260 nm was enhanced progressively upon addition of increasing quantities of *t,t*-MA (Figure S5). Titration profile indicated the formation of 1:1 dicopper(II) bistren cryptand-*t,t*-MA with a logarithm of the stability constant of 8.45 obtained by a nonlinear least-squares fitting.

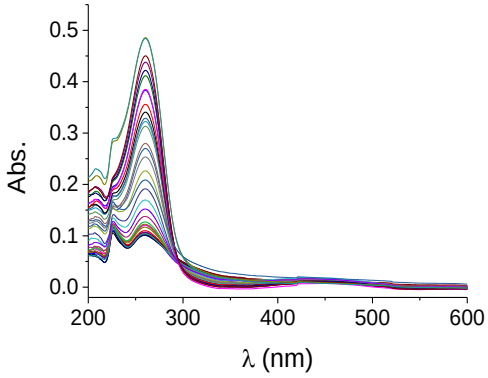

Figure S5. UV-vis titrations of HEPES (0.05 M, pH 7.0) solutions of dicopper (II) bistren cryptands with *t,t*-MA .

Calibration curve in HEPES

1 mg of **S4** was suspended in 1300 µL of HEPES (0.05 M, pH=7) and divided in two aliquots of 500 µL. Then, HEPES was added to the aliquots until a final volume of 1200 µL was reached. Afterward, 2 µL of a *t,t*-MA solution (6.8 mM) was added each 10 min. 150 µL samples were centrifuged for 3 min at 12000 rpm to remove the solid.

Fluorescence of the released SRh B was measured at 580 nm (λ_{exc} = 510 nm). From the calibration curve showed in Figure S6 a limit of detection of 0.027 mM for *t*,*t*-MA was determined and calculated based on the intersection point of the two slopes of the represented curve.

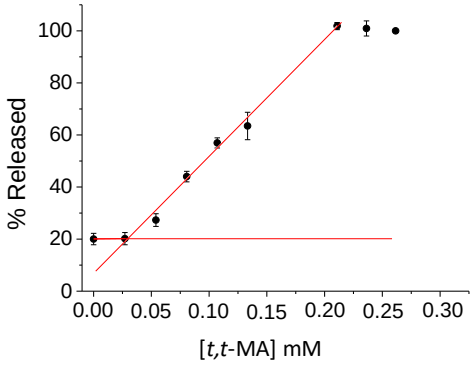

Figure S6. Calibration curve of **S4** nanoparticles with *t*,*t*-MA in HEPES (0.05M. pH=7). Error bars are expressed as 3σ for three independent experiments.

Selectivity studies with S4 in HEPES

2 mg of **S4** were suspended in 1300 µL of HEPES (0.05 M, pH=7) and divided into 8 aliquots of 150 µL. Aliquots were filled with HEPES until a 500 µL volume was reached. HEPES solutions of dicarboxylic acids (*t*,*t*-MA, adipic acid, maleic acid, fumaric acid, succinic acid, suberic acid and sebacic acid) were prepared (6.8 mM). 14 µL of the dicarboxylic acid solution were added to each **S4** aliquot to obtain a final concentration of 0.19 mM. Blank was obtained by the addition of 14 µL of HEPES. Aliquots were stirred for 10 min at 25°C and 150 µL of the samples were centrifuged for 3 min at 12000 rpm to remove the solid. Fluorescence of the released SRh B was measured at 580 nm (λ_{ex} = 510 nm) (Figure 2b).

Detection of *t,t*-MA in urine

Solid **S4** (1 mg) was suspended in real urine (1300 µL) and then divided in five aliquots of 250 µL each. Aliquots were filled with urine until 3 mL and then 12, 16, 20, 24 and 28 µL of a *t,t*-MA solution (6.8 mM) were added. Samples were stirred for 10 min and then centrifuged for 3 min at 12000 rpm (to remove the solid). Fluorescence of the released SRh B was measured at 580 nm (λ_{exc} = 510 nm). The amount of *t,t*-MA in each sample was measured using a calibration curve in urine (Table S4).

Table S4. Determination of *t,t*-MA spiked in urine using S4 nanoparticles.

Sample	*t,t*-MA spiked (µM)	*t,t*-MA determined (µM)	Recovery (%)
1	45.0	44.5	98.9
2	54.0	53.0	98.2
3	62.9	61.0	97.1

Table S5. Comparison of the present work with the other published analytical methods of *t,t*-MA detection. [1] High performance liquid chromatography, [2] Dispersive solid-phase extraction, [3] High performance liquid chromatography - Ultraviolet spectroscopy, [4] Combination of molecularly imprinted polymer (MIP) and microextraction by packed sorbent (MEPS) , [5] Partitioned dispersive liquid–liquid microextraction, [6] Micro-extraction by packed sorbent, [7] Gas chromatography - Mass spectrometry, [8] Solid-phase extraction,[9] High performance liquid chromatography–mass spectrometry, [10] Molecularly imprinted solid-phase extraction,[11] Liquid chromatography–mass spectrometry, [12] Not reported.

Method	Sample preparation technique	Limit of detection ($\mu g \cdot L^{-1}$)	Limit of quantitation ($\mu g \cdot L^{-1}$)	Recovery (%)	Ref.
HPLC[1]	DSPE[2]	1.0	3.0	96-98	[18]
HPLC-UV[3]	MIMEPS[4]	15	50	89.8-91.6	[19]
HPLC–UV[3]	PDLLME[5]	0.11	0.83	86-102	[20]
HPLC-UV[3]	MEPS[6]	32	100	93.3-99.4	[21]
GC-MS[7]	SPE[8]	37	109	83.3- 94.8	[8]
HPLC-MS/MS[9]	SPE[8]	0.5	1.5	>86	[23]
HPLC-UV[3]	MISPE[10]	100	300	87-112	[24]
LC-MS/MS[11]	Dilute-inject	69.6	231.6	NR[12]	[26]
Fluorimeter	-	0.002	0.006	97-99	Present study

3.5 CONCLUSION

In summary, we describe herein a nanoprobe based on gated mesoporous silica nanoparticles for the selective and sensitive *t,t*-MA detection in buffered aqueous solution and in urine. **S4** nanoparticles are composed by a mesoporous inorganic scaffold loaded with SRh B and capped by an inclusion complex formed between a grafted terephthalate derivative and a dicopper(II) bistren cryptand. The sensing mechanism arises from a displacement reaction by the formation of an inclusion complex between *t,t*-MA and the dicopper(II) bistren cryptand that results in cargo delivery. Pore opening and payload release is selectively induced with *t,t*-MA,

whereas this is not observed for other dicarboxylates. LOD for *t,t*-MA as low as 0.027 mM in HEPES and 0.017 mM in urine are determined. Finally, **S4** demonstrate to effectively determine the concentration of *t,t*-MA in spiked urine samples. This indicates the high potential of **S4** nanoprobe for the fast detection of *t,t*-MA (10 min) using a simple fluorimeter without sample pretreatment. This, or similar nanoparticles, could be useful for an effective control of benzene exposure in environments in which this highly toxic pollutant is used.

ACKNOWLEDGEMENTS

The authors thank the Spanish Government (RTI2018-100910-B-C41) and the Generalitat Valenciana (PROMETEO 2018/024) for support.

3.6 REFERENCES

1. B. Holeckova, E. Piesova, K. Sivikova, J. Dianovsky, *Ann. Agric. Environ. Med*. **2004**, *11*, 175-179.

2. Agency for Toxic Substances and Disease Registry, Toxicological Profile for Benzene, US Department of Health and Human Services, Public Health Service, ATSDR, Atlanta, GA, **2007**.

3. P. Gustafson, L. Barregard, B. Strandberg, G. S. Callsten, *J. Environ. Monit.* **2007**, *9*, 23-32.

4. R. Duarte-Davidson, C. Courage, L. Rushton, L. Levy, *Occup. Environ. Med.* **2001**, *58*, 13.

5. Toxicological Profile for Benzene, US Department of Health and Human Services, Agency for Toxic Substances and Disease Registry, Atlanta, GA, **2007**.

6. R. Snyder, J. *Toxicol. Environ. Health A*. **2000**, *61*, 339-346.

7. C. P. Weisel, *Chem. Biol. Interact*. **2010**, *184*, 58-66.

8. M. K. R. Mudiam, A. Chauhan, K. P. Singh, S. K. Gupta, R. Jain, R. Che, R. C. Murthy, *Anal. Bioanal. Chem.* **2013**, *405*, 341-349.

9. D. H. Koh, M. Y. Lee, E. K. Chung, J. K. Jang, D. U. Park, *Ind. Health.* **2018**, *56*, 346-355.

10. LARC, Benzene. **2012**.

11. V. Wiwanitkit, S. Soogarun, J. Suwansaksri, *Leukemia Lymphoma*. **2004**, *45*, 1643-1645.

12. S. Fustinoni, M. Buratti, L. Campo, A. Colombi, D. Consonni, A. C. Pesatori, M. Bonzini, P. Farmer, S. Garte, F. Valerio, D. F. Merlo, P. A. Bertazzi, *Chem. Biol. Interact.* **2005**, *153–154*, 253-256.

13. P. Lovreglio, M. N. D'Errico, S. Fustinoni, I. Drago, A. Barbieri, L. Sabatini, M. Carrieri, P. Apostoli, L. Soleo, *J. Environ. Monit*. **2011**, *13*, 2921-2928.

14. G. Scherer, T. Renner, M. Meger, *J. Chromatogr. B: Biomed. Sci. Appl*. **1998**, *717*, 179-199.

15. American Conference of Governmental Industrial Hygienists. Threshold Limit Values and Biological Exposure Indices, ACGIH, *Cincinnati*, **2010**.

16. S. Waidyanatha, N. Rothman, S. Fustinoni, M. T. Smith, R. B. Hayes, W. Bechtold, M. Dosemeci, L. Guilan, S. Yin, S. M. Rappaport, *Carcinogenesis*. **2001**, *22*, 279-286.

17. M. K. Mudiam, A. Chauhan, K. P. Singh, S. K. Gupta, R. Jain, C. Ratnasekhar, R. C. Murthy, *Anal. Bioanal. Chem.*, **2013**, *405*,341-349.

18. E. Soleimani, A. Bahramia, A. Afkhami, F. G. Shahna, *J. Chromatogr. B Biomed. Appl*. **2017**, *1061–1062*, 65–71.

19. M. Rismanchian, K. Ebrahim, Z. Ordudari, *Chem. Pap*. **2019**, *73*, 2485–2492

20. R. Rahimpoor, A. Bahrami, D. Nematollahi, F. G. Shahna, M. Farhadian*, Int. J. Environ. Anal. Chem.* **2020**, *102*, 885-898.

21. E. Soleimani, A. Bahrami, A. Afkhami, F. G. Shahna, *Toxicol. Environ. Health. Sci*. **2017**, *9*, 317-324.

22. M. K. R. Mudiam, A. Chauhan, K. P. Singh, Sh. K. Gupta, R. Jain, R. Ch, R. C. Murthy, *Anal. Bioanal. Chem.***2013**, 405, 341-349.

23. G. Tranfo, E. Paci, R. Sisto, D. Pigini, *J. Chromatogr. B.* **2008**, 867, 26-31.

24. A. C. Vieira, R. A. Zampieri, M.E. P. B. de Siqueira, I. Martins, E. C. Figueiredo, *Analyst*. **2012**, *137*, 2462-2469.

25. M. K. R. Mudiam, A. Chauhan, K. P. Singh, S. K. Gupta, R. Jain, Ch. Ratnasekhar, R. C. Murthy, *Anal. Bioanal. Chem*. **2013**, *405*, 341-349.

26. S. Gagné, Biomed. *Chromatogr.* **2013**, *27*, 664-668.

27. R. Mateos, S. Vera-López, M. Saz, A. M. Díez-Pascual, M. P. San Andrés*, J. Chromatogr. A*. **2019**, *1596*, 30-40.

28. Q. Ji, X. Qiao, X. Liu, H. Jia, J.-S. Yu, A. Katsuhiko, Bull. *Chem. Soc. Jpn.* **2018**, *91*, 391-397.

29. G. Alibrandi, V. Amendola, G. Bergamaschi, L. Fabbrizzi, M. Licchelli, *Org. Biomol. Chem*. **2015**, *13*, 3510-3524.

30. M. Boiocchi, M. Bonizzoni, L. Fabbrizzi, G. Piovani, A. Taglietti, *Angew. Chem. Int. Ed.* **2004**, *43*, 3847-3852.

31. R. Gomes, A. Sanson, F. Lobo, R. Alfonso, M. Coutrim, *Separations.* **2016**, *3*, 1-14.

32. V. Amendola, G. Bergamaschi A. Miljkovic, *Supramol. Chem*. **2018**, *30*, 236-242.

33. D. Merli, S. La Cognata, F. Balduzzi, A. Miljkovic, L. Toma, V. Amendola, *New J. Chem.* **2018**, *42*, 15460-15465.

34. C. Coll, R. Casasúsa, E. Aznar, M. D. Marcos, R. Martínez-Máñez, F. Sancenón, J. Soto, P. Amorós, *Chem. Commun.* **2007**, *19*, 1957-1959.

35. E. Aznar, C. Coll, M. D. Marcos, R. Martínez-Máñez F. Sancenón, J. Soto, P. Amorós, J. Cano, E. Ruiz, *Chem. Eur.* J. **2009**, *15*, 6877-6888.

36. E. Aznar, R. Villalonga, C. Giménez, F. Sancenón, M. D. Marcos, R. Martínez-Máñez, P. Díez, J. M. Pingarrón, P. Amorós, *Chem. Commun*. **2013**, *49*, 6391-6393.

37. L. Mondragón, N. Mas, V. Ferragud, C. de la Torre, A. Agostini, R. Martínez-Máñez, F. Sancenón, P. Amorós, E. Pérez-Payá, M. Orzáez, *Chem. Eur. J.* **2014**, *20*, 5271-5281.

38. S. El Sayed, M. Licchelli, R. Martínez-Máñez, F. Sancenón, *Chem. As.* J. **2017**, *12*, 2670-2674.

39. S. El Sayed, M. Milani, C. Milanese, M. Licchelli, R. Martínez-Máñez, F. Sancenón, *Chem. Eur. J.* **2016**, *22*, 13935-13945.

40. S. El Sayed, M. Milani, M. Licchelli, R. Martínez-Máñez, F. Sancenón, *Chem. Eur. J.* **2015**, *21*, 7002-7006.

41. S. El Sayed, C. Giménez, E. Aznar, R. Martínez-Máñez, F. Sancenón, M. Licchelli, *Org. Biomol. Chem*. **2015**, *13*, 1017-1021.

42. A. García-Fernández, E. Aznar, R. Martínez-Máñez, F. Sancenón, *Small*, **2020**, *16*, 1902242.

43. A. Llopis-Lorente, B. Lozano-Torres, A. Bernardos, R. Martínez-Máñez, F. Sancenón, *J. Mat. Chem.,* B. **2017**, *5*, 3069-3083.

44. C. T. Kresge, M. E. Leonowicz, W. J. Roth, J. C. Vartuli, J. S. Bec, *Nature.* **1992**, *359*, 710-712.

45. S.-H. Wu, C.-Y. Mou, H.-P. Lin, *Chem. Soc. Rev*. **2013**, *42*, 3862-3875.

46. M. Bührmann, J. Hardick, J. Weisner, L. Quambusch, D. Rauh, *Angew. Chem., Int. Ed.* **2017**, *56*, 13232-13236.

47. B. E. Huff, T. M. Koenig, D. Mitchell, M. Staszak, Org. Synth. 1998, 75, 53.

Chapter 4| NIR fluorescent probe for the detection of renal damage based on overrepresentation of alanine aminopeptidase enzyme.

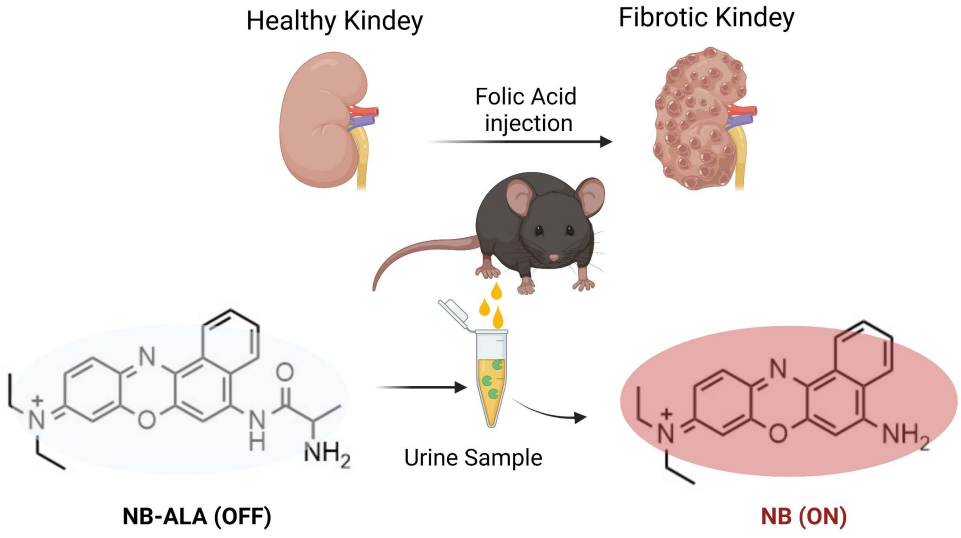

NIR fluorescent probe for the detection of renal damage based on overrepresentation of alanine aminopeptidase enzyme.

Marcia Domínguez,[a,b] Kathleen Meyer,[c] Félix Sancenón,[a,b,d,e] Juan F. Blandez,[a,b,d,*] Manuel Serrano,[b,f,*] and Ramón Martínez-Máñez,[a,b,d,e,*]

a. Interuniversitario de Investigación de Reconocimiento Molecular y Desarrollo Tecnológico (IDM), Uni-versitat Politècnica de València, Universitat de València, Spain.

b. CIBER de Bioingeniería, Biomateriales y Nanomedicina, Instituto de Salud Carlos III.

c. Institute for Research in Biomedicine (IRB Barcelona), Barcelona Institute of Science and Technology (BIST), Barcelona 08028, Spain.

d. Unidad Mixta de Investigación en Nanomedicina y Sensores, Universitat Politècnica de València, Instituto de Investigación Sanitaria La Fe, Spain.

e. Unidad Mixta UPV-CIPF de Investigación en Mecanismos de Enfermedades y Nanomedicina, Universitat Politècnica de València, Centro de Investigación Príncipe Felipe, Spain.

f. Catalan Institution for Research and Advanced Studies (ICREA), Barcelona 08010, Spain.

Published online: 31 January 2023

(Reprinted with permission from *ChemComm.*, **2023**, *59*, 2481 – 2484)

4.1 ABSTRACT

Kidney damage generates changes at phenotypic and genotypic levels that allow its monitoring using different biomarkers in blood, urine or serum. Among these biomarkers, kidney failure causes the urine overrepresentation of the alanine aminopeptidase (APN) enzyme. Here, we describe the design of a molecular probe (**NB-ALA**) based on Nile Blue fluorophore (NB), which can detect the APN enzyme in the urine by simple fluorometric measurements.

4.2 INTRODUCTION

The kidneys' primary function is to filter waste products from the blood and remove water excess. In addition, kidneys are responsible for preserving the balance of salts and minerals (such as calcium, phosphorus, sodium, and potassium), controlling blood pressure, regulating the production of erythropoietin to prevent anemia, and maintain the body homeostasis. However, kidneys are very sensitive organs that can suffer from a large number of pathologies that lead to renal fibrosis in the majority of cases. Early-stage detection of these diseases is of great importance because they usually progress over time, increasing the damage, and difficulting recovery treatments.[1,2]

One of the most common clinical complications in hospitalized and critically ill patients is acute kidney injury.[3] There are numerous factors that may predispose to the development of this disease, such as advanced age, chronic infections, diabetes, hypertension, immune disorders, underlying renal and hepatic problems, prostatic hypertrophy and bladder obstruction.[4]

Acute kidney injury is usually diagnosed by accumulation of end products of nitrogen metabolism (urea and creatinine) or by decreased urine output, or by both factors.[5] However, serum creatinine cannot be used as a sensitive early biomarker, since it requires a decrease in the glomerular filtration rate of at least 50% and a moderately long-time lag between this reduction and its translation into an increase in serum levels.[6,7] Moreover, these levels depend on multiple variables such as age, gender, diet, muscle metabolism, medication, or hydration. In the same way, serum urea levels may increase under certain conditions such as corticosteroid treatment, gastrointestinal bleeding, or a high-protein diet, limiting its use as renal dysfunction biomarker.[8,9] Besides of changes in creatinine or urea serum levels, kidney damage also induces urinary overrepresentation of the APN enzyme. Aminopeptidases

degrade the N-terminal residue of oligopeptides, producing smaller peptides and free amino acids. APN is an exopeptidase located in the renal microvillus membranes of the brush border/proximal renal epithelial cells and other plasmatic membranes within the intestine. Upon renal epithelium damage, enzymes such as APN are released and secreted into the urine.[10-12] For that, their presence in urine can be employed as a kidney degradation biomarker even when urinary macroglobulin remains in normal ranges, allowing its uses as an early biomarker of renal damage.[13,14] APN has also been used as a cancer biomarker, and several fluorogenic molecular probes had been developed for its monitoring.[15,16] However, APN detection in urine samples as potential early biomarker of kidney damage is a much less explored field (Table S1).[10,11]

Based on the above and in our interest in designing fluorogenic molecular probes for the detection of biomarkers,[17,18]we report herein the design and preparation of compound **NB-ALA**, which is a fluorescent APN probe based on Nile Blue (NB). NB is a low-cost commercial fluorophore, which meets the requirements established by the FDA for the use in humans, and whose emission band is centered in the near-infrared area (NIR).[19] **NB-ALA** can sensitively and selectively detect the APN enzyme in aqueous solutions and in doped urine. Besides, APN detection by **NB-ALA** is also validated in a murine model of acute kidney injury by direct urine fluorescence measurements (Figure 1).

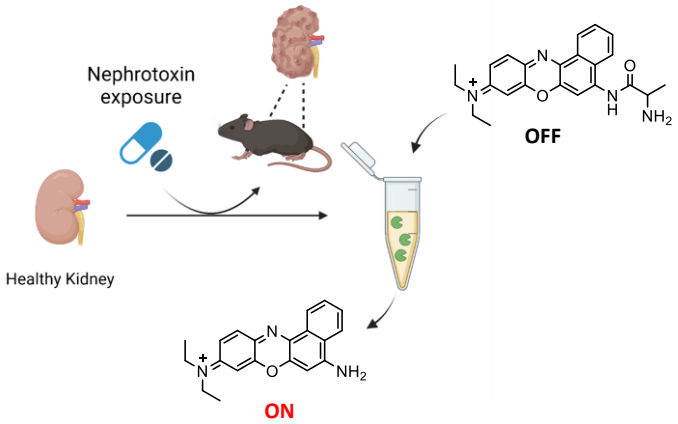

Figure 1. Schematic representation of the application of **NB-ALA** probe for the detection of kidney damage through urine samples.

4.3 RESULTS AND DISCUSSION

NB-ALA was synthetized using a two-steps protocol (Figure S1). In a first step, fluorenylmethyloxycarbonyl-L-alanine (Fmoc-Ala-OH) was covalently linked through the formation of an amide bond with the NB fluorophore. Then, in a second step, the fluorenylmethyloxycarbonyl protecting group (Fmoc) was removed with piperidine, yielding **NB-ALA** with a 31% global yield. **NB-ALA** and its intermediate were characterized by ^{1}H-NMR, ^{13}C-NMR and high-resoultion mass spectroscopy (HR-MS) (see Supporting Information). **NB-ALA** was designed in such a way that, after APN hydrolysis, NB was released (Figure 2A). H_2O-dimethyl sulfoside (DMSO) (99:1 v/v)solution of **NB-ALA** shows a weak emission band at 630 nm upon excitation at 530 nm ($\Phi_{\textbf{NB-ALA}}$ = 0.00028). However, in the presence of APN enzyme, a ca. 10-fold enhancement in emission band at 630 nm was observed (Figure 2B, Φ_{NB} = 0.01 and Table S2). This emission enhancement is ascribed to the APN-induced hydrolysis of **NB-ALA** probe, which yields free NB (Figure 2A).

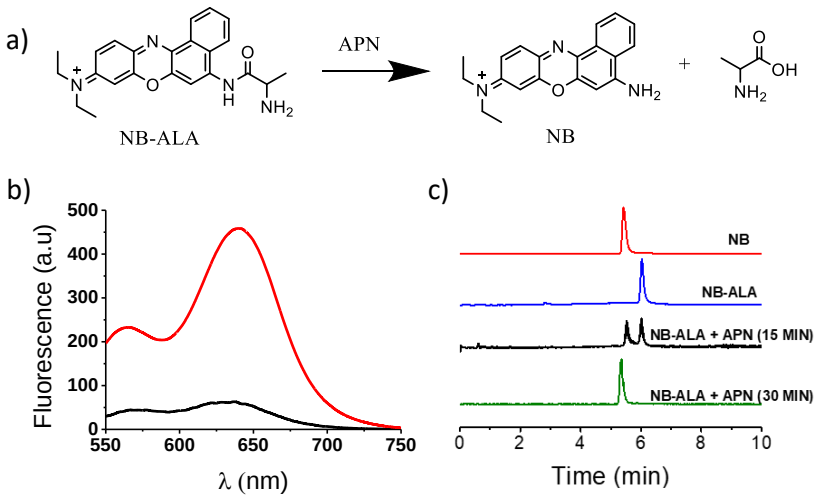

Figure 2. (A) APN-induced hydrolysis of the **NB-ALA** probe. (B) Fluorescence emission of **NB-ALA** (20 µM) + APN (2 µg/mL, 22.1 mU/mL) (red curve) and **NB-ALA** (20 µM) (black curve) in water/DMSO 99:1 v/v at pH 7.4 (λexc = 530 nm), after 30 minutes upon APN enzyme addition. (C) Chromatograms of aqueous free **NB-ALA** (20 µM) (blue), free NB (20 µM) (red), **NB-ALA** (20 µM) + APN (2 µg/mL, 22.1 mU/mL) after 15 minutes (black) and after 30 min (green) of enzyme addition. Conditions: KromasilC18 column, 0.7 mL/min, MeCN-methanol gradient elution from 70:30 v/v at 0 min to 50:50 v/v at 15 min.

HPLC-MS studies, carried out with **NB-ALA** probe alone or in the presence of APN enzyme, confirmed the proposed hydrolysis reaction. At this respect, chromatogram of the probe alone showed a single peak at 6.02 min, whereas after 15 min in the presence of enzyme, the intensity of this signal was reduced with the subsequent appearance of a new peak at 5.47 min, which was ascribed to NB formation upon **NB-ALA** hydrolysis (Figure 2C and S4). Besides, after 30 min of enzyme addition the 6.02 min peak of **NB-ALA** completely disappeared confirming the complete hydrolysis of the probe.

In an additional study, different amounts of APN were added to a solution of **NB-ALA** (H_2O-DMSO 99:1 v/v, 20 µM) and emission spectra (λ_{exc} = 530 nm) were recorded

after incubation of the samples at 37°C for 30 min. Activity of APN enzyme was calculated as 22.1 mU·mL^{-1}, using Ala-7-amido-4-methylcoumarin (Ala-AMC) as reference substrate (Figure S5 and equation S1). As shown in Figure 3A, a marked emission enhancement was observed proportional to the amount of the enzyme added and due to APN enzyme induced hydrolysis of **NB-ALA**, which the subsequent release of free NB. From these data, a LOD for APN as low as 1 ng·mL^{-1} was calculated using the equation S2 (Figure S6).

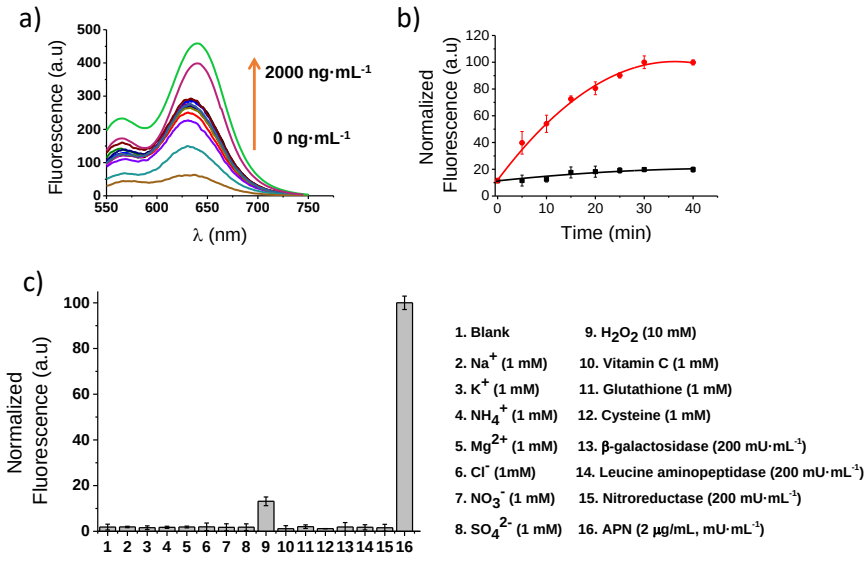

Figure 3. (A) Fluorescence emission spectra of **NB-ALA** (20 µM) in aqueous solution (H_2O-DMSO 99:1 v/v, pH 7.4) in the presence of different concentrations of APN enzyme (0-2000 ng·mL^{-1}). (B) Fluorescence of **NB-ALA** in (H_2O-DMSO 99:1 v/v, pH 7.4) at different time points in the absence (black curve) and in the presence of APN enzyme (2 µg·mL^{-1}) with an activity of 22.1 mU·mL^{-1} (red curve). Error bars are expressed as 3σ for three independent experiments. (C) Selectivity of **NB-ALA**. (H_2O-DMSO 99:1 v/v, pH 7.4). **NB-ALA** (20 µM) was incubated with the following interferents.

Additionally, a kinetic study of **NB-ALA** hydrolysis in the presence or absence of the APN enzyme (2 μg·mL^{-1}, 22.1 mU·mL^{-1}) was carried out (Figure 3B). Fluorescence emission of the **NB-ALA** solution (H_2O-DMSO 99:1 v/v, 20 μM) remained stable in the absence of APN enzyme. In sharp contrast, upon the addition of the APN enzyme (2 μg·mL^{-1}, 22.1 mU·mL^{-1}), a progressive fluorescence enhancement at 630 nm, due to NB, was observed reaching the maximum in ca. 30 min (Table S3). Finally, the emission response of **NB-ALA** in the presence of potentially interfering species such as anions, cations, small biomolecules (vitamin C, glutathione, cysteine) and enzymes (β-galactosidase, leucine aminopeptidase, nitroreductase, APN) was also tested (Figure 3C). The study demonstrated that only in the presence of APN a marked emission enhancement at 630 nm was observed.

Considering the promising results obtained with **NB-ALA** in aqueous solutions, we checked the ability of the probe to detect APN in a more clinically relevant environment. For this purpose, a human urine sample was collected from a healthy volunteer. The concentration of APN enzyme was negligible in this urine as confirmed using the aminopeptidase N/ANPEP Enzyme-linked immunosorbent assay (ELISA) kit (Table S4). In order to validate the ability of probe for APN enzyme detection in urine, **NB-ALA** was added to the human urine sample that was dopped with different amounts of APN (probe concentration 20 μM). Fluorescence signal was recorded after incubation at 37 °C for 30 min (Figure 4A). A progressive emission enhancement was obtained directly related to the amount of APN (5-fold at 2 μg·mL^{-1} of enzyme, 22.1 mU·mL^{-1}). From the obtained calibration curve (Figure 4B) a LOD of 5.4 ng·mL^{-1} for APN in doped human urine was calculated using the equation S2 (see Supporting Information).

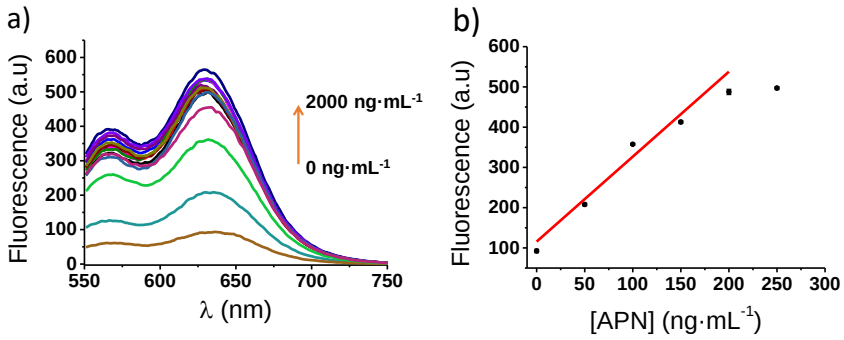

Figure 4. (A) Fluorescence emission spectra of **NB-ALA** in human urine samples (20 µM) doped with different concentrations of APN (0-2000 ng·mL^{-1}, 22.1 mU·mL^{-1}) after 30 min. (B) Calibration curve for APN concentration in urine. Error bars are expressed as 3σ for three independent experiments.

Subsequently, the urine sample was spiked with different amounts of APN (50, 100 and 200 ng·mL^{-1}), **NB-ALA** was added, and the mixture was incubated at 37 °C for 30 min. Finally, the emission at 630 nm was measured and the APN concentration was calculated using the calibration curve showed in Figure 4B. The obtained results are shown in Table 1. The probe **NB-ALA** successfully detected APN in human urine spiked with the enzyme with recoveries ranging from 98.5 to 99.0 %.

Table 1. Determination of APN in human urine.

APN spiked (ng/mL)	APN detected (ng/mL)	% of APN found by **NB-ALA**
50	49.5	99.0
100	98.5	98.5
200	97.8	98.9

To test the ability of **NB-ALA** to detect endogenous APN enzyme in a pre-clinical setting, urine samples from mice with acute kidney damage and fibrosis were evaluated. To generate an acute kidney damage, C57BL/6J mice were one time

injected intraperitoneally with a high concentration (250 mg·kg^{-1}) of folic acid (FA), which is a well-known experimental model of kidney damage.[20] The pathological features underlying FA-induced acute kidney injury are direct and indirect tubular damage and oxidative stress, which triggers tubular epithelial cell (TEC) necrosis, senescence, and cytokine release.[21] In this model, serum urea and serum creatinine levels were recover with time (or rather compensates while some renal damage remains) (Figure 5D)[22] and the only pathological reading that can be related with renal damage is urine density, which was monitored with time.

Urine samples of FA-treated mice were collected at 0 (control, CTR), 7 and 15 days after FA injection (Figure 5A). To analyse the animal model, mice were euthanized, kidneys harvested, and tissue sections were embedded in paraffin and stained with Sirius red/Fast green in order to visualize and quantify fibrosis (Figure 5B, 5C and S7). Control animals did not present signs of cortical fibrosis, whereas mice after 7 and 15 days of FA treatment developed fibrosis. In order to assess if fibrosis resulted in a decline of renal function, urine was collected, and their density measured (Figure 5E), showing a significative reduction in the values for sample of animals after 7 and 15 days of FA treatment, corroborating renal failure.

To validate the effectiveness of **NB-ALA** in determining kidney failure by APN detection, urine samples collected at 0, 7 and 15 days were treated with **NB-ALA** (final concentration of 20 μM) and incubated at 37°C for 30 min before fluorescence measure at 630 nm (λ_{exc} = 530 nm). Fluorescence measurements were performed without any previous treatment of urine. Interestingly, significant differences in fluorescence signal were found in urine samples 7 days after FA treatment (6-fold). Furthermore, urine samples from 15 days FA post-treatment showed an 11-fold enhancement, demostrating that **NB-ALA** can be used for the detection of renal damage in a mice model of kidney injury.

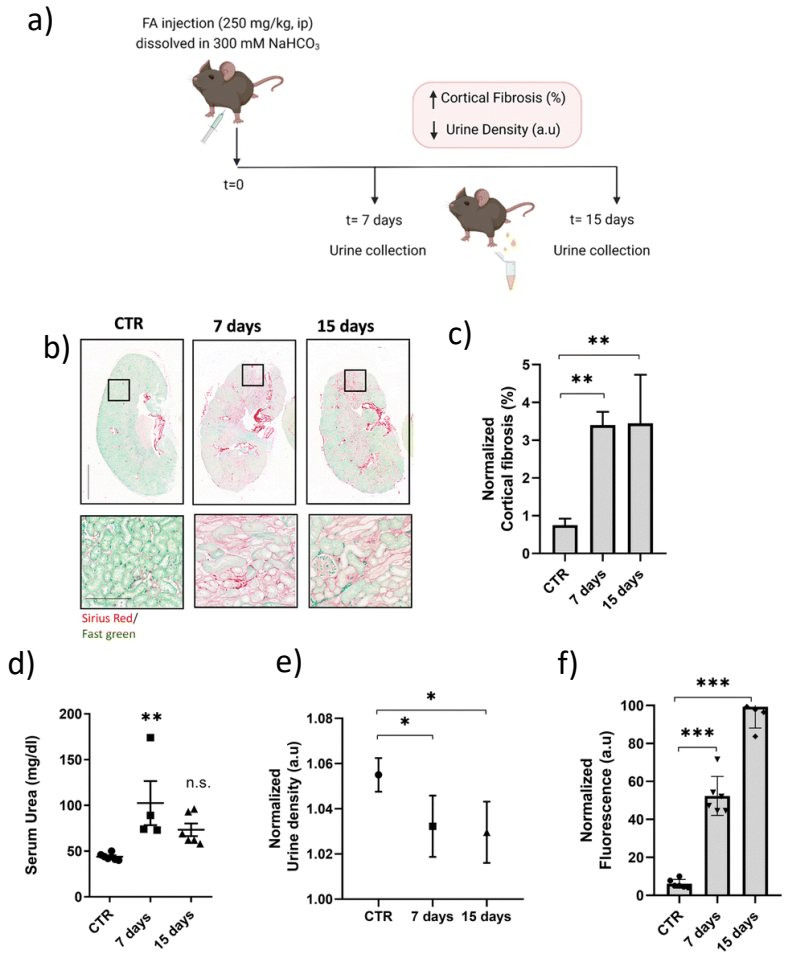

Figure 5. NB-ALA detection in urine of mice exposed to FA-induced kidney injury. (A) Timeline for the experimental procedure of FA–induced kidney injury. 8-10-week-old male BL6/J mice were treated intraperitoneally with 250 mg/kg folic acid dissolved in 300 mM sodium bicarbonate buffer. After 0, 7 and 15 days, urine was collected ("spot" urine) and mice were sacrificed. (B) Kidneys were harvested, paraffin-embedded, sectioned and stained for Sirius red/Fast green (fibrosis). Bar graphs within the upper row (whole kidneys) represents 250 mm and in the lower row (magnification) 250 nm. (C) Quantification of renal fibrosis. n=6;** P=0.0011. (D) Quantification of serum urea. For 7 days, n=4; ** P=0.0066 and for 15 days, n=6,

n.s. P=0.1183. (E) Urine density measured with a refractometer. n=6; * P=0.0113. (F) Fluorescence emission intensity of NB-ALA in urine samples. n=6; *** P < 0.001.

4.4 MATERIALS AND METHODS

Materials: NB, Fmoc-Ala-OH, 2-ethoxy-1-ethoxycarbonyl-1,2-dihydroquinoline (EEDQ), piperidine, triethylamine, DMSO, dichloromethane, $MgCl_2$, K_2CO_3, $NaHCO_3$, NH_4Cl, H_2O_2, vitamin C, glutathione, cysteine, β-galactosidase from *Escherichia coli*, phosphatase from bovine intestinal mucosa, nitroreductase from *Escherichia coli* and Leucine Aminopeptidase from porcine kidney (LAP) were obtained from Sigma-Aldrich. Recombinant Human Aminopeptidase N/CD13 Protein (APN) from mouse myeloma cell line, were purchased from R&D Systems. Invitrogen™ Human Aminopeptidase N/ANPEP ELISA Kit was obtained from Sigma-Aldrich. Urine samples employed for this work were from voluntary individuals and informed consents were obtained for experimentation. ^{1}H and ^{13}C NMR spectra were recorded on a Bruker FT-NMR Avance 400 (Ettlingen, Germany) spectrometer at 300 K, using TMS as an internal standard. Fluorescence spectroscopy was carried out in a JASCO spectrofluorometer FP-8500 and using a PerkinElmer multimode plate reader (EnSpire). Absorption spectra were collected in a JASCO V-650 spectrophotometer. HPLC-MS was recorded with an Agilent 1620 Infinity II HPLC coupled to a mass spectrometer Agilent Ultivo equipped with a triple QTOF detector.

Table S1. Comparison of the NB-ALA probe with other fluorescent probes for the detection of APN in urine as a biomarker of renal damage.

Probe	Excitation (nm)	Emission (nm)	Time (min)	LOD (water) ($ng \cdot mL^{-1}$)	LOD (urine) ($ng \cdot mL^{-1}$)	Lineal range ($ng \cdot mL^{-1}$)	*In vivo* model	
NB-ALA	530	630	30	0.5	2	0-200	Mice Folic Acid -Induced Acute Kidney Injury Model	This work
MUR2	480	590	60	Not reported	Not reported	0-100	Mice Cisplatin/ Doxorubicin-Induced Acute Kidney Injury Model	Pu et al, *Anal. Chem.* **2020**, 92, 8, 6166–6172
CVN	525	575/626	30	0.033	Not reported	0–6	Not reported	He et al, *Anal. Chem.* **2017**, 89, 5, 3217–3221

Synthesis and characterization of NB-ALA

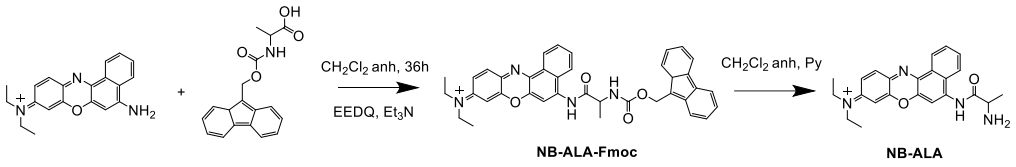

Figure S1. Synthetic route for the NB-ALA probe.

Synthesis of NB-ALA-Fmoc: Fmoc-Ala-OH (500 mg, 1.6 mmol), EEDQ (643 mg, 2.6 mmol), and triethylamine (360 µL, 2.6 mmol) were dissolved in dry dichloromethane (5 mL) with stirring at room temperature for 1 h. Then, NB (960 mg, 2.3 mmol) dissolved in dichloromethane (5 mL) was added and the reaction mixture was stirred

at room temperature for 36 h. The solvent was evaporated under reduced pressure and the residue was purified by silica gel chromatography with hexane as eluent, yielding compound **NB-ALA-Fmoc** (500 mg, yield 52%). ^{1}H NMR (400 MHz, $CDCl_3$) δ 8.69 (d, J = 4.7 Hz, 1H), 7.95 (d, J = 8.4 Hz, 1H), 7.88 (d, J = 8.0 Hz, 1H), 7.56 (d, J = 8.3 Hz, 2H), 7.48 (q, J = 8.0 Hz, 3H), 7.30 (t, J = 7.2 Hz, 2H), 7.20–7.04 (m, 4H), 6.52 (dd, J = 8.5, 6.1 Hz, 1H), 5.98 (dt, J = 14.3, 5.3 Hz, 1H), 4.14 (m, 1H), 3.93 (qd, J = 7.1, 2.0 Hz, 2H), 3.59–3.40 (m, 1H), 3.10 (d, J = 19.1 Hz, 1H), 1.83 (d, J = 7.6 Hz, 2H), 1.24–1.02 (m, 6H), 1.00–0.84 (m, 4H). ^{13}C NMR (101 MHz, $CDCl_3$) δ 143.79, 141.33, 129.53, 127.70, 127.06, 125.11, 124.08, 123.52, 119.99, 66.95, 61.37, 52.54, 47.23, 41.91, 31.93, 31.62, 29.70, 22.70, 21.89, 14.18. ESI-MS: theoretical ($M+H^+$): 611.72m/z; measured ($M+H^+$): 612.26 m/z.

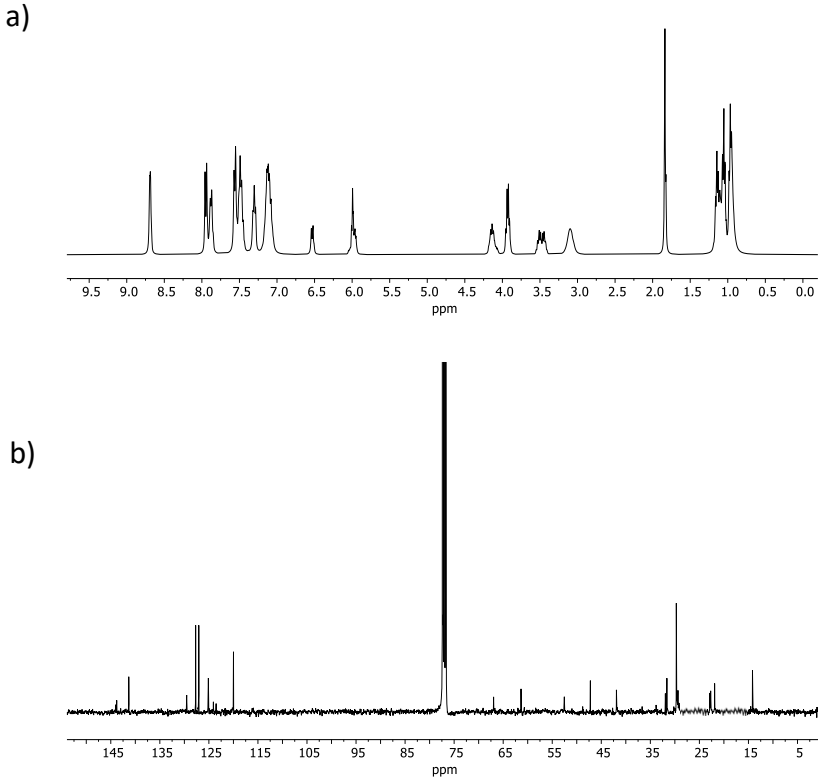

Figure S2. ^{1}H-NMR and ^{13}C-NMR of **NB-ALA-Fmoc**.

Synthesis of NB-ALA: Compound **NB-ALA-Fmoc** (500 mg, 0.8 mmol) was dissolved in CH_2Cl_2 (10 mL) containing piperidine (160 µL, 1.63 mmol) and stirred at room temperature overnight. The solvent was removed by evaporation under reduced pressure, and the crude product was purified by silica gel chromatography eluted with hexane-ethyl acetate (v/v, 1:1), affording probe **NB-ALA** (300 mg, yield 60%). ^{1}H NMR (400 MHz, $CDCl_3$) δ (ppm): 8.93 (d, J =2.9 Hz, 1H); 8.17 (d, J =8.1 Hz, 1H); 8.12 (d, J =8.6 Hz, 1H); 7.83 (d, J = 8.2 Hz, 1H); 7.2 (t, J =7.2 Hz, 1H); 7.55 (t, J = 13.5; 6.0 Hz, 1H); 7.41 (dd, J= 8.3; 4.2 Hz, 1H); 7.26 (s, 2H); 3.48 (dd, J=14.1; 7.0 Hz, 1H); 3.38 (dd, J=14.1; 7.1, 1H); 2.88 (s,1H); 1.55 (dd, J= 10.7; 5.4 Hz, 6H); 1.43 (dd, J=13,9; 8.8 Hz, 3H); 1.26 (d, J =6.1 Hz, 4H).^{13}C NMR (101 MHz, $CDCl_3$) δ (ppm): 150.91, 148.81,

136.52 , 129.95 , 128.78 , 128.26 , 127.01 , 121.55 , 53.51 , 30.16, 26.33 , 25.29. ESI-MS: theoretical ($M+H^+$): 389.47 m/z; ($M+H^+$) measured 390.18 m/z.

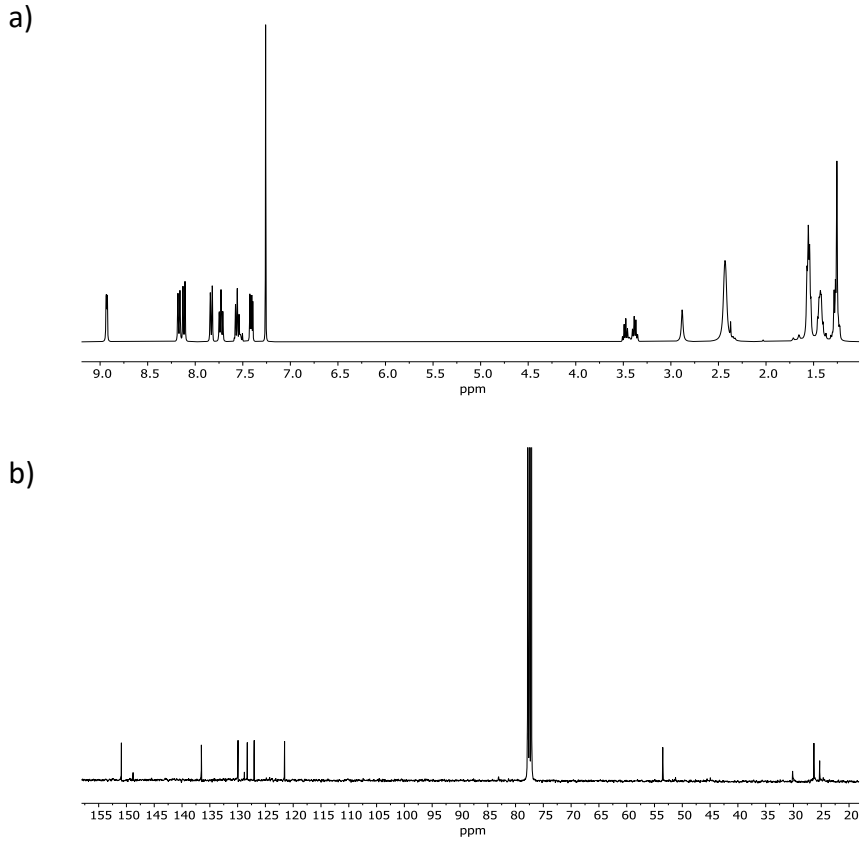

Figure S3. ^{1}H-NMR and ^{13}C-NMR of **NB-ALA**.

Photophysical characterization of NB and NB-ALA.

Molar extinction coefficients, stokes shift, and quantum yields were determined for **NB** and **NB-ALA** (Table S1). Quantum yields values were measured using **NB** dissolved in water as standard (Φ = 0.01)[23] while molar extinction coefficients were obtained in the adsorption maximum at 530 nm.

Table S2. Photophysical parameters for **NB**, **NB-ALA**

	NB	**NB-ALA**
Molar extinction coefficient [L·(mol·cm^{-1})$^{-1}$]	4.30 x 10^4	1005
Quantum yield	0.01	0.00028
Stokes shift	37	45

Hydrolysis of NB-ALA by APN.

4.5 µL of APN water solution were added to a water solution of **NB-ALA** (20 µM). Hydrolysis was monitored, after 15 min of incubation, through HPLC-MS measurements using a KromasilC18 column, 0.7 mL·min^{-1}, with MeCN: methanol gradient elution from 70:30 at 0 min to 50:50 at 15 min. Besides, chromatograms of **NB** and **NB-ALA** alone were also obtained using the same experimental conditions.

HPLC-MS characterization of NB and NB-ALA

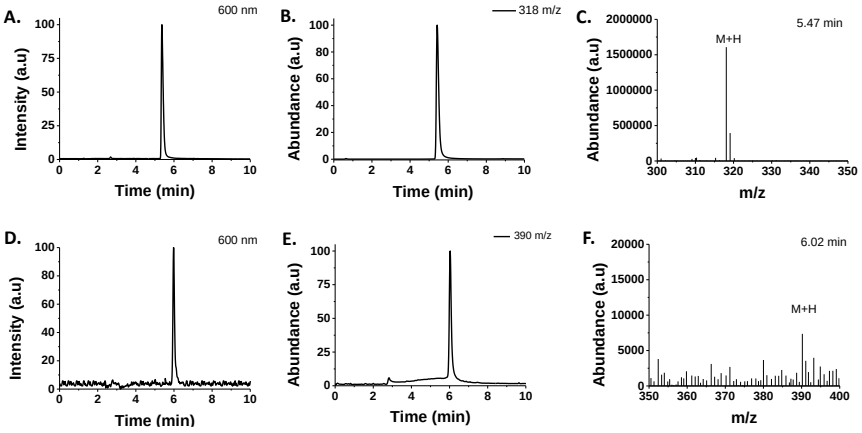

Figure S4. (A) UV chromatogram of **NB** at 600 nm; (B) Mass spectrum for **NB** obtained from the peak at 5.47 min; (C) Mass spectrum of B showing a signal at 318 m/z corresponding to M+H of **NB**; (D) UV chromatogram of **NB-ALA** at 600 nm; (E) Mass spectrum for **NB-ALA** obtained

from the peak at 6.02 min; (F) Mass spectrum of E showing a signal at 390 m/z corresponding to M+H of NB-ALA.

APN activity measurement.

The APN enzyme used in the different experiments have an activity of 22.1 mU·mL^{-1}. The activity of the enzyme was determined by its ability to cleave the fluorogenic peptide substrate Ala-AMC. For this purpose, solutions of 0.2 µg·mL^{-1} APN enzyme and 200 µM Ala-AMC in 50 mM trisaminometano buffer, pH 7.0 were prepared. Next, 50 µL of 0.2 µg·mL^{-1} APN enzyme was loaded onto a plate and the reaction was initiated by adding 50 µL of 200 µM Ala-AMC. An Ala-AMC blank containing 50 µL of assay buffer and 50 µL of substrate was included. Fluorescence on the multiplate reader (380 nm and 460 nm excitation and emission) in kinetic mode for 5 min was measured. Specific enzyme activity was determined using equation S1.

$$\textbf{Specific Activity}\ ((\text{pmol}\cdot\text{min}^{-1})\cdot\mu\text{g}^{-1}) = \frac{\textbf{Adjusted Vmax}^{*}\textbf{x Conversion Factor}^{**}}{\textbf{Amount of enzyme}} \quad (S1)$$

*Adjusted for substrate blank. **Derived using calibration standard Ala-AMC

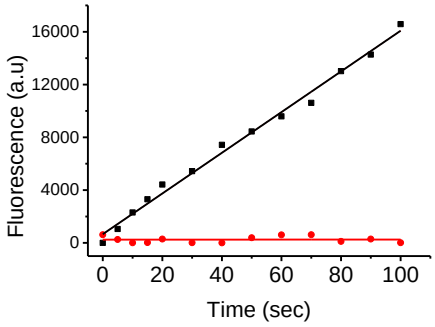

Figure S5. Monitoring of fluorescence at 460 nm due to alanine aminopeptidase activity, which induced the hydrolysis of fluorogenic peptide substrate Ala-7-amido-4-methyilcoumarin (Ala-AMC). Commercial enzyme solution (black) and blank (red).

General procedure for APN detection.

Fluorescence emission measurements of **NB-ALA** were carried out with 4.0 µL of the probe from a stock solution (1.0 x 10^{-3} M in DMSO), followed by addition of APN solution in water. Final volume was adjusted to 200 µL with distilled H_2O at pH 7.4. After incubation at 37°C for 30 min in a thermostat, solution was transferred to a quartz cell of 1 cm optical length to measure the fluorescence (λ_{ex} = 530 nm). A blank solution without APN was prepared and measured under the same conditions.

Calibration curve in water/DMSO.

LOD was obtained from the plot of fluorescence intensities at 630 nm upon excitation at 530 nm versus APN concentration in ng·mL^{-1}. LOD was calculated by using the equation (S2), where K=3; Sb is the standard deviation of the blank and *m* is the slope of the calibration curve. The resulting LOD was 1 ng·mL^{-1}.

$$LOD = K * \frac{Sb}{m} \text{ (S2)}$$

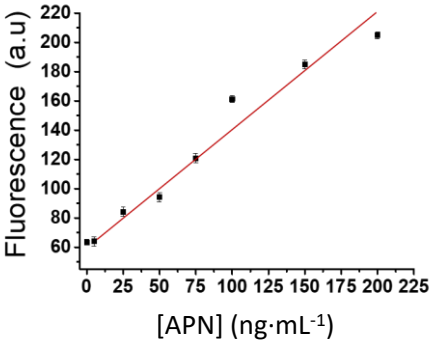

Figure S6. Calibration curve of NB-ALA (20 µM) at different APN concentrations in water-DMSO 99:1 v/v at pH 7.4. Fluorescence measures were taken 30 min after APN addition. Error bars are expressed as 3σ for three independent experiments.

Detection of NB-ALA in human doped urine.

Urine sample was taken from a healthy volunteer of 28 years old, from whom informed consent was obtained. In a common experiment of urine (10 µL) were diluted with distilled H_2O (1:20 v/v) and doped whit different amounts of APN followed by the addition of 4.0 µL of **NB-ALA** stock solution (1.0 x 10^{-3} M in DMSO). Distilled H_2O was added upon a final volume of 200 µL per vial. After incubation at 37°C for 30 min in a thermostat, the reaction solution was transferred to a quartz cell of 1 cm optical length to measure the fluorescence (λ_{ex}= 530 nm). Blank solutions without APN enzyme were prepared and measured under same conditions.

APN-induced hydrolysis of NB-ALA probe.

The emission intensity at 630 nm (excitation at 530 nm) after APN-induced hydrolysis of **NB-ALA** at different times and in the presence of different enzyme amounts was recorded. The obtained results are shown in Table S3.

Table S3. Hydrolysis of NB-ALA probe in the presence of several amounts of APN enzyme.

	Normalized Fluorescence at 630 nm (a.u.)			
Time (min)	0.05 ($\mu g \cdot mL^{-1}$)	0.2 ($\mu g \cdot mL^{-1}$)	1 ($\mu g \cdot mL^{-1}$)	2 ($\mu g \cdot mL^{-1}$)
0	0.18	6.40	11.79	11.50
5	0.67	9.28	21.33	39.78
10	1.29	12.63	30.81	54.01
15	1.82	21.58	38.09	72.52
20	15.89	27.30	49.19	80.55
30	24.19	35.93	53.40	90.16
40	36.56	47.14	66.70	99.99

50	46.89	58.50	83.10	-
60	59.83	63.36	-	-

Determination of APN in Urine by Human Aminopeptidase N/ANPEP ELISA Kit.

The concentration of APN in health human urine was determined by measuring the absorbance at 450 nm using a commercial Human Aminopeptidase N/ANPEP ELISA kit. A series of 100 µL of standard solutions of APN and 100 µL of diluted urine were added to the ELISA kit wells. After incubation with the antigen at room temperature for 2.5 h, the solution in each well was removed and washed 4 times with washing buffer, followed by addition of 100 µL of biotin conjugate and incubation at room temperature for 1 h. Later, all of the wells were washed 4 times with 300 µL of the washing buffer. Then, 100 µL of Streptavidin-HRP solution was added to each well and incubated at room temperature for 45 min. After that, all of the wells were washed 4 times with 300 µL of the washing buffer, followed by addition of 100 µL of 3,3',5,5'-Tetramethylbenzidine color developing agent solution. After further incubation at room temperature for 30 min in the dark, 50 µL of stop solution was added to each well, and the absorbance of each well was measured immediately on a microplate reader at 450 nm (see Table S4).

Table S4. APN in human urine determined by a human aminopeptidase N/ANPEP ELISA kit.

APN spiked ($ng \cdot mL^{-1}$)	APN detected by ELISA ($ng \cdot mL^{-1}$)	% of APN found by ELISA
0	0.10	-
1.0	0.98	98.0
2.5	2.41	96.0
5.0	4.85	97.0

Mouse model.

C57BL/6J male mice were maintained at the Institut de Recerca Biomèdica (IRB). All animal procedures were carried out in compliance with the regulations of the Animal Care and Use Ethical Committee of the Barcelona Science Park (CEEA-PCB) and the Catalan Government under the recommendations of the FELASA (11054-P2). To generate renal fibrosis, 8-10-week-old male C57BL/6J mice were treated intraperitoneally once with a high dose (250 $mg \cdot kg^{-1}$ body weight) of folic aci; dissolved in 300 mM sodium bicarbonate. After 2 days, blood was taken by puncturing the sub-mandibular vein and serum was generated (centrifugation of blood samples at 2500 g at room temperature for 15 min). Mice were monitored longitudinally by measuring the body weight and urine. Urine was taken in the early evening (= spot urine) and urine density was determined using a refractometer. At 7 and 15 days, mice were sacrificed, and kidneys were harvested, paraffin-embedded and sectioned. Sections were stored at room temperature until histochemical staining's were performed with a single dose of either 250 $mg \cdot kg^{-1}$ of FA or vehicle. Sirius red/ fast green staining was performed in order to corroborate the presence of renal fibrosis. Briefly, paraffin-embedded 6 µm kidney slides were incubated with the mordant thiosemicarbazide 99% for 10 min. Then they were washed in distilled water for 10 min prior incubation with 0.1% Fast green for 20 min and rinsed with 1% acetic acid for 1 min. Finally, the stained samples were dehydrated and mounted with Mounting Medium, toluene-free using a Dako CoverStainer.

Acute injury mice model characterization

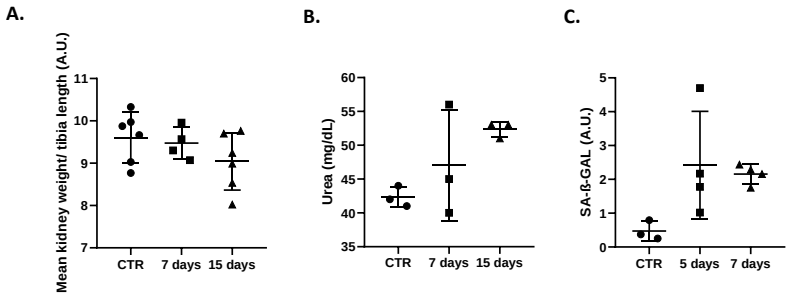

Figure S7. Macroscopic phenotyping (A), biochemical phenotyping (B) and senescence phenotyping for acute injury mice (C).

4.5 CONCLUSIONS

In summary, we show herein the synthesis and characterization of **NB-ALA**, a NIR fluorescent probe for APN detection. **NB-ALA** is weakly emissive, however, in the presence of APN enzyme, **NB-ALA** is hydrolyzed releasing the highly emissive NB fluorophore. **NB-ALA** was functional in water and in APN-doped human urine samples. Additionally, **NB-ALA** probe was validated in a murine renal fibrosis model induced by FA. Emission signal was only observed in urine from fibrotic kidneys of FA-treated mice. This study demonstrates the potential applications of **NB-ALA** probe for the sensitive and selective detection of APN to non-invasively determine the burden of renal damage. **NB-ALA** is a promising probe that could be employed for a range of applications including the monitoring of treatments with nephrotoxic drugs that induce acute kidney damage or to determine regeneration after renal damage.

ACKNOWLEDGEMENTS

The authors thank the Spanish Government (PID2021-126304OB-C41) and the Generalitat Valenciana (PROMETEO CIPROM/2021/007) for support. Thank the

financial support from the FEDER found of European Union (IDIFEDER/2021/044). This work was also supported by CIBER-Consorcio Centro de Investigación Biomédica en Red-(CB06/01/2012), Instituto de Salud Carlos III, Ministerio de Ciencia e Innovación. M. D. -R. thanks to his predoctoral fellowship Grisolias to the Genelalitat Valenciana (GRISOLIAP/2019/144). J.F.B. thanks to his postdoctoral fellowship Sara Borrell from ISCIII (CD19/00038).

4.6 REFERENCES

1. J. G. Abuelo, N. *Engl. J. Med.* **2007**, *357*, 797–805.
2. L. He, Q. Wei, J. Liu, et al., Kidney Int. **2017**, *92*, 1071-1083.
3. J.A. Kellum, P. Romagnani, G. Ashuntantang, C. Ronco, A. Zarbock, H. -J. Anders, *Nat. Rev. Dis. Primers.* **2021**, *7*, 52.
4. S. M. Bagshaw, R. Bellomo, *Curr. Opin. Crit. Care*. **2007**, *13*, 638-644.
5. J. Y. C. Soo, J. Jansen, R. Masereeuw, M. H. Little, *Nat. Rev. Nephrol.* **2018**, *14*, 378–393.
6. X. Wang, et al., *J. Am. Soc. Nephrol.* **2006**, *17*, 2900–2909.
7. P. K. Bhatraju, et al., *JAMA Netw. Open*. **2020**, *3,* 1-12.
8. M. A. Perazella, S. G. Coca, *Nat. Rev. Nephrol.* **2013**, *9*, 484–490.
9. O. Dong-Jin, *Renal failure*. **2020**, *42*, 154-165.
10. P. Cheng, Q. Miao, J. Huang, J. Li, K. Pu, *Anal. Chem.* **2020**, *92*, 6166−6172.
11. X. He, Y. Xu, W. Shi, H. Ma, *Anal. Chem.* **2017**, *89*, 3217–3221.
12. L. Z. Chen, W. Sun, W. H. Li, J. Li, L. P. Du, W. F. Xu, H. Fang, M. Y. Li, *Anal. Methods*. **2012**, *4*, 2661−2663.
13. L. Z. Chen, W. Sun, J. Li, Z. Z. Liu, Z. Ma, W. Zhang, L. P. Du, W. F. Xu, H. Fang, M. Y. Li, *Org. Biomol. Chem.* **2013**, *11*, 378−382.
14. J. Li, L. Z. Chen, W. X. Wu, W. Zhang, Z. Ma, Y. N. Cheng, L. P. Du, M. Y. Li, *Anal. Chem.* **2014**, *86*, 2747−2751.

15. H. Li, Q. Yao, W. Sun, K. Shao, Y. Lu, J. Chung, D. Kim; J. Fan, S. Long, J. Du, Y. Li, J. Wang, J. Yoon, X. Peng, *J. Am. Chem. Soc.* **2020**, *142*, 6381-6389.

16. X. Zhou, H. Li, Ch. Shi, F. Xu, Z. Zhang, Q. Yao, H. Ma, W. Sun, K. Shao, J. Du, S. Long, J. Fan, J. Wang, X. Peng, *Biomaterials*. **2020**, *253*, 120089.

17. M. Xiao, W. Sun, J. Fan, J. Cao, Y. Li, K. Shao, M. Li, X. Li, Y. Kang, W. Zhang, S. Long, J. Du, X. Peng, *Adv. Funct. Mater*. **2018**, *1805128*, 1-9.

18. W. Sun, Sh. Guo, Ch. Hu, J. Fan, X. Peng, *Chem. Rev.* **2016**, *116*, 7768–7817.

19. J. Mérian, J. Gravier, F. Navarro, I. Texier, *Molecules*. **2012**, *17*, 564 – 5591.

20. Zh. Hu, H. Zhang, Sh. Yang, X. Wu, D. He, K. Cao, W. Zhang, *Oxid. Med. Cell. Longev.* **2019**, *2019*, 1-8.

21. O.E. Aparicio-Trejo, P. Rojas-Morales, S.H. Avila-Rojas, J.C. León-Contreras, R. Hernández-Pando, A.P. Jiménez-Uribe, R. Prieto-Carrasco, L.G. Sánchez-Lozada, J. Pedraza-Chaverri, E. Tapia, *Int. J. Mol. Sci.* **2020**, *21*, 1-19.

22. J. A. Kellum, *Crit. Care Clin.* **2015**, *31*, 621-32.Jose, J., Ueno, Y., & Burgess, K. *Chem. Eur. J.*, **2009**, *15*, 418-423.

Chapter 5| Leucine aminopeptidase (LAP) activatable nile blue-based NIR fluorescent probe for cancer detection.

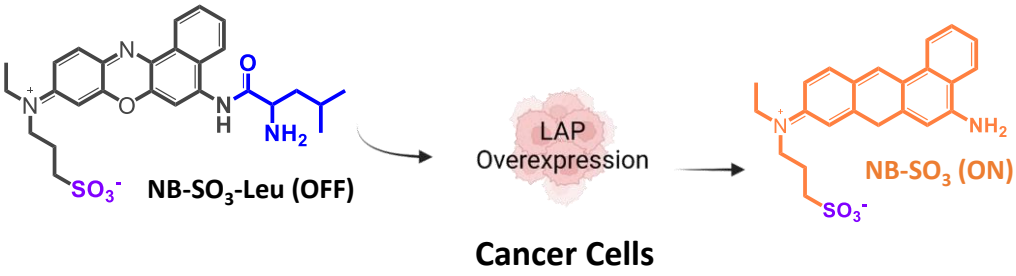

Leucine aminopeptidase (LAP) activatable nile blue-based NIR fluorescent probe for cancer detection.

Marcia Domínguez,[a,b] David Azorín-Soriano,[a,c] Vicente Martí-Centelles,[a,b] Alba García-Fernández,[a,b,c] Juan F. Blandez,[a,b,d,e] Félix Sancenón,[a,b,c,d,*] and Ramón Martínez-Máñez[a,b,c,d,*]

a. Instituto Interuniversitario de Investigación de Reconocimiento Molecular y Desarrollo Tecnológico (IDM), Universitat Politècnica de València, Universitat de València, Spain.
b. CIBER de Bioingeniería, Biomateriales y Nanomedicina, Instituto de Salud Carlos III.
c. Unidad Mixta UPV-CIPF de Investigación en Mecanismos de Enfermedades y Nanomedicina, Universitat Politècnica de València, Centro de Investigación Príncipe Felipe, Spain.
d. Unidad Mixta de Investigación en Nanomedicina y Sensores, Universitat Politècnica de València, Instituto de Investigación Sanitaria La Fe, Spain.
e. Department of Chemical Engineering and Biotechnology, University of Cambridge, Philippa Fawcett Dr, Cambridge CB3 0AS.

5.1 ABSTRACT

Leucine aminopeptidase (LAP) is one of the most widely used cancer biomarkers, being overexpressed in many cancer types. Here, we report the design and synthesis of a NIR fluorescent probe (**NB-SO_3-Leu**) based on NB fluorophore skeleton modified with sulfonic groups to increase its solubility, facilitating cellular trafficking. NB was selected as signaling unit due to its unique features because is a FDA approved fluorophore for its use in humans. Besides, its emission wavelength in the NIF-I window avoids the overlap with the strong autofluorescence signal of cancer cells. The ability of the **NB-SO_3-Leu** probe to detect LAP enzyme is successfully tested in PBS-DMSO solutions. The initial low-fluorescence signal of **NB-SO_3-Leu** shows a marked 4-fold enhancement when probe was incubated with LAP enzyme for 15 minutes. **NB-SO_3-Leu** has a LOD of 7.2 ng·mL^{-1} for LAP enzyme. **NB-SO_3-Leu** probe is also successfully validated *in vitro* in SK-Mel-103 cells (human melanoma cells), characterized by high endogenous levels of LAP. Our study demonstrates the high potential of **NB-SO_3-Leu** for the selective and sensitive detection of LAP overexpression *in vitro*.

5.2 INTRODUCTION

According to studies conducted by the World Health Organization (WHO), it is expected that by 2035 there will be 24 million new cases of cancer worldwide and more than 14.5 million cancer-related deaths per year. Approximately, 30% of these lives could be saved with an early diagnosis, pointing out the great importance of improve cancer early diagnostic tools.[1] Among developed techniques for early diagnosis, those based on the evaluation of cancer-related biomarkers are becoming established as the most promising for detection and treatment monitoring.[2] A large number of potential cancer biomarkers have been described in recent years. Among them, overexpressed enzymes are gaining interest due to the important roles that play in both, physiological and pathological processes. In the same way, not only the levels of the enzymes, but also their location, intra- or extracellular, or their accumulation at subcellular level can allow determining the presence of a wrong homeostasis state. The importance of deregulated enzymes in cancer process underlines the need of developing techniques that allow their easy, sensitive, and selective detection. Fluorescence measurements stand out among these techniques, as they have high selectivity and sensitivity with good spatio-temporal resolution and are usually low-cost procedures, which do not require specialised personnel or expensive equipment. However, a number of problems remain unresolved. One main drawback in the use of fluorescent probes is the shallow tissue depth at which they can be used, as tissues are not transparent to fluorescent radiation, cornering techniques that exploit this effect only for surface measurements. To overlap this problem, some researchs have been directed towards the development of NIR fluorophores. However, molecules with this characteristic are usually based on fused aromatic rings, which drastically decreases their solubility in biofluids and increases their toxicity, making them difficult to be used *in vivo*.[3-5] Moreover, most developed

probes are mainly eliminated by the RES, which leads to their accumulation in the liver and spleen with the consequent potential organ toxicity and side effects, which is also an important drawback.[6] To dodge this elimination route, it has been reported that the presence of zwitterionic moieties on a fluorophore structure promotes its renal excretion, reducing fluorophore binding to proteins and nonspecific uptake in normal tissues.[7-9] These features have been used to design probes that can be activated in tissues or cell *in vivo,* and subsequently excreted in urine, allowing direct measurement of probe fluorescence in this biofluid and, consequently, a non-invasive detection of the biomarker.[10-12] However, this concept has not been widely employed.

LAP, one of the most extensive exopeptidases in the body, has become one of the most relevant biomarkers in early cancer detection.[13] LAP is an enzyme that catalyzes the hydrolysis of peptide bonds, in which the amino group at the N-terminal position of a peptide or protein is a leucine.[14] In addition, LAP performs the split up of the peptide bond between terminal leucine and the following amino acid in the chain, releasing the free leucine amino acid with an amine group (leucinamide). LAP is involved in a large number of physiological and pathological progressions such as tumour cell proliferation, invasion, and drug resistance,[15] processes that are characterized by an important LAP overexpression.[16] Several studies have corroborated a direct relationship between high LAP levels and cancer disease. High levels of LAP in tissues have been reported in epithelial ovarian cancer, breast cancer, liver cancer and skin cancer (specifically melanoma).[17-19] A particularly important example is LAP overexpression in melanoma, for which early detection is essential for resection treatment. However, due to the aggressiveness of this type of cancer, tumoral cells rapidly spreads progressing to a metastatic stage with limited therapeutic options.[21,22] Besides, LAP enzyme has been described as a decisive regulator of vascular endothelial growth factor (VEGF), a protein that stimulates

angiogenesis. Some studies have verified that VEGF levels are higher in patients with melanoma, being correlated with tumour progression.[23] Therefore, LAP enzyme can be involved in melanoma progression by increasing VEGF production with the subsequent tumour angiogenesis and invasion. These findings suggest that LAP can not only be used as an early biomarker of melanoma, yet its level might allow monitoring melanoma progression and longitudinal studies in melanoma treaments. Highly selective fluorescent probes have been developed for the *in vitro* and *in vivo* detection of high levels of LAP, most of them containing a leucinamide moiety directly linked to a highly emissive fluorophore (Table S1). Generally, these probes presented a weak fluorescence, due to the presence of the leucinamide directly linked with the fluorophore (OFF state), yet hydrolysis in the presence of LAP results in a restoration of the fluorophre emission (ON state).[24-26] However, these probes display some of the problems described above (such as poor solubility, accumulation and poor renal excretion).

In line with the above-discussed ideas, we report herein the synthesis and characterization of a molecular fluorescent probe (**NB-SO_3-Leu**) for the detection of LAP and its possible application for early-cancer detection. This probe is based on the NB fluorophore chemically modified with a sulfonic group to originate a zwitterionic structure, and a leucine derivative as LAP substrate. The probe (**NB-SO_3-Leu**) shows a weak emission which increases markedly in the presence of the LAP enzyme due to LAP-induced hydrolysis that results in a highly emissive NB derivative (NB-SO_3). Prospective *in vitro* studies with SK-Mel-103 melanoma cells indicate the possibility of using the **NB-SO_3-Leu** probe in cancer detection protocols.

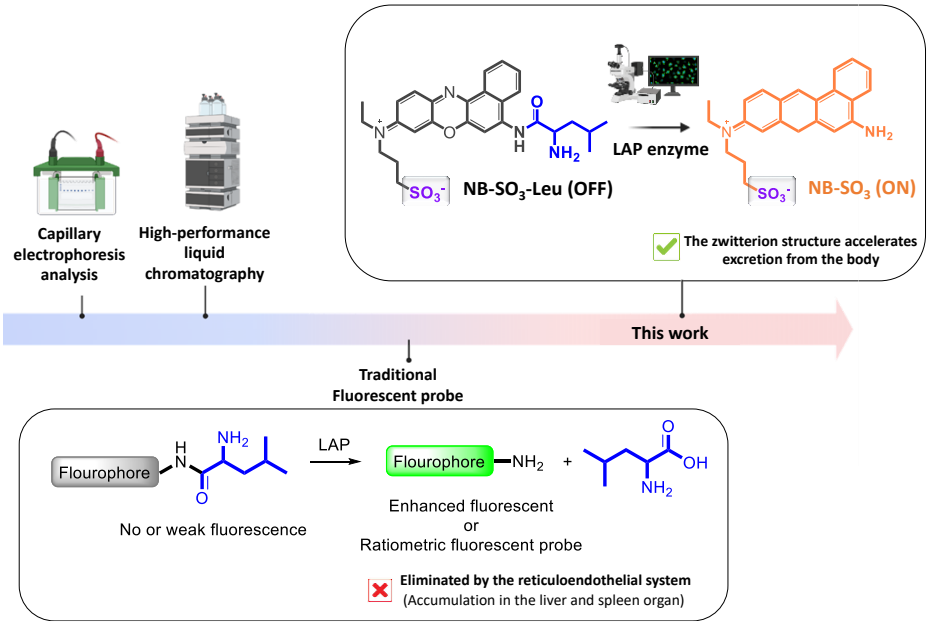

Figure 1. Different protocols developed for the detection of LAP enzyme as a cancer biomarker including the fluorescent probe **NB-SO$_3$-Leu** proposed in the present work.

5.3 RESULTS AND DISCUSSION

NB-SO$_3$ fluorophore was synthesized following the procedure shown in Figure 2a. In a first step, 3-aminophenol was alkylated with iodoethane by an S_N2 reaction, yielding (3-ethylamino) phenol (**1**). Next, compound **1** reacted with 1,3-propanesultone, again by a bimolecular nucleophilic substitution (S_N2) reaction, yielding the sulfonic acid derivative **2**. Then, in a third step, compound **2** was nitrosylated with sodium nitrite to obtain product **3**. Finally, NB-SO$_3$ fluorophore was obtained by a condensation reaction between **3** and 1-naphthylamine (68% global yield). In addition, the **NB-SO$_3$-Leu** probe was synthetized from NB-SO$_3$ fluorophore using a two-step protocol (Figure 2b). In the first step, tert-butyloxycarbonyl-L-leucine (Boc-Leu-OH) was covalently linked, through the formation of an amide bond,

with the NB-SO_3 fluorophore. Then, in a second step, the tert-butyloxycarbonyl (Boc) protecting group was removed with trifluoroacetic acid, yielding **NB-SO_3-Leu** (55% global yield). NB-SO_3 fluorophore, **NB-SO_3-Leu** probe and the intermediates were further characterized by ^{1}H-NMR, ^{13}C-NMR and HRMS (Figure S1-S6).

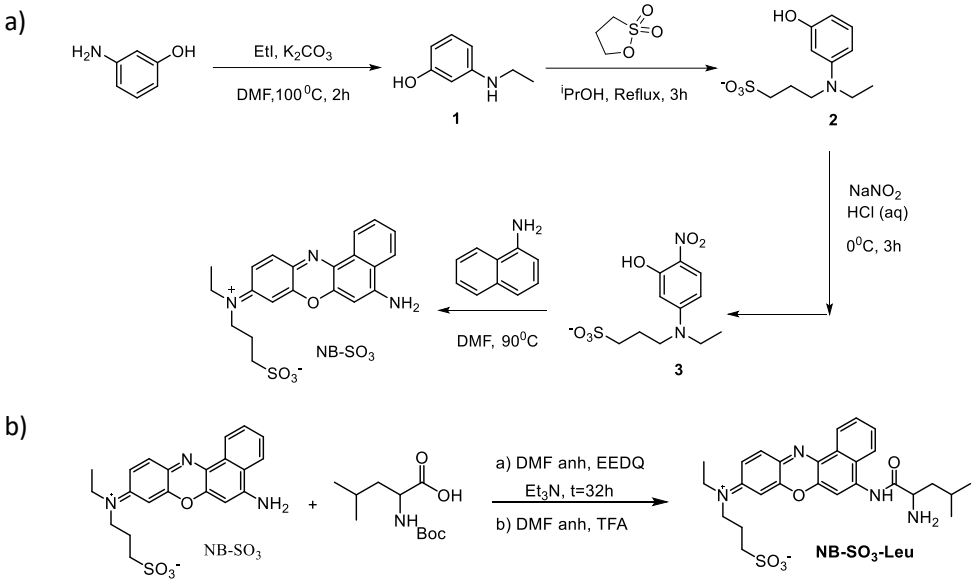

Figure 2. (a) Synthesis of NB-SO_3 fluorophore. (b) Synthetic sequence used to prepare **NB-SO_3-Leu** probe.

NB-SO_3-Leu was designed in such a way that, in the presence of LAP enzyme, its hydrolysis releases the highly emissive NB-SO_3 fluorophore (Figure 3a). Dealing with the photophysical features of NB-SO_3, PBS-DMSO 99:1 v/v (pH 7.4) solutions of the fluorophore (5 µM) showed a marked emission band at 660 nm (λ_{ex} = 630 nm, $\Phi_{NB\text{-}SO_3}$= 0.0730). Besides, the emission of NB-SO_3 fluorophore (5 µM in PBS-DMSO, 99:1 v/v) remained unchanged in the 5.0-9.0 pH interval (Figure S7), which is a suitable characteristic for its use in biological media. In marked contrast, PBS-DMSO 99:1 v/v (pH 7.4) solutions of **NB-SO_3-Leu** probe (5 µM) show a weak emission band at ca. 660

nm (λ_{exc} = 630 nm, $\Phi_{\text{NB-SO}_3\text{-Leu}}$ = 0. 0002) (Table S2). This reduced emission of the **NB-SO$_3$-Leu** probe is ascribed to the presence of an alanine residue directly linked, through an amide bond, with the NB-SO_3 fluorophore, which quenches its emission through ICT.[27]

To determine the capability of **NB-SO$_3$-Leu** probe to detect the LAP enzyme, further fluorescence studies were carried out. Emission of **NB-SO$_3$-Leu** in PBS-DMSO 99:1 v/v was monitored in the presence and absence of the LAP enzyme. A marked emission enhancement was observed at ca. 660 nm (λ_{exc} = 630 nm) (Figure 3b). Emission enhancement was ascribed to the proposed mechanism, in which LAP-induced hydrolysis of **NB-SO$_3$-Leu** probe yielded the highly emissive NB-SO_3 fluorophore. LAP-induced enzymatic hydrolysis of **NB-SO$_3$-Leu** probe was also corroborated through HPLC studies (Figure 3c). As could be seen in Figure 3c, HPLC chromatograms of **NB-SO$_3$-Leu** probe (5 μM) in PBS-DMSO 99:1 v/v (pH 7.4) showed a single peak at 12.3 min. However, after probe incubation with LAP enzyme for 10 min, a marked reduction of the **NB-SO$_3$-Leu** peak and the appearance of a new signal at 17.4 min was observed (see also Figure 3c), which corresponds to the NB-SO_3 fluorophore.

On the other hand, a kinetic study of **NB-SO$_3$-Leu** probe hydrolysis in the presence or absence of the LAP enzyme was carried out (Figure 3d and Figure S8). As could be seen in Figure 3d, the weak fluorescence emission of the **NB-SO$_3$-Leu** probe (PBS-DMSO 99:1 v/v at pH 7.4) remained practically unchanged in the absence of LAP enzyme. However, **NB-SO$_3$-Leu** probe incubation with LAP enzyme (750 ng·mL^{-1}) shows a progressive fluorescence enhancement centered at 660 nm that reached the maximum value 15 min after enzyme addition (4-fold).

Changes in fluorescence emission intensity of **NB-SO$_3$-Leu** probe were also monitored in the presence of increasing concentrations of LAP enzyme (0-750 ng·mL^{-1}). Samples were incubated with LAP for 15 minutes at 37°C before monitoring the

emission intensity at 660 nm. As shown in Figure 3e, the fluorescence emission recorded at 660 nm (λ_{exc} = 630 nm) was enhanced as a function of the increase in the amount of the LAP enzyme added. The calibration curve obtained from these data exhibits a linear range from 0 to 40.0 ng LAP·mL^{-1} (R^2 = 0.97) with LOD 7.2 ng·mL^{-1} and a LOQ of 21.8 ng·mL^{-1} (equation 1) (Figure 3f).

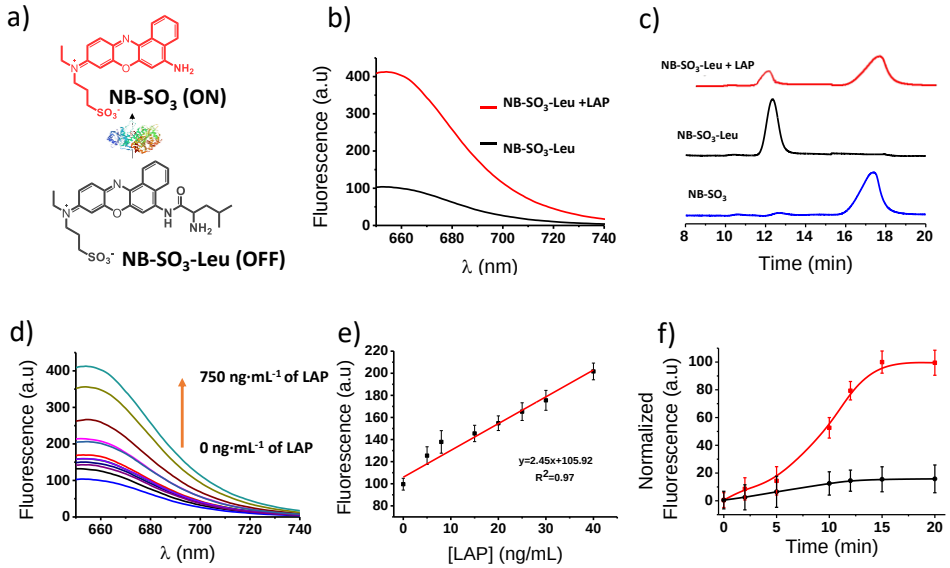

Figure 3. (a) LAP-induced hydrolysis of **NB-SO$_3$-Leu** probe. (b) Fluorescence emission **of NB-SO$_3$-Leu** (5 µM) + LAP (750 ng·mL^{-1}) (red curve) and **NB-SO$_3$-Leu** (5 µM) (black curve) in PBS-DMSO 99:1 v/v at pH 7.4 (λexc = 630 nm), after 15 min upon LAP enzyme addition. (c) Chromatograms of **NB-SO$_3$-Leu** (5 µM) + LAP (750 ng·mL^{-1}) after 10 min upon enzyme incubation (red curve), **NB-SO$_3$-Leu** (black curve) and NB-SO$_3$ (5 µM) (blue curve) in PBS-DMSO 99:1 v/v at pH 7.4. Conditions: ODS Hypersil column, 1.8 mL·min^{-1}, Buffer (0.2 M of KH_2PO_4 solution, pH = 3 ± 0.1)-MeCN-Ethanol (90:10:2 v/v/v) elution at 20 min. (d) Fluorescence of **NB-SO$_3$-Leu** (5 µM) in (PBS–DMSO 99: 1 v/v, pH 7.4) at different time points in the absence (black curve) and in the presence of LAP enzyme (750 ng·mL^{-1}) (red curve). (e) Fluorescence emission spectra of **NB-SO$_3$-Leu** (5 µM) in PBS-DMSO 99:1 v/v, pH 7.4 in the presence of different concentrations of LAP enzyme (0-750 ng·mL^{-1}). (f) Calibration curve of **NB-SO$_3$-Leu** (5 µM) at different APN

concentrations in PBS-DMSO 99:1 v/v at pH 7.4. Fluorescence measurements were taken 15 min after LAP addition. Error bars are expressed as 3σ for three independent experiments.

To determine the selectivity of **NB-SO_3-Leu**, the probe was incubated with several potentially interfering species (including cations, small biomolecules and other enzymes).[28] Only in the presence of LAP enzyme, a marked emission at 660 nm was recorded (Figure 4a). To further assess the sensing mechanism, **NB-SO_3-Leu** probe was incubated with LAP in the presence of bestatin, a well-known competitive reversible inhibitor of LAP.[29] While a strong fluorescence is recorded at 660 nm upon probe incubation with LAP enzyme, this signal is reduced 2.4-fold when the probe is incubated with LAP enzyme in the presence of bestatin (Figure 4b).

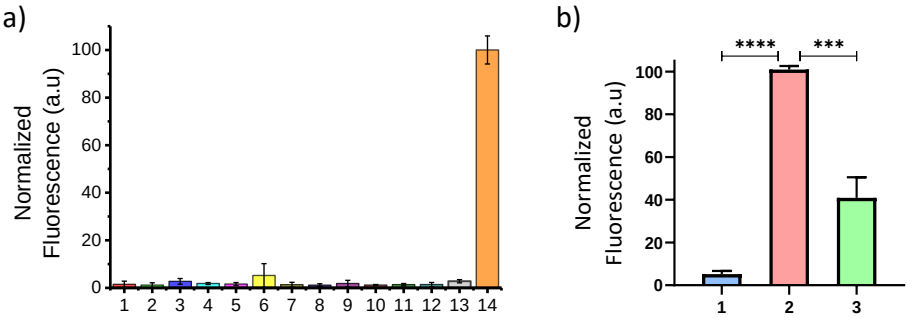

Figure 4. (a) Fluorescence emission of **NB-SO_3-Leu** (5 μM) in PBS-DMSO 99:1 v/v at pH 7.4 in the presence of different interferents at 660 nm (excitation at 630 nm): 1.Blank (5 μM); 2. Ca^{2+} (1 mM); 3. Fe^{3+} (1 mM); 4. Mg^{2+} (1 mM); 5. Mn^{2+} (1 mM); 6. H_2O_2 (10 mM); 7. Glutathione (1 mM); 8. Cysteine (1 mM); 9. Monoamine oxidase-A (100 mgmL); 10. α-Glutamyltransferase (100 mg·mL^{-1}); 11. Nitroreductase (100 mg·mL^{-1}); 12. Arginine (1 mM); 13. Glycine (1 mM); 14. LAP (750 ng·mL^{-1}). (B) Fluorescence at 660 nm of: (1) **NB-SO_3-Leu** (5 μM) alone, (2) **NB-SO_3-Leu** (5 μM) + LAP (750 ng·mL^{-1}) and (3) **NB-SO_3-Leu** (5 μM) + LAP (750 ng·mL^{-1}) + bestatin (100 μM) in PBS-DMSO 99:1 v/v at pH 7.4. Error bars are expressed as 3σ for three independent experiments. Values are expressed as mean ± SD. Statistical analysis was assessed by applying Student's T-test (****p< 0.0001, ***p< 0.05).

Encouraged by the high sensitivity and selectivity of **NB-SO$_3$-Leu** toward LAP detection, *in vitro* studies were carried out using SK-Mel-103 cells (human melanoma cells), which has been reported to have high levels of endogenous LAP enzyme. The expression of LAP enzyme in SK-Mel-103 cells was in fact corroborated by Western blot assays (Figure 5a). Besides, toxicity studies demonstrated the high biocompatibility of **NB-SO$_3$-Leu** probe in SK-Mel-103 cells after their incubation for 24 h, even at high concentrations (Figure 5b). In addition, confocal assays were carried out to assess the selective activation of the **NB-SO$_3$-Leu** probe in SK-Mel-103 cells. A strong fluorescence signal was observed in SK-Mel-103 cells incubated with **NB-SO$_3$-Leu** probe when compared with untreated SK-Mel-103 cells (15-fold) (Figure 5c and 5d).

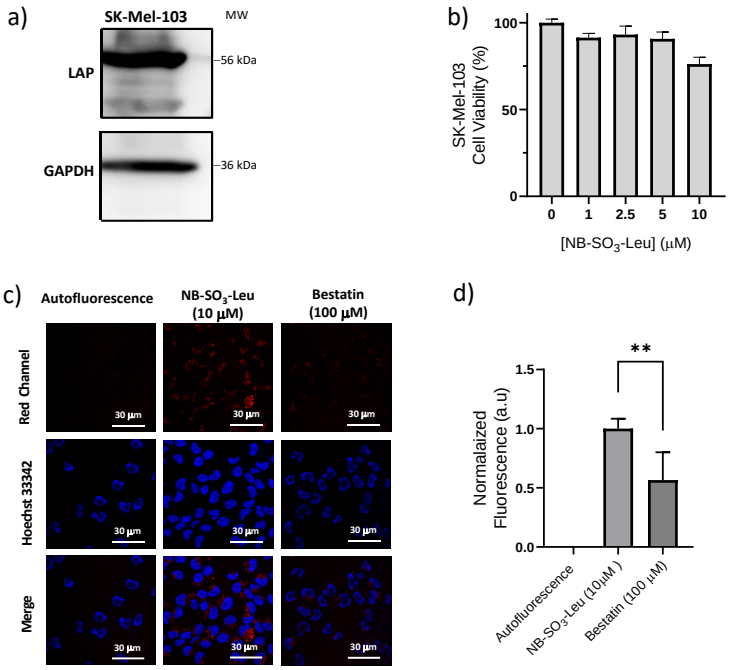

Figure 5. (a) Western blot assay for LAP expression in SK-Mel-103 cells. (b) Cell viability in SK-Mel-103 cells incubated with different concentrations of **NB-SO$_3$-Leu** probe for 24 h. (c)

Confocal images of not treated SK-Mel-103 cells, SK-Mel-103 cells incubated with **NB-SO_3-Leu** (10 µM), and SK-Mel-103 cells incubated whit **NB-SO_3-Leu** (10 µM) + bestatin (100 µM). (d) Fluorescence quantification of confocal images. Error bars are expressed as 3σ for three independent experiments. Values are expressed as mean ± SD. Statistical analysis was assessed by applying Student's T-test (**p< 0.05).

These studies also corroborated a strong signal dose-dependent reduction when cells were incubated with **NB-SO_3-Leu** probe and the LAP inhibitor bestatin for 30 min (56% of fluorescence signal) (Figure 6). The results confirmed the proposed mechanism, in which **NB-SO_3-Leu** probe was hydrolysed by LAP enzyme, overexpressed in SK-Mel-103 cells, yielding the emissive NB-SO_3 fluorophore.

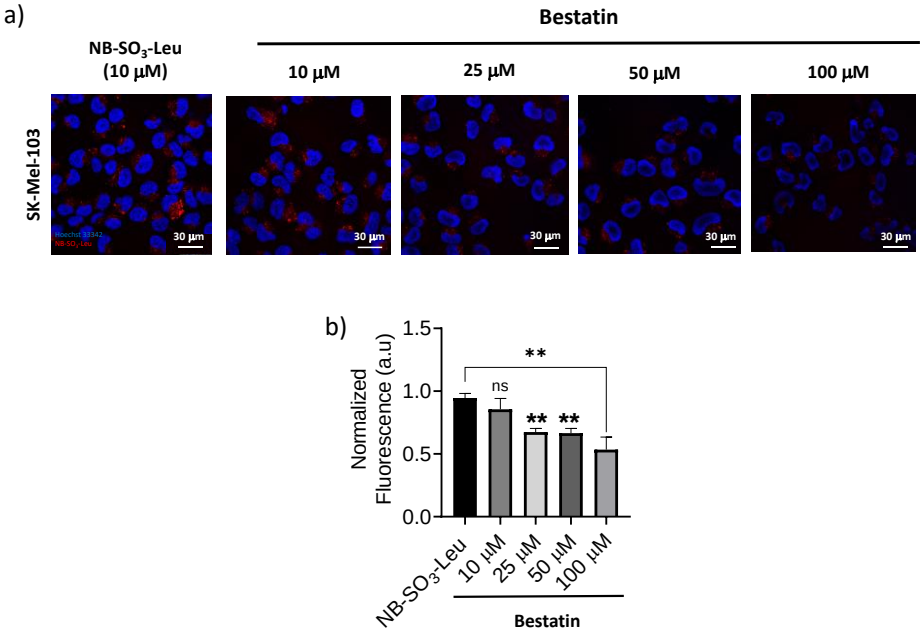

Figure 6. (a) Confocal images of SK-Mel-103 cells untreated and treated whit LAP inhibitor (10, 25, 50 and 100 µM of bestatin), incubated with **NB-SO_3-Leu** (10 µM). (b) Fluorescence quantification of confocal images. Error bars are expressed as 3σ for three independent

experiments. Values are expressed as mean ± SD. Statistical analysis was assessed by applying Student's T-test (**p< 0.05).

5.4 EXPERIMENTAL SECTION

Materials. 3-aminophenol, iodoethane, 1,3-propanesultoneBoc-Ala-OH), 2-ethoxy-1-ethoxycarbonyl-1,2-dihydroquinoline, *N*,*N*-dimethylformamide (DMF), triethylamine, *N*-(tert-butoxycarbonyl)-L-alanine, $NaNO_2$, K_2CO_3, $FeCl_3$, $CaCl_2$, $MnCl_2$, $MgCl_2$, H_2O_2, glutathione, cysteine, arginine, glycine, bestatin, monoamine oxidase A from *baculovirus* infected BTI insect cells (MAO-A), γ-glutamyltransferase from porcine kidney, nitroreductase from *Escherichia coli* and leucine aminopeptidase from porcine kidney (LAP) were obtained from Sigma-Aldrich. ^{1}H and ^{13}C NMR spectra were recorded on a Bruker FT-NMR Avance 400 (Ettlingen, Germany) spectrometer at 300 K. Fluorescence spectroscopy was carried out in a JASCO spectrofluorometer FP-8500 and absorption spectra were collected in a JASCO V-650 spectrophotometer. HPLC-MS was recorded with an Agilent 1620 Infinity II HPLC coupled to a mass spectrometer Agilent Ultivo equipped with a triple QTOF detector. PuriFlash XS 520 Plus was used for purification.

Table S1. Comparison of the NB-SO_3-Leu probe with other fluorescent probes for the detection of LAP overexpression.

Probe	λ exc/ λ em (nm)	Time (min)	LOD	*In vitro* (Cell lines)	*In vivo* model	Ref.
DCD-Leu	525/605	30	Not reported	HCT 116	Not reported	Young H. et al. *Bioorg. Med. Chem. Lett.* **2011**,*21*, 2403–2405
CV-Leu	585/625	20	0.42 ng/mL	HepG2 A549	Not reported	Gong Q. et al. *Chem. Sci.*, **2016**, *7*, 788–792

DCM–Leu	455/660	40	46 ng/mL	QSG-7701 c SMMC-7721 HeLa	Not reported	Gu K. et al. *ACS Appl. Mater. Interfaces* **2016**, *8*, 26622–26629
BODIPY-C-Leu	480/ (I_{578}/I_{601})	30	41.9 ng/mL	HeLa	Zebrafish imaging	Zhou Zh. et al. *Anal. Chem.* **2017**, *89*, 11576–11582
TMN-Leu	460/658	70	0.38 ng/mL	HCT116	HCT116 tumour-bearing mice	Zhang W. et al. *Anal. Chem.* **2017**, *89*, 12319–12326
HCAL	670/705	90	10.5 ng/mL	LO2 HepG2	Drug-induced liver injury model	He X. et al. *Chem. Sci.*, **2017**, *8*, 3479–3483
UUSQ-Leu	650/710	30	0.61 ng/mL	HepG2 LO2 L929	Xenograft tumour in BALB/c nude mice	Wu B. et al. *Anal. Chem*. **2018**, *90*, 9359–9365
DPA-TPE-Leu	359/505	30	8.87 ng/mL	HepG2	Not reported	Huang Sh. et al. *Anal. Chim. Acta.* **2018**, *1031*, 169-177
CHMC-M-Leu	530/625	30	50 ng/mL	HeLa	Not reported	Chai Y. et al. *Analyst*, **2019**, *144*, 463–467
DLP	705/733	30	0.26 ng/mL	HepG2	Not reported	Huang Y. et al. *Anal. Chem.* **2019**, *91*, 8085–8092
hCy-CA-LAP	680/710	Not reported	0.0067 U/mL	LO2 HepG2	Mice model of RFP-induced cholestatic liver injury	Zhang Y. et al. *Chem. Sci.*, **2021**, *12*, 14855-14862
Probe 1	λ_{em}=550	10	0.008 U/L	HepG2 LO2	HepG2 tumour-bearing BALB/c nude	Wang B. et al. *Chem. Sci.*, **2022**, *13*, 2324-2330
DCM-LAP	440/656	90	168 mU/L	A549 HeLa HepG2 MCF-7	Breast cancer tumour model.	Zhong R. et al. *Anal. Chem.* **2023**, *95*, 2428–2435

MCL	400/550	60	0.001136 U/L	HCT116 HepG2 A549 BJ	Tumour bearing mice model	Gunduz H. et al. *Sens. Actuators B Chem.*,**2023**, *383*, 1-10
NB-SO_3-Leu	630/660	15	7.2 ng/mL	SK-Mel-103	Not reported	This work

Synthesis of NB-SO_3. The synthesis of products **1**, **2** and **3** were adapted from *Chem. Eur. J.* **2009**, *15*, 418-442.

Synthesis of (3-ethylamino) phenol (1).

3-aminophenol (2.10 g, 19.3 mmol) and potassium carbonate (2.52 g, 18.2 mmol) were mixed in a round bottom flask under argon atmosphere and dissolved in anhydrous DMF (10 mL). The reaction mixture was stirred for 15 min under argon atmosphere at room temperature until complete solution of reagents. Then, iodoethane (1.5 mL, 18.7 mmol, 0.05 mL·min^{-1} was added dropwise for 30 min at 100°C. After complete addition, the whole reaction mixture was stirred 2 h at 100°C. The reaction is then cooled to room temperature and K_2CO_3 removed by filtration. Solvent was removed under reduced pressure and the obtained oil resuspended in 10 mL water and extracted 2 times with ethyl acetate. The solvent was eliminated under vacuum. The residue was purified by column chromatography on silica gel (hexane-ethyl acetate 5:1 v/v as eluent) to obtain product **1** as brown oil (82 % yield). ^{1}H NMR (400 MHz, $CDCl_3$) δ (ppm): 7.02 (td, J = 8.0, 2.2 Hz, 1H), 6.23 (ddt, J = 7.9, 4.0, 2.3 Hz, 2H), 6.10 (dt, J = 4.3, 2.3 Hz, 1H), 4.17 (qd, J = 7.2, 3.7 Hz, 1H), 3.07 (qd, J = 7.2, 2.9 Hz, 2H), 1.20 (td, J = 7.1, 2.1 Hz, 3H). ^{13}C NMR (101 MHz, $CDCl_3$) δ (ppm): 156.97, 149.73, 130.19, 106.23, 105.24, 100.79, 38.80, 14.63.

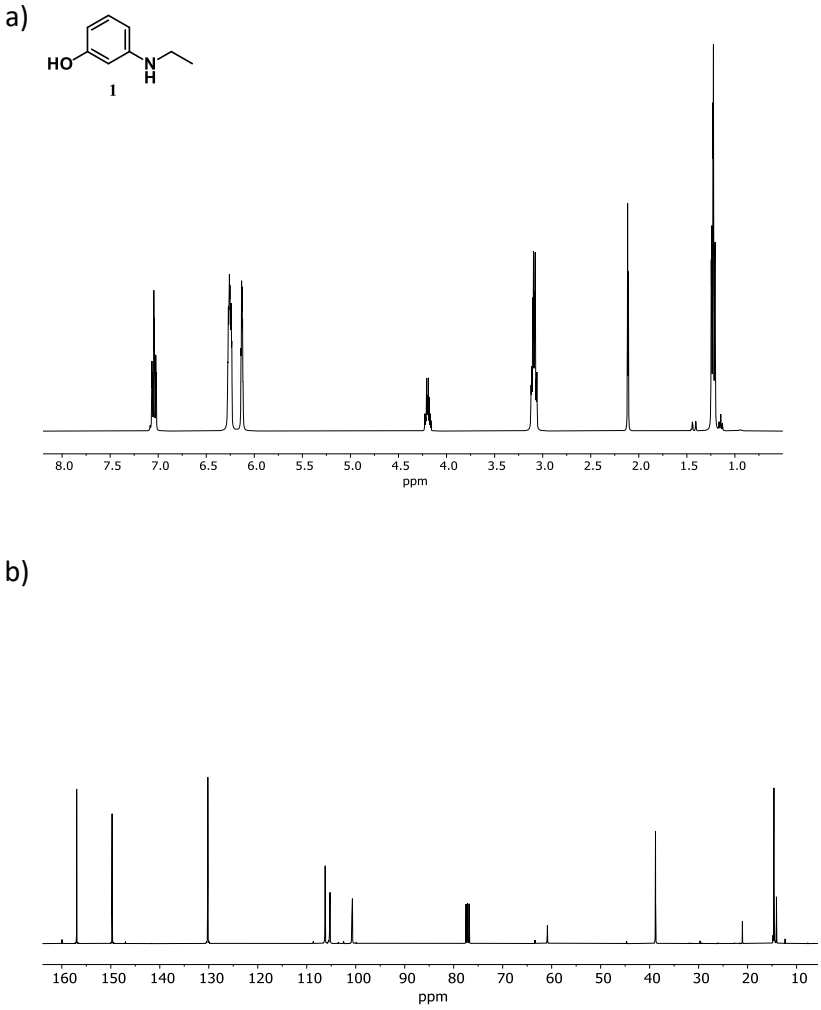

Figure S1. ^{1}H-NMR and ^{13}C-NMR of compound **1**.

Synthesis of (3-(ethyl(3-hydroxyphenyl)amino)propane-1-sulfonate) (2).

Compound **1** (316.8 mg, 2.30 mmol) and 1,3-propanesultone (336.1 mg, 2.75 mmol) were mixed in a bottom round flask of 10 mL and dissolved in isopropanol (3 mL). The reaction mixture was heated under reflux at 90°C for 3 h. The appearance of the reaction mixture changes rapidly to a light pink colour, followed by the

appearance of a white precipitate. Finally, the reaction is cooled to room temperature. Precipate was isolated by filtration and washed with cold isopropanol. The solid is collected and dried overnight under vacuum. Compound **2** was used in the next synthetic step without further purification (52% yield). ^{1}H NMR (400 MHz, D_2O) δ (ppm): 7.52 (t, J = 8.2 Hz, 1H), 7.12–7.08 (m, 2H), 7.04 (t, J = 2.3 Hz, 1H), 3.80–3.74 (m, 2H), 3.68 (q, J = 7.2 Hz, 2H), 2.92 (t, J = 7.2 Hz, 2H), 1.97 (q, J = 7.6 Hz, 2H), 1.16 (t, J = 7.2 Hz, 3H). ^{13}C NMR (101 MHz, D_2O) δ (ppm): 158.90, 137.66, 133.04, 117.73, 113.71, 109.04, 56.38, 54.38, 47.57, 20.40, 8.91.

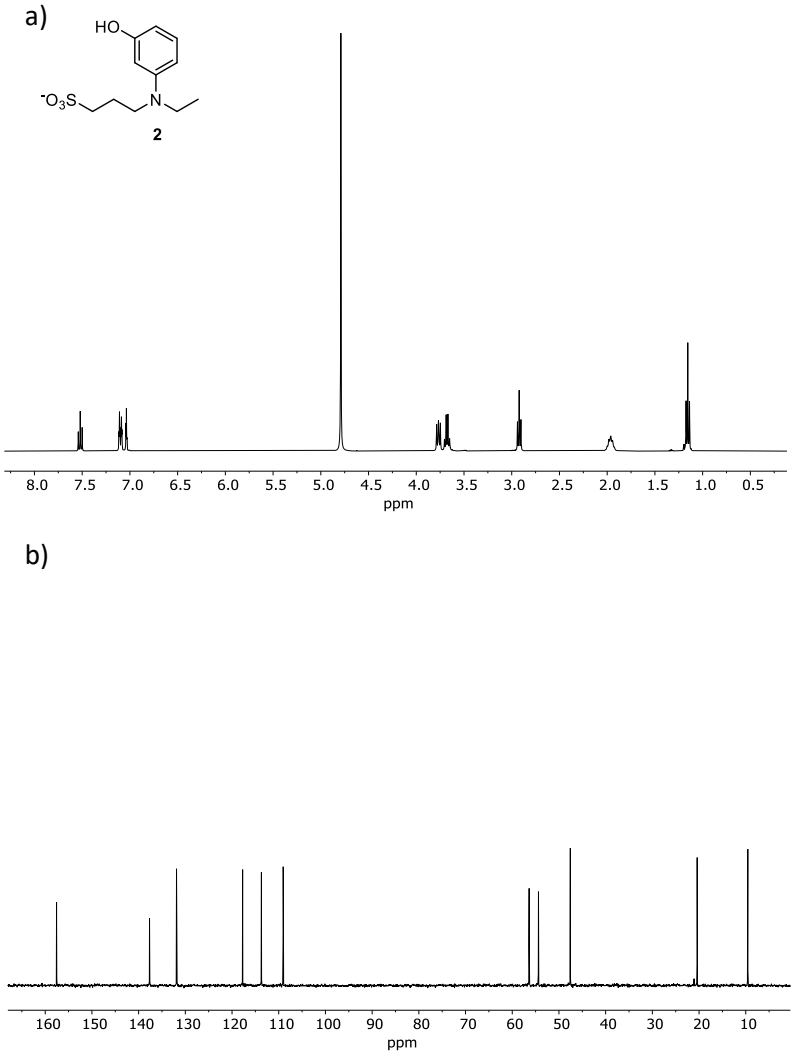

Figure S2.^{1}H-NMR and ^{13}C-NMR of compound **2**.

Synthesis of (3-(ethyl(3-hydroxy-4-nitrophenyl)amino)propane-1-sulfonate) (3).

Compound **2** (193.2 mg, 0.75 mmol) was dissolved in 1 mL of HCl-H_2O 13:7 v/v and cooled in an ice bath. Then, a $NaNO_2$ solution (60 mg, 0.87 mmol) in H_2O (1.2 mL)

was added dropwise to reaction mixture. The colour changes immediately to bright yellow. The stirring was kept for 3 h. Then, the reaction mixture was filtered off and the solvent removed under reduced pressure to obtain compound **3** as a black-brownish solid and employed immediately in the next step (91 % yield).

Synthesis of NB-SO_3.

3 (200 mg, 0.66 mmol) and 1-naphthylamine (95 mg, 0.66 mmol) were mixed in a round bottomed flask under argon atmosphere and dissolved in anhydrous DMF (5 mL). The reaction mixture was stirred at 90°C under argon atmosphere overnight. The solvent was eliminated under vacuum. The crude reaction was purified through a Soxhlet extraction to obtain NB-SO_3 as a blue solid (68 % yield). ^{1}H NMR (400 MHz, MeOD) δ (ppm): 8.85 (d, J = 8.2 Hz, 1H), 8.26 (d, J = 8.2 Hz, 1H), 7.89–7.70 (m, 3H), 7.25 (d, J = 9.4 Hz, 1H), 6.95 (s, 1H), 6.82 (s, 1H), 3.73 (t, J = 7.7 Hz, 2H), 3.68–3.60 (m, 2H), 2.85 (t, J = 6.8 Hz, 2H), 2.08 (d, J = 14.7 Hz, 2H), 1.29–1.15 (m, 3H).^{13}C NMR (101 MHz, MeOD) δ (ppm): 148.18, 147.41, 140.10, 136.03, 132.87, 130.28, 130.18, 130.00, 129.77, 128.83, 128.72, 127.91, 126.87, 124.41, 122.46, 97.34, 96.11, 45.49, 25.69, 10.70. HR-MS: Theoretical ($M+H^+$): 411.47 m/z; Experimental ($M+H^+$): 412.13 m/z.

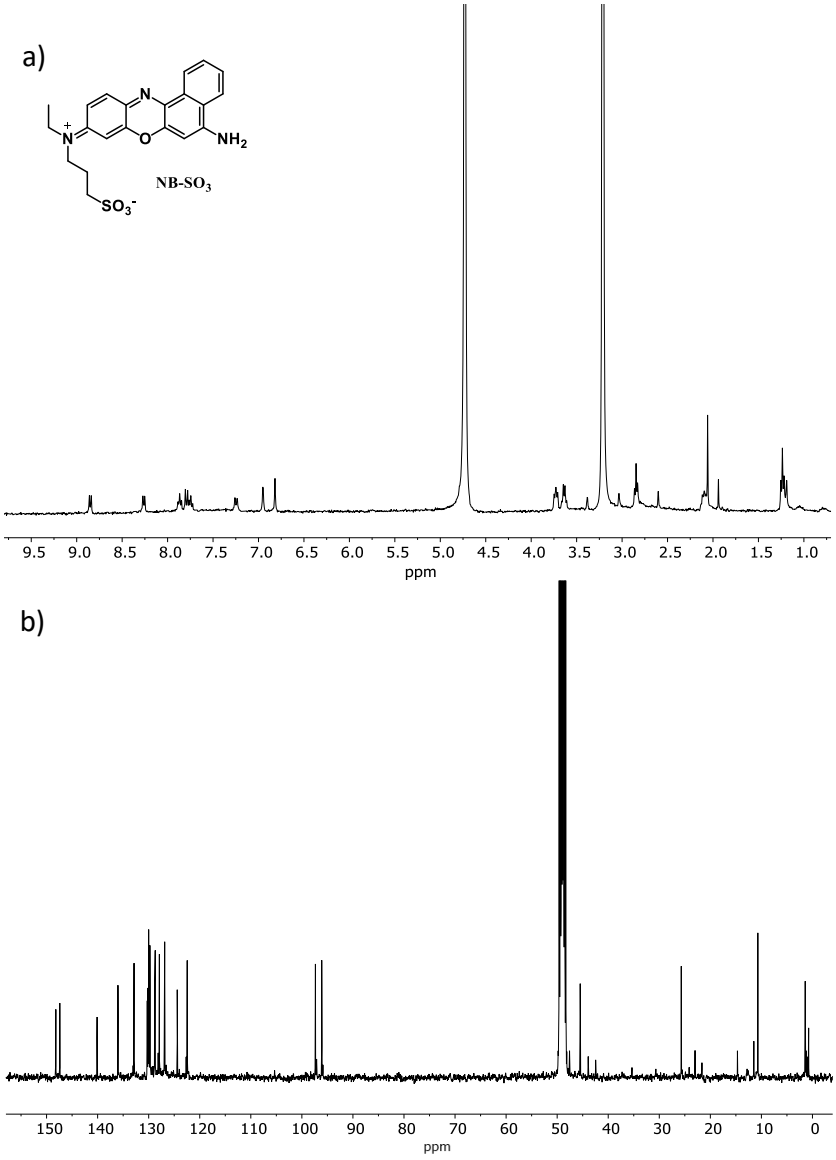

Figure S3. ^{1}H-NMR and ^{13}C-NMR of NB-SO_3.

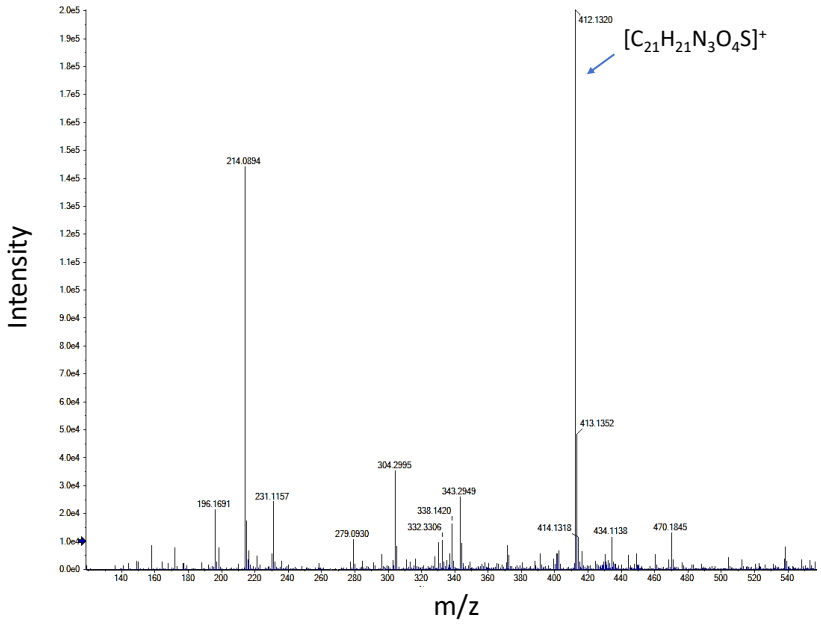

Figure S4. HRMS of NB-SO_3

NB-SO_3 fluorescence emission at different pH

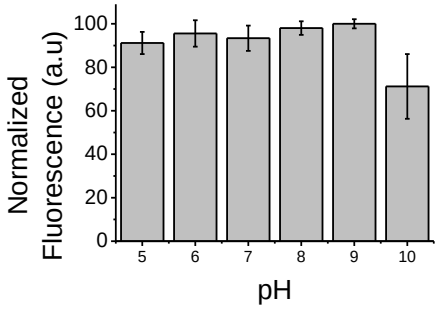

Figure S7. Emission intensity at 660 nm (λ_{exc} = 630 nm) of PBS/DMSO 99:1 v/v (pH 7.4) solutions of NB-SO_3 (5 µM) at pH 5, 6, 7, 8, 9 and 10.

Synthesis of NB-SO_3-Leu.

Boc-Leu-OH (138.8 mg, 0.6 mmol), triethylamine (68.2 µL, 0.49 mmol) and 2-ethoxy-1-ethoxycarbonyl-1,2-dihydroquinoline (123.6 mg, 0.49 mmol) were mixed in a round bottom flask under argon atmosphere and dissolved in anhydrous DMF (5 mL). The reaction mixture was stirred at room temperature for 1 h. Then, NB-SO_3 (200 mg, 0.49 mmol) dissolved in anhydrous DMF (2 mL) were added dropwise to the reaction mixture. The crude was heated at 70°C for 32 h. After this time trifluoroacetic acid (TFA) dilution (5 mL DMF and 0.75 mL TFA) was added to the reaction mixture and stirred for 24 h. The solvent was eliminated under vacuum. The product was purified in the PuriFlash XS 520 Plus using a PF-30C18HP-F0004 column (hexane-ethyl acetate 95:5 v/v as eluent, 5.0 mL·min^{-1} of flow rate) to obtain **NB-SO_3-Leu** probe as purple solid (55 % yield). ^{1}H NMR (400 MHz, DMSO) δ (ppm): 9.41 (s, 1H), 9.09 (dd, J = 4.7, 1.7 Hz, 1H), 8.73 (dd, J = 8.4, 1.6 Hz, 1H), 8.15 (d, J = 8.1 Hz, 2H), 7.93 (ddd, J = 8.6, 7.0, 1.5 Hz, 1H), 7.80–7.74 (m, 2H), 3.09 (qd, J = 7.3, 4.4 Hz, 6H), 1.36 m, 4H), 1.18 (t, J = 7.3 Hz, 9H), 0.88–0.84 (m, 2H).^{13}C NMR (101 MHz, DMSO) δ (ppm)158.54, 158.18, 148.48, 143.65, 140.25, 131.55, 128.54, 128.16, 127.80, 125.65, 121.71, 117.60, 114.68, 77.84, 45.67, 45.62, 28.16, 24.30, 23.07, 22.94, 21.48, 8.52. HRMS: Theoretical ($M+H^+$): 524.636 m/z. Experimental ($M+H^+$): 525.216 m/z.

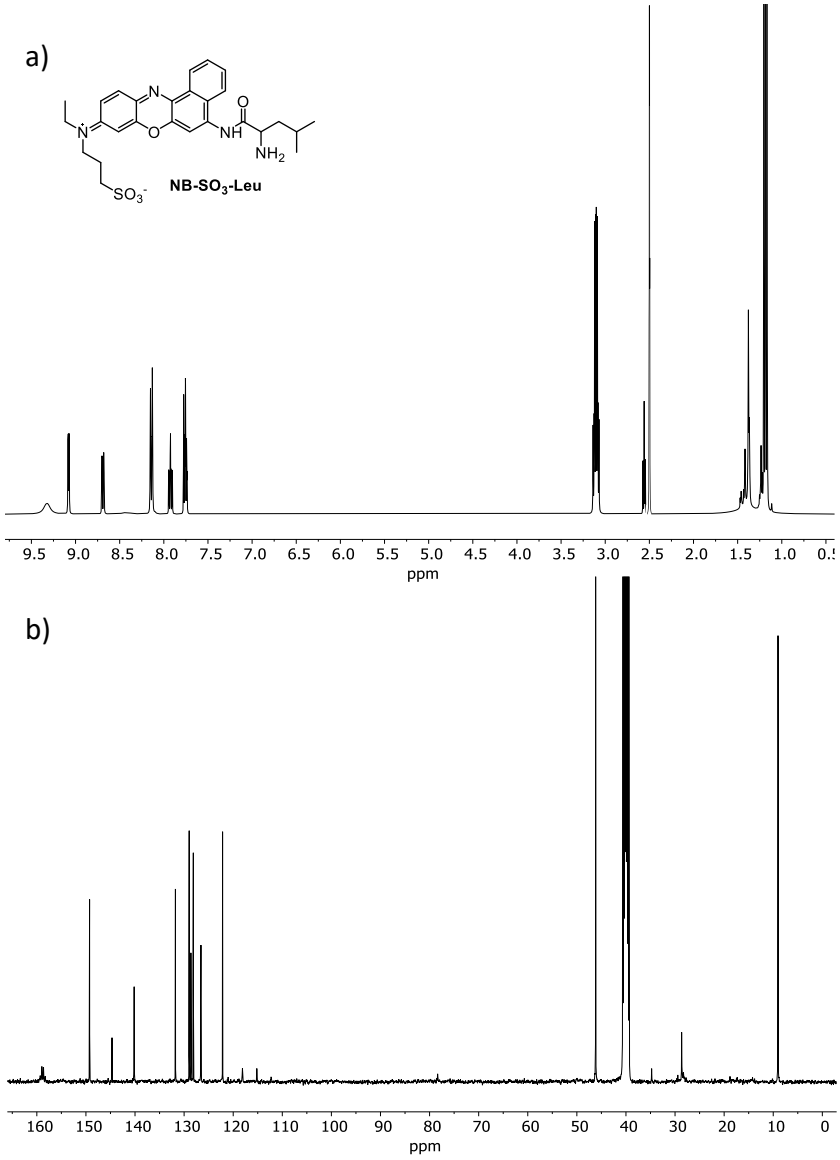

Figure S5. ^{1}H-NMR and ^{13}C-NMR of **NB-SO$_3$-Leu**.

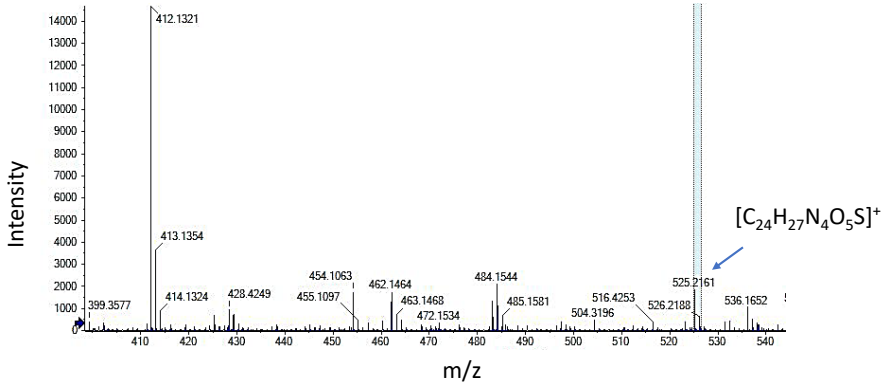

Figure S6. HRMS of NB-SO_3-Leu.

HPLC measurements of LAP-induced hydrolysis of NB-SO_3.

Pure probe and fluorophore samples were taken from a 1.0 x 10^{-3} M stock solution to obtain a final concentration of 5 µM. The hydrolysis sample chromatogram was recorded 10 min after incubating **NB-SO_3-Leu** probe (5 µM) with LAP enzyme (750 ng·mL^{-1}). HPLC chromatograms were obtained using a Hypersil Gold CN column, flow rate of 1.8 mL·min^{-1}, with buffer (0.2 M KH_2PO_4 solution, pH = 3.0 ± 0.1)-acetonitrile-ethanol (90:10:2 v/v/v) at 17 min.Additionally, chromatograms of NB-SO_3 and **NB-SO_3-Leu** alone were obtained under the same experimental conditions.

General procedure for LAP detection.

Fluorescence emission measurements of **NB-SO_3-Leu** were carried out with 1 µL of the probe from a stock solution (1.0 x 10^{-3} M in DMSO), followed by addition of LAP solution in PBS (10 mM, pH 7.4). Final volume was adjusted to 200 µl with PBS at pH 7.4. After incubation at 37°C for 15 min in a thermostat, solution was transferred to a quartz cell of 1 cm optical length to measure the fluorescence (λ_{exc} = 630 nm). Control samples, without LAP enzyme, were prepared and measured under the same conditions.

Calibration curve for LAP.

LOD and the LOQ were obtained from the plot of fluorescence intensities at 660 nm (upon excitation at 630 nm) versus LAP concentration in ng/ml. LOD and LOQ were calculated by using the equation 1:[26]

$$LOD/LOQ=K*Sb\cdot m^{-1} \text{ (Equation 1)}$$

where K=3 for LOD and K=10 for LOQ; Sb is the standard deviation of the control measures and *m* is the slope of the calibration curve. The resulting LOD and LOQ were 7.2 $ng\cdot mL^{-1}$ and 21.8 $ng\cdot mL^{-1}$ respectively.

Photophysical characterization of NB and NB-SO_3-Leu.

Molar extinction coefficients, stokes shift and quantum yields for NB-SO_3 and **NB-SO_3-Leu** were determined (Table S2). Quantum yields values were measured using Nile Blue (NB) dissolved in water as standard (Φ = 0.01)[30] using the equation S1:[31]

$$\frac{\Phi_x}{\Phi_s} = \frac{S_x}{S_s} \times \frac{1-10^{-A_S}}{1-10^{-A_x}} \times \frac{n_x^2}{n_s^2} \text{ (Equation S1)}$$

where x and s indicate the unknown and standard solution, respectively, Φ is the quantum yield, S is the area under the emission curve, A is the absorbance at the excitation wavelength and n is the refraction index. Molar extinction coefficients were obtained in the adsorption maximum at 630 nm.

Table S2. Photophysical parameters for NB-SO_3, **NB-SO_3-Leu.**

	NB	**NB-SO_3**	**NB-SO_3-Leu**
Molar extinction coefficient [L·(mol·cm^{-1})$^{-1}$]	10500	20000	1960
Quantum yield	0.0100	0.0730	0.0002
Stokes shift (nm)	37	38	34

Kinetic studies.

Fluorescence spectra of the reaction mixture were recorded every 5 min to show the fluorescence responses triggered by the reaction between 750 ng·mL^{-1} of LAP and 5 µM of **NB-SO_3-Leu** within 15 min.

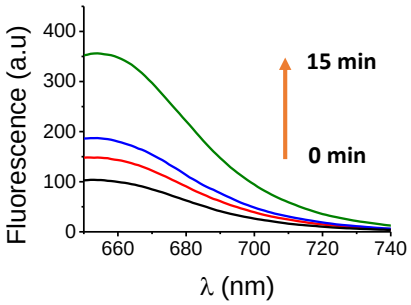

Figure S8. Fluorescence of **NB-SO_3-Leu** in (PBS/DMSO 99:1 v/v, pH 7.4) at different time points in the absence and in the presence of LAP enzyme (750 ng·mL^{-1}).

Cell Culture.

SK-Mel-103 cell line was purchased from the American Type Culture Collection (ATCC), cultured in Dulbecco's Modified Eagle Medium (DMEM) supplemented with 10% Fetal bovine serum (FBS). Cells were maintained in a 20% O_2 and 5% CO_2 atmosphere at 37°C.

Western blot assays.

To determine the levels of LAP enzyme in SK-Mel-103 cells, whole cell extracts were obtained by using lysis buffer (25 mM Tris-HCl pH 7.4, 1 mM EDTA, 1% SDS, plus protease and phosphatase inhibitors). Cell lysates were resolved in 12% SDS-PAGE gels, transferred to nitrocellulose membranes, blocked with 5% non-fat milk, and incubated overnight with the primary antibody for LAP (#PA5-80533, Invitrogen). Besides, GAPDH (#14C10 from Cell Signalling) was used as reference protein for normalization. Then, membranes were washed and probed with the secondary antibody conjugated to horseradish peroxidase, anti-rabbit IgG peroxidase antibody (#A6154, Sigma) for enhanced chemiluminescence detection (Amersham Pharmacia Biotech).

***In vitro* cytotoxicity studies.**

For the *in vitro* cytotoxicity studies, SK-Mel-103 cells were seeded in a 96-well plate (10,000 cells/well) and incubated for 24 h. Then, the cells were incubated with varying concentrations of the **NB-SO_3-Leu** probe (diluted in DMEM) for 24 h. The cell viability was determined by WST-1 reagent which was added for 30 min and then absorbance was measured at 450 nm.

Confocal *in vitro* experiments.

SK-Mel-103 cells were seeded in a cover slip in a 6-well plate at 250,000 of cells·mL^{-1}. After 24 h cells, some cells were treated with **NB-SO_3-Leu** (10 µM) alone and other cells with the bestatin inhibitor also for 30 min. Then cells were washed, and coverslips mounted to confocal visualization. Hoechst 33342 was added at 2 µg·ml^{-1} for nuclei staining. Confocal images were acquired in a Leica TCS SP8 AOBS

confocal microscope (λ_{exc} = 552 nm; λ_{em} = 574-765 nm). Images were quantified by using the Image J software.

Inhibitor experiments.

SK-Mel-103 cells were incubated with 10 µM of **NB-SO_3-Leu** probe 30 min (Figure 5) and other SK-Mel-103 cells were previously treated with **NB-SO_3-Leu** probe and different concentration of bestatin inhibitor (10, 25, 50 and 100 µM) for 30 min.

5.5 CONCLUSIONS

We report herein the design and synthesis of a fluorogenic probe (**NB-SO_3-Leu**) for the sensitive and selective detection of LAP overrepresentation. LAP enzyme monitorization is performed by following the fluorescent signal of the highly emissive NB-SO_3 fluorophore, which was produced after LAP-induced hydrolysis of the low emissive **NB-SO_3-Leu** probe. Fluorophore was initially modified with sulfonic groups to potentially facilitate a rapid renal clearance thus decreasing possible toxic effects. Finally, confocal studies confirmed the ability of **NB-SO_3-Leu** to detect the LAP enzyme in SK-Mel-103 melanoma cells, with endogenous overexpression of LAP.

ACKNOWLEDGEMENTS

This research was supported by project PID2021-126304OB-C41 funded by MCIN/ AEI /10.13039/501100011033/ and by European Regional Development Fund - A way of doing Europe. This study was also supported by Generalitat Valenciana (CIPROM/2021/007). Thank the financial support from the FEDER found of European Union (IDIFEDER/2021/044). This research was supported by CIBER-Consorcio Centro de Investigación Biomédica en Red-(CB06/01/2012), Instituto de Salud Carlos III, Ministerio de Ciencia e Innovación. M. D. -R. thanks to his predoctoral fellowship

Grisolia to the Genelalitat Valenciana (GRISOLIAP/2019/144). J. F. B. thanks to his postdoctoral fellowship APOSTD from Generalitat Valenciana (CIAPOS/2021/198).

5.6 REFERENCES

1. Guo, Z., Park, S., Yoon, J., & Shin, I. Recent progress in the development of near-infrared fluorescent probes for bioimaging applications. *Chem. Soc. Rev.*, **2014**, *43*, 16-29.

2. Kobayashi, H., Ogawa, M., Alford, R., Choyke, P. L., & Urano, Y. New strategies for fluorescent probe design in medical diagnostic imaging. *Chem. Rev.*, **2010**, *110*, 2620-2640.

3. Hanash, S. Disease proteomics. *Nature*, **2003**, *422*, 226-232.

4. Thiry, A., Dogne, J. M., Masereel, B., & Supuran, C. T. Targeting tumor-associated carbonic anhydrase IX in cancer therapy. *Trends Pharmacol. Sci.*, **2006**, *27*, 566-573.

5. Copeland, R. A., Harpel, M. R., & Tummino, P. J. Targeting enzyme inhibitors in drug discovery. *Expert Opin. Ther. Targets*, **2007**, *11*, 967-978.

6. Huang, J., Weinfurter, S., Daniele, C., Perciaccante, R., Federica, R., Della Ciana, L., Pill, J. & Gretz, N. Zwitterionic near infrared fluorescent agents for noninvasive real-time transcutaneous assessment of kidney function. *Chem. Eng. Sci.*, **2017**, *8*, 2652-2660.

7. Huang, J., Xie, C., Zhang, X., Jiang, Y., Li, J., Fan, Q., & Pu, K. Renal-clearable molecular semiconductor for second near-infrared fluorescence imaging of kidney dysfunction. *Angew. Chem. Int. Ed.*, **2019**, *58*, 15120-15127.

8. Zhu, W., Kang, M., Wu, Q., Zhang, Z., Wu, Y., Li, C., Li, K., Wanga, L., Wang, D. & Tang, B. Z. Zwitterionic AIEgens: Rational Molecular Design for NIR-II Fluorescence Imaging-Guided Synergistic Phototherapy. *Adv. Funct. Mater.*, **2021**, *31*, 1-11.

9. Huang, J., Lyu, Y., Li, J., Cheng, P., Jiang, Y., & Pu, K. A Renal-Clearable Duplex Optical Reporter for Real-Time Imaging of Contrast-Induced Acute Kidney Injury. *Angew. Chem. Int. Ed.*, **2019**, *131*, 17960-17968.

10. Huang, J. Li, J. Lyu, Y. Miao, Q. & Pu, K. Molecular optical imaging probes for early diagnosis of drug-induced acute kidney injury. *Nat. Mater.*, **2019**, *18*, 1133-1143.

11. Choi, H. et al. Renal clearance of quantum dots. *Nat. Biotechnol.*, **2017**, *25*, 1165-1170.

12. Loynachan, C. N., et al. Renal clearable catalytic gold nanoclusters for *in vivo* disease monitoring. *Nat. Nanotech.*, **2019**, *14*, 883–890.

13. Scott, J. I., Deng, Q., & Vendrell, M. Near-infrared fluorescent probes for the detection of cancer-associated proteases. *ACS Chem. Biol.*, **2021**, *16*, 1304-1317.

14. Tsujimoto, M., Goto, Y., Maruyama, M., & Hattori, A. Biochemical and enzymatic properties of the M1 family of aminopeptidases involved in the regulation of blood pressure. *Heart Fail. Rev*., **2008**, *13*, 285-291.

15. Kondo, C., Shibata, K., Terauchi, M., Kajiyama, H., Ino, K., Nomura, S., Nawa, A., Miztutani, Sh., & Kikkawa, F. A novel role for placental leucine aminopeptidase (P-LAP) as a determinant of chemoresistance in endometrial carcinoma cells. *Int. J. Cancer Manag.,* **2006**, *118*, 1390-1394.

16. Wang, B., Chen, Z., Cen, X., Liang, Y., Tan, L., Liang, E., Zheng, L., Zheng, Y., Zhan, Z. & Cheng, K. A highly selective and sensitive chemiluminescent probe for leucine aminopeptidase detection *in vitro*, *in vivo* and in human liver cancer tissue. *Chem. Eng. Sci.*, **2022**, *13*, 2324-2330.

17. Li, R., Guo, J., Duan, Y., Liu, X., Gui, L., Xu, Y., Kong, X., Li, Y., Chen, H. & Yuan, Z. Monitoring inflammation-cancer progression by cell viscosity, polarity and leucine aminopeptidase using multicolor fluorescent probe. *Chem. Eng. J.*, **2022**, *435*, 1-13.

18. Cifaldi, L., Romania, P., Lorenzi, S., Locatelli, F., & Fruci, D. Role of endoplasmic reticulum aminopeptidases in health and disease: from infection to cancer. *Int. J. Mol. Sci.*, **2012**, *13*, 8338-8352.

19. Valyi-Nagy, I., Shih, I.M., Györfi, T., Greenstein, D., Juhasz, I., Herlyn, M., & Elder, D.E. Spontaneous and induced differentiation of human melanoma cells. *Int. J. Cancer Manag.*, **1993**, *54*, 159-165.

20. Gray-Schopfer, V., Wellbrock, C., & Marais, R. Melanoma biology and new targeted therapy. *Nature*, **2007**, *445*, 851-857.

21. Mattia, G., Puglisi, R., Ascione, B., Malorni, W., Carè, A., & Matarrese, P. Cell death-based treatments of melanoma: conventional treatments and new therapeutic strategies. *Cell Death Dis.*, **2018**, *9*, 1-14.

22. Mizutani, S., Shibata, K., Kikkawa, F., Hattori, A., Tsujimoto, M., Ishii, M., & Kobayashi, H. Essential role of placental leucine aminopeptidase in gynecologic malignancy. *Expert Opin. Ther. Targets*, **2007**, *11*, 453-461.

23. Yoon, H. Y., Shim, S. H., Baek, L. J., & Hong, J. I. Small-molecule probe using dual signals to monitor leucine aminopeptidase activity. *Bioorganic Med. Chem. Lett.,* **2011**, *21*, 2403-2405.

24. Chen, Y. Fluorescent probes for detection and bioimaging of leucine aminopeptidase. *Mater. Today Chem.*, **2020**, *15*, 1-19.

25. Cheng, P., & Pu, K. Molecular imaging and disease theranostics with renal-clearable optical agents. *Nat. Rev. Mater.*, **2021**, *6*, 1095-1113.

26. Chen, Y. Fluorescent probes for detection and bioimaging of leucine aminopeptidase. *Mater. Today Chem.*, **2020**, *15*, 100216.

27. Liu, H. W., Chen, L., Xu, C., Li, Z., Zhang, H., Zhang, X. B., & Tan, W. Recent progresses in small-molecule enzymatic fluorescent probes for cancer imaging. Chemical Society Reviews, **2018**, *47*, 7140-7180.

28. Hitzerd, S. M., Verbrugge, S. E., Ossenkoppele, G., Jansen, G., & Peters, G. J. Positioning of aminopeptidase inhibitors in next generation cancer therapy. *Amino Acids*, **2014**, *46*, 793-808.

29. Shrivastava, A., & Gupta, V. B. Methods for the determination of limit of detection and limit of quantitation of the analytical methods. *Chron. Young Sci.*, **2011**, *2*, 21-25.

30. Jose, J., Ueno, Y., & Burgess, K. Water-soluble Nile blue derivatives: syntheses and photophysical properties. Chem. Eur. J., **2009**, *15*, 418-423.

31. Lakowicz, J. R. (Ed.). Principles of fluorescence spectroscopy. Boston, MA: springer US, **2006**.

Chapter 6| NIR fluorescent probe for detection of alanine aminopeptidase (APN) overrepresentation as a cancer biomarker.

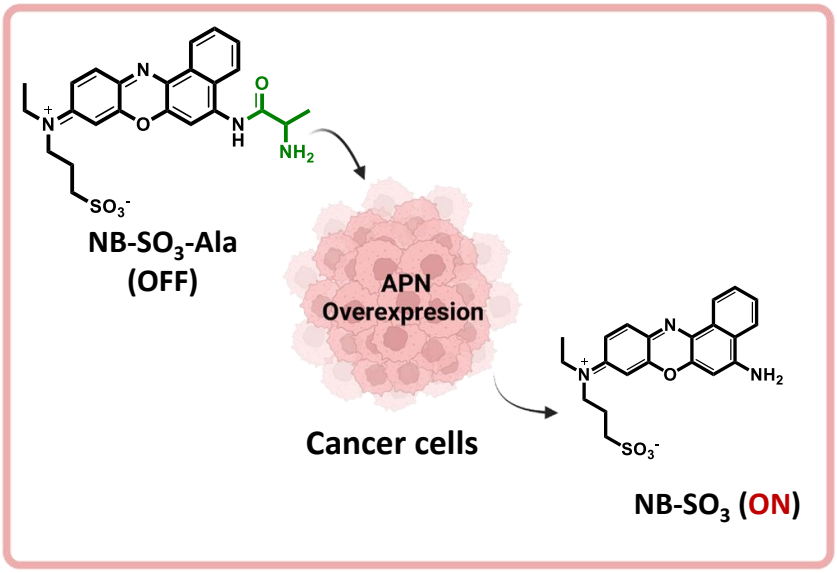

NIR fluorescent probe for detection of alanine aminopeptidase (APN) overrepresentation as a cancer biomarker.

Marcia Domínguez,[a,b] David Azorín-Soriano,[a,c] Vicente Martí-Centelles,[a,b] Alba García-Fernández,[a,b,c] Juan F. Blandez,[a,b,d,e] Félix Sancenón,[a,b,c,d,*] and Ramón Martínez-Máñez[a,b,c,d,*]

a. Instituto Interuniversitario de Investigación de Reconocimiento Molecular y Desarrollo Tecnológico (IDM), Universitat Politècnica de València, Universitat de València, Spain.
b. CIBER de Bioingeniería, Biomateriales y Nanomedicina, Instituto de Salud Carlos III.
c. Unidad Mixta UPV-CIPF de Investigación en Mecanismos de Enfermedades y Nanomedicina, Universitat Politècnica de València, Centro de Investigación Príncipe Felipe, Spain.
d. Unidad Mixta de Investigación en Nanomedicina y Sensores, Universitat Politècnica de València, Instituto de Investigación Sanitaria La Fe, Spain.
e. Adsorption & Advanced Materials Laboratory (A2ML), Department of Chemical Engineering & Biotechnology, University of Cambridge, Philippa Fawcett Drive, Cambridge CB3, 0AS, U.K.

6.1 ABSTRACT

Aminopeptidase N (APN) is a metalloprotease that plays a critical role in the preservation of normal physiological functions and whose overexpression is deeply related to the progression, invasion, and migration of malignant tumours. Thus, a specific and early detection of APN overrepresentation can be of interest in clinical diagnosis, prognosis, and drug treatment of cancer diseases. Based on this, we report herein the design and synthesis of a new NIR fluorescent probe (**NB-SO_3-Ala**) based on the NB fluorophore, whose backbone was modified with a sulfonic moiety. It has been demonstrated that the presence of a zwitterionic structure in molecules increases solubility and can induce a fast renal clearance, reducing tissue accumulation, cytotoxicity, and side-effects. In addition, the sulfonic-modified NB fluorophore was conjugated to an alanine residue, which acts as APN substrate. **NB-SO_3-Ala** is weakly fluorescent in the NIR I region, yet the emission increased progressively over time with the addition of APN, reaching the maximum value at 30 min, with an overall 3.5-fold increase. This emission enhancement is ascribed to an APN-induced hydrolysis of the probe which generates the emissive NB-SO_3 fluorophore. A LOD of 17.2 ng·mL^{-1} for the APN enzyme is determined. **NB-SO_3-Ala** probe is successfully validated *in vitro* in the 4T1, HeLa, and A549 cancer cell lines. Viability studies confirmed that **NB-SO_3-Ala** probe is not toxic at concentrations up to 10 μM. Confocal images of the **NB-SO_3-Ala** probe incubated with 4T1, HeLa, and A549 cells show fluorescence emission in the order A549 > 4T1 > HeLa which is in agreement with APN levels found by Western-blot analysis.

6.2 INTRODUCTION

Following the criteria of the WHO, cancer leads the world ranking as the main death cause in developed countries, being the major obstacle to increasing life and health span.[1, 2] The main drawback in cancer treatment lies in its late detection due to, among other reasons, the lack of pain and body scans at the first stages of the disease. Besides, in the absence of external manifestations, patients are also unaware of the presence of the tumour. Thus, cancers are often detected in the middle and advanced stages, employing conventional medical instrumentation such as MRI,[3] CT,[4] US,[5] and PAI.[6] However, it has been widely demonstrated that when cancer is detected early, a large number of patients can be cured, reducing the risk of recurrence.[7] Therefore, real-time, dynamic, and visual monitoring of tumour onset, progression and treatment has a decisive role in personalized treatments. However, despite the large number of efforts applied in the development of early-cancer detection techniques, no universal method able to detect cancer has been described, among other causes, because the initial changes and biomarkers related to cancer are present at molecular and cellular level. Currently, preclinical trials and clinical practices are focused on monitoring reactive oxygen species (ROS), [8] antigens, [9] and enzymes, [10] in tissues from biopsies, body fluids and excretions, to explore early tumour detection.

Enzymes are generally located in groups with a particular subcellular localization. The size of these groups, as well as their location, change according to the biological enzyme function and can therefore also be used for the early detection of diseases. [11-13] In this way, levels of enzymes have great importance as biomarker for early detection and prognosis, as well as for the formulation of personalized treatments and their monitorization.[14] In this scenario, fluorescence imaging techniques have emerged as powerful tools that allow real-time monitoring of enzyme levels with

spatio-temporal resolution, which is significant to both fundamental research and biomedical applications.[15,16]

Among enzymes as biomarkers, APN, also known as CD13, arises as one of the main enzymes related to cancer cell growth, migration, and tumour metastasis.[17-19] APN is a Zn^{2+} dependent membrane enzyme that cleaves N-terminal neutral amino acids expressed in normal tissues.[20,21] The over-expression, dysregulation, and alterations in the function of this enzyme have been related to several types of cancer, notably in those with aggressive characteristics.[22] For example, in breast,[23] ovarian,[24] thyroid,[25] pancreatic,[26] colorectal[27], and lung cancer the activity of APN has been strongly related to tumour progression, metastasis, and tumour cell survival due to its function in supplying amino acids to cell growth.[28-30] Besides, APN proteolytic activity has also been associated with the degradation of the extracellular matrix, promoting tumor cell migration and thus metastasis.[31] Furthermore, APN overexpression has been related to poor prognosis, as well as with the development of drug resistance in several cancer types.[32,33] Therefore, considering the crucial role of APN in tumors, its activity is an attractive target biomarker for tumor imaging.[34]

In the last years, a large number of analytical methods, such as hyperpolarized nuclear magnetic resonance,[35] or HR-MS have been developed for the detection of overexpressed APN levels in early cancer detection.[38,39] However, these techniques have numerous drawbacks, such as the requirement for bulky and expensive equipment or the need of trained personnel. An attractive alternative to these systems is the use of fluorogenic molecular probes constituted by an enzymatic recognition moiety, which performs sensitive and selective detection of APN overexpression (Table S1).[40] However, fluorogenic probes for imaging have, as main drawback, their usually high hydrophobicity, which results in their entrapment in the RES, which can lead to accumulation in the liver and spleen, with the subsequent problems of organ toxicity and side effects.[41]

Based on the above, and given the need to develop new systems with high sensitivity and selectivity for the detection of APN overexpression as a cancer biomarker, we report herein the design and synthesis of the highly soluble **NB-SO_3-Ala** probe to detect levels of APN enzyme. **NB-SO_3-Ala** is based on the the fluorophore NB modified with a sulfonic group (as reporting unit), covalently linked to an alanine amino acid (as APN substrate). The probe is chemically designed with a sulfonic group that provides a negative charge that together with the positive charge located into the imine group of NB configures a final zwitterionic structure. This zwitterionic configuration has been described as improving solubility, increasing cell diffusion, and preventing entrapment by the RES. Additionally, the zwitterionic character could facilitate a rapid renal clearance of the probe, reducing tissue accumulation and the subsequent cytotoxicity and side-effects.[42] The underlying idea is that the weakly emissive **NB-SO_3-Ala** (off state) will be transformed into the highly emissive NB-SO_3 fluorophore (on state) due to the APN-induced hydrolysis of the amide bond that linked alanine with the fluorophore (Figure 1). We also report the use of the **NB-SO_3-Ala** to detect APN overexpression in several cancer lines.

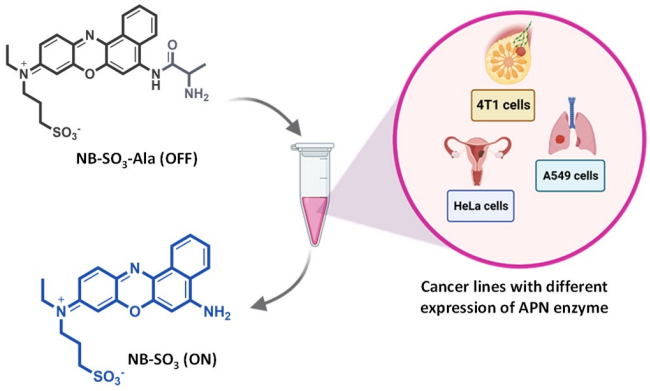

Figure 1. Schematic representation of the application of the **NB-SO_3-ALA** probe for the detection of overexpression of APN enzyme in different cancer lines.

6.3 RESULTS AND DISCUSSION

NB-SO_3 fluorophore was synthesized and characterized following the previously reported protocol (**Chapter 5: Leucine Aminopeptidase activatable Nile Blue-based NIR fluorescent probe for cancer detection)** (Figure S1). **NB-SO_3-Ala** probe was synthetized by a two-step protocol (Figure 2a). In the first step, tert-butyloxycarbonyl-L-alanine (Boc-Ala-OH) was covalently linked, through the formation of an amide bond, with the NB-SO_3 fluorophore. Then, in the second step, the Boc protecting group was removed with TFA, yielding **NB-SO_3-Ala** with a 58% global yield. NB-SO_3 fluorophore, **NB-SO_3-Ala** probe and intermediates were characterized by ^{1}H-NMR, ^{13}C-NMR and HRMS (Figure S2-S4).

After the synthesis and characterization of **NB-SO_3-Ala** and its fluorophore, we procede to the photochemical characterization. First, the quantum yields in PBS-DMSO (99:1 v/v at pH 7.4) of NB, **NB-Ala** (synthesized and characterized as reported in Chapter 4), NB-SO_3 (synthesized and characterized as reported in Chapter 5), and **NB-SO_3-Ala** (Table S2) were determined. We found that compounds containing sulphonic acid moieties show higher quantum yields ($\Phi_{\text{NB-SO}_3}$ = 0.0730**,** $\Phi_{\text{NB-SO}_3\text{-Ala}}$ = 0.0007) that their counterparts without the sulfonic group (Φ_{NB} = 0.0010**,** $\Phi_{\text{NB-Ala}}$ = 0.0002). It is also evident that the alanine group reduces significantly the quantum yield of the Nile Blue fluorophore both in **NB-SO_3-Ala** and **NB-Ala**.

As stated above, **NB-SO_3-Ala** was designed in such a way that the NB-SO_3 fluorophore is expected to be released after hydrolysis with APN enzyme (Figure 2b). **NB-SO_3-Ala** solutions in PBS-DMSO (99:1 v/v at pH 7.4) show a weak emission at ca. 660 nm upon excitation at 630 nm ($\Phi_{\text{NB-SO}_3\text{-Ala}}$ = 0.0007) (Figure 2c). In sharp contrast, when **NB-SO_3-Ala** probe was incubated with APN enzyme at the same conditions, a broad emission band centered at ca. 660 nm (λ_{exc} = 630 nm) was observed (3.5-fold). This emission enhancement at ca. 660 nm is ascribed to APN-induced hydrolysis of

the **NB-SO_3-Ala** probe that gives the high emissive NB-SO_3 fluorophore ($\Phi_{NB\text{-}SO_3}$= 0.0730). In fact, enzymatic hydrolysis of **NB-SO_3-Ala** by APN was verified by HPLC studies. At this respect, HPLC chromatogram of **NB-SO_3-Ala** probe in PBS-DMSO (99:1 v/v at pH 7.4) showed a single peak at 10.7 min (Figure 2d). Besides, HPLC chromatograms of **NB-SO_3-Ala** in PBS-DMSO (99:1 v/v at pH 7.4) in the presence of APN enzyme after 20 min of incubation, displayed two peaks at ca. 10.7 min and 12.5 min ascribed to **NB-SO_3-Ala** and NB-SO_3, respectively (Figure 2d).

The fluorescence emission of **NB-SO_3-Ala** in the absence of APN enzyme remained nearly unchanged with time (Figure 2e and Figure S5). However, upon addition of APN (750 ng·mL^{-1}), a time progressive fluorescence enhancement at 660 nm was observed, reaching the maximum value at 30 min, with an overall 3.5-fold enhancement. Besides, to determine the LOD, **NB-SO_3-Ala** in PBS-DMSO (99:1 v/v at pH 7.4) was incubated for 30 min in the presence of different amounts of APN enzyme (0-750 ng·mL^{-1}). The emission enhancement at 660 nm (λ_{exc}= 630 nm) was proportional to the amount of enzyme added (Figure 2f). From these data, the calibration curve shown in Figure 2g was obtained, which is linear over the APN concentration range 0–40.0 ng·mL^{-1} (R^2 = 0.93). LOD and LOQ of 17.2 ng·mL^{-1} and 57.8 ng·mL^{-1} were determined, respectively (using equation 1).

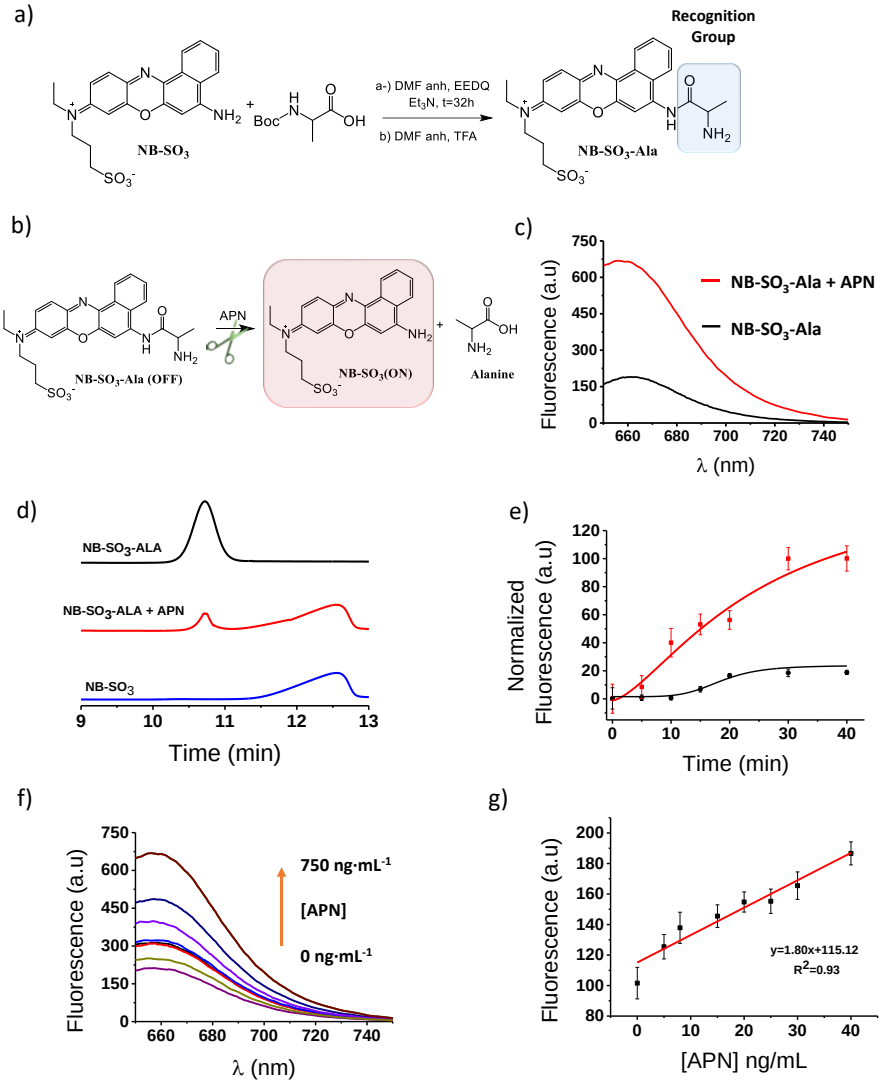

Figure 2. (a) Synthetic route of **NB-SO$_3$-Ala** probe. (b) APN-induced hydrolysis of the **NB-SO$_3$-Ala** probe. (c) Fluorescence emission of **NB-SO$_3$-Ala** (5 µM) in the presence of APN enzyme (750 ng·mL^{-1}) (red curve) and the absence of APN enzyme (black curve) in PBS-DMSO 99:1 v/v at pH 7.4 (λ_{exc} = 630 nm), after 30 min of incubation at 37°C. (d) Chromatograms of **NB-SO$_3$-Ala** (5 µM) + APN (750 ng·mL^{-1}) after 20 minutes upon enzyme addition (red curve), **NB-SO$_3$-Ala** (5 µM) (black curve) and NB-SO$_3$ (5 µM) (blue curve) in PBS-DMSO 99:1 v/v, pH 7.4. Conditions:

ODS Hypersil column, 1.8 mL·min^{-1}, Buffer (0.2 M of KH_2PO_4 solution, pH=3±0.1)-MeCN-Ethanol (90:10:2) elution, during 15 min. (e) Fluorescence of **NB-SO$_3$-Ala** (5 μM) in PBS/DMSO 99:1 v/v, pH 7.4 at different time points. Error bars are expressed as 3σ for three independent experiments. (f) Fluorescence emission spectra of **NB-SO$_3$-Ala** (5 μM) in PBS/DMSO 99:1 v/v, pH 7.4 with increasing concentrations of APN enzyme (0-750 ng·mL^{-1}). (g) Calibration curve of **NB-SO$_3$-Ala** (5 μM) at different APN concentrations in PBS/DMSO 99:1 v/v at pH 7.4. Fluorescence measures were taken 30 min after APN addition.

Finally, to evaluate the selectivity of the **NB-SO$_3$-Ala** probe towards APN, several potentially interfering species were added to **NB-SO$_3$-Ala** solutions. [13] As could be seen in Figure 3A, a clear emission enhancement was observed only in the presence of APN, while no changes in fluorescence were found for other potential interferents reported in the literature (i.e. Ca^{2+}, Fe^{3+}, Mg^{2+}, Mn^{2+}, H_2O_2, glutathione, cysteine, monoamine oxidase A, α-glutamyltransferase, nitroreductase, arginine and glycine).[43] The enzymatic hydrolysis mechanism was also validated with bestatin, a selective APN inhibitor. Thus, APN enzyme previously incubated with bestatin followed by the addition of the **NB-SO$_3$-Ala** probe showed a marked decreased emission (33 % lower) compared to that obtained in the presence of the APN enzyme alone (Figure 3b).

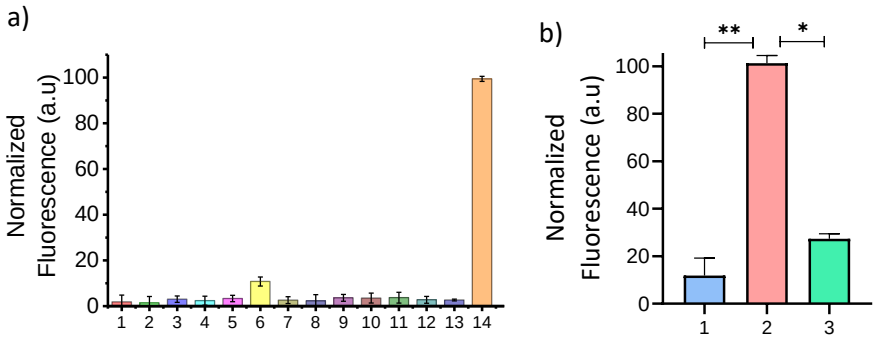

Figure 3. (a) Fluorescence emission of **NB-SO_3-Ala** (5 μM) in PBS/DMSO 99:1 v/v, pH 7.4 in the presence of different interferents at 660 nm (excitation at 630 nm): 1. Blank (5 μM); 2. Ca^{2+} (1 mM); 3. Fe^{3+} (1 mM); 4. Mg^{2+} (1 mM); 5. Mn^{2+} (1 mM); 6. H_2O_2 (10 mM); 7. Glutathione (1 mM); 8. Cysteine (1 mM); 9. Monoamine oxidase-A (100 mg/mL); 10. α-Glutamyltransferase (100 mg·mL^{-1}); 11. Nitroreductase (100 mg·mL^{-1}); 12. Arginine (1 mM); 13. Glycine (1 mM); 14. APN (750 mg·mL^{-1}). (B) Fluorescence at 660 nm of: (1) **NB-SO_3-Ala** (5 μM) only, (2) **NB-SO_3-Ala** (5 μM) + APN (750 mg·mL^{-1}) and (3) **NB-SO_3-Ala** (5 μM) + APN (750 mg·mL^{-1}) + Bestatin (100 μM) in PBS-DMSO 99:1 v/v at pH 7.4. Error bars are expressed as 3σ for three independent experiments. Values are expressed as mean ± SD. Statistical analysis was assessed by applying Student's T-test (*$p < 0.02$, **$p < 0.05$).

Encouraged by the selectivity observed for **NB-SO_3-Ala** towards APN enzyme, the probe was validated for the *in vitro* detection of endogenous APN levels associated with cancer. Among the most aggressive tumour types is lung cancer in which APN is considered to be highly overexpressed.[44] Despite advances in first-line standard treatment for lung cancer, the prognosis for this disease remains poor, with an estimated overall survival rate of only 23 % for all stages, thus evidencing the need for early diagnostic tests.[36] **NB-SO_3-Ala** probe was validated in WI-38 fibroblasts derived from lung tissue (healthy tissue) and lung cancer A549 cells. A549 cells were selected considering the significant APN overexpression in patient samples in many studies.[45,46] APN expression in WI-38 and A549 cells was tested using Western-blot

assay (Figure 4a and 4b) and it was found an overexpression of APN in A549 lung cancer cells compared with WI-38. **NB-SO_3-Ala** was also tested for toxicity against A549 cells, showing no toxic effect after 24 h of incubation at concentrations up to 10 μM (Figure 4c). Based on the results above, WI-38 and A549 cells were treated with **NB-SO_3-Ala** (10 μM) for 30 minutes prior to confocal image acquisition.

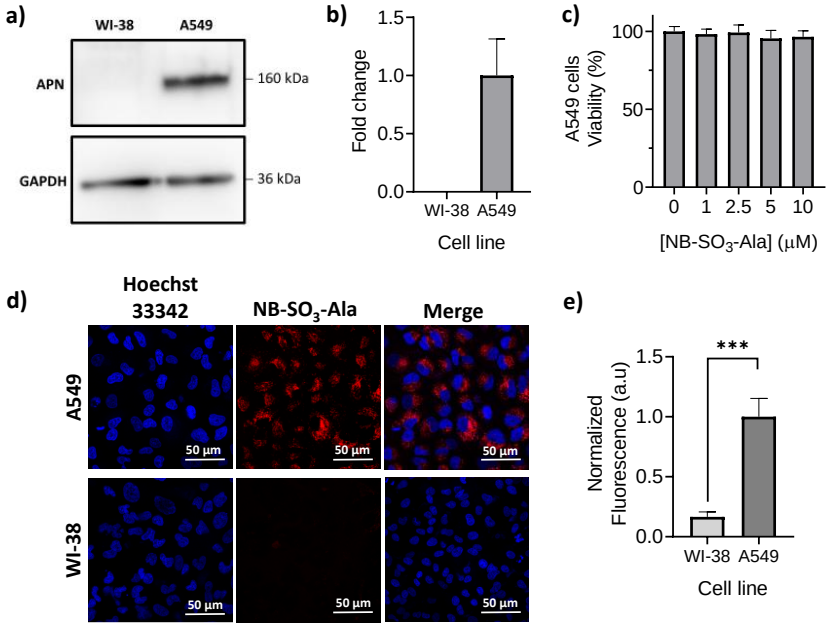

Figure 4. (a) APN expression determined by Western-blot assay in WI-38 and A549 cells. (b) Quantification of Western-blot assay. (c) Cell viability in A549 (human lung carcinoma cancer line) cells incubated with different concentrations of **NB-SO_3-Ala** probe for 24 h. The results are expressed as mean ± SD from tree independent studies (n=3) (d) Confocal images of WI-38 (negative APN cells) and A549 (positive APN cells) incubated with **NB-SO_3-Ala** (10 μM) for 30 minutes. (e) Fluorescence quantification of confocal images. The results exhibited representative images from three independent studies (n=3) and values are expressed as mean ± SD. Statistical analysis was assessed by applying Student's T-test (***$p < 0.001$).

As shown in Figure 4d, WI-38 cells did not exhibit any noticeable fluorescence signal after treatment, while A549 cells incubated with **NB-SO_3-Ala** showed a bright emission. Fluorescence quantification of confocal images showed a 7-fold emission enhancement in A549 cells when compared with WI-38 control cells (Figure 4e) in agreement with the high levels of APN and APN-induced probe hydrolysis that generated the highly emissive NB-SO_3 fluorophore.

Once the specificity of the **NB-SO_3-Ala** probe for the APN enzyme was confirmed, the probe was additionally tested in different types of cancer cells. Considering the aggressiveness of triple-negative breast cancer, 4T1 cells were selected to evaluate APN expression. HeLa cells were also tested although APN has not been extensively described in this cervical cancer type.[47-49] The level of endogenous APN enzyme in the selected cancer cells were determined by Western-blot assay. The highest expression of APN enzyme was found in lung cancer cells A549, followed by breast cancer 4T1 cells, whereas the lowest expression was observed for HeLa cells (Figure 5a and 5b). Viability studies confirmed that the **NB-SO_3-Ala** probe was not toxic to either 4T1 cells (Figure 5c) or for HeLa cells (Figure 5d) at concentrations up to 10 μM. Confocal images of **NB-SO_3-Ala** probe incubated with 4T1, HeLa and A549 cells showed fluorescence emission in the order A549 > 4T1 > HeLa (Figure 5e and 5f) which is in agreement with APN levels found in Western-blot analysis. These results confirm the use of the **NB-SO_3-Ala** probe to detect APN enzyme in cells.

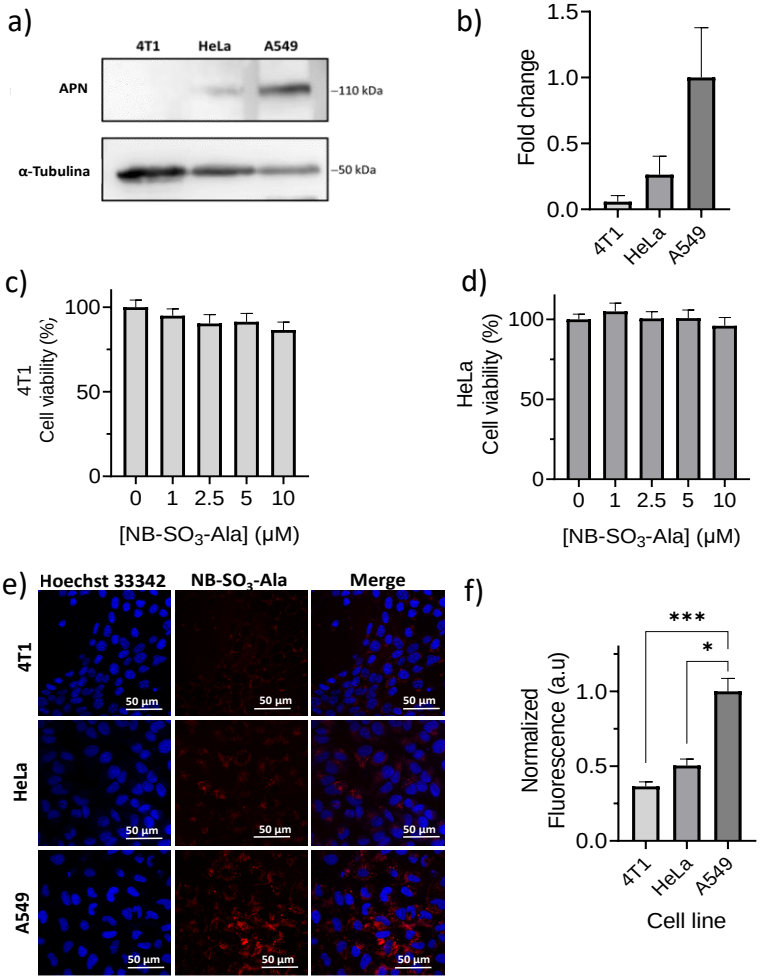

Figure 5. (a) Western blot assay for APN expression in 4T1, HeLa and A549 cells. (b) Quantification of Western-blot assay. (c and d) Cell viability in 4T1 (murine mammary cancer cell line) and HeLa (human cervix epitheloid carcinoma cell line) cells incubated with different concentrations of **NB-SO$_3$-Ala** probe for 24 h. The results are expressed as mean ± SD from tree independent studies (n=3). (e) Confocal images of 4T1, HeLa, and A549 cells incubated with **NB-SO$_3$-Ala** (10 μM) for 24 h. (f) Fluorescence quantification of confocal images. The greatest fluorescence variation was observed in A549 cells treated with **NB-SO$_3$-Ala** probe. The results exhibited representative images from three independent studies (n=3) and values are

expressed as mean ± SD. Statistical analysis was assessed by applying Student's T-test (***p < 0.001, *p< 0.05).

6.4 EXPERIMENTAL SECTION

Materials.

3-aminophenol, iodoethane, 1,3-propanesultone, Boc-Ala-OH, 2-ethoxy-1-ethoxycarbonyl-1,2-dihydroquinoline, anhydrous DMF, triethylamine, TFA, Boc-L-Ala, $NaNO_2$, K_2CO_3, $FeCl_3$, $CaCl_2$, $MnCl_2$, $MgCl_2$, H_2O_2, glutathione, cysteine, arginine, glycine, bestatin, monoamine oxidase A from *baculovirus* infected BTI insect cells (MAO-A), γ-glutamyltransferase from porcine kidney, and nitroreductase from *Escherichia coli* were obtained from Sigma-Aldrich. Recombinant Human Aminopeptidase N/CD13 Protein (APN) from mouse myeloma cell line, were purchased from R&D Systems. **NB-Ala** probe and NB-SO_3 fluorophore were synthetized following the procedures reported in Chapter 4 and 5, respectively. ^{1}H and ^{13}C NMR spectra were recorded on a Bruker FT-NMR Avance 400 (Ettlingen, Germany) spectrometer at 300 K. Fluorescence spectroscopy was carried out in a JASCO spectrofluorometer FP-8500 and absorption spectra were collected in a JASCO V-650 spectrophotometer. HPLC-MS was recorded with an Agilent 1620 Infinity II HPLC coupled to a mass spectrometer Agilent Ultivo equipped with a triple QTOF detector. PuriFlash XS 520 Plus was used for purification. Confocal fluorescence images were taken on a Leica TCS SP8 AOBS. Images were analyzed using Image J software.

Table S1. Comparison of NB-SO_3-Ala with other fluorescent probes for the detection of APN overexpression.

Probe	λ exc/ λ em (nm)	Time (min)	LOD	*In vitro* (Cell lines)	*In vivo* model	Ref.
HCAN	665/705	45	0.8 ng/mL	HepG2	Tumor-bearing BALB/c nude mice	X. He, et al. *ChemComm.***2017**, *53*, 9438–9441.
NBFMel	635/680	20	0.75 ng/mL	C8161 HT1080 B16/BL6	B16/BL6-tumor-bearing mice	M. Xiao,et al. *Adv.Funct.Mater.***2018**,*28*,1805128
DCM-APN	470/664	120	0.25 ng/mL	HepG-2 B16/BL6	Bearing HepG-2 xenograft tumors in nude BALB/c mice	H. Li, et al. *Chem.Sci*.**2019**, *10*, 1619 – 1625.
CyP1	675/720	Not reported	Not reported	5637 4T1	Bladder cancer in living mice	J. Huang, et al. *Angew.Chem*.**2020**,*132*,4445 –4450
YH-APN	λ em= 650	30	0.13 ng/mL	HepG-2 B16/BL6	BABL/c mice bearing HepG-2 xenograft tumor	H. Li, et al. *J. Am. Chem. Soc.* **2020**, *142*, 6381–6389
HBPQ	475/545	120	1.50 ng/mL	HepG2	Not reported	Y. Liu, et al. *Anal. Chem.* **2021**, *93*, 6463–6471
TMN-Abu	500/660	30	0.57 mg/mL	HepG2 A549 HCT-116	Tumor-bearing nude mice Diabetic model mice	S.-Y. Liu et al. *Sensors and Actuators: B. Chemical.***2022**, *363*, 1-9
NB-SO_3-Ala	630/660	30	17.2 ng/mL	4T1 HeLa A549	Not Reported	This work

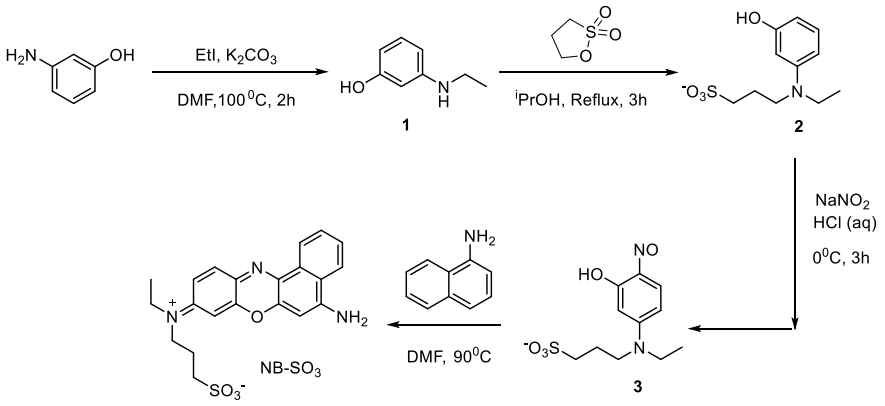

Figure S1. Synthetic route of NB-SO_3 fluorophore.

Synthesis of NB-SO_3-Ala.

Boc-Ala-OH (104.06 mg, 0.55 mmol), triethylamine (76.60 µL, 0.55 mmol) and EDDQ (136.00 mg, 0.55 mmol) were mixed in a 10 mL round bottom flask under argon atmosphere and dissolved in 5 mL of anhydrous DMF. The reaction mixture was stirred at room temperature under argon atmosphere for 1 h. Then, NB-SO_3 (150.00 mg, 0.37 mmol) in 2 mL of anhydrous DMF was added dropwise. Final reaction mixture was heated at 70°C for 32 h. After that, TFA solution (5 mL DMF: 750 µL TFA) was added to the reaction mixture and stirred for another 24 h. The solvent was removed under vacuum pressure. **NB-SO_3-Ala** was purified as purple solid with PuriFlash XS 520 Plus using a PF-30C18HP-F0004 column (hexane-ethyl acetate 95:5 v/v as eluent, 5.0 mL·min^{-1} of flow rate) (58 % yield). ^{1}H NMR (400 MHz, MeOD) δ (ppm) 9.21–9.18 (m, 1H), 9.15 (d, J = 8.4 Hz, 1H), 8.33 (d, J = 8.3 Hz, 1H), 8.26 (d, J = 8.6 Hz, 1H), 8.16 (ddd, J = 8.6, 6.9, 1.4 Hz, 1H), 8.06 (dd, J = 8.4, 5.3 Hz, 1H), 7.97 (t, J = 7.7 Hz, 2H), 3.31 (p, J = 1.7 Hz, 3H), 3.00 (s, 1H), 2.86 (s, 1H), 1.51 (s, 3H), 1.44 (t, J = 2.5 Hz, 3H), 1.30 (d, J = 7.3 Hz, 9H). ^{13}C NMR (101 MHz, DMSO) δ (ppm): 148.47,

143.66, 140.25, 131.55, 128.53, 128.16, 127.80, 125.65, 121.71, 45.67, 45.62, 28.17, 8.52. HRMS: Theoretical ($M+H^+$): 482.5554 m/z. Experimental ($M+H^+$): 483.1699 m/z.

Characterization of NB-SO_3-Ala

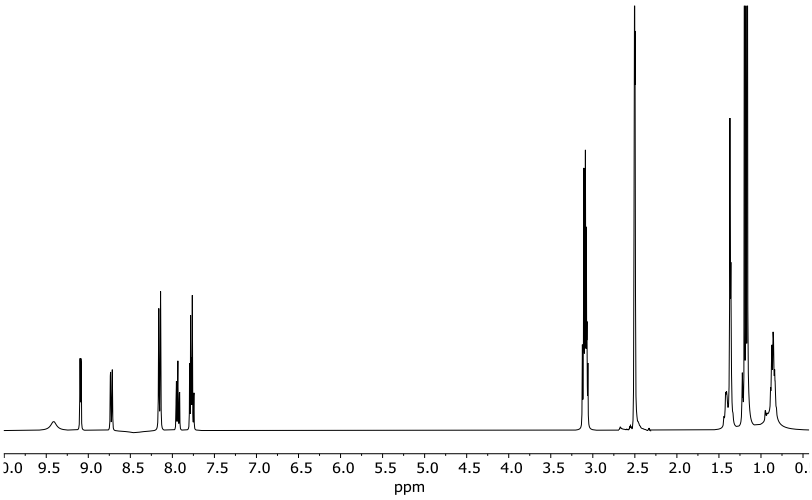

Figure S2. ^{1}H-NMR of **NB-SO_3-Ala**.

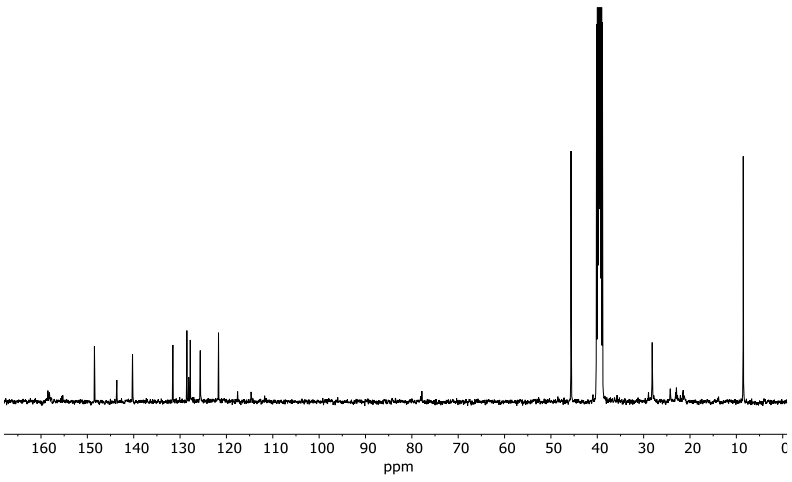

Figure S3. ^{13}C-NMR of **NB-SO_3-Ala**.

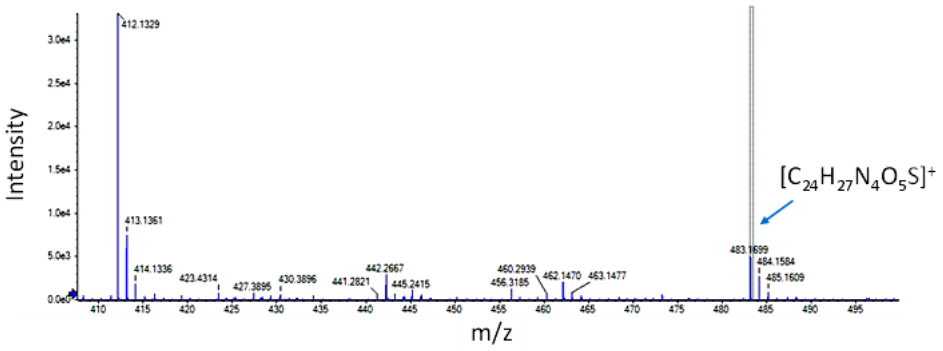

Figure S4. HRMS of **NB-SO$_3$-Ala.**

HPLC monitoring NB-SO$_3$-Ala hydrolysis.

HPLC chromatograms were obtained employing a Hypersil Gold CN column in an isocratic flow rate of (1.8 mL·min^{-1}, water Buffer (KH_2PO_4 0.2 M, pH = 3 ± 0.1)-MeCN-Ethanol (90:10:2 v/v/v) for 15 min. Pure reagent samples of NB-SO$_3$ and **NB-SO$_3$-Ala** were prepared from a 1.0 x 10^{-3} M stock solution for a final concentration of 5 µM, while hydrolysis sample chormatogram was recorder 20 min after incubation of **NB-SO$_3$-Ala** probe (5 µM) with APN enzyme (750 ng·mL^{-1}).

General procedure for APN detection.

For fluorescence measurements, a **NB-SO$_3$-Ala** stock solution was prepared (1.0 x 10^{-3} M in DMSO). Samples were prepared from 1 µL of probe stock solution, followed by the addition of APN enzyme dissolved in PBS (10 mM, pH 7.4). Final volume of samples was adjusted to 200 µL with PBS solution (pH 7.4). Samples were incubated at 37°C for 30 min in a thermostat before taking the fluorescence measurements, which were recorded upon excitation at 630 nm. A control solution, without APN, was measured under the same conditions.

Calibration curve in PBS/DMSO.

LOD and LOQ were obtained from the plot of fluorescence intensities at 660 nm, upon excitation at 630 nm, versus APN concentration in ng·mL^{-1}. LOD and LOQ were calculated by using equation 1:[50]

LOD/LOQ=K*Sb/m (Equation 1)

K is a constant with a value of 3 or 10 for LOD or LOQ, respectively; Sb is the standard deviation of the blank and *m* is the slope of the calibration curve. The resulting LOD and LOQ were 17.2 ng·mL^{-1} and 57.8 ng·mL^{-1}, respectively.

Photophysical characterization of NB-SO_3 and NB-SO_3-Ala.

Molar extinction coefficients, stokes shifts and quantum yields were determined for NB-SO_3 and **NB-SO_3-Ala** (Table S1). Quantum yields values were measured using NB dissolved in water as standard (Φ = 0.01)[51] using the equation S1:[52]

$$\frac{\Phi_x}{\Phi_s} = \frac{S_x}{S_s} \times \frac{1-10^{-A_S}}{1-10^{-A_x}} \times \frac{n_x^2}{n_s^2} \quad \text{(S1)}$$

where x and s indicate the unknown and standard solution, respectively, Φ is the quantum yield, S is the area under the emission curve, A is the absorbance at the excitation wavelength and n is the refraction index. Molar extinction coefficients for NB, **NB-Ala**, NB-SO_3 and **NB-SO_3-Ala** were obtained at the adsorption maximum of 630 nm.

Table S2. Photophysical parameters for NB, **NB-Ala**, NB-SO_3, **NB-SO_3-Ala.**

	NB	**NB-Ala**	**NB-SO_3**	**NB-SO_3-Ala**
Molar extinction coefficient [L·(mol·cm^{-1})^1]	10500	1500	20000	2004
Quantum yield	0.0100	0.0002	0.0730	0.0007
Stokes shift (nm)	37	45	38	31

Kinetic studies.

Fluorescence spectra of the reaction mixture were recorded every 5 min to show the fluorescence responses triggered by the reaction between 750 ng·mL^{-1} of APN and 5 µM of **NB-SO_3-Ala** within 30 min.

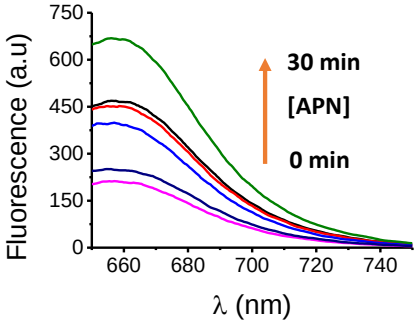

Figure S5. Fluorescence of **NB-SO_3-Ala** in (PBS/DMSO 99:1 v/v, pH 7.4) at different time points in the absence and in the presence of APN enzyme (750 ng·mL^{-1}).

Table S3. Fluorescence at 660 nm and Fluorescence enhancement (F (t)/F (t=0)) of NB-SO_3-Ala in PBS-DMSO (99:1 v/v at pH 7.4) solution at different times in the presence of APN enzyme (750 ng·mL^{-1}).

	NB-SO_3-Ala + APN	
Time (min)	**Fluorescence at 660 nm (a.u)**	**F(t)/F(t=0)**
0	205.0	1
5	246.9	1.2
10	391.0	1.9
15	449.1	2.2
20	466.1	2.3
30	666.5	3.3

Cell Culture.

4T1 breast cancer cell line, HeLa human cervical carcinoma cells WI-38 lung-tissue human fibroblast cell line and A549 human lung carcinoma cell line were purchased from the ATCC, cultured in DMEM (Dulbecco's Modified Eagle Medium) supplemented with 10% FBS (Fetal bovine serum) (Sigma), and for WI-38 cells supplemented with 1X Non-Essential aminoacids (Gibco). Cells were maintained in 20% O_2 and 5% CO_2 atmosphere at 37°C.

Western blot assays.

To determine the levels of APN protein in each cellular line (4T1, HeLa, WI-38 and A549) whole-cell extracts were obtained using lysis buffer (25 mM Tris-HCl pH 7.4, 1 mM EDTA, 1% SDS, plus protease and phosphatase inhibitors). Cell lysates were resolved in 8% SDS-PAGE gels, transferred to nitrocellulose membranes, blocked with

5% non-fat milk, and incubated overnight with the primary antibody for APN (ab108310, abcam). Besides, GAPDH (#85925 from CellSignalling) was used as reference protein for normalization. Then, membranes were washed and probed with the secondary antibody conjugated to horseradish peroxidase, anti-rabbit IgG peroxidase antibody (#A6154, Sigma) for enhanced chemiluminescence detection (Amersham Pharmacia Biotech).

Confocal *in vitro* experiments.

4T1, HeLa, WI-38 and A549 cells were seeded in a cover slip in a 6-well plate at 250,000 cells per well. After 24 h cells were incubated with **NB-SO_3-Ala** (10 µM) for 30 minutes, washed with PBS washed, and coverslips were mounted to confocal visualization. Hoechst 33342 was added at 2 $\mu g \cdot mL^{-1}$ for nuclei staining. Confocal images were acquired in a Leica TCS SP8 AOBS confocal microscope (λ_{exc} = 638 nm; λ_{em} = 656-781 nm). Images were quantified by using the Image J software.

***In vitro* cytotoxicity studies.**

For the *in vitro* cytotoxicity studies, A549 cells were seeded in a 96-well plate (10,000 cells per well) and incubated for 24 h. Then, the cells were incubated with varying concentrations of the **NB-SO_3-Ala** probe (diluted in DMEM) for 24 h. The cell viability was determined by WST-1 reagent which was added for 30 min and then absorbance was measured at 638 nm at Wallac 1420 Victor2 Microplate Reader (Perkin Elmer).

6.5 CONCLUSIONS

This study shows the synthesis and characterization of **NB-SO_3-Ala,** a fluorogenic molecular probe selective to the APN enzyme detection. **NB-SO_3-Ala** is weakly

fluorescent. However, in the presence of APN enzyme, **NB-SO_3-Ala** is hydrolysed releasing the highly emissive NB-SO_3 fluorophore. **NB-SO_3-Ala** contains a sulfonic group to improve its solubility and cell trafficking, minimizing tissue time exposure and the consequent potential toxicity. **NB-SO_3-Ala** probe was successfully validated *in vitro* for APN detection in differenct cancer cell lines. Confocal images showed fluorescence signal in APN-positive cells, which is proportional to the APN levels determined by Western-blot analysis.

ACKNOWLEDGEMNTS

This research was supported by project PID2021-126304OB-C41 funded by MCIN/ AEI /10.13039/501100011033/ and by European Regional Development Fund - A way of doing Europe. This study was also supported by Generalitat Valenciana (CIPROM/2021/007). Thank the financial support from the FEDER found of European Union (IDIFEDER/2021/044). This research was supported by CIBER -Consorcio Centro de Investigación Biomédica en Red- (CB06/01/2012), Instituto de Salud Carlos III, Ministerio de Ciencia e Innovación. M. D. -R. thanks to his predoctoral fellowship Grisolia to the Genelalitat Valenciana (GRISOLIAP/2019/144). J.F.B. thanks to his postdoctoral fellowship Sara Borrell from ISCIII (CD19/00038) and CIAPOS/2021/198 funded by the Generalitat Valenciana. V.M.-C. thanks the financial support from project CIDEGENT/2020/031 funded by the Generalitat Valenciana.

6.6 REFERENCES

1. World Health Organization (WHO). Global Health Estimates 2020: Deaths by Cause, Age, Sex, by Country and by Region, 2000-2019. Accessed December 11, **2020**.

2. Bray, F., Laversanne, M., Weiderpass, E., & Soerjomataram, I. The ever-increasing importance of cancer as a leading cause of premature death worldwide. *Cancer*, **2021**, *127*, 3029-3030.

3. Lawrentschuk, N., Haider, M. A., Daljeet, N., Evans, A., Toi, A., Finelli, A., Trachtenberg, J., Zlotta A. & Fleshner, N. 'Prostatic evasive anterior tumours': the role of magnetic resonance imaging. *BJU Int.*, **2010**, *105*, 1231-1236.

4. Paulus, M. J., Gleason, S. S., Kennel, S. J., Hunsicker, P. R., & Johnson, D. K. High resolution X-ray computed tomography: an emerging tool for small animal cancer research. *Neoplasia*, **2000**, *2*, 62-70.

5. Frangioni, J. V. New technologies for human cancer imaging. *J. Clin. Oncol.*, **2008**, *26*, 4012.

6. Valluru, K. S., & Willmann, J. K. Clinical photoacoustic imaging of cancer. *Ultrasonography*, **2016**, *35*, 267-280.

7. Vermorken, J. B., & Specenier, P. Optimal treatment for recurrent/metastatic head and neck cancer. *Ann. Oncol.*, **2010**, *21*, 252-261.

8. Zhu, H., Zhang, Z., Long, S., Du, J., Fan, J., & Peng, X. Synthesis of an ultrasensitive BODIPY-derived fluorescent probe for detecting HOCl in live cells. *Nat. Protoc.*, **2018**, *13*, 2348-2361.

9. Grunnet, M., & Sorensen, J. B. Carcinoembryonic antigen (CEA) as tumor marker in lung cancer. *Lung cancer*, **2012**, *76*, 138-143.

10. Kim, W. Y., Won, M., Salimi, A., Sharma, A., Lim, J. H., Kwon, S. H., Jeon, J. Y., Lee, J. Y. & Kim, J. S. Monoamine oxidase-A targeting probe for prostate cancer imaging and inhibition of metastasis. *ChemComm*, **2019**, *55*, 13267-13270.

11. Zhang, J., Chai, X., He, X. P., Kim, H. J., Yoon, J., & Tian, H. Fluorogenic probes for disease-relevant enzymes. *Chem. Soc. Rev.*, **2019**, *48*, 683-722.

12. Wu, X., Shi, W., Li, X., & Ma, H. Recognition moieties of small molecular fluorescent probes for bioimaging of enzymes. *Acc. Chem. Res.*, **2019**, *52*, 1892-1904.

13. Liu, Y., Xu, C., Liu, H. W., Teng, L., Huan, S., Yuan, L., & Zhang, X. B. Precipitated fluorophore-based molecular probe for in situ imaging of aminopeptidase N in living cells and tumors. *Anal. Chem.*, **2011**, *93*, 6463-6471.

14. Borrebaeck, C. A. Precision diagnostics: moving towards protein biomarker signatures of clinical utility in cancer. *Nat. Rev. Cancer.*, **2017**, *17*, 199-204.

15. Gu, K., Zhu, W. H., & Peng, X. Enhancement strategies of targetability, response and photostability for *in vivo* bioimaging. *Sci. China Chem.*, **2019**, *62*, 189-198.

16. Wu, X., Li, H., Lee, E., & Yoon, J. Sensors for in situ real-time fluorescence imaging of enzymes. *Chem*, **2020**, *6*, 2893-2901.

17. Schreiber, C. L., & Smith, B. D. Molecular imaging of aminopeptidase N in cancer and angiogenesis. *Contrast Media Mol. Imaging*, **2018**, *2018*, 1-15.

18. Aozuka, Y., Koizumi, K., Saitoh, Y., Ueda, Y., Sakurai, H., & Saiki, I. Anti-tumor angiogenesis effect of aminopeptidase inhibitor bestatin against B16-BL6 melanoma cells orthotopically implanted into syngeneic mice. *Cancer Lett.*, **2004**, *216*, 35-42.

19. Hata, R., Nonaka, H., Takakusagi, Y., Ichikawa, K., & Sando, S. Design of a hyperpolarized molecular probe for detection of aminopeptidase N activity. *Angew. Chem. Int. Ed.*, **2016**, *128*, 1797-1800.

20. Mina-Osorio, P. The moonlighting enzyme CD13: old and new functions to target. *Trends Mol. Med.*, **2008**, *14*, 361-371.

21. Dixon, J., Kaklamanis, L., Turley, H., Hickson, I. D., Leek, R. D., Harris, A. L., & Gatter, K. C. Expression of aminopeptidase-n (CD 13) in normal tissues and malignant neoplasms of epithelial and lymphoid origin. *J. Clin. Pathol.*, **1994**, *47*, 43-47.

22. Lendeckel, U., Karimi, F., Al Abdulla, R., & Wolke, C. The Role of the Ectopeptidase APN/CD13 in Cancer. *Biomedicines*, **2023**, *11*, 1-21.

23. Ranogajec, I., Jakić-Razumović, J., Puzović, V., & Gabrilovac, J. Prognostic value of matrix metalloproteinase-2 (MMP-2), matrix metalloproteinase-9 (MMP-9) and aminopeptidase N/CD13 in breast cancer patients. *Med. Oncol.*, **2012**, *29*, 561-569.

24. Van Hensbergen, Y., Broxterman, H. J., Hanemaaijer, R., Jorna, A. S., Van Lent, N. A., Verheul, H. M., Pinedo, H. M. & Hoekman, K. Soluble aminopeptidase N/CD13 in malignant and nonmalignant effusions and intratumoral fluid. *Clin. Cancer Res.*, **2002**, *8*, 3747-3754.

25. Kehlen, A., Lendeckel, U., Dralle, H., Langner, J., & Hoang-Vu, C. Biological significance of aminopeptidase N/CD13 in thyroid carcinomas. *Cancer Res.*, **2003**, *63*, 8500-8506.

26. Ikeda, N., Nakajima, Y., Tokuhara, T., Hattori, N., Sho, M., Kanehiro, H., & Miyake, M. Clinical significance of aminopeptidase N/CD13 expression in human pancreatic carcinoma. *Clin. Cancer Res.*, **2003**, *9*, 1503-1508.

27. Hashida, H., Takabayashi, A., Kanai, M., Adachi, M., Kondo, K., Kohno, N., Yamaoka, Y. & Miyake, M. Aminopeptidase N is involved in cell motility and angiogenesis: its clinical significance in human colon cancer. *Gastroenterology*, **2002**, *122*, 376-386.

28. Zhang, Q., Wang, J., Zhang, H., Zhao, D., Zhang, Z., & Zhang, S. Expression and clinical significance of aminopeptidase N/CD13 in non-small cell lung cancer. *J. Cancer Res. Ther.*, **2015**, *11*, 223-228.

29. Guzman-Rojas, L., Rangel, R., Salameh, A., Edwards, J. K., Dondossola, E., Kim, Y. G., Saghatelian, A.; Giordano, R. J., Kolonin, M. G., Staquicini, F. I., Koivunen, E., Sidman, R. L., Arap, W. & Pasqualini, R. Cooperative effects of aminopeptidase N (CD13) expressed by nonmalignant and cancer cells within the tumor microenvironment. *Proc. Natl. Acad. Sci.*, **2012**, *109*, 1637-1642.

30. Lendeckel, U., Karimi, F., Al Abdulla, R., & Wolke, C. The Role of the Ectopeptidase APN/CD13 in Cancer. *Biomedicines*, **2023**, *11*, 1-21.

31. Siegal, R., Miller, K. D., & Jemal, A. Cancer statistics, 2012. *CA Cancer J. Clin.*, **2014**, *64*, 9-29.

32. H. Hashida, A. Takabayashi, M. Kanai, M. Adachi, K. Kondo, N. Kohno, Y. Yamaoka, M. Miyake. Aminopeptidase N is involved in cell motility and angiogenesis: its clinical significance in human colon cancer. *Gastroenterology*, **2002**, *122*, 376-386.

33. H. Murakami, A. Yokoyama, K. Kondo, S. Nakanishi, N. Kohno, M. Miyake Circulating aminopeptidase N/CD13 is an independent prognostic factor in patients with non-small cell lung cancer. *Clin. Cancer Res.*, **2005**, *11*, 8674-8679.

34. Taylor, A. Aminopeptidases: structure and function. *FASEB J.*, **1993**, *7*, 290-298.

35. Siegal, R., Miller, K. D., & Jemal, A. Cancer statistics, 2012. *CA Cancer J. Clin.*, **2014**, *64*, 9-29.

36. Cokkinides, V., Albano, J., Samuels, A., Ward, M., & Thum, J. American cancer society: Cancer facts and figures. Atlanta: American Cancer Society, **2005**, *2017*.

37. Smida, T., Bruno, T. C., & Stabile, L. P. Influence of estrogen on the NSCLC microenvironment: a comprehensive picture and clinical implications. *Front. Oncol.*, **2020**, *10*, 1-15.

38. Brahmer, J. R., Tykodi, S. S., Chow, L. Q., Hwu, W. J., Topalian, S. L., Hwu, P., Drake, Ch. G., Camacho, L. H., Kauh, J., Odunsi, K., Pitot, H. C., Hamid, O., Bhatia, Sh., Martins, R., Eaton, K., Chen, Sh., Salay, T. M., Alaparthy, S., Grosso, J. F., Korman A. J., Parker, S. M., Agrawal, Sh.,Goldberg, S. G., Pardoll, D. M., Gupta, A. & Wigginton, J. M. Safety and activity of anti–PD-L1 antibody in patients with advanced cancer. *N. Engl. J. Med.*, **2012**, *366*, 2455-2465.

39. Sharma, P., Hu-Lieskovan, S., Wargo, J. A., & Ribas, A. Leading edge review primary, adaptive, and acquired resistance to cancer immunotherapy. *Cell*, **2017**, *168*, 707-723.

40. Saito, Y., Yatabe, H., Tamura, I., Kondo, Y., Ishida, R., Seki, T., Hiraga, K., Eguchi, A., Takakusagi, Y., Saito, K., Oshima, N., Ishikita, H., Yamamoto, K., Krishinina, M. C. & Sando, S. Structure-guided design enables development of a hyperpolarized

molecular probe for the detection of aminopeptidase N activity *in vivo*. *Sci. Adv.*, **2022**, *8*, 1-10.

41. Basile, F., Ferrer, I., Furlong, E. T., & Voorhees, K. J. Simultaneous multiple substrate tag detection with ESI-ion trap MS for *in vivo* bacterial enzyme activity profiling. *Anal. Chem.*, **2002**, *74*, 4290-4293.

42. Hata, R., Nonaka, H., Takakusagi, Y., Ichikawa, K., & Sando, S. Design of a hyperpolarized molecular probe for detection of aminopeptidase N activity. *Angew. Chem. Int. Ed.*, **2016**, *12*, 1797-1800.

43. Li, H., Yao, Q., Sun, W., Shao, K., Lu, Y., Chung, J., Kim, D., Fan, J., Long, S., Du, J., Li, Y., Wang, J., Yoon, J. & Peng, X. Aminopeptidase N activatable fluorescent probe for tracking metastatic cancer and image-guided surgery via in situ spraying. *J. Am. Chem. Soc*. **2020**, *142*, 6381-6389.

44. Paracha, N., Abdulla, A., & MacGilchrist, K. S. Systematic review of health state utility values in metastatic non-small cell lung cancer with a focus on previously treated patients. Health Qual. *Life Outcomes*, **2018**, *16*, 1-30.

45. Schmidt, L. H., Brand, C., Stucke-Ring, J., Schliemann, C., Kessler, T., Harrach, S., Mohr, M., Gorlich, D., Marra, A., Hilejan, L., Muller-tidow, C., Wardelmann, E., Wiewrodt, R., Berdel, W. E., Schwoppe, Ch. & Hartmann, W. Potential therapeutic impact of CD13 expression in non-small cell lung cancer. *PLoS One*, **2017**, *12*, 1-16.

46. Zhang, Q., Wang, J., Zhang, H., Zhao, D., Zhang, Z., & Zhang, S. Expression and clinical significance of aminopeptidase N/CD13 in non-small cell lung cancer. *J. Cancer Res. Ther.*, **2015**, *11*, 223-228.

47. Ranogajec, I., Jakić-Razumović, J., Puzović, V., & Gabrilovac, J. Prognostic value of matrix metalloproteinase-2 (MMP-2), matrix metalloproteinase-9 (MMP-9) and aminopeptidase N/CD13 in breast cancer patients. *Med. Oncol.*, **2012**, *29*, 561-569.

48. Tsukamoto, H., Shibata, K., Kajiyama, H., Terauchi, M., Nawa, A., & Kikkawa, F. (2008). Aminopeptidase N (APN)/CD13 inhibitor, Ubenimex, enhances radiation sensitivity in human cervical cancer. *BMC Cancer*, **2008**, *8*, 1-8.

49. Barnieh, F. M., Loadman, P. M., & Falconer, R. A. Is tumour-expressed aminopeptidase N (APN/CD13) structurally and functionally unique? *Biochimica et Biophysica Acta (BBA)-Reviews on Cancer*, **2021**, *1876*, 1-9.

50. Shrivastava, A., & Gupta, V. B. Methods for the determination of limit of detection and limit of quantitation of the analytical methods. *Chron. Young Sci.*, **2011**, *2*, 21-25.

51. Jose, J., Ueno, Y., & Burgess, K. Water-soluble Nile blue derivatives: syntheses and photophysical properties. *Chem. Eur. J.*, **2009**, *15*, 418-423.

52. Lakowicz, J. R. (Ed.). Principles of fluorescence spectroscopy. Boston, MA: springer US, **2006**.

Chapter 7| A renal clearable probe for *in vivo* monoamine oxidase (MAO) detection.

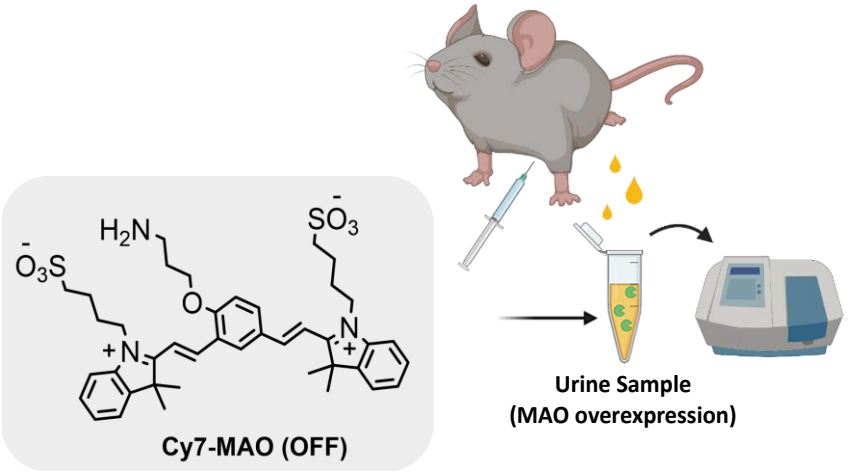

A renal clearable probe for *in vivo* monoamine Oxidase (MAO) detection.

Marcia Domínguez,[a,b] Araceli Lérida-Viso,[a,b,c,d] David Azorín-Soriano,[c] Vicente Martí-Centelles,[a,b] Juan F. Blandez,[a,b,d,e*] Alba García-Fernández,[a,b,c,d] Félix Sancenón,[a,b,c,d*] and Ramón Martínez-Máñez[a,b,c,d*]

a. Instituto Interuniversitario de Investigación de Reconocimiento Molecular y Desarrollo Tecnológico (IDM), Universitat Politècnica de València, Universitat de València, Spain.
b. CIBER de Bioingeniería, Biomateriales y Nanomedicina, Instituto de Salud Carlos III.
c. Unidad Mixta UPV-CIPF de Investigación en Mecanismos de Enfermedades y Nanomedicina, Universitat Politècnica de València, Centro de Investigación Príncipe Felipe, Spain.
d. Unidad Mixta de Investigación en Nanomedicina y Sensores, Universitat Politècnica de València, Instituto de Investigación Sanitaria La Fe, Spain.
e. Adsorption & Advanced Materials Laboratory (A2ML), Department of Chemical Engineering & Biotechnology, University of Cambridge, Philippa Fawcett Drive, Cambridge CB3, 0AS, U.K.

7.1 ABSTRACT

Hyperactivation of monoamine oxidase enzymes (MAO) is related to an uncontrolled production of neurotoxic compounds such as H_2O_2 and other ROS, whose accumulation can be linked with the development of neurodegenerative, chronic, and age-related diseases. Although the use of chromo-fluorogenic probes for the detection and quantification of MAO enzyme *in vitro* and *in vivo* has been reported in the literature, simple, and non-invasive procedures for monitoring the overexpression of MAO enzyme *in vivo* have not been described to date. Here we describe the design, synthesis, and characterization of a renal clearable fluorogenic probe based on cyanine-7 fluorophore (**Cy7-MAO**) for the *in vivo* detection of MAO enzymatic overexpression through fluorescence measurements in urine. The probe is functionalised with sulfonic groups and a propylamino group that is a substrate of the MAO enzyme. Upon administration of the probe to animals the **Cy7-MAO** probe is hydrolyzed at site in the presence MAO enzyme, resulting in the release of highly emissive Cy7-fluorophore that is renally cleared and can be quantified in urine. **Cy7-MAO** is successfully validated *in vitro* using HepG2 liver human cells, with endogenous high levels of MAO enzyme. We also provided evidence of the use of the **Cy7-MAO** probe to monitor different burden of MAO enzymes *in vivo*. We found that the expression of MAO in healthy elderly mice increases significantly compared with young animals, suggesting that MAO overexpression can be used as a biomarker of aging. The results suggest that this could be a strategy to facilitate longitudinal studies of physiological processes or diseases associated with MAO overactivity.

7.2 INTRODUCTION

MAO enzymes belong to the family of flavoenzymes that can be found in most cells type in the body. MAO enzymes can be present in two isoforms, MAO-A and MAO-B, which show a 70% homology sequence.[1] Both are vital for the inactivation of monoaminergic neurotransmitters but with different specificities. MAO-A cleaves mainly serotonin, melatonin, noradrenaline, and adrenaline, whereas MAO-B cleaves preferably phenethylamine and benzylamine.[2] Moreover, MAO enzymes induce the generation ofROS in the catalytic oxidation of amine to imine.[3-6] ROS compounds raise oxidative stress and, ultimately, accelerate the development of neurodegenerative diseases, such as Parkinson, Alzheimer or amyotrophic lateral sclerosis.[7-10] In the same way, it has been described that high levels of ROS, generated by MAO overexpression, may be a key factor in the development of chronic diseases such as endothelial dysfunction in hypertension, metabolic disorders, and chronic kidney disease, all associated with different burdens of inflammatory process. [11, 12]

In the same way, tissue-specific changes in MAO levels have also been described in age-related disorders.[13] The increased longevity in the population is associated with a higher prevalence of chronic diseases, suggesting the existence of a common process of functional decline in organ systems.[14] Increased oxidative stress and mitochondrial dysfunction are key factors in cellular and organs function in the ageing process. Building on these data, an increasing number of studies have associated the possible involvement of MAO enzymes in age-related disorders and their connection in ROS formation via H_2O_2 produced in the MAO enzymatic processes.[13,15]

Several procedures have been described in the literature to detect MAO overexpression such as ELISA,[16] HPLC[17] or spectrophotometric assay.[18]

Nevertheless, these processes require specific equipment, long testing times, and trained personnel and do not allow MAO detection *in vivo*.[19,20] On the other hand, fluorometric detection methods are particularly engaging due to its cost-effectiveness, high sensitivity and selectivity (Figure 1a).[21] Several probes have been reported for MAO enzymes detection *in vitro* and in damaged tissues (Table S1). However, most of these probes cannot be used *in vivo* nor in longitudinal studies. An attractive alternative to classical probes is the design of diagnostic systems capable of detecting target biomarkers and have a rapid renal clearance. A few reports have been described based on this concept, employing ofr that protease-responsive nanoparticles,[22,23] fluorescent and chemiluminescent derivatives equipped β-cyclodextrin (HPβCD) derivatives,[24,25] or nanosensor based on ultra-small renally removable gold nanoparticles.[26] However, an alternative to these still complex techniques (using nanoparticles or requiring complex instrumentation) is the design of fluorophores having renal clearance properties. In this approach the probe, in an OFF state, is specifically transformed to an ON state by the action of a certain biomarker in cells/tissues *in vivo* and is designed to have a rapid elimination by the kidney into the urine where it can be easily measured. However, as far as we are aware, such approach has not been reported. Besides, these renal clearable probes might have high potential in clinical applications due to their rapid elimination, avoiding tissue accumulation and diminishing toxic side-effect. Such simple platforms could also be applicable in low-resource environments and might democratize access to advanced and sensitive diagnoses.

Building on the above discussed, we report herein a fluorescent molecular probe based on a modified cyanine-7 fluorophore (**Cy7-MAO**) containing a propylamine group as recognition moiety (Figure 1b.1).[27-32] The probe backbone has been modified with two sulfonic groups that increases it solubility and promotes rapid renal clearance in *in vivo* studies (Figure 1b.2).[33] In addition, the zwitterionic

character of the probe reduces the binding to proteins and the non-specific uptake in normal tissues and organs, which also increased its renal elimination.[34] The probe mechanism is based on an increase of the fluorescence signal in the presence of MAO enzymes that transform the weakly emissive **Cy7-MAO** molecule in the high-emissive Cy7-fluorophore, that is time-degradated in its also emissive Cy7-subproducts. The probe has been tested *in vitro* in HepG2 in which there is an endogenous MAO overexpression and *in vivo* were we demonstrated that there is higher load of MAO enzymes in elderly BALB/c compared with young animals.

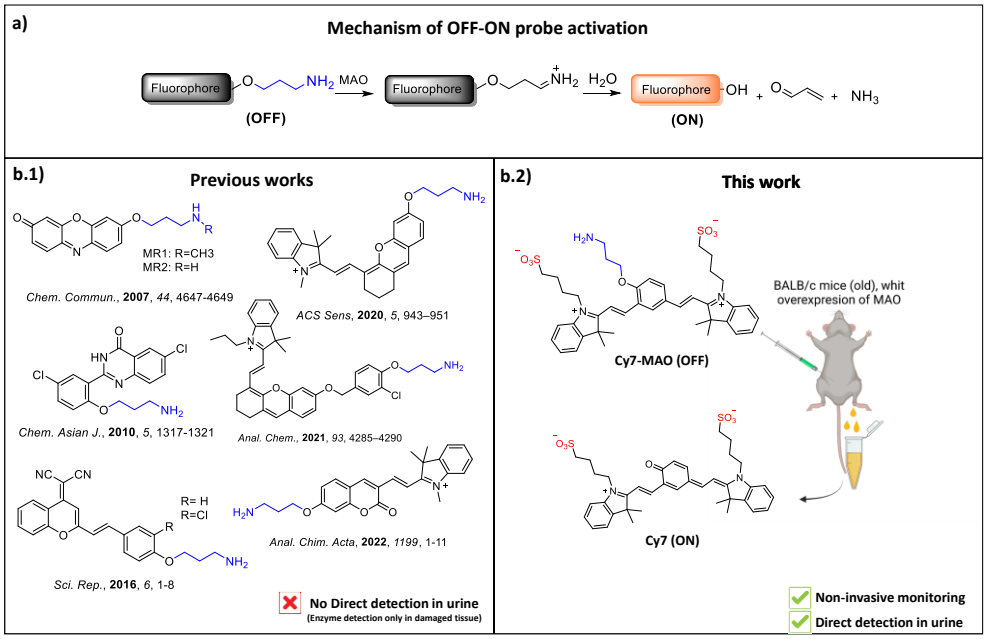

Figure 1. (a) Scheme illustration of the activatable fluorescence probes for MAOs by MAO enzymes that induce hydrolysis of the propylamine moiety. (b) Structure of fluorescent probes for the detection of MAOs reported in previous works (b.1) and in this work (b.2).

7.3 RESULTS AND DISCUSSION

Cy7-MAO probe was synthesized by a two-step procedure (Figure 2a). First, a nucleophilic substitution reaction was carried out between BOC-protected 3-

bromopropylamine and 5-formylsalycilaldehyde in anhydrous MeCN, followed by deprotection of the BOC-protecting group with TFA, yielding the intermediate compound **1**. Then, in a second step, a Knoevenagel condensation between **1** and the commercially available reagent 2,3,3-trimethyl-1-(4-sulfobutyl) indolium (**2**) yielded the final **Cy7-MAO** probe. **Cy7-MAO** was purified by silica gel chromatography and fully characterized by ^{1}H-NMR, ^{13}C-NMR and HRMS (Figures S1-S5 in Supporting Information). In addition, the Cy7-fluorophore was synthesized according to previously reported procedures (Figure S6).[35] On the other hand, emission of Cy7-fluorophore solutions (20 µM in HEPES, 10 mM, pH 7.4) at different pH values corroborated fluorophore stability in the pH range 5-10 (Figure S7).

The photophysical properties of **Cy7-MAO** probe were evaluated under simulated physiological conditions in the presence or absence of MAO-A or MAO-B enzymes (Table S1). **Cy7-MAO** (5 µM) solution in HEPES (10 mM, pH 7.4) is weakly emissive upon excitation at 450 nm. In sharp contrast, a broad fluorescence emission peak centered at 535 nm was observed upon enzyme addition (MAO-A or MAO-B at 100 $\mu g \cdot mL^{-1}$) under the same conditions (Figures 2b). 24 h after enzyme addition, an emission enhancement of 13.2-fold and 9.7 was observed for MAO-A and MAO-B, respectively (Table S2) that is ascribed to the enzymatic hydrolysis of **Cy7-MAO**, which releases the highly emissive Cy7 modified fluorophore. According to literature reports, the Cy7-fluorophore is inestable under biological condition, leading to its degradation to aldehyde (Cy7- subproduct) (Figure 2c).[36] To verify this, a study on the stability of Cy7 fluorophore was conducted through measurements of absorbance and fluorescence over time (Figure S8). Absorbance spectra indicate that, over time, the band around 600 nm gradually disappears, while a new band around 500 nm emerges, clearly indicating the degradation process of the Cy7 fluorophore. These observations were corroborated by fluorescence measurements, in chich under excitation at 590 nm, the distinctive cyanine band

(emission peaks at 670 nm) diminishes until nearly vanishing after 24 h. Conversely, under excitation at 450 nm, a notable increase in fluorescence intensity is observed.

The MAO-induced enzymatic hydrolysis of the **Cy7-MAO** probe was furtherly studied through HPLC. For this purpose, **Cy7-MAO** (5 μM) in HEPES buffer solution (10 mM, pH 7.4) was incubated with MAO-A enzyme (100 $\mu g \cdot mL^{-1}$) for 30 min. After this time, HPLC chromatograms clearly showed the disappearance of the **Cy7-MAO** peak and the appearance of the Cy7-fluorophore prior to its degradation in the Cy7-subproducts (Figure S9).

Next, the fluorescence emission of **Cy7-MAO** probe (5 μM) was monitored in the presence of different amounts of MAO-A or MAO-B enzymes (0-100 $\mu g \cdot mL^{-1}$) after 24 h of enzyme incubation (Figures 2c and 2e). A significant increase in emission at ca. 535 nm, aldehyde Cy7-subproduct, proportional to the amount of enzyme added was observed for the range of 0–60.0 $\mu g \cdot mL^{-1}$. These data were employed to determine the LOD 6.4 and 10.9 $\mu g \cdot mL^{-1}$ and LOQ of 29.3 and 52.1 $\mu g \cdot mL^{-1}$ for MAO-A and MAO-B, respectively (Figures 2d and 2f). These results indicate that **Cy7-MAO** probe can be used for the qualitative and quantitative detection of both isoforms of MAO enzyme.

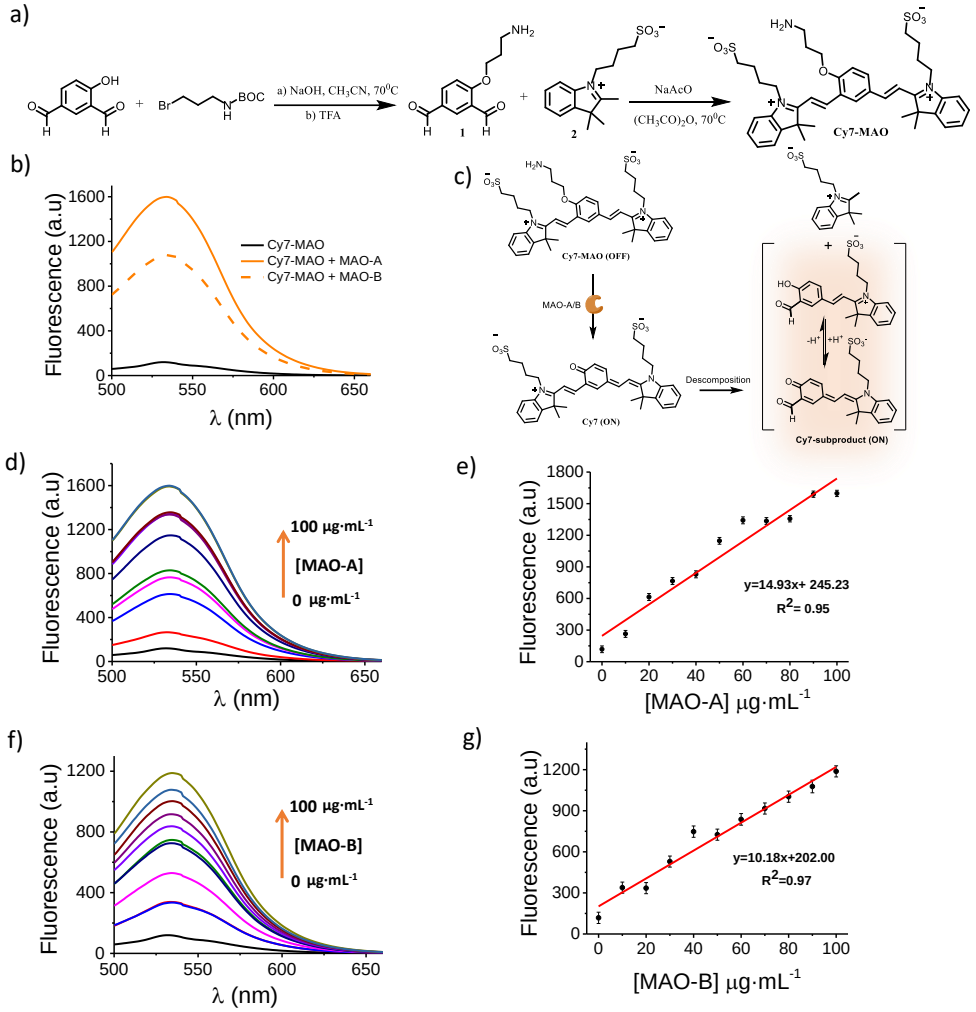

Figure 2. (a) Synthetic sequence used to prepare **Cy7-MAO** probe.(b) Fluorescence emission spectra (λ_{exc} = 450 nm) of **Cy7-MAO** (5 µM) (black curve) and **Cy7-MAO** (5 µM) + MAO-A/B (100 µg·mL^{-1}) (orange curves) in HEPES solution (10 mM, pH 7.4) after 24 h of incubation at 37°C. (c) MAO-induced hydrolysis of **Cy7-MAO** probe. (d and f) Fluorescence spectra of **Cy7-MAO** (5 µM) in the presence of increasing MAO-A/B concentrations (0-100 µg·mL^{-1}) after 24 h of incubation at 37°C. (e and g) Calibration curve of **Cy7-MAO** for MAO-A/B in HEPES solution (10 mM, pH 7.4). Error bars are expressed as 3σ for three independent experiments.

The selectivity of **Cy7-MAO** probe was also assessed in the presence of several potentially interfering species.[37] Only both MAO isoforms induced a remarkable emission enhancement (Figure 3a) at 535 nm, whereas no changes were found in the presence of selected cations, small molecules, or enzymes. Besides, additional experiments were performed in the presence MAO enzymes and MAO inhibitors (Clorgyline for MAO-A and Pargyline for MAO-B).[38,39] In both cases, the fluorescence signal of **Cy7-MAO** in presence of inhibitors was a 70% lower than the signal in its absence, confirming the proposed mechanism, i.e. the emission enhancement is due to the hydrolysis of **Cy7-MAO** by MAO enzymes (Figure 3b).

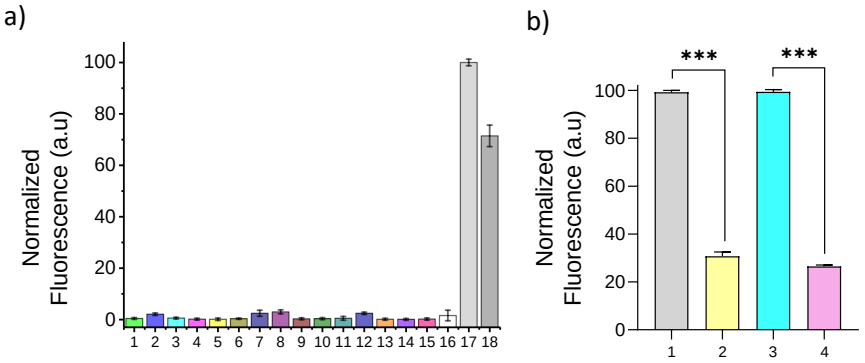

Figure 3. (a) Fluorescence emission of Cy7-MAO (5 µM) in HEPES (10 mM, pH=7.4, 37°C) in the presence of different interferents at 535 nm (excitation at 450 nm): 1, Na^+ (1 mM); 2, K^+ and NO_3^- (1 mM); 3, Ca^{2+} (1 mM); 4, Mg^{2+} (1 mM); 5, Fe^{3+} (1 mM); 6, H_2O_2 (10 mM); 7, Vitamin C (1 mM); 8, Arginine (1 mM); 9, Urea (20 mM); 10, Glucose (10 mM); 11, Acetyl Cholinesterase (150 mg·mL^{-1}); 12, Leucine Aminopeptidase (150 mg·mL^{-1}); 13, β-Galactosidase (150 mg·mL^{-1}); 14, Phosphatase (150 mg·mL^{-1}); 15, Lysozyme (150 mg·mL^{-1}); 16, Glutathione (1 mM); 17, MAO-A (100 µg·mL^{-1}) and 18, MAO-B (100 µg·mL^{-1}). (b) Fluorescence intensity: 1: Cy7-MAO + MAO-A; 2: Cy7-MAO + MAO-A + CL (clorgyline, a specific MAO-A inhibitor); 3: Cy7-MAO + MAO-B; 4: Cy7-MAO + MAO-B + PA (pargyline, a specific MAO-B inhibitor). The solutions used were prepared in HEPES (10 mM, pH=7.4, 37°C) with the following concentrations: Cy7-MAO (10 µM), MAO-A/B (10 µM), CL and PA (10 µM).

Error bars are expressed as 3σ for three independent experiments. Values are expressed as mean ± SD. Statistical analysis was assessed by applying Student's T-test (***$p < 0.001$).

Encouraged by the high sensitivity and selectivity of **Cy7-MAO** probe, we studied the possibility to use **Cy7-MAO** for the *in vitro* detection of endogenous MAO-A/B enzymes. For these studies human-derived HepG2 (hepatocellular carcinoma) cells were selected because they are known to display MAO-A and MAO-B overexpression.[40] Initially, **Cy7-MAO** toxicity was tested in HepG2 cells, showing no toxic effect after 48 h of incubation, even at concentrations as high as 200 µM (Figure 4a). Besides, MAO expression in HepG2 was further confirmed by Western Blot, exhibiting endogenous high levels of MAO-A and MAO-B (Figure 4b). In sharp contrast, Western Blot of SK-Mel-103 human melanoma cells, used as control, showed low levels of MAO-A and MAO-B enzymes (Figure 4b). Confocal images of the cells incubated with **Cy7-MAO** probe showed strong fluorescence signal in HepG2 cells compared to SK-Mel-103 cells (2-fold), which displayed a negligible signal (Figures 4c and 4d). The hydrolysis of **Cy7-MAO** only occurs in HepG2 cells which overexpress MAO-A/B. Besides, no emission was observed in the absence of probe in both cell lines (Figure S10).

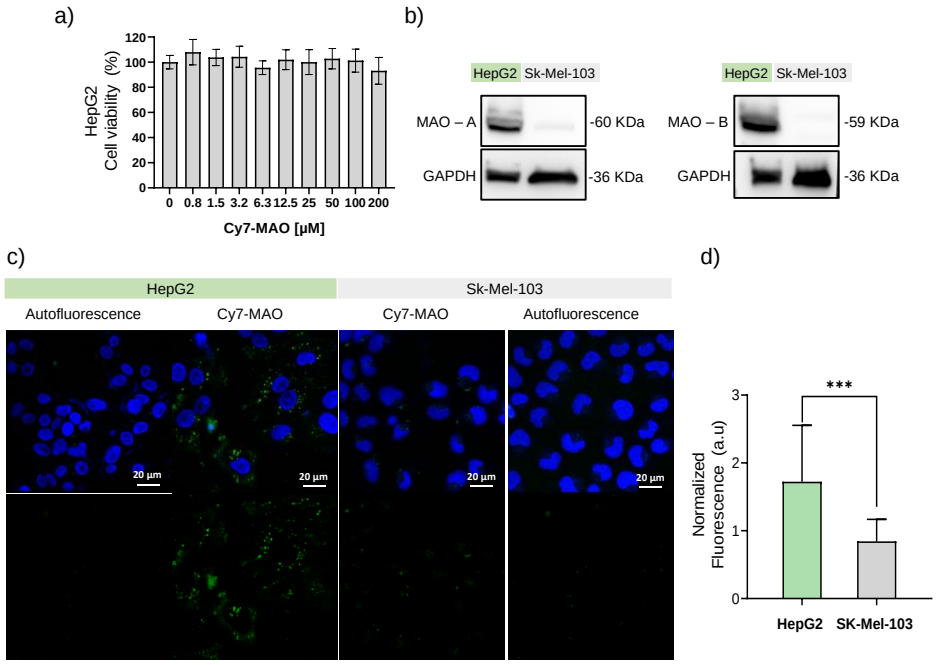

Figure 4. (a) Cell viability in HepG2 cells incubated with different concentrations of **Cy7-MAO** probe for 48 h. The results are expressed as mean ± SD from tree independent studies (n=3). (b) Western blot assay for MAO-A/B expression in HepG2 and SK-Mel-103 cells. (c) Confocal images of HepG2 (positive MAO cells) versus SK-Mel-103 (control cells) incubated with **Cy7-MAO** (100 µM) for 24 h. (D) Fluorescence quantification of confocal images. Images show a 2-fold emission enhancement in HepG2 cells when compared with SK-Mel-103 cells. The results exhibited representative images from three independent studies (n=3) and values are expressed as mean ± SD. Statistical analysis was assessed by applying Student's T-test (***p < 0.001).

The fact that MAO-A and/or MAO-B enzymes levels are frequently elevated in aged or dysfunctional organs has opened new perspectives on their role in aging. Although MAO high levels were first described in brains with neurodegenerative diseases, currently, it has been demonstrated that MAO is also expressed in a variety of peripheral not nerveous system organs, arising interest in the extra-cerebral roles of these enzymes.[13] In this context, high levels of MAOs enzymes can

play a potential role in the decline of organ functions, as major producers of mitochondrial ROS, and thus in natural aging and aging-related diseases such as cardiovascular disorders, neurodegenerative diseases or liver diseases, among others.[40] Bearing these facts in mind, we have aimed to test the **Cy7-MAO** probe for monitoring overall MAO activity in healthy young and old individuals. For this purpose, BALB/cByJ mice of different ages (12 and 2 months old) were intraperitoneally administrated with **Cy7-MAO** (10 mM) and the fluorescence emission was monitored by IVIS technique (Figure 5a). Fluorescence analysis *in vivo* using IVIS images 15 min post-injection clearly showed fluorescence signal accumulation in the bladder (Figure 5b, 5c), suggesting a rapid renal clearance. Fluorescent signal detected by IVIS imaging in the bladder from elderly mice was 4.2 -fold stronger than from young mice (Figure 5b). Moreover, urine was collected after mice recovered from anaesthesia. We found that the emission from urine collected samples of elderly mice was 5.6-fold higher that the obtained for 12-month mice (Figure 5d and 5e). In addition, the amount of excreted Cy7 (µmol) was quantified using a fluorometer and a calibration curve (Figure 5f). We found a detectable amount of Cy7 in the urine (ca. 0.40 µmol) of elderly animals. In contrast, the Cy7 fluorophore was basically undetectable in urine from **Cy7-MAO** injected young mice (0.01 µmol. A simple mass balance of the amount of **Cy7-MAO** injected and Cy7 recovery by urine allows calculatie that aprotxmatly the ca. 60% of injected doses **Cy7-MAO** was excreted through urine as Cy7 in old mice (100 mg/kg) while the excretion of Cy7 in young mice was negligible (0.0001%) (Figure 5f). After euthanasia, the brain, lungs, liver, kidneys and speel were studied by IVIS imaging. However, quantification of the emission intensity did not reveal significant changes in aged mice when compared to young animals, except for the bladders where higher fluorescence was observed for elderly mice (Figure S11). The data suggests

that hydrolysis of **Cy7-MAO** and elimination of Cy7 through the urine is an efficient and fast process.

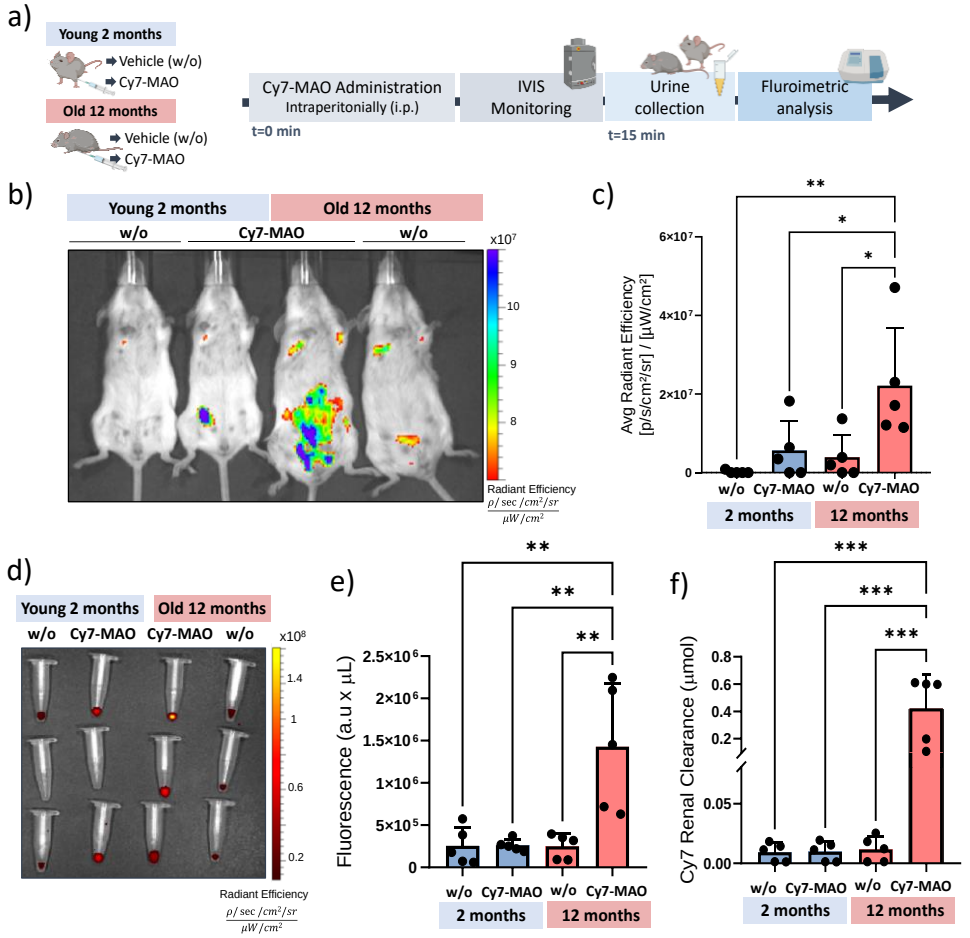

Figure 5. (a) Timeline for the *in vivo* evaluation of **Cy7-MAO** probe in naturally aged BALB/cByJ mice (n=5 animals per group). (b and c) Representative IVIS images of BALB/cByJ mice injected with **Cy7-MAO** and quantification. (d) Representative IVIS image of urine samples from young (2 months) and old (12 months) mice recorded 15 min after **Cy7-MAO** or vehicle treatment (w/o). Image shows that only urine from old mice treated with Cy7-MAO exhibits a strong fluorescence signal. (e) Quantification of IVIS images of urine samples. Note that this value is normalized to the total volume of urine recovered. (f) Cy7 (μmol) excreted through

urine from BALB/c mice. Values are expressed as mean ± SD. Statistical analysis was assessed by applying One-Way ANOVA with multiple comparisons (***p <0,0001, **p < 0.05, *p < 0,02).

Despite mechanisms that control enzymatic MAO expression being only partially understood and relying on indirect evidence, the higher emission found in 12 old animals compared to young mice suggested that MAO (either A and/or B) are overexpressed in elderly mice. To demonstrate this, we determined MAO expression by real-time PCR in 12 and 2-month mice (Figure 6a). The relative mRNA expression in the different tissues reveals a significant increase of MAO-A and MAO-B in liver from elderly mice compared to young ones (Figure 6b and S12). As the heat map of gene expression shows, MAO-A moderately increased in the liver of 12-month mice compared to young animals (ca 3-fold). Remarkably, the expression of MAO-B is clearly higher in the liver of old mice (ca 24-fold compared with young animals) and also to a lesser extent in kidneys (Figure S11). In contrast there is no change in MAO mRNA expression in other organs. These results determine that expression of MAO (especially MAO-B) in elderly animals increases significantly compared with young one. Overall, these results confirm a good correlation between global overexpression of MAO enzyme and aging (elderly versus young mice) through the simple *in vivo* fluorescence measurements recorded through urine upon **Cy7-MAO** administration.

To determine biological aging, considerable efforts have been devoted to identifying biomarkers.[41,42] Biomarkers of aging have been reported to have a great potential for early diagnosis, prognosis of age-related diseases and for the monitorization of the effectiveness of their prevention and treatment. Aging biomarkers are also indicators of preclinical stage of further aging-related diseases. Using probe **Cy7-MAO** we have demonstrated that expression of the MAO enzymes in liver showed about a 24-fold increase in healthy elderly mice samples compared

with healthy young subjects, which is, as far as we are aware, the first evidence suggestive of MAO's utility as a biomarker of aging. MAO can also be an indicator of one hallmark of aging; namely oxidative stress, as it has been reported that MAO enzymes induce the generation of ROS. Although the potential use of overexpression of MAO as biomarker remains uncertain and more experiments need to be performed, our research demonstrate the potential use of renal clearable probes for the non-invasive monitoring of certain biomarkers (such as dysregulated enzymes) in urine.

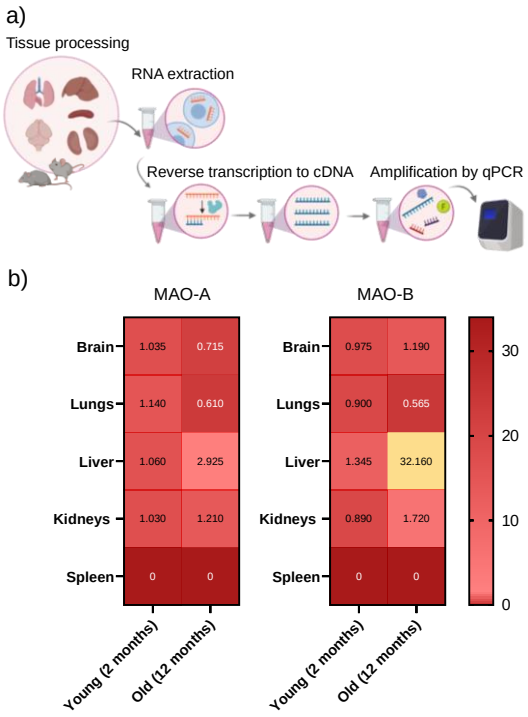

Figure 6. (a) Evaluation of MAO-A/B expression in major organs by real-time qPCR. Animals were euthanatized and tissues (brain, lung, liver, kidney, spleen) digested to obtain RNA. Then cDNA is obtained and amplified by qPCR to determine mRNA expression levels of MAO. (b) Heat map of MAO expression corroborated by real-time qPCR. Values represent the mean

of relative MAO mRNA expression (n=5). Actin-A was used for input normalization. MAO-A/B expression significantly increased in the liver of old mice versus young mice.

7.4 MATERIALS AND METHODS.

3-(Boc-amino) propyl bromide, potassium carbonate, 1-(4-sulfobutyl)-2,3,3-trimethylindolium inert salt (**2**), sodium acetate, sodium hydroxide, acetic anhydride, tertbutyldimethylsilyl chloride (TBSCl), dichloromethane and monoamine oxidase A and B (MAO-A and MAO-B) were obtained from Sigma-Aldrich and used without further purification. 5-formylsalicylaldehyde was purchased from Fluorochem. Anhydrous MeCN was obtained from Acros Organics. Cy7 fluorophore was synthetized following the literature.[30] ^{1}H and ^{13}C NMR spectra were recorded on a Bruker FT-NMR Avance 400 (Ettlingen, Germany) spectrometer at 300 K. HRMS data were obtained with a TRIPLETOF T5600 (ABSciex, USA) spectrometer. Fluorescence spectroscopy was carried out in a JASCO spectrofluorometer FP-8500 and absorption spectra were collected in a JASCO V-650 spectrophotometer. Confocal fluorescence images were taken on a Leica TCS SP8 AOBS. Images were analyzed using ImageJ software. Monitoring of fluorescence in animals was carried out in an IVIS Spectrum *In Vivo* Imaging System (PerkinElemer) and images were analyzed by using the Living Image software.

Table S1. Comparison of **Cy7-MAO** with other fluorescent probes for the detection of MAO overexpression.

Probe	λ exc/ λ em (nm)	Time	LOD	Selectivity	*In vitro* (Cell lines)	*Animal model*	Ref.
MR1/ MR2	544/590	1 h	Not reported	MAO-A/B	PC12	Not reported	Albers et al, *ChemCom m.* **2007**, *44*, 4647-4649
MAO-HPQ1	360/530	2 h	Not reported	MAO-A/B	C6 gliom PC12	Not reported	Aw et al. *Chem. Asian J.***2010**,*5*, 1317-1321
Imino POS	448/585	90 min	Not reported	MAO-A/B	C6 glioma	Not reported	Kim et al. *ChemCom m.* **2012**, *48*, 6833-6835.
U1	304/449	2 h	Not reported	MAO-B	HepG2 SH-SY5Y	Drosophi la Brain of mice (*ex vivo*)	Li et al. *Nat.Comm*. **2014**, 3276
Probe 1-4	470/535	40 min	3.5 µg /mL (MAO-A) 6.0 µg /mL (MAO-B)	MAO-A/B	MCF-7	Not reported	Li et al. Org. *Biomol. Chem.* **2014**, 12, 2033-2036.
Probe 1-2	475/570	2 h	34.7 µg/ mL	MAO-A/B	HepG2, HeLa, MCF-7, RAW, SH-SY5Y, BV2	Not reported	Li et al. *Analyst*. **2014**, 139, 6092-6095
M2	410/510	Not reported	Not reported	MAO-B	HepG2 SHSY5Y	Not reported	Li et al. *Angew. Chem. Int. Ed.* **2015**, 54, 10821-10825

MAO-Red-1/2	420 /664	40 min	1.2 µg/ mL	MAO-A/B	HeLa HepG2	Not reported	Li et al, *Sci. Rep.* **2016**, 6:31217, 1-8
Probe 1	425/550	4.5 h	1.1 ng/mL	MAO-A	HeLa NIH-3T3	Not reported	Wu et al. *Anal. Chem.* **2016**, 88, 1440-1446
Probe 3	550/586	3h	2.7 ng/mL	MAO-A	SY-SY5Y HepG2	Not reported	Wu et al. *Angew. Chem., Int. Ed.* **2017**, 56, 15319-15323
MitoHCy-NH_2	730/770	2 h	Not reported	MAO-B	HepG2 SMMC7721	BALB/c mice (*ex vivo* and *in vivo*)	Wang et al. *Anal. Chem.* **2018**, 90, 4054-4061
Probe 3	530/675	2h	2.6 ng/mL	MAO-A	SH-SY5Y NIH-3T3 HepG2	Tumor-bearing nude mice (*in vivo*)	Yang et al. *Chem. Commun.* **2019**, 55, 2477
OTNP-3-Piperazine	340/400	Not reported	Not reported	MAO-A/B	NIH/3T3 HpeG2	Not reported	Zhang et al. *Talanta*. **2020**, 209,1-5
F1/FD1	430/618	2h	Not reported	MAO-A	SY-SY5Y	Mice Tissues of human (*ex vivo*)	Fang et al, *Angew. Chem. Int. Ed.* **2020**, 59, 7536-7541
Probe A	425/550	4 h	1.1 ng/mL	MAO-A	Hela	Zebrafish (*in vivo*)	Meng et al. *Dyes Pigments*. **2020**,176, 108208
DHMP2	680/710	12 h	13.0 ng/mL	MAO-A	SH-SY5Y PC-3	Zebrafish Tissues of rats/mice	Yang et al, *ACS Sens*. **2020**, 5, 943–951

						(*in vivo*)	
Rma-1/2	680/708	1 h	4.5 ng/mL (MAO-A) 13-fold (MAO-B)	MAO-A/B	HeLa	Zebrafish Tumor-bearing BALB/c mice (*in vivo*)	Shang et al. *Anal. Chem.* **2021**, 93, 4285−4290
HCCP	540/626	Not reported	Not reported	MAO-A	U251 Hela	Tissues of mice (*ex vivo*)	Wu et al. *Anal. Chim. Acta.* **2022**, 1199,339573
Cy7-MAO	450/550	24 h	6.9 μg/mL (MAO-A) 10.9 9 μg/mL (MAO-B)	MAO-A/B	HepG2	Naturally aged BALB/cByJ mice (*in vivo*)	This work

Synthesis and characterization of 4-(3-aminopropoxy)isophthalaldehyde (compound 1).

5-formylsalicylaldehyde (500 mg, 3.3 mmol), sodium hydroxide (133 mg, 3.3 mmol), and 3-(Boc-amino) propyl bromide (786 mg, 3.3 mmol) were dissolved in anhydrous MeCN (5 mL). The reaction mixture was stirred under argon atmosphere at 70 °C overnight. After that, TFA (5 mL DMF: 750 μL TFA) was added to the reaction mixture and stirred for 24 h. Solvent was removed under vacuum yielding product **1** as a yellow solid (457.5 mg, 91.5% yield). This product was used without further purification. ^{1}H NMR (400 MHz, DMSO-d_6) δ (ppm): 10.71 (s, 1H), 10.20 (s, 1H), 8.53 (d, J = 2.3 Hz, 1H), 8.31 (dd, J = 8.8, 2.3 Hz, 1H), 7.43 (d, J = 8.7 Hz, 1H), 4.60–4.53 (m, 2H), 3.58 (td, J = 6.1, 2.3 Hz, 2H), 2.28–2.14 (m, 2H). ^{13}C NMR (101 MHz, DMSO-d_6) δ (ppm): 190.67, 190.45, 169.45, 153.14, 135.27, 133.28, 126.38, 120.16, 66.43, 39.15, 21.18.

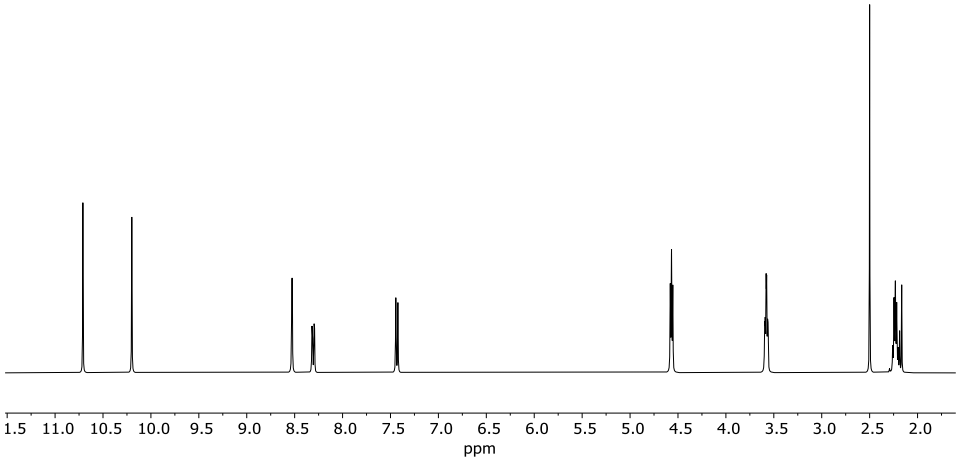

Figure S1. ^{1}H-NMR of compound **1**.

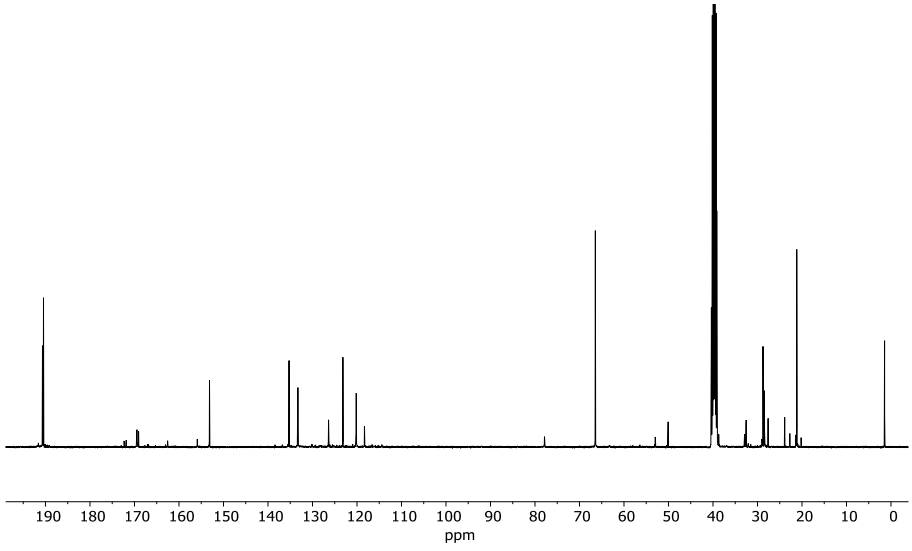

Figure S2. ^{13}C-NMR of compound **1**.

Synthesis and characterization of Cy7-MAO.

Compound **1** (250 mg, 1.2 mmol), commercial reagent 1-(4-sulfobutyl)-2,3,3-trimethylindolium) innert salt (**2**) (709 mg, 2.4 mmol) and sodium acetate (196.8 mg, 2.4 mmol) were dissolved in acetic anhydride (5 mL). The reaction mixture was heated to 70 °C and stirred under argon atmosphere overnight. The solvent was removed by evaporation under reduced pressure, and the crude product was purified by silica gel chromatography eluted with hexane-ethyl acetate (v/v, 1:1), affording probe **Cy7-MAO** as yellow-brown oil (300 mg, 60% yield). ^{1}H NMR (400 MHz, MeOD) δ (ppm): 7.37–7.34 (m, 1H), 7.19–7.15 (m, 1H), 7.14–7.08 (m, 5H), 7.00–6.95 (m, 1H), 6.90 (dd, J = 7.4, 0.9 Hz, 2H), 6.87 (d, J = 2.9 Hz, 2H), 6.84 (d, J = 1.0 Hz, 1H), 5.44 (s, 2H), 4.22–4.18 (m, 1H), 4.04 – 3.97 (m, 1H), 3.72–3.63 (m, 6H), 2.81–2.75 (m, 6H), 1.59 (s, 12H), 1.31–1.26 (m, 4H). ^{13}C NMR (101 MHz, MeOD) δ (ppm): 196.96, 190.81, 168.75, 160.88, 147.06, 140.74, 139.15, 135.26, 134.17, 131.44, 130.11, 129.94, 128.63, 127.31, 124.57, 122.73, 120.96, 118.87, 117.93, 115.78, 109.75, 105.91, 85.11, 54.53, 52.83, 51.04, 44.54, 26.64, 25.06, 22.66, 22.40, 21.89. HRMS: Theoretical ($C_{39}H_{47}N_3O^{2\bullet 2+}$): 573.3708 m/z and ($C_{26}H_{33}N_2O_4S^{2\bullet +}$): 469.2156 m/z. Experimental ($C_{39}H_{47}N_3O_2{}^{\bullet 2+}$): 572.1935 m/z and ($C_{26}H_{33}N_2O_4S^{2\bullet +}$): 470.1615 m/z respectively.

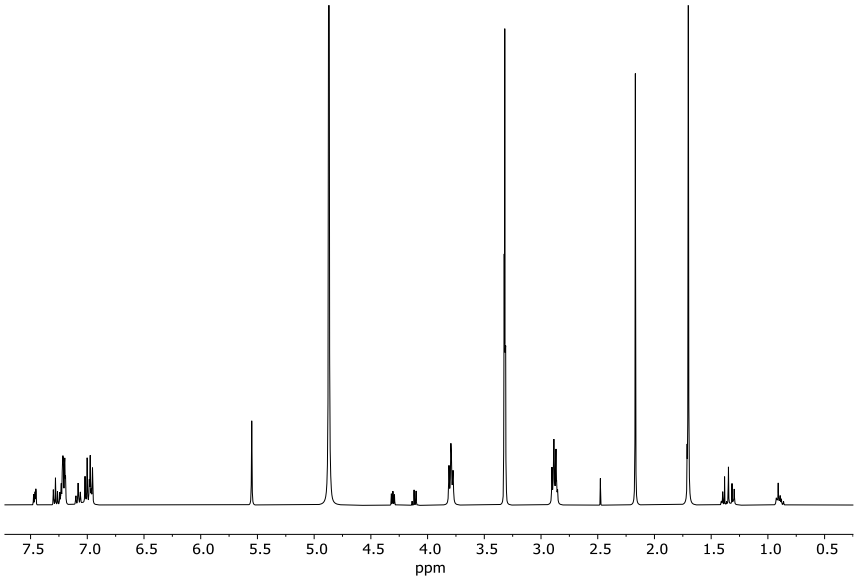

Figure S3. ^{1}H-NMR of **Cy7-MAO**.

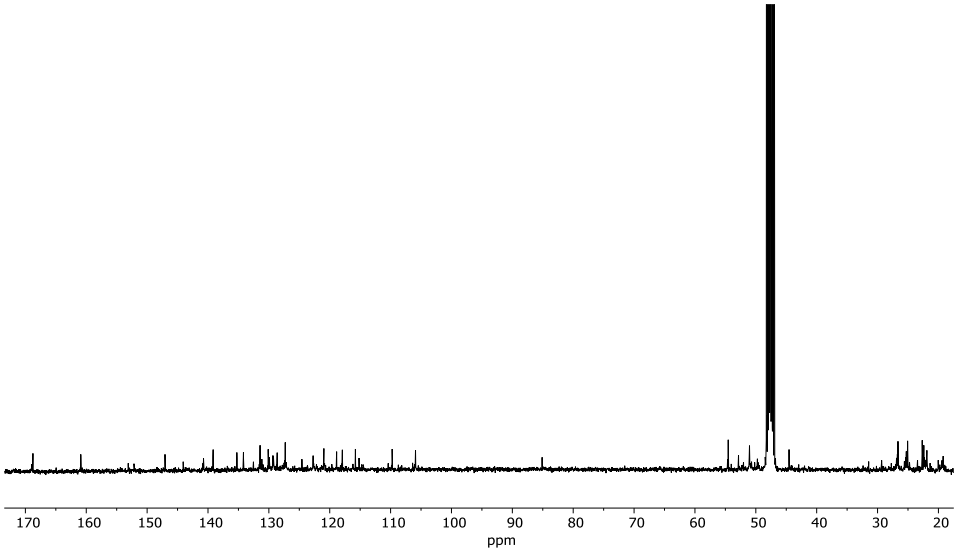

Figure S4. ^{13}C-NMR of **Cy7-MAO**.

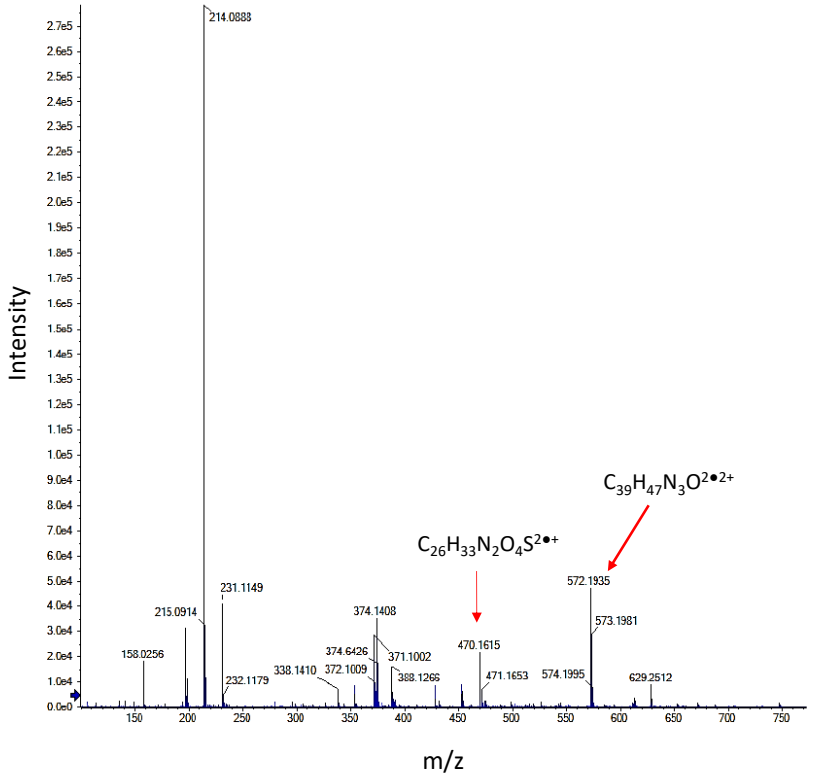

Figure S5. HRMS of **Cy7-MAO**.

Synthesis of Cy7 fluorophore

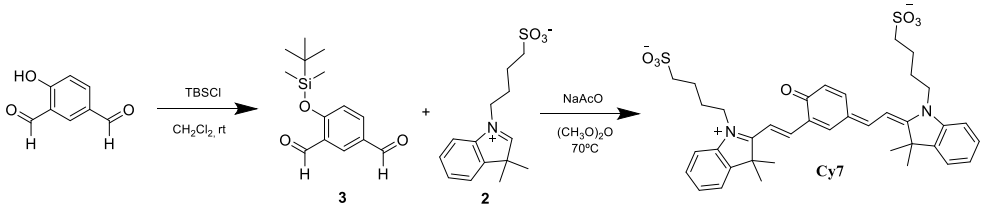

Figure S6. Synthetic route of Cy7 fluorophore.

Cy7 fluorescence emission at different pH

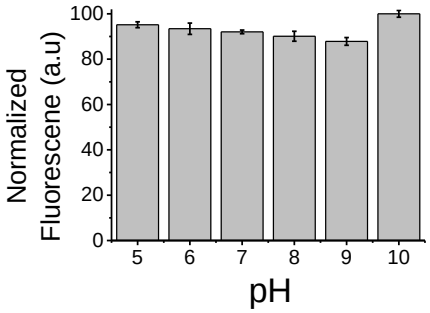

Figure S7. Emission intensity at 660 nm (λ_{ex} = 580 nm) of Cy7 fluorophore (5 µM) HEPES solutions at pH 5, 6, 7, 8, 9 and 10. Error bars are expressed as 3σ for three independent experiments.

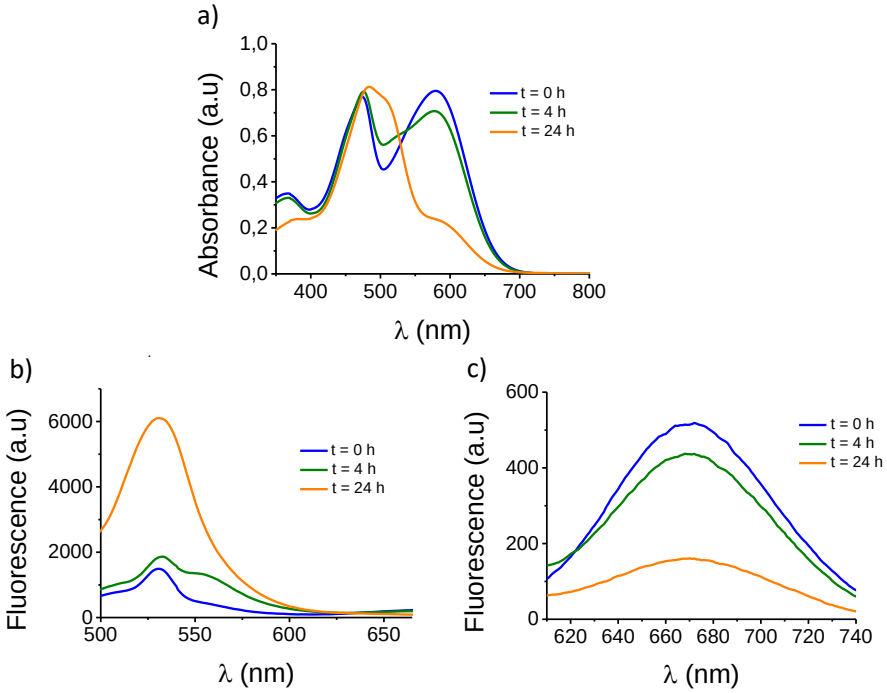

Figure S8. Study of the stability of cy7 fluorophore. (a) Absorption spectra of the Cy7 fluorophore (10^{-4} M in HEPES solution (10 mM, pH 7.4)) at different time points. (b and c)

Fluorescence emission spectra of the Cy7 fluorophore (10^{-6} M in HEPES solution (10 mM, pH 7.4)) were recorded at various time points, with excitation wavelengths at 450 nm and 580 nm, respectively.

General Procedure for MAO Detection.

Fluorescence emission measurements of **Cy7-MAO** were carried out with 1.0 µL of the probe from a stock solution (1.0 x 10^{-3} M in HEPES solution), followed by addition of MAO-A and MAO-B solution in HEPES (10 mM, pH 7.4). Final volume was adjusted to 200 µL with HEPES at pH 7.4. After incubation at 37°C for 30 min in a thermostat, solution was transferred to a quartz cell of 1 cm optical length to measure the fluorescence (λ_{exc} = 450 nm). A blank solution without MAO-A and MAO-B were prepared and measured under the same conditions.

Hydrolysis of Cy7-MAO by monoamine oxidase.

MAO (100 µg·mL^{-1}) was added to HEPES (pH 7.4) solutions of **Cy7-MAO** (5 µM). Chromatograms of **Cy7-MAO**, Cy7 and **Cy7-MAO** + MAO-A after 30 min of incubation were obtained by HPLC using a KromasilC18 column stationary phase. Samples were elucidated in a mixture water-methanol under gradient conditions (flow: 0.8 mL·min^{-1}, from 90:10 at 0 min to 10:90 at 20 min) as mobile phase and a photodiode array detector (λ=215 nm).

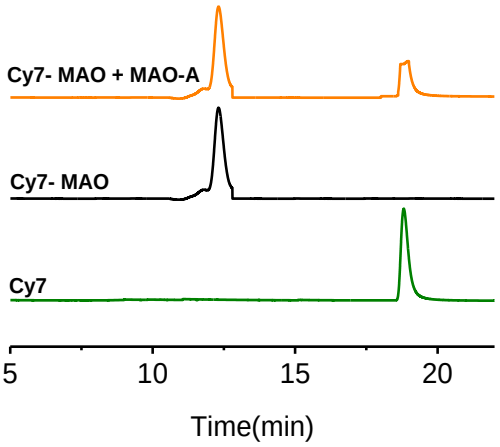

Figure S9. HPLC chromatograms of Cy7, Cy7-MAO, and Cy7-MAO + MAO-A.

Calibration curve in HEPES solution.

LOD and LOQ were obtained from the plot of fluorescence intensities at 535 nm (upon excitation at 450 nm) versus MAO-A/B concentration. LOD and LOQ were calculated by using the equation S2,[44] where K=3 for LOD and K=10 for LOQ; Sb is the standard deviation of the blank and m is the slope of the calibration curve. The resulting LOD were 6.4 and 10.9 $\mu g \cdot mL^{-1}$ for MAO-A and MAO-B respectively. On the other hand, LOQ were 29.3 $\mu g \cdot mL^{-1}$ for MAO-A and 52.1 $\mu g \cdot mL^{-1}$ for MAO-B.

$$LOD/LOQ=K*Sb/m \quad \text{(Eq. S2)}$$

Table S2. Fluorescence enhancement (F(t)/F(t=0)) of Cy7-MAO in HEPES solution at different times in the presence of MAO-A or MAO-B respectively (100 $\mu g \cdot mL^{-1}$).

	Cy7-MAO + MAO-A	Cy7-MAO + MAO-B
Time (h)	**Fluorescence enhancement**	
0	1.0	1.0
4	3.0	3.4
5	3.4	4.3
6	4.4	5.3
12	9.1	9.6
24	13.2	9.7

Cell Culture.

HepG2 hepatocellular carcinoma cells and SK-Mel-103 human melanoma cells were purchased from the American Type Culture Collection (ATCC), cultured in DMEM (Dulbecco's Modified Eagle Medium) supplemented with 10% FBS (Fetal bovine serum) (Sigma). Cells were maintained in 20% O_2 and 5% CO_2 at 37°C.

Western blot assays.

To determine the levels of MAO protein in each cellular line (SK-Mel-103 and HepG2) whole-cell extracts were obtained by using lysis buffer (25 mM Tris-HCl pH 7.4, 1 mM EDTA, 1% SDS, plus protease and phosphatase inhibitors). Cell lysates were resolved in 12% SDS-PAGE gels, transferred to nitrocellulose membranes, blocked with 5% non-fat milk, and incubated overnight with the primary antibody for MAO-A (#ab126751, Abcam) and MAO-B (#ab137778, Abcam), respectively. Besides, GAPDH (#14C10 from Cell Signalling) was used as reference protein for normalization. Then, membranes were washed and probed with the secondary antibody conjugated to horseradish peroxidase, anti-rabbit IgG peroxidase antibody

(#A6154, Sigma) for enhanced chemiluminescence detection (Amersham Pharmacia Biotech).

Confocal *in vitro* experiments.

SK-Mel-103 and HepG2 cells were seeded in a cover slip in a 6-well plate at 300,000 cells per well. After 24 h cells were incubated with **Cy7-MAO** (100 µM) for 4 h. Then cells were washed, and coverslips mounted to confocal visualization. Hoechst 33342 was added at 2 $\mu g \cdot mL^{-1}$ for nuclei staining. Confocal images were acquired in a Leica TCS SP8 AOBS confocal microscope (λ_{exc} = 552 nm; λ_{em} = 574-765 nm). Images were quantified by Image J software.

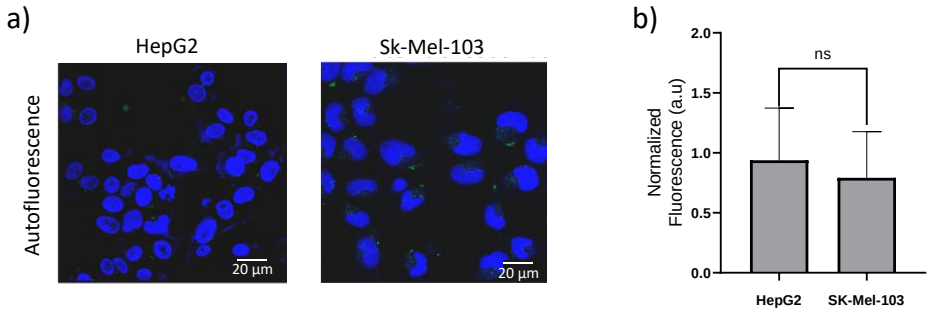

Figure S10. (a) Autofluorescence of HepG2 and Sk-Mel-103 cells. (b) Fluorescence quantification of confocal images a.

***In vitro* cytotoxicity studies.**

For the *in vitro* cytotoxicity studies, HepG2 cells were seeded in a 96-well plate (10,000 cells per well). After 24 h, cells were incubated with different concentrations of **Cy7-MAO** probe (diluted in DMEM) for 24 h. The cell viability was determined by WST-1 reagent which was added for 30 min and then absorbance was measured at 450 nm at Wallac 1420 Victor2 Microplate Reader (Perkin Elmer).

Young and naturally aged BALB/cByJ mice.

BALB/cByJ mice of different ages, 2 and 12 months, were acquired from Envigo and maintained at the Spanish Centro de Investigación Príncipe Felipe (CIPF). All animal procedures were approved by the CIPF and UV Ethics Committees for Research and Animal Welfare (CEBA) and conducted in accordance with the recommendations of the Federation of European Laboratory Animal Science Associations (FELASA).

Renal clearance of Cy7-MAO.

Mice were anesthetized and intraperitoneally injected with **Cy7-MAO** (10 mM, 100 µl) in DMEM. Fluorescence was monitored in an IVIS spectrum (Perkin Elmer) for 15 min taking photographs every 2 minutes (λ_{exc} = 535 nm; λ_{em} = 640 nm; time exposure: 10 s). Urine was collected after mice recovered from anaesthesia in an Eppendorf tube and analysed directly by IVIS (λ_{exc} = 535 nm; λ_{em} = 640 nm; time exposure: 1s). Finally, mice were euthanized, and organs were harvested for further MAO expression characterization. Fluorescence measurements of collected urine samples were also analysed with a fluorescence spectrophotometer (JASCO FP-8500). For this purpose, 5 µl of urine was diluted in 95 µL of distilled water and fluorescence spectra were recorded at 535 nm (λ_{exc} = 450 nm). The amount of Cy7 fluorophore excreted in urine was calculated through a calibration curve. For the calibration curve, a stock solution of Cy7 in blank urine from an untreated young mouse was prepared. Serial dilutions were prepared in the same urine and 5 µl of each Cy7 urine solution was added to 95 µl of distilled water and measured in the fluorimeter under the same condition.

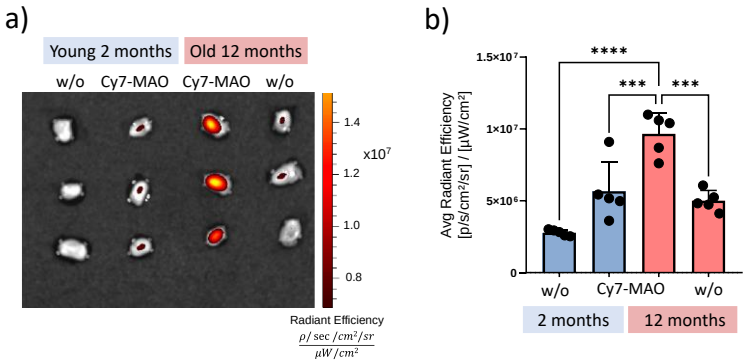

Figure S11. (a) *Ex vivo* IVIS spectrum imaging of bladder from young (2 months) and old (12 months) after **Cy7-MAO** or vehicle treatment (w/o). Image shows that only bladder from old mice treated with **Cy7-MAO** exhibits a strong fluorescence signal. (b) Quantification of IVIS images of bladders. Values are expressed as mean ± SD. Statistical analysis was assessed by applying One-Way ANOVA with multiple comparisons (****p <0,0001, ***p < 0. 0,0010).

MAO *expression* by *Real Time-PCR*.

The frozen organ samples (brain, lungs, liver, kidneys, and spleen) were employed for total RNA extraction. The tissue was disrupted with Trizol according to the manufacturer's instructions (Merck, T9424) and the total RNA was quantified using NanoDrop™. Samples were treated with *DNase I* (Nzytech, MB19901) to avoid genomic DNA contamination. The retrotranscription reaction of total RNA was performed using the NZY First-Strand cDNA Synthesis Kit (Nzytech, MB12502) following the manufacturer's protocol. qRT-PCR reactions were performed using qPCR Green Master Mix (2x) (Nzytech, MB22402) with each sample loaded in triplicate and were run in a LightCycler® 480 System (Roche) following the manufacturer's protocol. Data were analyzed using the LightCycler 480 relative quantification software. Nucleotide sequences of the primers used for mRNA expression analyses are listed below:

Gene	Primer	Sequence (5'→3')
MAO-A	Forward	AACTTACCCATTCCGTGGTG
	Reverse	CCACAGGGCAGATACCTCAT
MAO-B	Forward	CCTTGCTGAAGAGTGGGACT
	Reverse	TGTCCTCCATTGGTTGTTGA
Actin-A	Forward	GTCCACACCCGCCACC
	Reverse	ACCCATTCCCACCATCACAC

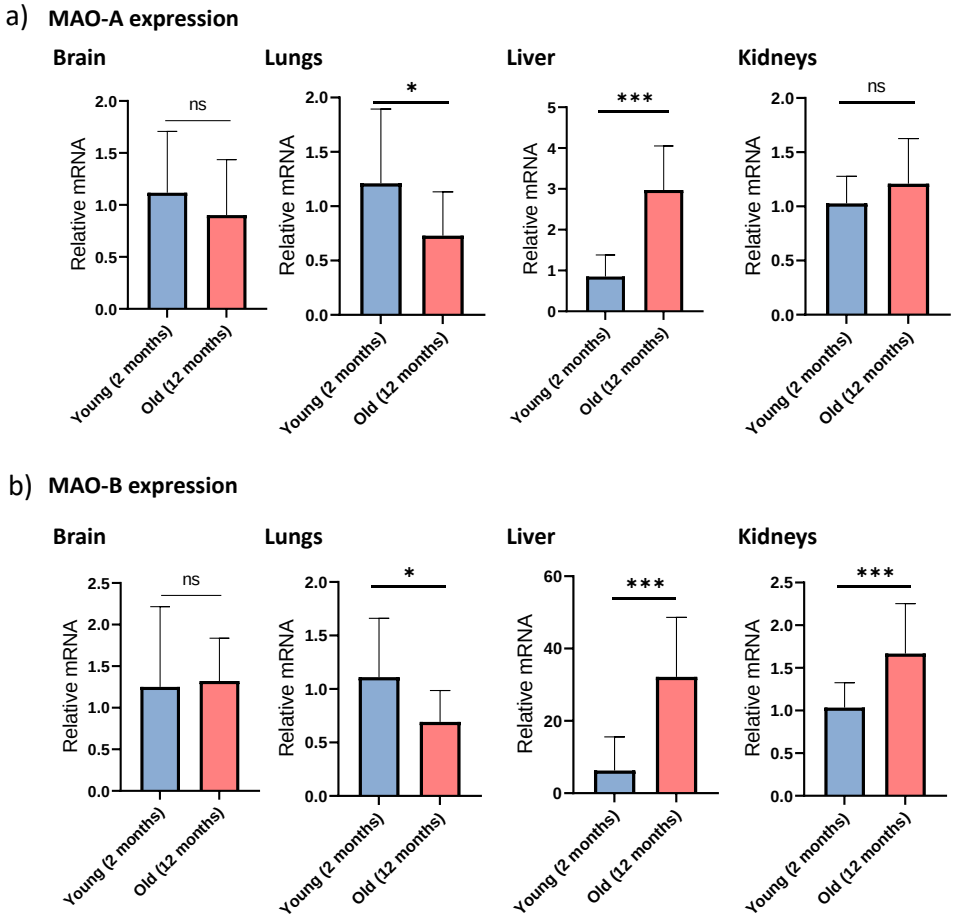

Figure S12. (a) mRNA expression levels of MAO-A and (b) MAO-B in major organs corroborated by real-time PCR. Expression of MAO significantly changed in old mice versus

young mice. Actin-A was used for input normalization. Values are relative to control mice and are expressed as mean ± SD. Statistical significance was assessed by the two-tailed Student's t-test: *p < 0.05; **p < 0.01; ***p < 0.001; ****p < 0.0001 (n=5).

7.5 CONCLUSIONS

In the context of precision medicine, one attractive approach is to detect biomarkers form accessible biofluids using simple detection systems to guide healthcare decisions. One approach towards this aim is the design of probes in an OFF state that can be transformed by certain biomarkers in cells or tissues *in vivo* to give an ON highly emissive product that can be renally cleared, allowing fluorescence detection in urine by simple techniques. Based on this concept, we report herein a fluorogenic molecular probe (**Cy7-MAO**) to selectively detect MAO enzymes through fluorescence measurements in collected urine samples. MAO enzymes hydrolyses the poorly fluorescent **Cy7-MAO** probe to give the highly emissive Cy7-fluorophore and its degradation products. Confocal studies confirmed the ability of **Cy7-MAO** to detect MAO enzymes *in vitro* in HepG2, in which there is an endogenous MAO overexpression. We also provided evidence on the reliability that the fluorophore intensity in urine correlates with the burden of MAO in elderly and young BALB/c mice *in vivo*. We found that urine emission in 12-month healthy mice was 5.6-fold higher than in 2-month animals. This are directly related with the relative mRNA expression. These studies reveal that MAO-A, and specially, MAO-B expression, are clearly higher in the liver of 12-month-old mice (ca. 24-fold compared with young mice).. As far as we know, this is the first evidence suggesting that MAO expression can be used as a biomarker of aging and an indicator of oxidative stress (a hallmark of aging) due to the generation of ROS by MAO enzymes. Our findings demonstrate that renal clearable fluorogenic probes can be a versatile modular tool that opens new opportunities to develop simple monitorization in

urine for physiological process (such as aging) or diseases where dysregulated enzymatic activity is a biomarker. We are also aware that this simple technology can be applied to the monitoring of therapeutic treatments and longitudinal studies.

ACKNOWLEDGEMENTS

This research was supported by project PID2021-126304OB-C41 funded by MCIN/ AEI /10.13039/501100011033/ and by European Regional Development Fund - A way of doing Europe. This study was also supported by Generalitat Valenciana (CIPROM/2021/007). Thank the financial support from the FEDER found of European Union (IDIFEDER/2021/044). This research was supported by CIBER - Consorcio Centro de Investigación Biomédica en Red- (CB06/01/2012), Instituto de Salud Carlos III, Ministerio de Ciencia e Innovación. M. D. -R. thanks to his predoctoral fellowship Grisolia to the Genelalitat Valenciana (GRISOLIAP/2019/144). J.F.B. thanks to his postdoctoral fellowship Sara Borrell from ISCIII (CD19/00038) and CIAPOS/2021/198 funded by the Generalitat Valenciana. V.M.-C. thanks the financial support from project CIDEGENT/2020/031 funded by the Generalitat Valenciana.

7.6 REFERENCES

1. Iacovino, L.G., Magnani, F. & Binda, C. The structure of monoamine oxidases: past, present, and future. *J. Neural Transm.*, **2018**, *125*, 1567–1579.

2. Da Prada, M., Kettler, R., Keller, H. H., Cesura, A. M., Richards, J. G., Marti, J. S., Muggli-Maniglio, D., Wyss, P.-C., Kyburz, E. & Imhof, R. From moclobemide to Ro 19-6327 and Ro 41-1049: the development of a new class of reversible, selective MAO-A and MAO-B inhibitors. In Neurotransmitter Actions and Interactions: Proceedings of a Satellite Symposium of the 12th International Society for

Neurochemistry Meeting, Algarve, Portugal, Springer Vienna, April 29–30, **1989**, 279-292.

3. Wu, X., Shi, W., Li, X., & Ma, H. Recognition moieties of small molecular fluorescent probes for bioimaging of enzymes. *Acc. Chem. Res.*, **2019**, *52*, 1892-1904.

4. Huang, J., Hong, D., Lang, W., Liu, J., Dong, J., Yuan, C., Lou, J., Ge, J. & Zhu, Q. Recent advances in reaction-based fluorescent probes for detecting monoamine oxidases in living systems. *Analyst*, **2019**, *144*, 3703-3709.

5. Qin, H., Li, L., Li, K., & Xiaoqi, Y. Novel strategy of constructing fluorescent probe for MAO-B via cascade reaction and its application in imaging MAO-B in human astrocyte. *Chin. Chem. Lett.*, **2019**, *30*, 71-74.

6. Mattson, M. P. Apoptosis in neurodegenerative disorders. *Nat. Rev. Mol. Cell Biol.*, **2000**, *1*, 120-130.

7. Shih, J. C., Chen, K., & Ridd, M. J. Monoamine oxidase: from genes to behavior. *Annu. Rev. Neurosci.*, **1999**, *22*, 197-217.

8. Youdim, M. B., Edmondson, D., & Tipton, K. F. The therapeutic potential of monoamine oxidase inhibitors. *Nat. Rev. Neurosci.*, **2006**, *7*, 295-309.

9. Wang, R., Han, X., You, J., Yu, F., & Chen, L. Ratiometric near-infrared fluorescent probe for synergistic detection of monoamine oxidase B and its contribution to oxidative stress in cell and mice aging models. *Anal. Chem.*, **2018**, *90*, 4054-4061.

10. Nicotra, A., Pierucci, F., Parvez, H., & Senatori, O. Monoamine oxidase expression during development and aging. *Neurotoxicology*, **2004**, *25*, 155-165.

11. Mathew, B., E Mathew, G., Suresh, J., Ucar, G., Sasidharan, R., Anbazhagan, S., K. Vilapurathu, J. & Jayaprakash, V. Monoamine oxidase inhibitors: Perspective design for the treatment of depression and neurological disorders. *Curr. Enzym. Inhib.*, **2016**, *12*, 115-122.

12. Kunugi, H., & Mohammed Ali, A. Royal jelly and its components promote healthy aging and longevity: from animal models to humans. *Int. J. Mol. Sci.*, **2019**, *20*, 1-26.

13. Santin, Y., Resta, J., Parini, A., & Mialet-Perez, J. Monoamine oxidases in age-associated diseases: New perspectives for old enzymes. *Ageing Res. Rev.*, **2021**, *66*, 1-13.

14. Cesari, M., Calvani, R., & Marzetti, E. Frailty in older persons. *Clin. Geriatr. Med.*, **2017**, *33*, 293-303.

15. Janssens, G. E., Meinema, A. C., Gonzalez, J., Wolters, J. C., Schmidt, A., Guryev, V., Bischoff, R., Wit, E. C, Veenhoff, L. M. & Heinemann, M. Protein biogenesis machinery is a driver of replicative aging in yeast. *eLife*, **2015**, *4*(e08527),1-24.

16. Pang, F. Y., Hucklebridge, F. H., Forster, G., Tan, K., & Clow, A. The relationship between isatin and monoamine oxidase-B inhibitory activity in urine. *Stress med.*, **1996**, *12*, 35-42.

17. Herraiz, T., Flores, A., & Fernández, L. Analysis of monoamine oxidase (MAO) enzymatic activity by high-performance liquid chromatography-diode array detection combined with an assay of oxidation with a peroxidase and its application to MAO inhibitors from foods and plants. *J. Chromatogr. B*, **2018**, *1073*, 136-144.

18. Huang, G., Zhu, F., Chen, Y., Chen, S., Liu, Z., Li, X., Gan, L., Zhang, L. & Yu, Y. A spectrophotometric assay for monoamine oxidase activity with 2,4-dinitrophenylhydrazine as a derivatized reagent. *Anal. Biochem*, **2016**, *512*, 18-25.

19. Edelstein, S. B., & Breakefield, X. O. Monoamine oxidases A and B are differentially regulated by glucocorticoids and “aging” in human skin fibroblasts. *Cell. Mol. Neurobiol.*, **1986**, *6*, 121-150.

20. Zhou, M., & Panchuk-Voloshina, N. A one-step fluorometric method for the continuous measurement of monoamine oxidase activity. *Anal. Biochem.*, **1997**, *253*, 169-174.

21. Huang, J., Hong, D., Lang, W., Liu, J., Dong, J., Yuan, C., Lou, J., Ge, J. & Zhu, Q. Recent advances in reaction-based fluorescent probes for detecting monoamine oxidases in living systems. *Analyst*, **2019**, *144*, 3703-3709.

22. Kwong, G. A., von Maltzahn, G., Murugappan, G., Abudayyeh, O., Mo, S., Papayannopoulos, I. A., Sverdlov, D. Y., Liu, S. B., Warren, A. D., Popov, Y., Schuppan, D., & Bhatia, S. N. Mass-encoded synthetic biomarkers for multiplexed urinary monitoring of disease. *Nat. Biotech.*, **2013**, *31*, 63-71.

23. Lin, K. Y., Kwong, G. A., Warren, A. D., Wood, D. K. & Bhatia, S. N. Nanoparticles that sense thrombin activity as synthetic urinary biomarkers of thrombosis. *ACS Nano*, **2013**, *7*, 9001-9009.

24. Huang, J. Li, J. Lyu, Y. Miao, Q. & Pu, K. Molecular optical imaging probes for early diagnosis of drug-induced acute kidney injury. *Nat. Mater.*, **2019**, *18*, 1133-1143.

25. Choi, H. Liu, W., Misra, P., Tanaka, E., Zimmer, J. P., Ipe, B. I., Bawendi, M. G. & Frangioni, J. V. Renal clearance of quantum dots. *Nat. Biotechnol.*, **2007**, *25*, 1165-1170.

26. Loynachan, C. N., Soleimany, A. P., Dudani, J. S., Lin, Y., Najer, A., Bekdemir, A., Chen, Q., Bhatia S. N. & Stevens, M. M. Renal clearable catalytic gold nanoclusters for *in vivo* disease monitoring. *Nat. Nanotech.*, **2019**, *14*, 883–890.

27. Albers, A. E., Rawls, K. A., & Chang, C. J. Activity-based fluorescent reporters for monoamine oxidases in living cells. *ChemComm*, **2007**, *44*, 4647-4649.

28. Aw, J., Shao, Q., Yang, Y., Jiang, T., Ang, C., & Xing, B. Synthesis and characterization of 2-(2'-hydroxy-5'-chlorophenyl)-6-chloro-4-(3H)-quinazolinone-

based fluorogenic probes for cellular imaging of monoamine oxidases. *Chem. Asian J.*, **2010**, *5*, 1317-1321.

29. Li, L. L., Li, K., Liu, Y. H., Xu, H. R., & Yu, X. Q. Red emission fluorescent probes for visualization of monoamine oxidase in living cells. *Sci. Rep.*, **2016**, *6*, 1-8.

30. Yang, Z. M., Mo, Q. Y., He, J. M., Mo, D. L., Li, J., Chen, H., Zhao, S. L. & Qin, J. K. Mitochondrial-targeted and near-infrared fluorescence probe for bioimaging and evaluating monoamine oxidase activity in hepatic fibrosis. *ACS Sens.*, **2020**, *5*, 943-951.

31. Shang, J., Shi, W., Li, X., & Ma, H. Water-soluble near-infrared fluorescent probes for specific detection of monoamine oxidase A in living biosystems. *Anal. Chem.*, **2021**, *93*, 4285-4290.

32. Wu, J., Han, C., Cao, X., Lv, Z., Wang, C., Huo, X., Feng, L., Zhang, B., Tian, X. & Ma, X. Mitochondria targeting fluorescent probe for MAO-A and the application in the development of drug candidate for neuroinflammation. *Anal. Chim. Acta.*, **2022**, *1199*, 1-11.

33. Huang, J., Weinfurter, S., Daniele, C., Perciaccante, R., Federica, R., Della Ciana, L., Pill, J. & Gretz, N. Zwitterionic near infrared fluorescent agents for noninvasive real-time transcutaneous assessment of kidney function. *Chem. Sci.*, **2017**, *8*, 2652-2660.

34. Cheng, P., & Pu, K. Molecular imaging and disease theranostics with renal-clearable optical agents. *Nat. Rev. Mater.*, **2021**, *6*, 1095-1113.

35. Wu, H., Alexander, S. C., Jin, S., & Devaraj, N. K. A bioorthogonal near-infrared fluorogenic probe for mRNA detection. *J. Am. Chem. Soc.*, **2016**, *138*, 11429-11432.

36. Bokan, M., Bondar, K., Marks, V., Gellerman, G., & Patsenker, L. D. Switchable phenolo-cyanine reporters containing reactive alkylcarboxylic

groups for fluorescence-based targeted drug delivery monitoring. *Dyes Pigm.*, **2018**, *159*, 18-27.

37. Wang, R., Han, X., You, J., Yu, F., & Chen, L. Ratiometric near-infrared fluorescent probe for synergistic detection of monoamine oxidase B and its contribution to oxidative stress in cell and mice aging models. *Anal. Chem.*, **2018**, *90*, 4054-4061.

38. Silverman, R. B. Radical ideas about monoamine oxidase. *Acc. Chem. Res.*, **1995**, *28*, 335-342.

39. Brunner, H. G., Nelen, M., Breakefield, X. O., Ropers, H. H., & Van Oost, B. A. Abnormal behavior associated with a point mutation in the structural gene for monoamine oxidase A. *Science*, **1993**, *262*, 578-580.

40. Shih, J. C., & Chen, K. Regulation of MAO-A and MAO-B gene expression. *Curr. Med. Chem.*, **2004**, *11*, 1995-2005.

41. Yan, F., Tian, X., Luan, Z., Feng, L., Ma, X., & James, T. D. NAG-targeting fluorescence based probe for precision diagnosis of kidney injury. *ChemComm*, **2019**, *55*, 1955-1958.

42. Biomarkers of Human Aging, Healthy Ageing and Longevity 10, Series Editor: Suresh I. S. Rattan. Springer, **2019**.

43. Moskalev, A. Biomarkers of human aging. Cham: Springer International Publishing, **2019**, 10.

44. Shrivastava, A., & Gupta, V. B. Methods for the determination of limit of detection and limit of quantitation of the analytical methods. *Chron. Young Sci.*, **2011**, *2*, 21-25.

Chapter 8| Conclusions and Perspectives

Chapter 8| Conclusions and Perspectives

Despite significant developments in medicine in recent years, the diagnosis of many diseases remains a major challenge, mainly due to the high cost of tests, the need to use invasive techniques, or the problematic management of samples. Consequently, the design and development of new, cost-effective, and easy-to-use diagnostic tools remains a major challenge in medical research. In this regard, it is interesting the study and development of new probes for the easy detection of diseases. To achieve this goal, one approach has been the development of sensors based on nanoparticles commonly consisting of inorganic or organic scaffolds whose surface is usually modified with different (bio)organic molecules that increase the selectivity and sensitivity of the systems. Another approach is the development of molecular sensors (probes), which are composed of a signalling unit, which are fluorophores or chromophores, directly or undirectly attached to a reactive moiety, which interacts/reacts selectively with the analyte to be detected (in disease diagnosis mainly a biomarker).

In the field of functionalized nanomaterials, our group has considerable experience in the design and application of gated mesoporous silica nanoparticles (MSNs) for the detection of a large number of analytes, both *in vitro* and *in vivo*. For this purpose, the pores of the mesoporous nanoparticles are loaded with selected chromophores or fluorophores and the outer surface is functionalized with different organic compounds, supramolecular ensembles, or biomolecules, which act as molecular gates (also known as gatekeepers or nanovalves) blocking the pores of the materials. In the absence of a targeted analyte, the pores remained blocked and no cargo release occurs. However, when the analyte is present, its interaction with the molecular gates leads to the opening of the pores and the release of the cargo confined into the silica matrix. This release can be monitored through colour and/or fluorescence changes and allowed the detection of the

analyte or biomarker. Despite all the research carried out with gated MSNs, even *in vivo*, their use for the direct analyte recognition in a biofluid, such as urine, has been less explored.

On the other hand, the detection of analytes related to diseases can also be carried out using molecular probes. Among the different techniques capable of achieving this objective, chromo-fluorogenic detection is one of the more desirable due to its easy sample management, low cost, and broad detection spectrum both *in vitro* and *in vivo*. One of the most relevant analytes that can be detected with these molecular probes are enzymes, whose level changes, as well as their cellular or subcellular location, can be related to different pathologies. Traditionally, enzymes detection have been carried out by immunoassay techniques employing antibodies, which have a high limitation, namely the lack of spatiotemporal resolution and most importantly, the loss of information about their *in-situ* activity *in vivo*. In this way, fluorescent molecular probes have gained importance for enzymatic activity detection without the drawbacks of immunostaining analysis, allowing the detection *in vivo* and real-time monitoring of enzyme activity with excellent spatiotemporal resolution. However, UV-visible radiation is not invisible through tissues and suffers scattering and absorption with the consequent loss of resolution and signal, enabling their use only in superficial areas. With the hope to overpass these drawbacks, new fluorescent molecular probes design have been focused on NIR-I (760-900 nm) and NIR-II (900-1700 nm) windows. These new fluorophores are mainly constituted by fused aromatic rings that can impart a marked hydrophobicity to the final probe markedly reducing its water solubility and, consequently, their *in vivo* accumulation in organs such as the liver or spleen, with the subsequent increase in toxicity and side effects. A possible solution to these problems may lie in the introduction of zwitterionic structures that not only increase the solubility of the probes, yet, as we have demonstrated, promote the rapid clearance of probes through the urinary system, avoiding their accumulation

in the body. This clearance mechanism can be used in the design of fluorogenic molecular probes that are capable of being activated by specific biomarkers at tissue or cell level, followed by a fast excretion of the activated probe by urine. This allows for a simple and fast reading of biomarkers through urine measurements, making it possible to use them for the detection of diseases and monitoring of treatments. In line with this background, the present doctoral thesis has attempted to contribute to the growth of this research field. Specifically, the detection of analytes through fluorescence measurements in urine, either (i) by the presence of the analytes in urine or (ii) by the *in vivo* activation at the site of disease of the molecular probes and the recovery of the activated derivatives in urine after their elimination from the body by the renal system.

With these aims in mind, the third chapter of this PhD thesis describes a nanodevice constituted by sulforhodamine B-loaded MSNs, whose external surface was functionalized with a derivative of terephthalic acid. Coordination of this terephthalic acid derivative with a Cu_2bistren complex induced pore blocking (allowing the encapsulation of the dye) yielding the final solid **S4**. Sulforhodamine-B is a highly emissive dye with a strong fluorescence signal centred at 580 nm. This nanodevice was employed for the detection of muconic acid (*t,t*-MA), whose presence in urine is indicative of exposure to high benzene levels in humans. Cu_2bistren complex exhibits a strong affinity towards *t,t*-MA, and in its presence, the supramolecular complex in the external surface of **S4** is dethreaded resulting in pore opening and release of the confined fluorophore. The difference between binding constants of Cu_2bistren-therephthalic acid or Cu_2bistren-*t,t*-MA is the responsible of the selectivity of **S4** towards *t,t*-MA detection. Besides, *t,t*-MA sensing with **S4** was validated in doped human urine by fluorescence measurements recorded at 580 nm. These studies showed a strong selectivity with a low limit of detection for *t,t*-MA in urine, being one of the first examples based

on MSNs employed for the detection of biomarkers in urine.

On the other hand, chapter four presented a fluorescent molecular probe for detection of alanine aminopeptidase (APN) enzyme in urine. The **NB-ALA** probe is constituted by the Nile Blue fluorophore, acting as signalling unit, linked to an alanine aminopeptidase substrate. **NB-ALA** was employed for APN enzyme detection in urine samples, whose presence can be related with renal diseases. In the presence of APN enzyme **NB-Ala** is hydrolysed, releasing the Nile Blue dye and restoring its initial fluorescence, which was quenched in the probe by the presence of the alanine unit linked to the fluorophore. This mechanism allows the selective detection of APN enzyme in different scenarios with high selectivity and sensitivity. Its application for the detection of kidney-related diseases was validated in a fibrotic kidney mouse model. Versus traditional renal function assays, **NB-ALA** showed a progressive enhancement of signal, proportional to the time elapsed since the damage occurred. Thus, the first significant differences were observed at a shorter time compared to globular filtration test and creatinine serum levels, two of the most common biomarkers employed to kidney function monitoring.

Despite the results obtained with **NB-ALA** described in chapter four, molecular probes have a crucial drawback for their *in vivo* application. Their usually high hydrophobicity promotes accumulation in organs of the RES such as liver or spleen, increasing probe toxicities and side effects. Although NB fluorophore exhibits a relatively low water solubility, its modification with sulfonic acid improves its solubility by the formation of a zwitterionic structure. In addition, it has been widely described that the presence of zwitterionic groups not only increases solubility, but also can promote rapid renal clearance. With these ideas in mind, we synthesised and characterized two new fluorogenic molecular probes based on the modification of the Nile Blue dye with sulfonic groups. In chapters five and six, we focused on the synthesis and characterization of these probes, **NB-SO_3-Leu** and **NB-SO_3-Ala**, which were employed for the detection of leucine aminopeptidase (LAP) and

alanine aminopeptidase (APN), respectively. Both, LAP and APN enzymes are well described as cancer biomarkers.

Chapter five described the synthesis, characterization, and *in vitro* application of **NB-SO_3-Leu** probe for the detection of LAP enzyme that is overexpressed in SK-Mel-103 cells (human melanoma cell). **NB-SO_3-Leu** probe presented a very weak emission that was highly increased in the presence of LAP enzyme. This emission enhancement is ascribed to LAP-induced hydrolysis of the probe which yielded the highly emissive **NB-SO_3** fluorophore. Sensing mechanism is corroborated using LAP inhibitors, which induced a remarkable decrease in the fluorescent signal. Besides, the selectivity of the probe was assessed. In a similar way, chapter six presented the results obtained with the **NB-SO_3-Ala** probe which was employed for the detection of the APN enzyme. In this case, *in vitro* detection of APN was performed in different cancer cells lines. For both probes, the results showed an improvement of solubility. In both cases, *in vitro* confocal images showed a selective detection of the enzymes in cancer cell lines.

As mentioned above, an important goal of this thesis is the development of a probe capable of determining the presence of specific biomarkers in tissues *in vivo*, and have a rapid real clearance allowing detection in urine of the presence of the biomarker in the tissue. This system can be employed in disease detection using a easily readable way on urine samples. This issue has been addressed in chapter seven, in which the synthesis, characterization, and *in vivo* validation of the **Cy7-MAO** probe for the detection of overexpressed monoamine oxidase (MAO) enzyme in a natural aged mouse model is described. **Cy7-MAO** is based on a cyanine-7 fluorophore modified with sulfonic groups which increased probe solubility and allowed rapid renal clearance. The sulfonic modified-Cy7 fluorophore was linked to a MAO substrate that quenched its fluorescence. The mechanism of **Cy7-MAO** is based on its ability to restore fluorophore emission after the hydrolysis of the MAO

substrate in the presence of the MAO enzyme. Both, the activated and non-activated molecules, are excreted by the urinary system, an effect that is promoted by their zwitterion structures. Considering that MAO is overexpressed in different aging-related diseases, and its levels increase with aging, **Cy7-MAO** probe is used for the non-invasive *in vivo* detection and quantification of this enzyme in young and naturally aged BALB/cByJ mice through direct fluorescence measurements in urine.

The development molecular probes for the detection of specific analytes, such as toxic compounds, proteins, enzymes, or other biomarkers, either directly in the urine or through urine, is a promising strategy for the design of new accessible and less invasive diagnostic techniques. However, considering that these systems are still in the early stages of research, some potential drawbacks must still be studied more in detail, such as possible side effects, biodistribution and organ accumulation, or related toxicities. The results shown in this PhD thesis can be a first step in the development of new research with the principal objective of developing systems able to characterize and monitor a large number of diseases by simple fluorometric measurements in urine, decreasing the care span of patients and increasing their lifespan.